Nuclear magnetic resonance spectroscopy and enzyme kinetic investigation of acetylcholinesterase inhibition by organophosphates and reactivation by oximes

2019

Joe Perkins

A thesis submitted to the university of Kent for the degree of

Doctor of philosophy

University of Kent

Department of Biosciences

A. Acknowledgments

I would like to thank my academic supervisors **Dr Gary Robinson** and **Dr Richard Williamson** for their continued support and patience throughout my PhD, and for their very thorough feedback on draft versions of this thesis. **Dr Gary Thompson** has provided expert assistance in the practical aspects of NMR and taken the time to teach me the theoretical concepts, for this I would like to thank him.

I would also like to thank the members of the Defence Science and Technology Laboratory (DSTL) at Porton Down who have offered there expert opinions and advise on the project and in particular **Dr Becky Williams** who supervised my work at DSTL and made all of the samples containing organophosphate chemical warfare agents.

Thank you to **Dr Sarel Fleishman** for providing the genes for wild type acetylcholinesterase and the mutated isoform of the enzyme which enabled much of this work.

Thank you to DSTL and the Engineering and Physical Sciences Research Council who provided the funding for this work.

B. Contents

C. Abbreviations

AChE	Acetylcholinesterase
AChE-d	Acetylcholinesterase designed
AChE-S	Acetylcholinesterase synaptic
AChE-E	Acetylcholinesterase erythrocyte
AChE-R	Acetylcholinesterase read-through
ACh	Acetylcholine
AMPS	Ammonium persulfate
ATCh	Acetylthiocholine
BChE	Butyrylcholinesterase
BSA	Bovine serum albumin
CSA	Chemical shift anisotropy
CWC	Chemical warfare agents convention
CPMG	Carr Purcell Meiboom Gill
cv	Column volume
DDT	Dichlorodiphenyltrichloroethane
DMSO	Dimethyl sulfoxide
DTNB	5,5-dithio-bis-2-nitrobenzoic acid
DTT	Dithiothreitol
E. coli	*Escherichia coli*
EDTA	Ethylenediaminetetraacetic acid
FID	Free induction decay
GdmCl	Guanidinium chloride
GSH	Reduced glutathione
GSSH	Oxidised glutathione
GST	Glutathione s transferase (EC 2.5.1.18)
HEK293	Human embryonic kidney cells 293
His tagged	Hexa histidine tagged
HMQC	Heteronuclear multiple quantum coherence
HSQC	Heteronuclear single quantum coherence

IPTG	Isopropyl β-D-1-thiogalactopyranoside
kDa	Kilodalton
LB	Lysogeny broth
MW	Molecular weight
NMR	Nuclear magnetic resonance
OP	Organophosphate
PCR	Polymerase chain reaction
PDB	Protein data bank
ppm	Parts per million
SDS-PAGE	Sodium dodecyl sulphate polyacrylamide gel electrophoresis
Sf9	*Spodoptera frugiperda* cell line
SOFAST	Selective optimized flip angle short transient
STD	Saturation transfer difference
TEMED	Tetramethylethylenediamine
TRX	Thioredoxin
2YT	2 X yeast tryptone

D. Abstract

Organophosphates (OPs) are a class of compounds that have been predominantly used as insecticides but also as chemical warfare agents. They covalently inhibit the enzyme acetylcholinesterase (AChE) which plays a key role in terminating muscle contractions. Due to the toxic nature of these compounds, methods are needed that can assess the threat posed by new OPs and inform on the effectiveness of medical countermeasures.

In this project the recombinant expression and purification of a mutated isoform of AChE (AChE-d) was optimised to allow *in vitro* kinetic assays to be carried out on OP inhibition of AChE-d and the reactivation of the OP-AChE-d conjugates by oximes. The isotopic labelling of AChE-d was optimised resulting in ^{15}N uniformly labelled AChE-d being produced. Heteronuclear 2D NMR spectra were collected of labelled AChE-d inhibited by OPs. This data was analysed along with the reactivation data to determin if OPs with similar reactivation rates caused similar peaks to shift. Saturation transfer difference (STD) NMR spectra were collected on an AChE-d mutant that could not be phosphorylated by OPs.

The inhibition rates of OPs did not correlate with their toxicity. The reactivation data for AChE-d differed from data collected using human AChE. The NMR spectra of OP inhibited AChE-d indicated that reactivation resistant OPs did cause similar peak shifts but further investigation is needed to confirm this due to the low resolution/signal of the NMR spectra. STD data indicated that phosphorylation was the rate limiting step in the inhibition reaction of an OP with AChE-d

1. Chapter 1 Introduction

1.1 Acetylcholinesterase (AChE) variants, mechanism of action and importance in disease.

1.1.1 Isoforms of AChE.

In mammals there are three isoforms of AChE. AChE-S (for synaptic) is found at the neuromuscular junction and cholinergic synapses in the brain, it contains a cysteine at the C-terminus that forms a covalent dimer with another AChE, this dimer can then non-covalently bind to another covalent dimer of AChEs to form a tetramer (1). A proline rich collagen-like domain binds exon 6 (Figure 1) of the AChEs in the tetramer and anchors it to the post synaptic membrane (2). This isoform is particularly prevalent in the neuromuscular junction where it hydrolyses the neurotransmitter acetylcholine (ACh) (Figure 2), this terminates muscle contractions (3).

AChE is also found bound to the outer membrane of erythrocytes by a Glycosylphosphatidylinositol (GPI) anchor (4), this isoform is referred to as AChE-E (for erythrocyte). The physiological role of AChE-E isn't definitively known, but the presence of ACh in plasma has been shown to increase NO efflux from erythrocyte and, the NO efflux has been shown to stop when AChE inhibitors were added to the assay, indicating that the breakdown of ACh by AChE-E stimulates the signal cascade that results in NO efflux from erythrocytes (5). NO stimulates vasodilation (6) which could indicate that AChE-E has a role in increasing blood flow to tissues exposed to high concentrations of ACh, for example contracting muscles.

A soluble monomer of AChE also exists, called AChE-R (for read-through). This isoform is the result of an intron 4 (Figure 1) being incorporated into the enzyme. Like AChE-E the exact function of this isoform isn't known but it has been shown to be overexpressed in mice after psychological and chemical stress (7) and certain reversible AChE inhibitors have also been shown to upregulate the expression of this

isoform (8). This indicates that AChE-R is expressed in response to certain stress but doesn't explain its function.

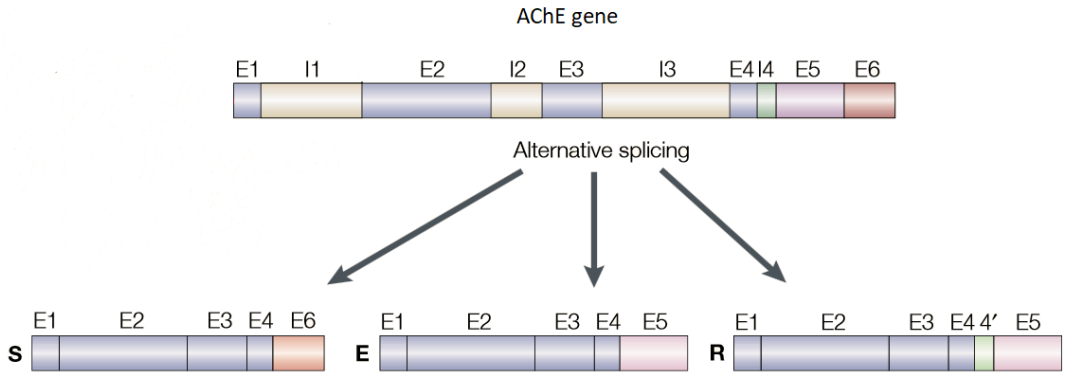

Figure 1. A schematic diagram showing the AChE gene and the three different mRNAs that arise from its alternative splicing. I stands for intron and E stands for exon. This Figure is an altered version of one found in reference (9)**.**

This nomenclature based on physiological role and localisation is useful when comparing AChE isoforms within mammals but problems are encountered when comparing the AChE isoforms of distant species. For example *Drosophila* has a single AChE isoform which is only found in the synaptic cleft of cholinergic neurons meaning functionally it would be classed as AChE-S, but structurally it shows more similarity to the AChE-E isoform in mammals (10). A second nomenclature exists based on the structure of the isoform and its mode of anchoring to membranes, an overview of this is shown in Figure 3. In this nomenclature AChE-H (for hydrophobic) is used to describe AChE isoforms that have a hydrophobic C-terminus containing a Cys that allows the formation of a covalent dimer and a GPI anchor which fixes the isoform to the membrane (11). Mammalian AChE-E and *Drosophila* AChE are examples of AChE-H.

The C-terminus of AChE-T (for tailed) contains a Cys residues which allows the formation of a dimer which can then form a tetramer with another AChE-T dimer. The C-terminus also contains the residues necessary for association with collagen and other similar proteins which can anchor the tetramer to the membrane or form larger bundles of tetramers (Figure 3 AChE-T 5) (12)(2). AChE-T 1,2 and 4 in Figure 3 are less physiologically relevant as they only exist when AChE-T is recombinantly

expressed in the absence of a collagen-like binding partner (2). Mammalian AChE-S is included in this category.

Confusingly AChE-S (for snake or soluble) is also used in this nomenclature. It's a monomeric form of AChE possessing a highly charged C-terminus that's missing the usual Cys residue. AChE-S is only found in *Elapid* snake venom where its purpose is a mystery since it doesn't add any toxicity to the venom (13). All future uses of AChE-S will be referring to the synaptic isoform of AChE.

Vertebrates also contain a second type of cholinesterase called butyrylcholinesterase (BChE), this enzyme is predominantly found in plasma but also exists in the brain (14). Unlike AChE-S, the activity of BChE doesn't appear to be vital for the survival as around 4% of the human population have a genotype that reduces BChE activity by a factor of 10, and the only negative phenotype associated with this genotype is an increased sensitivity to the muscle relaxant succinylcholine which is commonly administered along with an anaesthetic to patients undergoing surgery (15).

The three different mammalian isoforms of AChE (S, E and R) have very similar kinetic properties (16) for inhibition with Diisopropyl fluorophosphate (DFP). This is unsurprising since only the C-terminus of these isoforms (exons 5 and 6, Figure 1) are altered, these exons encode residues responsible for dimerization and method of attachment to membranes (9). The AChE from different species shows a larger variation in kinetic parameters. The sarin inhibition rate for rhesus monkeys AChE-S was shown to be 3 times higher than guinea pig and 2 times higher than pig AChE-S (17). This shows that AChE from a single species needs to be used in a set of experiments and care needs to be taken when extrapolating AChE kinetic data from one species to another.

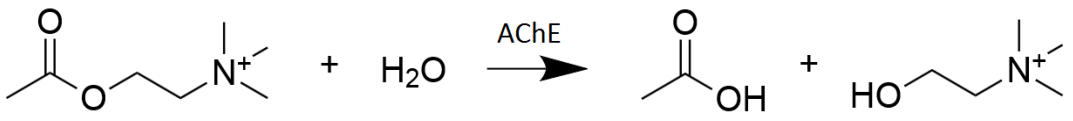

Figure 2. ACh being hydrolysed into acetic acid and choline catalysed by AChE.

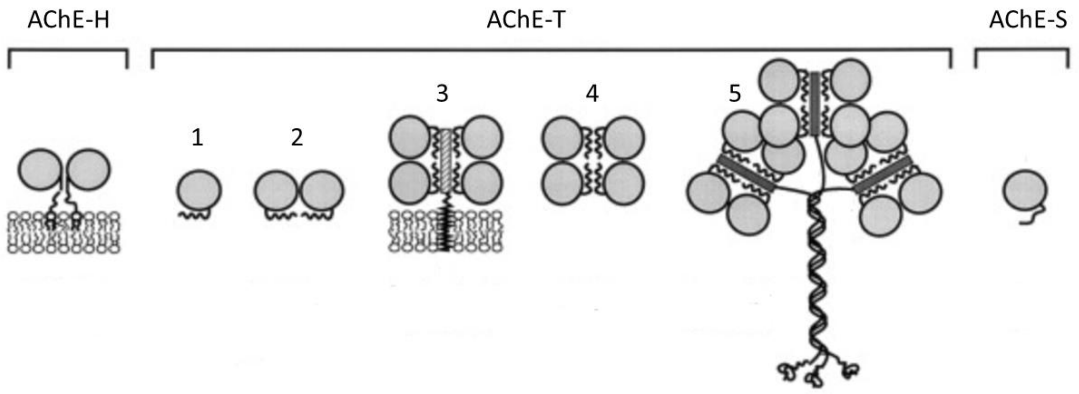

Figure 3. A cartoon representation of the different quaternary structures of AChE isoforms and their varying methods of associating with membranes. AChE-H (for hydrophobic) has a hydrophobic C-terminus that contains a post translational modification site for GPI that anchors it to the membrane, AChE-T (for tailed) contains a C-terminal peptide that allows association with a college like protein meaning higher order oligomeric structures can be formed and AChE-S (for soluble or snake) contains a highly charged C-terminus that lacks a Cys residue so can't form dimers. This figure is an altered version of one found in reference (2).

1.1.2 AChE structure and activity

The rate that AChE breaks down ACh is remarkably fast. The catalytic rate (k_{cat}/K_m) of AChE for ACh is around 1 X 10^8 M/s (18) this is higher than the average catalytic rate of 1 X 10^5 M/s (19), and is close to the diffusion limited rate of 1.5 X 10^{10} M/s (20). The high catalytic rate of AChE is particularly surprising as its active site is located at the bottom of a deep gorge shown in Figure 4 A.

Some studies have suggested mechanisms to explain how the presence of the active site gorge could increase the catalytic rate. First of all, the presence of a relatively weak binding site for ACh was discovered at the top of the gorge (Figure 4 B and Figure 5), it's been suggested that ACh first interacts with this before being passed down the gorge (21). The gorge itself contains several highly conserved acidic residues that are positioned to create a charge gradient with the strongest negative charge being at the base of the gorge (Figure 5), the charge gradient is enhanced by 14 highly conserved aromatic residues which modulate the dielectric constant of the acidic residues local environment (22).

Once ACh has bound to the low affinity peripheral binding site its 2D diffusion towards the active site is facilitated by its attraction to the negative charge of the

acidic residues and its interaction with certain aromatic residues. The combination of these two factors bring it into close proximity to the active site serine where it is hydrolysed (23)(24). The acetyl and choline groups then diffuse out of the active site gorge leaving the enzyme ready to hydrolyse another acetylcholine molecule (25).

The active site of AChE is made up of a catalytic triad which is similar to that of other serine hydrolases. Although the AChE catalytic triad does differ in two ways, firstly the triad in AChE is made up of a serine, histidine and glutamic acid, whereas in other serine hydrolases the glutamic acid is replaced with an aspartic acid. Secondly the handedness of the catalytic triad is reversed in AChE (26). The positioning of the residues that interact with ACh during catalysis are shown in Figure 6. The NH groups of Gly 121, Gly 122 and Ala 204 are found in close proximity to the catalytic triad, these form the oxyanion hole which stabilises the serine ACh intermediate by forming hydrogen bonds with the acyl group of ACh. The side chains of Glu 202, Trp 86 and Tyr 337 form the anionic binding site which interact with the choline moiety of ACh to ensure the correct positioning of the substrate for catalysis (27). Once the ACh molecule is at the catalytic triad and stabilised by the oxyanion hole and anionic binding site, His 447 deprotonates Ser 203 which causes the nucleophilic attack of the ACh carbonyl, the choline moiety accepts a proton from His 447 and breaks off from the acyl group. His 447 then deprotonates a water molecule creating a hydroxyl ion which reacts with the acetylated Ser 203 to produce acetic acid and a regenerated enzyme (18), this process is illustrated in Figure 7. The action of Glu 334 in the process is not fully understood but it is generally thought that it acts to stabilise the transition state by forming a hydrogen bond with either the acyl group (28) or with His 447 (29).

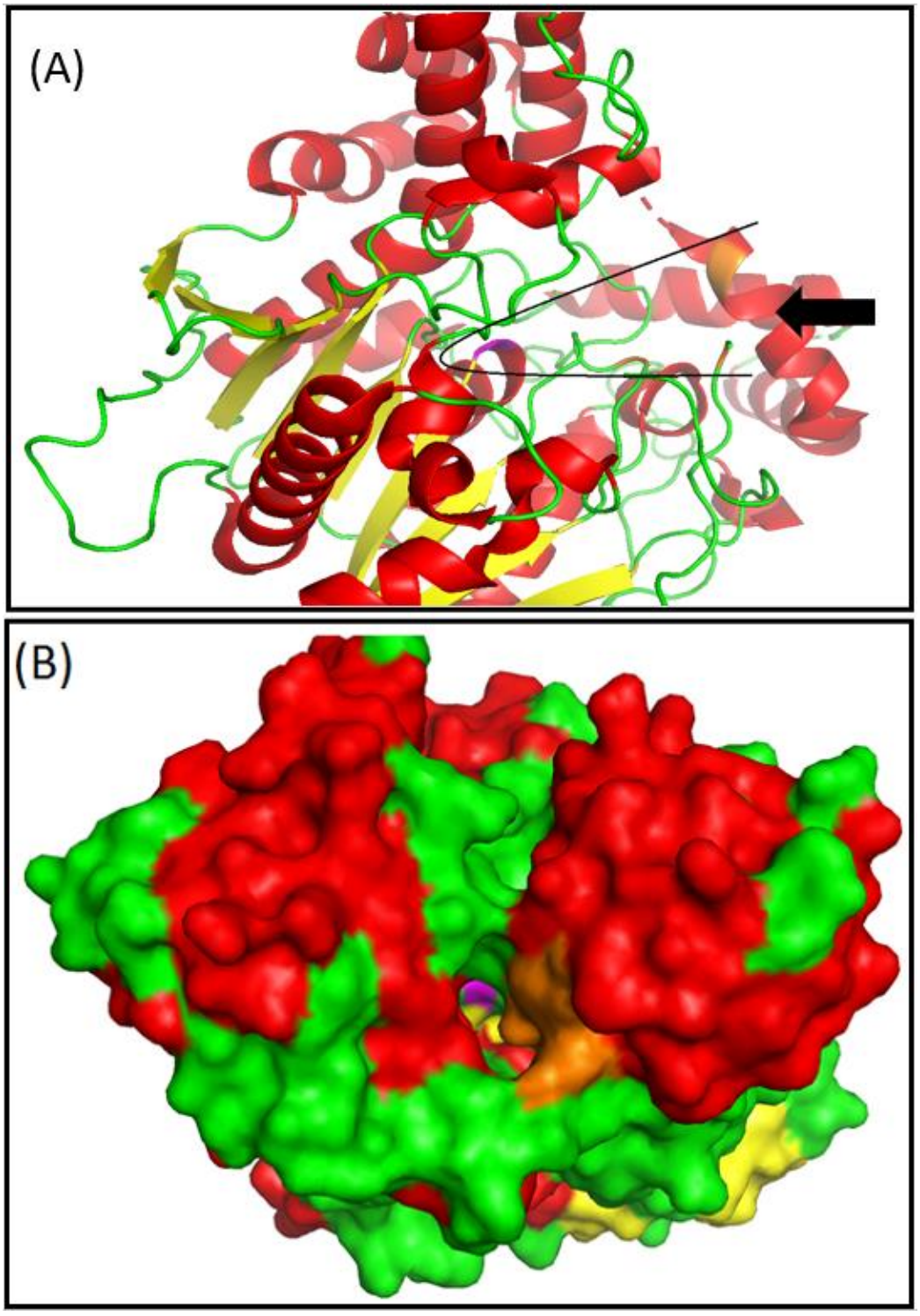

Figure 4. (A) Cross section of a cartoon representation of the crystal structure of human AChE-S subunit. The active site serine which covalently interacts with ACh is coloured pink and the residues of the peripheral anionic site are coloured orange. The approximate outline of the gorge is shown in black and an arrow points to the opening. (B) The same model from a different view to highlight the peripheral anionic site (orange). The PDB id 4pqe structure was used to generate both images.

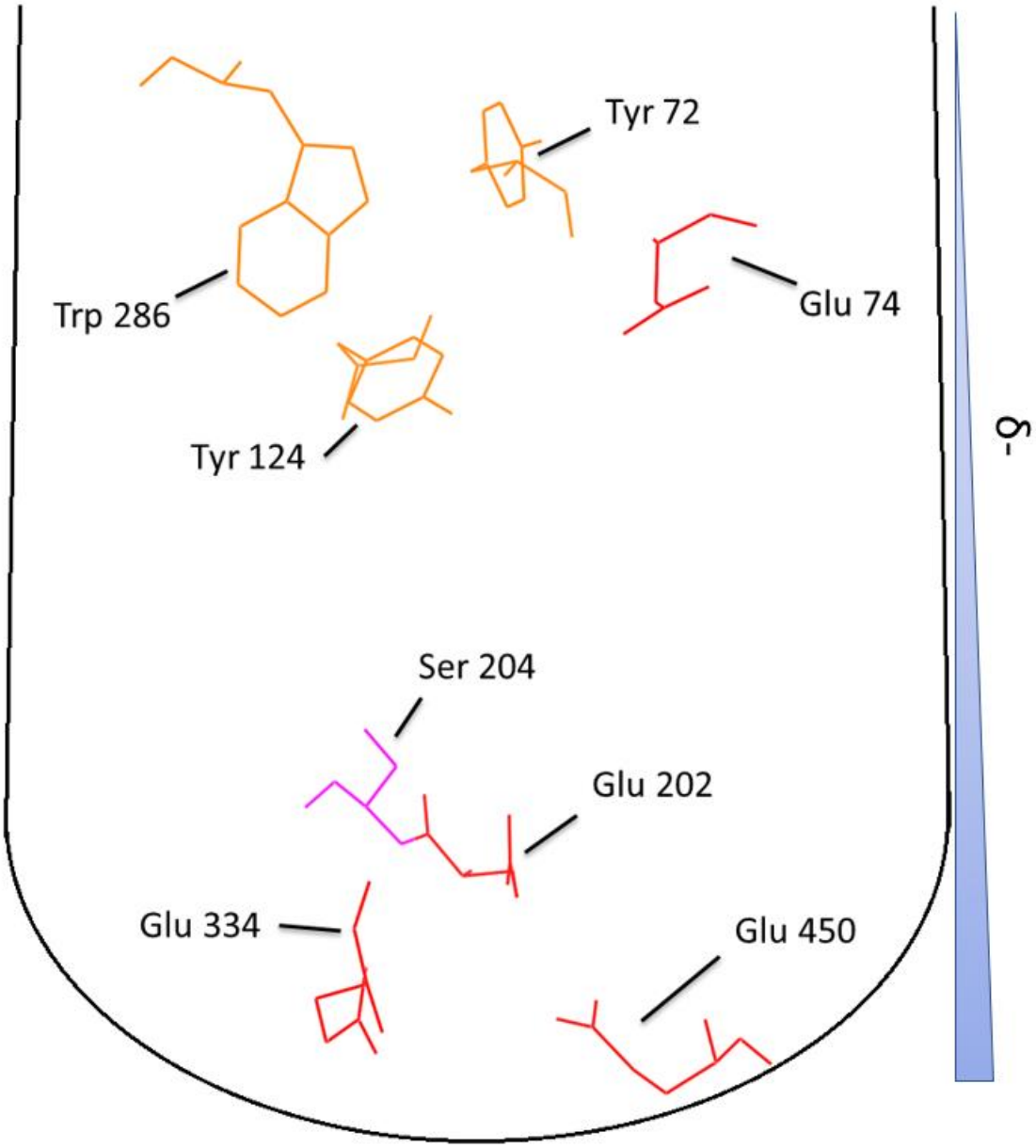

Figure 5. The AChE residues that form the peripheral anionic binding site (orange) located at the opening of the active site gorge (Figure 4 B) and the negatively charged residues (red) that attract the ACh molecule to the active site cysteine (pink) at the base of the gorge. Glu 74 can also be considered as part of the peripheral anionic site but is coloured red due to its negative charge (24)(30). The approximate outline of the gorge is shown in black and a rising wedge is included to indicate the electronegativity of the gorge. The PDB id 4pqe structure was used to generate the image.

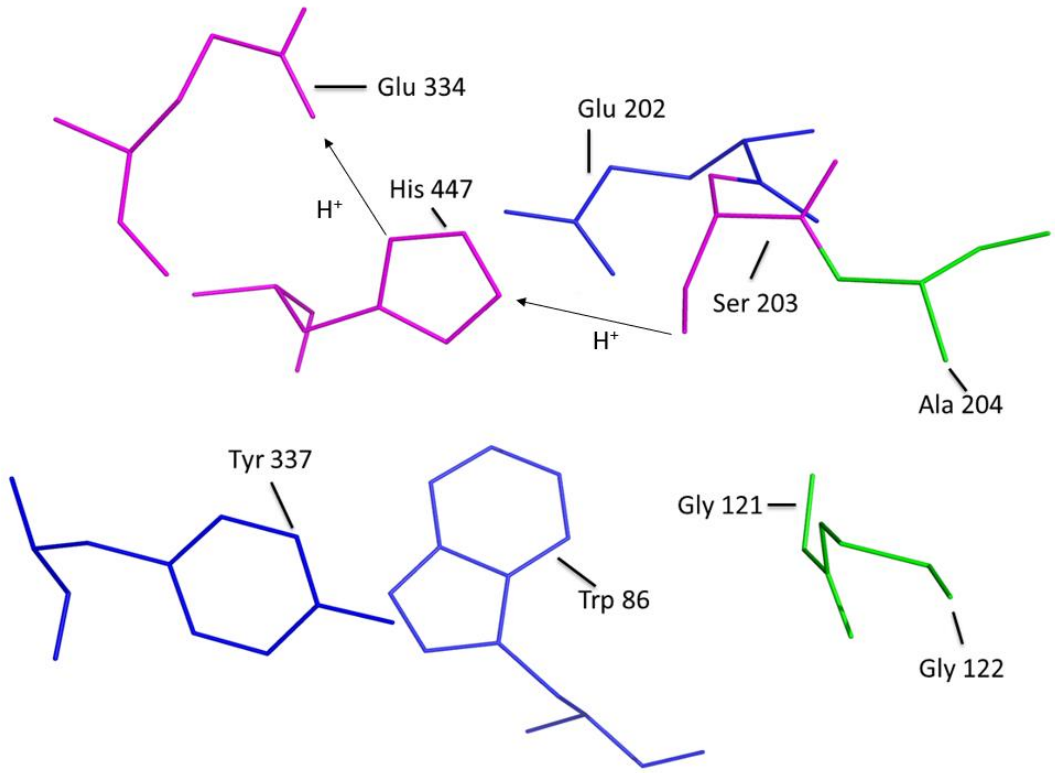

Figure 6. The arrangement of residues important to the catalytic activity of AChE. The catalytic triad is coloured pink, the oxyanion hole is coloured green and the blue residues form the anionic binding site. Arrows indicate the movement of H^+ ions between the catalytic triad during catalysis. This figure was generated using the crystal structure of human AChE-S. PDB id 4pqe.

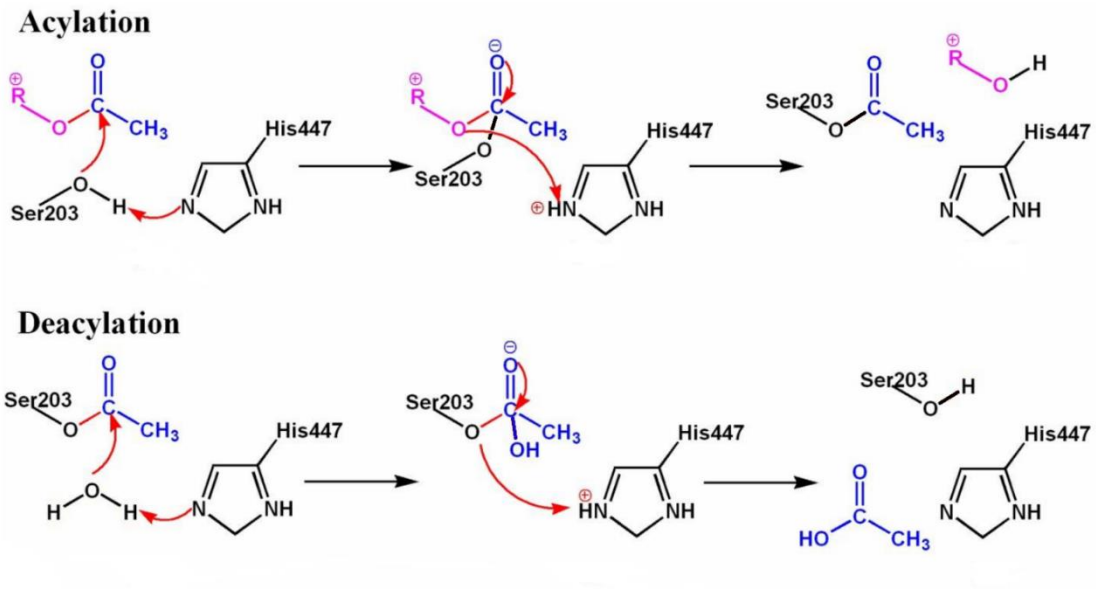

Figure 7. The reaction mechanism of AChE catalysing the breakdown of ACh. Blue represents the acyl moiety, pink represents the choline moiety and a red bond indicates that it is being broken in the reaction step. This figure is an altered version of a figure in reference (27).

1.1.3 AChE relevance to disease.

AChE has been shown to have relevance to several diseases. For instance, the upregulation of AChE-R expression in response to certain stresses mentioned in 1.1.1 has been shown to be detrimental to head injured mice, the inhibition of AChE-R overexpression with AChE-R antisense mRNA injections increased the survivability and lessened the drop in long term cognitive function in the head injured mice (31). Interestingly AChE-R has also been shown to be upregulated in the brains of people suffering from Alzheimer's disease (32). The mechanism that AChE-R plays in these conditions is poorly understood but these studies indicate that AChE-R further study as it could result in better treatments for these conditions.

AChE-S is linked to Alzheimer's disease in two ways. Alzheimer's disease is partly characterised by the loss of cholinergic neurones in the brain, this has led several reversible inhibitors of AChE to be developed to combat the symptoms. The rationale behind this method is that by inhibiting AChE the stimulation of cholinergic neurons can be prolonged by slowing the breakdown rate of ACh in the synapses. This can partially offset the reduction in cholinergic neuron activity seen in Alzheimer's patients. This method of treatment doesn't target the causes of Alzheimer's but can

alleviate the symptoms in mild to moderate cases of the disease (33). AChE also interacts with β-amyloid plaques which along with neurofibrillary tangles, are thought to be the causal agent of the neurodegeneration seen in Alzheimer's disease (34). The association of AChE with β-amyloid has been shown to speed up the formation of β-amyloid plaques which increases the rate of cognitive decline. Inhibitors targeting the peripheral anionic binding site of AChE were shown to slow the formation of β-amyloid plaques, however, inhibitors that only affected the catalytic triad of AChE showed no effect on the rate of plaque formation (35). This indicated that the peripheral anionic site may have a chaperone function for the formation of β-amyloid plaques, which opens the possibility that inhibitors of the interaction between AChE and β-amyloid can be produced to prevent or at least slow the onset of Alzheimer's disease. However, more research is needed to study the off-target effect of inhibiting the peripheral anionic site of AChE.

BChE has also been shown to have relevance to certain diseases. It was shown that when BChE was inhibited plasma concentrations of very low density lipoproteins and triglycerides decreased, indicating that it might function in the metabolism of these compounds (36). Concentration of BChE in the brain increase with age and are elevated further in people with Alzheimer's disease (37). BChE has also been found to associate with the plaques that cause Alzheimer's disease (38) indicating, that like AChE, BChE might play a role in the formation of the plaques. This means that BChE could potentially be a drug target for the treatment of Alzheimer's disease.

Cholinesterases have potential applications in protection against certain types of chemical warfare agents. If mice were given intravenous injection of BChE they could survive higher doses of the organophosphate (OP) chemical warfare agent soman (39) which irreversibly inhibits cholinesterase. The increased concentration of BChE in the blood stream of the mice will be irreversibly inhibited by soman which reduces the physiological concentration of the OP so less is available to inhibit AChE at the neuromuscular junction. Injections of recombinant BChE or AChE have the potential to be medically useful by removing OPs from people intoxicated by these compounds and as a pre-treatment to people entering situations that entail a high probability of OP exposure.

1.2 AChE inhibiting molecules.

1.2.1 AChE inhibiting insecticides.

AChE is an industrially important enzyme as it is the target for OP and carbamate insecticides (40). these types of insecticides are the most commonly used in agriculture and the domestic setting (41) meaning information on their interaction with AChE is of high importance in assessing the threat they pose to health and, developing antidotes to poisoning by these compounds. The mechanism of their inhibition of AChE is shown in Figure 8.

Until the 70s, the most commonly used pesticides were organochlorides, with Dichlorodiphenyltrichloroethane (DDT) being the most wildly used. It proved very effective at controlling insect populations and had low acute toxicity. However, its long environmental half-life (up to 15 years), accumulation in adipose tissue and link to cancer has persuaded the vast majority of countries to ban its use (42). This led to an increase in the use and development of carbamates and OP insecticides. The half-lives of these compounds are in the range of tens of days (43) meaning they have a much lower long term environmental impact compared to DDT and, because of their relatively high reactivities, bioaccumulation isn't seen. One negative trait that is shared by both DDT and the AChE inhibiting insecticides is their toxicity to bees (44)(45). A selection of AChE inhibiting insecticides (pirimiphos-methyl, malathion and pirimicarb) were tested against cabbage aphids and the species of wasp (*Diaeretiella rapae)* that parasitizes them (46). It was found that the relative toxicities of the insecticides for each species differed (Table 1), with pirimicarb being the most toxic insecticide to the aphid but least toxic to the wasp. This highlights the potential for AChE inhibiting insecticides to be developed that have a high toxicity to a few specific pest insects while having limited toxicity to beneficial insects, but further work is required to confirm if this is possible.

The major downside of AChE inhibiting insecticides is their toxicity to mammals. The oral LD_{50} in rats for DDT has been reported in the range of 133-800 mg/kg (47). The

oral LD_{50} in rats for the OP insecticides show a wide range, the values for Malathion, Ethion and Parathion-methyl are 619, 25.9 and 2.45 mg/kg respectively (48).

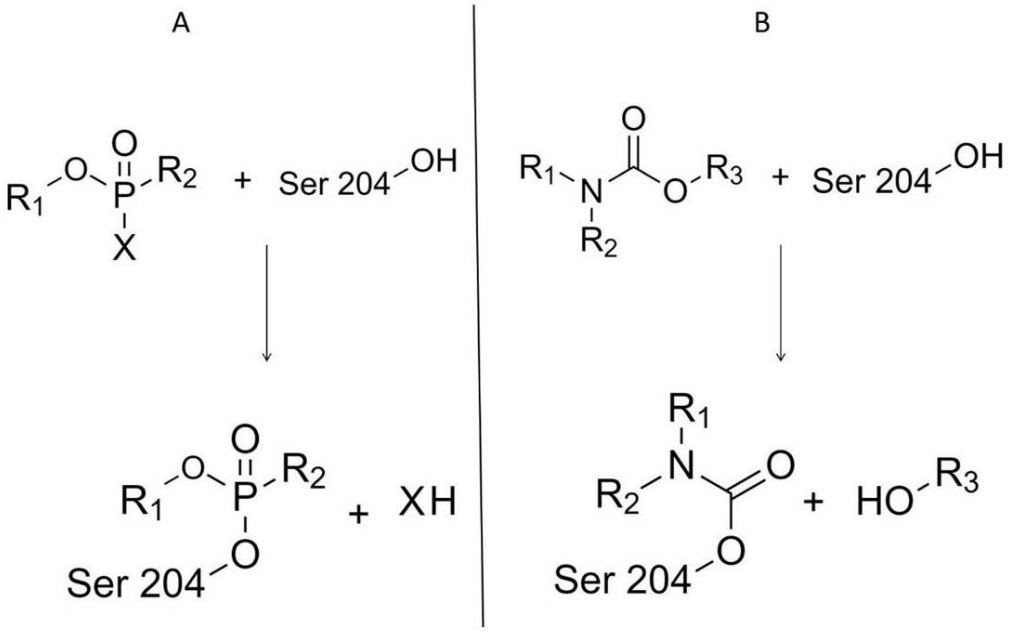

Figure 8. A shows a schematic of an OP reacting with the active site serine of AChE, X represents the leaving group R_1 and R_2 can be any other chemical group and the O which has a double bond to the P is sometimes replaced with an S. B is a schematic of a carbamate reacting with the active site serine of AChE. R_1, R_2 and R_3 can be any other chemical group.

Table 1. The relative toxicities of two OPs (malathion and pirimiphos-methyl) and one carbamate (pirimicarb) to cabbage aphids and the species of wasp (*Diaeretiella rapae*) that parasitizes them. Data taken from reference (46).

Relative toxicity	Aphid	Wasp
High	pirimicarb	pirimiphos-methyl
	pirimiphos-methyl	malathion
Low	malathion	pirimicarb

For a pesticide to be registered in Britain the manufacturers must carry out a series of experiments to determine the maximum dose that can be ingested every day

without any observable side-effects developing. The maximum doses that can be tolerated through inhalation and skin contact also need to be known to inform on the threat posed to agricultural workers. The maximum safe dose values are then decreased by a safety margin of 10-100 fold depending on the quality of the data. If the concentration needed to effectively control the target insect is likely to cause exposure to either the consumer or farm workers that exceeds the maximum safe dose then the application is rejected. The environmental impact of the pesticide is also considered, such as it's off target toxicity and environmental persistence (49). As these regulations came into place some of the more toxic OPs like parathion were banned (50). However, these regulations aren't global which means certain parts of the developing world, such as Nepal, still use the more toxic insecticides where they cause sporadic poisoning of rural workers by either accidental exposure or suicide attempt (51). This highlights the need for more research into AChE so insecticides can be developed that target any specific changes seen in the AChE of pest insects. One commonly proposed solution to the negative health and environmental impact of insecticides is to prohibit their use and rely on organic farming methods, however, it was shown that halving the amount of insecticide used on a wheat crop reduced the final crop yield by around 15% (52) and the reduction in crop yield caused by a 100% drop in pesticide use has been estimated to range from 26-80% depending on the crop (53). Insecticides have also been used to save lives by controlling the populations of disease carrying insects. DDT alone is thought to have prevented around 700 million cases of malaria in Africa (54). On average people infected with malaria have a 1.8% chance of dying from the disease (55) meaning over its lifetime DDT has saved approximately 12.6 million lives. This calculation doesn't consider other insecticides, continents or diseases. Although insecticides have negative effects on the environment and public health, stopping their use would likely result in large scale habitat destruction to make up for the reduced yield in agricultural crops and an increase in deaths from insect borne diseases. This highlights the need for detailed study of AChE to aid in the design of insecticides with minimal off target effects.

1.2.2 OPs as chemical warfare agents.

Highly toxic OPs have been used as chemical warfare agents meaning AChE is also of interest to the defence sector. The first chemical warfare agent OP was developed in Nazi Germany as an insecticide. Its potential for weaponisation was quickly realised and within a few years several new OP chemical warfare agents were developed. These OPs were named the G series agents as they were all first made in Germany, and some of their structures are shown in Figure 9 A. By the start of the 1950s, British chemists had designed a new generation of OP chemical warfare agents called the V series agents (Figure 9 B), these were more toxic than the G series agents, had lower volatility and were more environmentally persistent (56). The LD_{50}s of some OP chemical warfare agents are shown in Table 2. The 1950s also saw a third wave of OP chemical warfare agent development which took place in America and aimed to develop the V and G series agents as binary weapons. These would mix two non or mildly toxic chemicals in a warhead to produce the chemical warfare agent, ideally after firing the munition. Binary weapons greatly reduce the risk associated with the storage and handling of chemical warfare agent munitions.

All countries apart from Israel, Egypt, South Sudan and North Korea have signed up to the 1997 CWC which prohibits the production, stockpiling, development, transfer and use of all chemicals listed by the convention. All signatory countries also agreed to destroy all pre-existing stockpiles of chemical warfare agents and their pre cursors. Chemicals are considered on a case by case basis for inclusion in the CWC based on the following factors, the toxicity of the chemical, structural similarity to chemicals already included, the likelihood the chemical can be used as a precursor to a chemical warfare agent and historical uses of the chemical as a weapon or as a precursor to a weapon. Chemicals included in the CWC are separated into three “schedules”, schedule 1 chemicals have no use other than as weapons or pre cursors to weapons, schedule 2 chemicals can have some legitimate uses such as in medicine or research and schedule 3 chemicals are produced in large quantities for commercial uses. For schedule 2 and 3 chemicals only their implementation or development as weapons is prohibited by the CWC (57).

A range of OP pesticides are given in Figure 9 D and, when compared to the structures of OP chemical warfare agents in Figure 9 A and B several structural differences are clear. Firstly, the insecticides include compounds with a P=S instead of a P=O. This is due to the fact that OPs with a P=S are relatively weak inhibitors of AChE so have toxicities around 100 times lower than their P=O counterparts (58)(59). This is presumably because O is more electronegative than S meaning the O in P=O attracts electrons away from P giving it a more positive charge than an S would, making it more susceptible to nucleophilic attack by the Ser 204 of AChE, meaning P=O containing molecules would inhibit AChE at a faster rate than P=S containing molecules. P=S containing compounds need to be activated to become toxic, this is done by the oxidation of the P=S to P=O by cytochrome P450 in the human liver (60) and all tissues of insects (61). OP detoxifying enzyme, such as paraoxonase, phosphotriesterase, carboxylesterase and glutathione-S-transferase are more prevalent in mammals than in insects (62). This means that OPs are broken down at a faster rate in mammals than in insects, so in insects P=S containing insecticides are likely to be converted to the toxic P=O form whereas in mammals they're likely to be broken down before this conversion happens. This gives P=S containing insecticides a selective toxicity to insects. Interestingly, several insecticide resistance mechanisms have been attributed to upregulation of these enzymes in insects. For instance upregulation of glutathione-S-transferase-3 in *Plutella xylostella* was shown to confer resistance to methyl-parathion (63), and upregulation of a carboxylesterase was shown to give *Lucilia cuprina* resistance to malathion (64). The other main difference seen between OP insecticides and chemical warfare agents is that the chemical warfare agents routinely have a methyl group directly bound to the phosphorus, this is not seen in any commonly used insecticide (40). It has been noted that in general, OPs that have a methyl as their R_2 group (Figure 8 A) inhibit AChE at a faster rate than OPs with either an amide or an O alkyl group (65).

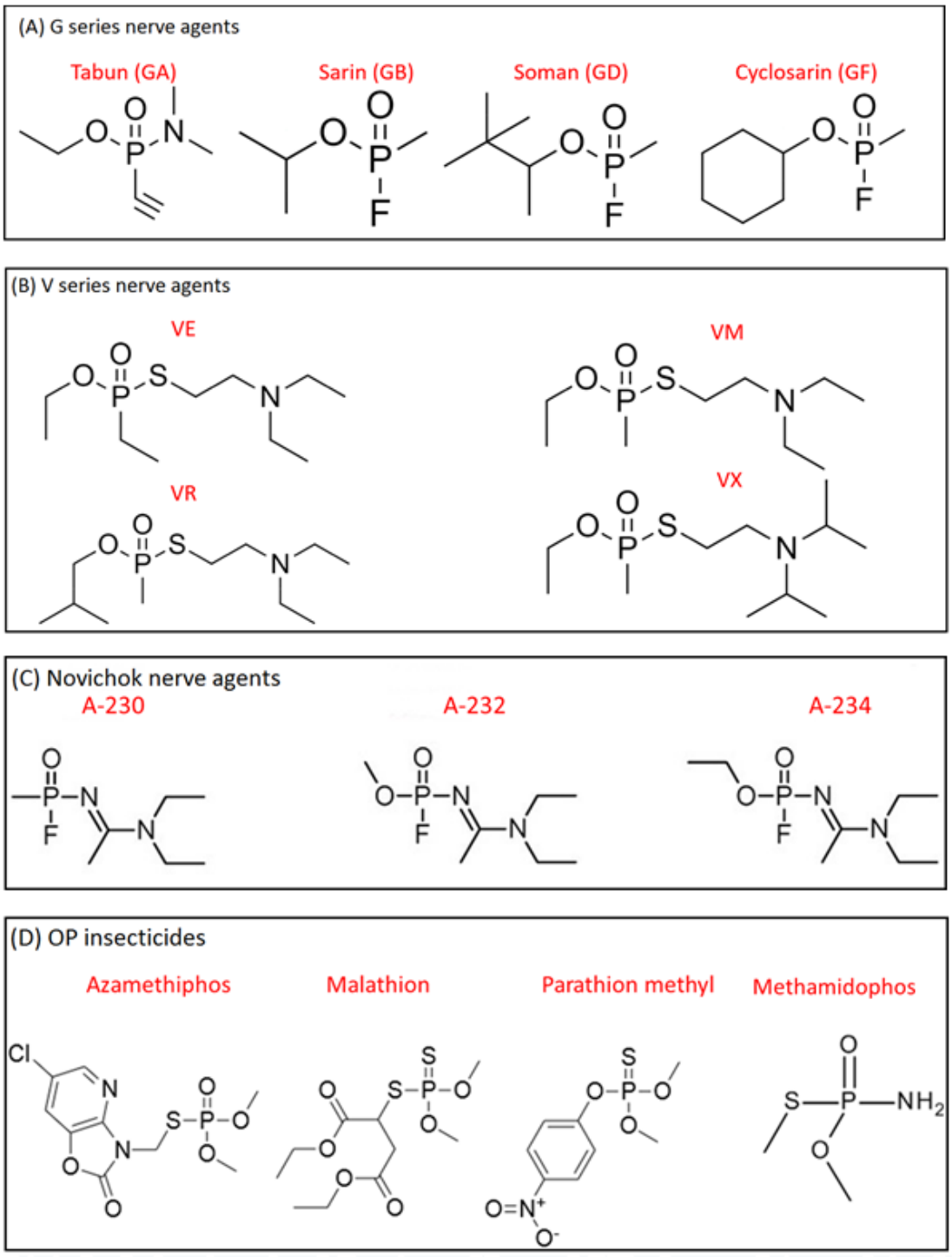

Figure 9. (A) Structures of some G series nerve agents, both their common and two letter NATO names are given. (B) Structures of some V series nerve agents. (C) Suggested but unconfirmed structures of some Novichock agents (66)**. (D) Structures of some common OP insecticides.**

Table 2. Toxicity of some commonly studied OP chemical warfare agents as the LD_{50} of intravenously administered agents in mice. The LD_{50} values were taken from (56). The two letter NATO designated name of the G series agents are given in brackets.

OP chemical warfare agent name	Intravenous LD_{50} in mice (μg/kg)
Soman (GD)	38
Sarin (GB)	41
Tabun (GA)	119
VX	12.6

1.3 Assessment and treatment of OP poisoning

1.3.1 Treatment of OP poisoning.

The main cause of death in patients with acute OP poisoning is asphyxiation caused by overstimulation of respiratory muscles, for this reason the first step in treating OP poisoning is to ensure the airways are open and to administer oxygen. A competitive inhibitor of ACh receptors is then administered to the patient to reduce the overstimulation of muscles caused by the excess ACh in the synapses. The most commonly used inhibitor of ACh receptors is atropine (Figure 10) which is a potent toxin if given to people not poisoned by OPs as, it desensitises the neuromuscular tissue to ACh preventing muscle contraction (67). However, as this has the opposite effect to OPs, atropine can counteract some of the dangerous effects of OP poisoning (68).

Oximes (Figure 10) can be effective reactivators of AChE inhibited with certain OPs. They function through a pin pong mechanism in that the AChE must first be inhibited by an OP after which an oxime can bind and reactivate the AChE. But some OPs show a high resistance to reactivation and the ability of the oxime to reactivate AChE is also dependent on the OP it is inhibited with. For instance, different homologues of tabun were shown to have a high variability in their reactivation times and the optimal oxime to reactivate with also differed (69). Consequently, there is no universal oxime which would serve as an effective treatment for all types of OP poisoning. Another factor that complicates treatment with oximes is that OP inhibited AChE can undergo a de-alkylation reaction which leaves the phosphate adduct with a negative charge, this process is referred to as ageing and is shown in Figure 11.

Oximes have a negative charge so function through a nucleophilic attack on the phosphorus atom, if the phosphate adduct becomes negatively charged it will repel the oxime meaning no reactivation can take place (70). Although the reactivation kinetics of different oxime OP pairs are well studied *in vitro* (69)(65)(71), well controlled clinical trials have not been carried out meaning that there isn't a

universally accepted procedure for oxime treatment of OP poisoned patients. Reviews of case studies usually conclude that the available data contains too many uncontrolled variables to definitively say if oxime treatment is effective but, due to *in vitro* studies showing oximes can be effective against certain OPs, it is better to administer the oxime than not (68)(72).

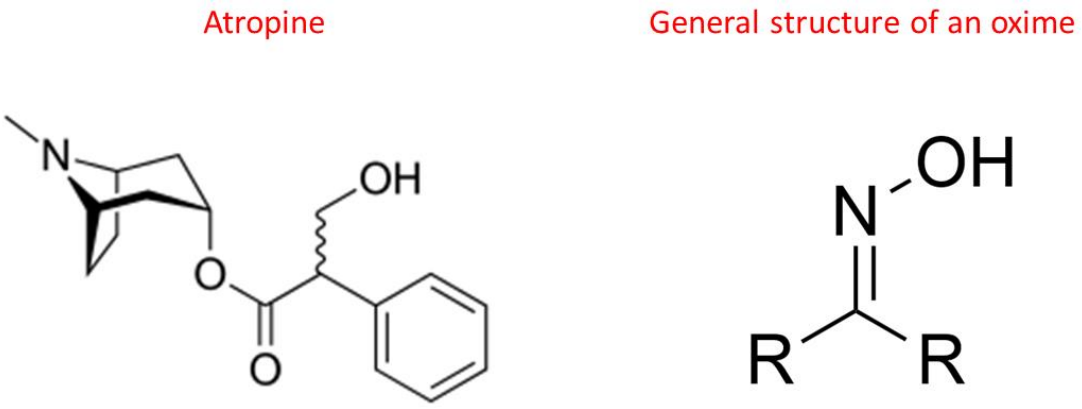

Figure 10. Structures of atropine and, the oxime functional group. These are the two drugs usually given to treat OP poisoning.

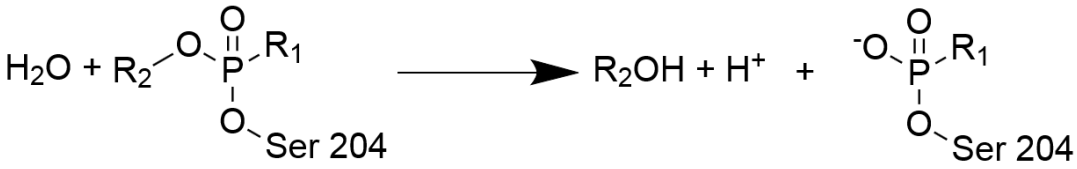

Figure 11. Schematic of the ageing process of the OP adducts bound to the active site serine of AChE, this process results in an OP AChE conjugate that can't be reactivated.

The three main factors affecting an OPs susceptibility to reactivation are ageing rate, electronegativity of the phosphorus atom and the size of the phosphate adduct (73). Some data has also shown that after inhibition with an OP, the active site gorge of AChE undergoes structural changes (74). These structural changes could also affect the ability of an oxime to reactivate an OP inhibited enzyme.

1.3.2 Assessment of OP toxicity.

Many current methods for assessing the toxicity of OPs rely on exposing animals to them and measuring the dose that results in the death of 50% of the tested animals, this gives the lethal dose (LD_{50}) values. A variety of different animals have been used in toxicity studies including rats (75), guinea pigs (76), mice, rabbits (77) and non-human primates (78). Guinea pigs and non - human primates are the preferred animals to use in toxicity studies as their plasma levels of OP degrading enzymes such as BChE and carboxylesterase are more similar to humans than the other model organisms (79).

For the foreseeable future, animals are likely to remain indispensable in the process of OP toxicity determination. However, protocols that approximate toxicity by studying the interactions of currently available OPs with AChE and correlating these results with those of animal toxicity experiments could have a value in reducing the number of animal experiments needed. For example, if currently available OPs with a high toxicity routinely produced a particular set of results in an *in vitro* assay, new OPs that produced the same or similar result could potentially be toxic. If this *in vitro* assay could (with reasonable accuracy) indicate a new OPs toxicity was several orders of magnitude lower than that of organophosphorus chemical warfare agents then, it could be safely assumed that the new OP didn't pose a threat as a chemical warfare agent and no animal experiment would be needed. However, if the assay indicated a toxicity value close to or higher than organophosphorus chemical warfare agents, then animal experiments would be needed to more accurately assess the threat posed by the OP. Similarly assays that produced results which correlate with the effectiveness of prophylactic or reactivating compounds could be useful in identifying compounds unlikely to be more effective than the current countermeasures. This would prevent unnecessary animal experiments from being carried out on compounds that pose little threat and have no medical use. The success of this approach would be dependent on the degree to which the parameters measured by the *in vitro* assay correlated with the toxicity or medical usefulness of the compound.

The "Animals (Scientific Procedures) Act 1986" that regulates animal experiments in Britain requires high standards in the care, sheltering and treatment of all animals

used for experimentation and that appropriately skilled people are employed to be accountable for each of these requirements. This ensures the distress and suffering the animals are exposed to is minimised but greatly increases the cost of using animals in scientific experiments. So assays that can be used to reduce the amount of animal experiments needed in OP threat detection and countermeasure development would lower the cost of these procedures and improve animal welfare.

1.3.3 Project aims.

An engineered isoform of human AChE (AChE-d) was created using a computational algorithm. The algorithm used a multiple sequence alignment of wild type human AChE-S against "several dozen" naturally occurring homologue sequences, for each residue in the wild type sequence the likelihood of it being mutated to each of the other 19 residues in the homologues sequences was calculated. The theory being that mutations that are more common in nature are less likely to have negative effects on the enzyme as they haven't been selected against by evolution. Any mutations that occurred in residues within 8 Å of the active site gorge were discarded. Rosetta computational mutation scanning was applied to each of the mutations deemed "likely" to occur in nature. For this a protein data bank structure of wild type human AChE-S was used. The energy difference between the wild type structure and the one containing the mutation was calculated, this was repeated for each of the mutations and the ones that reduced the activity below a certain threshold were selected. The threshold for a mutations likelihood to occur in nature and the reduction in structural energy were both altered to produce five variants of AChE-d, each containing a different set of mutations. The soluble expression yield, catalytic activity, and thermal stability of each variant were measured. The variant showing the highest thermal stability and expression yield whilst having the least change to the catalytic activity was chosen. The chosen variant (AChE-d) contained 51 mutations (Figure 12)(80). The catalytic activity was reported to be 11.4% lower in AChE-d than the wild type indicating success at minimising the effect on enzymatic activity. Table 3 shows the percentage similarity between AChE from different sources and Figure 13 shows the multiple sequence alignment used to generate these values. AChE-d and human AChE are 90.7% similar which is higher than the

similarity between human and electric ray AChE (61.6%) but slightly lower than human and guinea pig (92.4%). AChE from guinea pig (81), rat (82) and electric eel (83) are routinely studied. So while AChE-d is not completely comparable to wild type human AChE, its sequence homology and similar activity indicate that it is likely to provide data that's representative of wild type human AChE. For this reason, AChE-d was chosen for further study in this project.

The principle aims of this project were to:

1. Test the AChE-d construct and optimise its overexpression and purification.

2. Develop NMR methods to study the interactions of AChE with a range of OPs, and to develop protocols for use in assessing the threat of any newly discovered OPs.

3. To gain data on the mechanism of inhibition and reactivation that could be used to understand whether inhibition of AChE by certain OPs causes structural changes in the protein that could lower the affinity of certain oximes for that particular OP AChE conjugate. This would help to explain the differential reactivation rates that oximes have for different OP AChE conjugates.

Ligand observe studies using STD and CPMG experiments can be done with non-isotopically labelled AChE purified from a natural source, but to get NMR data on structural changes in AChE after inhibition with an OP, isotopically labelled recombinant AChE was required.

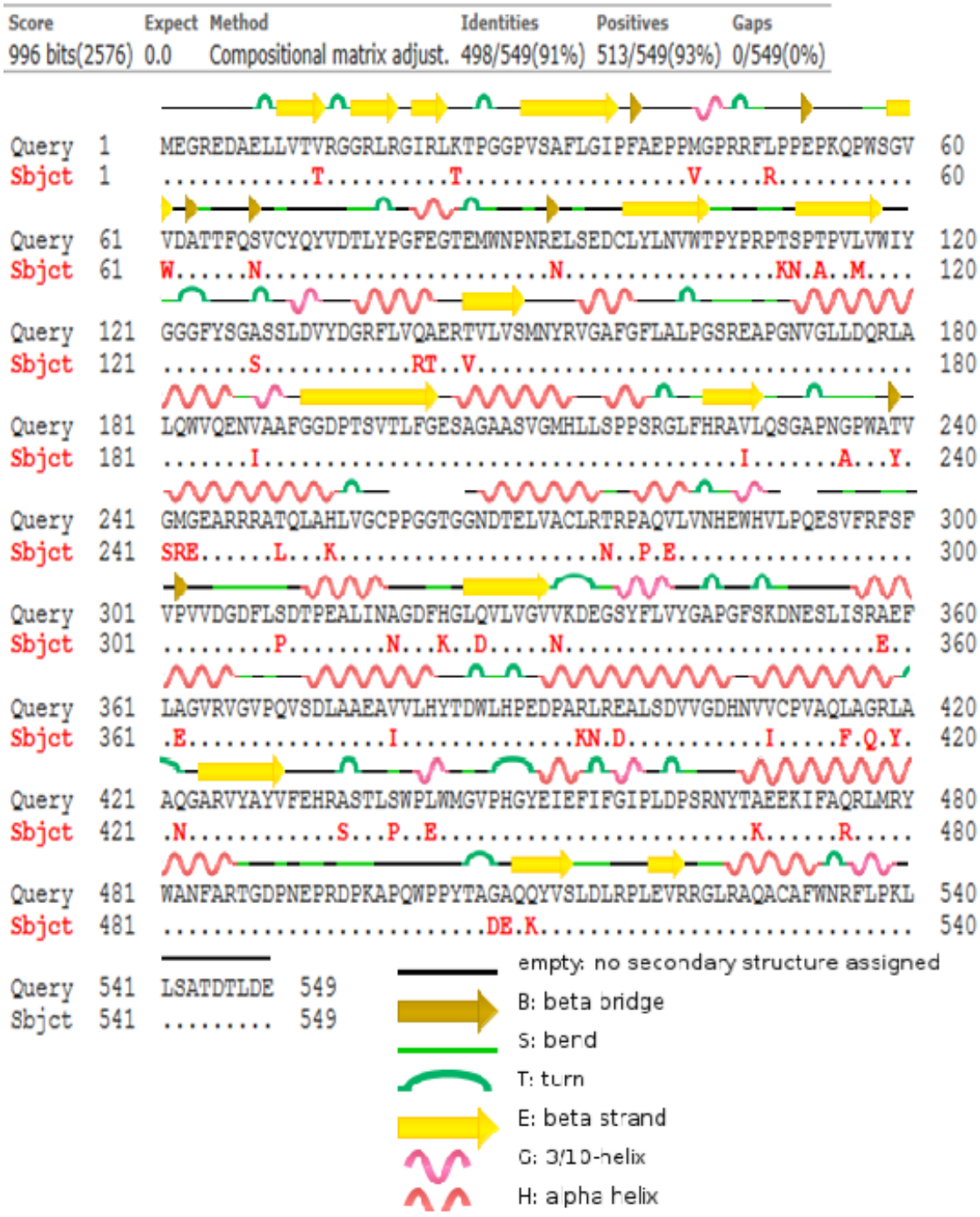

Figure 12. A comparison of the protein sequences of wild type AChE and AChE-d. The wild type sequence is shown in black and the mutated residues are shown in red. The secondary structure of wild type AChE is shown alongside the sequence and a key to the figure is included at the bottom of the image.

Table 3. Shows the percent similarity between AChE protein sequences from different sources. The signal sequences and the last intron containing the cysteine that forms an inter subunit disulphide bond were removed from sequences as they were not present in the AChE-d protein. Clustal omega was used for the sequence alignment.

Source of AChE	Electric eel	Rat	AChE-d	Human	Guinea pig
Electric eel	100.00	62.29	63.77	61.55	62.11
Rat	62.29	100.00	83.39	88.69	90.69
AChE-d	63.77	83.39	100.00	90.71	85.25
Human	61.55	88.69	90.71	100.00	92.35
Guinea pig	62.11	90.69	85.25	92.35	100.00

Figure 13. Multiple sequence alignment of AChE-S from different sources. Residues are colour coded based on their physical properties. Red are hydrophobic, blue are negatively charged, pink are positively charged and green polar. Residues marked with a * are conserved in all sequences and – indicate a gap has been introduced into the sequence to allow for a better alignment.

Chapter 2. Optimisation of the expression and purification of a designed isoform of acetylcholinesterase.

2.1 Introduction

2.1.1 Recombinant expression of AChE.

E. coli was the expression system of choice for this project because of the low cost and relative simplicity of the protocol compared to expression in more complex cells (84). Isotopic labelling of recombinant proteins is also much cheaper in *E. coli* due to the simplicity of the growth media needed. This makes it the ideal expression system for proteins to be used in NMR experiments (85). Unfortunately, human AChE is a 62 kDa protein containing three intra chain disulphide bonds and one inter chain disulphide bond (UniProtKB - P22303 (ACES_HUMAN)). For this reason attempts to express it in *E. coli* have had very limited success. Previous attempts to express AChE in *E. coli* resulted in the production of insoluble inclusion bodies (86). Attempts to refold the inclusion bodies produced only 4.15 mg of active protein from 750 L of media (87). Expression of the protein in other cell types has had more success. No exact figure for the recombinant expression yield of AChE in mammalian cells could be found, but usable quantities of AChE suitable for kinetic experiments have been expressed in HEK293 cells (88)(89). Active AChE (0.5 – 3.7 mg/l) was produced using the Baculovirus expression system in sf9 insect cells (90). AChE has been recombinantly produced in tobacco plants with yields of around 700 – 900 mg/kg, 8 – 10 weeks were needed to produce AChE by this method (91) making it relatively time consuming.

2.1.2 Ellmans assay.

The use of 5,5-dithio-bis-(2-nitrobenzoic acid) (DTNB) and acetylthiocholine (ATCh) to assess the activity of AChE was first described in reference (136) and the technique was named the Ellman's assay after the author of the paper. A schematic of the

reactions that take place in the Ellman's assay are shown in Figure 14. AChE catalyses the hydrolysis of ATCh to acetic acid and thiocholine which then reacts with DTNB, one of the products of this reaction is 5-mercapto-2-nitrobenzoic acid (5M2NA) which has a yellow colour. The A_{412} can be used to measure the concentration of 5M2NA and because one 5M2NA is released for every ATCh that is hydrolysed, the A_{412} is an indirect measure of how much ATCh has been hydrolysed.

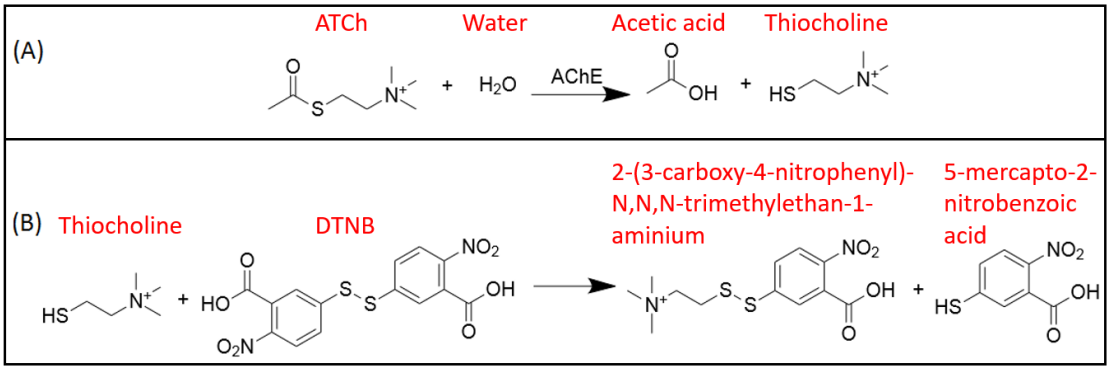

Figure 14. Schematic for the two chemical reactions that are coupled by the Ellman's assay. (A) Is the AChE catalysed hydrolysis of ATCh which releases acetic acid and thiocholine as products. (B) Is the reaction between thiocholine and DTNB which produces 2-(3-carboxy-4-nitrophenyl)-N,N,N-trimethylethan-1-aminium and 5M2NA which has a yellow colour.

The Ellman's assay has been used to study AChE in a variety of ways; including its use in combination with site directed mutagenesis to identify the amino acid residues that are important for catalytic activity (137) and to identify the mutations in mosquito AChE that confer resistance to certain insecticides (138). This assay has also been used to study the inhibition of AChE (139) and the effectiveness of oxime reactivators that are used to treat poisoning with these inhibitors (140).

2.1.3 Uniform ^{15}N labelling in different cell types.

Although insect and mammalian cells can produce active AChE, uniformly labelling the expressed protein with ^{15}N requires expensive media containing multiple ^{15}N labelled organic compounds (92)(93). Labelling media can be purchased from Cambridge Isotope Laboratories, the costs are around £5000/l and £5500/l for insect and mammalian cells respectively. Media used to uniformly label an *E. coli* expressed protein with ^{15}N is by contrast very simple. Only one source of ^{15}N is needed. 1 g/l of

NH_4Cl which costs around £13 a gram is the most expensive part of the media. It was for these reasons that an *E. coli* expression system was desired over other cell lines.

2.1.4 Designed isoform of AChE.

It was reported that a designed isoform of human AChE containing 51 mutations and a thioredoxin (TRX) fusion partner could be expressed in SHuffle® *E. coli* and the mutations in the gene had a minimal effect on the kinetic parameters of the enzyme (80). Shuffle *E. coli* was specifically developed to express disulphide bonded proteins by reducing the activity of the cytoplasmic reductive pathway and adding a disulphide bond isomerase to the cytoplasm (94). It was decided that the expression, purification and isotope labelling of this isoform (AChE-d) should be investigated. In (80) AChE was one of many proteins chosen for its lack of soluble expression in *E. coli*. The aim of the paper was to use a computer program to predict mutations that should be made to increase soluble expression and have minimal effect on activity. The optimal expression conditions and vector were not investigated. We intended to use heteronuclear multiple quantum coherence-selective optimized flip angle short transient (HMQC-SOFAST) NMR experiments for this work. Samples needed to be roughly 320 µl for a 5 mm Shigemi tube and over 25 µM so large amounts of protein are needed (roughly 0.5 mg of labelled AChE per sample) which made the optimisation of expression very important.

2.2 Materials and methods

2.2.1 Transformation and glycerol stock production.

Competent Shuffle express T7 *E. coli* were purchased from New England bio labs, the pET-32b vector containing AChE-d-TRX was kindly provided by Dr Sarel Fleishman. All other AChE-d constructs were made following the procedure described in section 2.2.8.

Plasmid (10 ng) was mixed with 50 µl of competent shuffle *E. coli* in a sterile 1.5 ml Eppendorf tube. This was left on ice for 10 minutes then heat shocked at 42^{o}C for 45 s in a temperature controlled water bath then left on ice for another 5 min. 150 µl of sterile 2YT media (16 g/l tryptone, 10 g/l yeast extract, 5 g/l NaCl) was added, the Eppendorf containing the transformation media was then placed in a shaking incubator at 37^{o}C 180 rpm for 1 h. After incubation the mixture was spread on LB agar plates containing ampicillin at 100 µg/ml these were then placed in an incubator at 37^{o}C for roughly 19 hours.

Single colonies were used to inoculate four 50 ml cultures of 2YT media containing 100 µg/ml ampicillin in 250 ml conical flasks which were incubated at 37^{o}C in a shaking incubator at 180 rpm until the OD_{600} was around 0.6. To create glycerol stocks, 840 µl of culture was transferred to cryo vials and 160 µl of sterile 50% glycerol, 50% water was added, these were then flash frozen in liquid nitrogen and kept on dry ice. The remaining cell cultures were induced with IPTG and placed back in the incubator for 3 hours. After this the cells were lysed using the protocol described below, and the AChE-d activity was measured. The glycerol stock that came from the culture with the highest AChE-d activity was kept at -80^{o}C and the others were discarded.

2.2.2 Protein expression.

2YT media was used to grow *E. coli* for unlabelled expression. Ampicillin (100 µg/ml) was added so only *E. coli* harbouring the expression plasmid would grow. Test growths were carried out in 250 ml conical flasks containing 50 ml of cell culture.

Large growths that were intended to produce protein for kinetic or NMR experiments were carried out in 2.5 L baffled conical flasks containing 1 L of media.

The glycerol stock of the desired transformant was streaked on LB agar containing 100 µg/ml ampicillin and incubated at 37^{o}C for 17 hours. Starter cultures of 2YT media were inoculated and incubated at 30^{o}C with shaking at 180 rpm for 17 hours. Starter cultures were then centrifuged at 3220 g for 20 minutes at 4^{o}C, the supernatant was discarded, and the pellet was re-suspended in 2 ml of fresh 2YT media for each 50 ml starter culture, the OD_{600} of this was then taken. The volume of concentrated starter culture needed to inoculate the main cultures to an OD_{600} of 0.2 was calculated (usually around 2.5 ml per L of main culture). After inoculation cultures were incubated at 37^{o}C with shaking at 180 rpm until OD_{600} reached 0.4 (around 1.5 hours) at which point the temperature was dropped to 25^{o}C and incubation was continued until OD_{600} was between 0.6 and 0.8 (around 1 hour). Protein expression was then induced by adding IPTG to a final concentration of 0.45 mM and cultures were returned to the incubator and left over night. The next day cultures were centrifuged at 3220 g for 20 minutes at 4^{o}C, the supernatant was discarded and the pellet was re-suspended in 10 ml lysis buffer (20 mM sodium phosphate, 100 mM NaCl, pH 7.3) for every litre of cell culture. Once cells were re-suspended in lysis buffer they could either be frozen at -20^{o}C or lysed.

2.2.3 Cell lysis.

Once cells were re-suspended in lysis buffer, Triton X-100 and lysozyme were added to a final concentration of 0.1 % v/v and 0.1 mg/ml respectively. After 20 minute incubation at room temperature, $MgCl_2$ and Bovine DNase 1 were added to final concentrations of 5 mM and 20 µg/ml respectively, this mixture was then incubated at room temperature until viscosity reduced. The mixture was then sonicated at amplitude of 15 microns for 3 minutes with a 10 second on/off cycle. The lysate was centrifuged at 20,000 g for 20 minute at 4^{o}C. The lysate supernatant was passed through a 0.45 µm syringe filter and the lysate pellet was re-suspended in a volume of lysis buffer equal to the lysate supernatant using a glass homogenizer.

2.2.4 Ni affinity, Procainamide affinity and size exclusion chromatography.

The buffers used in Ni affinity chromatography were all made in Milli-Q water, they were;

1. Charging buffer: 0.2 M $NiSO_4$

2. Sodium acetate buffer: 20 mM sodium acetate, 0.5 M NaCl, pH 4

3. Lysis buffer: 20 mM sodium phosphate, 100 mM NaCl, pH 7.3

4. Wash buffer: 20 mM sodium phosphate, 100 mM NaCl, 50 mM imidazole, pH 7.3 (unless otherwise stated)

5. Strip buffer: 20 mM sodium phosphate, 100 mM NaCl, 20 mM ethylenediaminetetra acetic acid (EDTA), pH 7.3

A Ni column was made using 2 ml of chelating Sepharose fast flow in a 20 ml Bio-Rad gravity flow column. First the column was washed with 10 column volumes (cv) of Milli-Q water followed by 2 cv of charging buffer (buffer 1), then 3 cv sodium acetate buffer (buffer 2), after this the column was washed with 10 cv lysis buffer (buffer 3). Up to 20 ml of lysis supernatant was loaded onto the column, after it had all flowed through, the column was washed with 10 cv lysis buffer (buffer 3) and then 10 cv wash buffer (buffer 4). The protein was eluted with 10 cv strip buffer (buffer 5). After strip buffer (buffer 5) was added the flow through was collected in 1 ml fractions. The column was then washed with 10 cv Milli-Q water and stored in 20 % ethanol. The A_{280} of all strip buffer fractions was measured to identify the ones containing protein, these were pooled and concentrated using a 6 ml 50 kDa cut off centrifugal concentrator to a volume of between 1-2 ml to increase separation on the size exclusion column.

Procainamide Sepharose purification was optimised using a batch method. 40 µl of procainamide Sepharose slurry was added to 1.5 ml Eppendorf tubes. Procanamide

Sepharose was washed by adding 1 ml of Milli-Q water then allowing to mix on a rotary mixer, after 5 minutes the samples were centrifuged at 4,000 g for 1 minute and the supernatant was removed. This was repeated with lysis buffer. 0.5 ml of lysate supernatant was then added to beads and allowed to mix. Samples were then washed again with 1 ml lysis buffer then mixed with 1 ml lysis buffer containing the specified concentration of NaCl. Samples of the elution were taken for analysis by SDS-PAGE gels and activity assays.

The size exclusion column used had a cv of 260 ml and was packed with Superdex 200. The column was equilibrated with 2 cv of lysis buffer before the 1-2 ml concentrated protein sample was loaded, lysis buffer was used to elute the protein. 5 ml elution fractions were collected, samples with high A_{280} were analysed by SDS-PAGE to assess purity. Samples containing only AChE-d were concentrated to around 30 µM using a 15 ml 50 kDa cut off centrifugal concentrator.

2.2.5 Ellmans assay of Lysate supernatant.

A 100 mM stock of 5,5-dithio-bis-(2-nitrobenzoic acid) (DTNB) was made in dimethyl sulfoxide (DMSO). This was added to lysis buffer along with acetylthiocholine (ATCh) to give a final concentration of 1 mM DTNB and 2 mM ATCh. This was made up just before the experiment starts as the DTNB and ATCh react over time. 990 µl of the lysis buffer containing DTNB and ATCh was added to a 1 ml cuvette, this was used to blank the spectrophotometer. 10 µl of lysate supernatant was then added to the cuvette and mixed. The absorbance at 412 nm was taken every 2 s for 20 s using the kinetics mode on a Nanodrop One and an initial delay of 1 s was included as required by the Nanodrop. Highly concentrated lysate supernatant produced a nonlinear graph of absorbance vs time, when this happened the lysate supernatant was diluted with lysis buffer and the dilution was taken into account in the final calculation. The rates were calculated using equation 1.

$$Rate = (A_{412t21} - A_{412t1}) * 3 * df$$

Equation 1. Used to calculate the rate of reaction of the AChE catalysed breakdown of ATCh. The units are absorbance units/min/10 µl lysate supernatant. A_{412t21} is the absorbance of the recording at 21 s, A_{412t1} is the absorbance of the recording at 1 s and df is the dilution factor.

Samples eluted from procainamide Sepharose with low NaCl concentrations had low AChE-d activity which precluded the method described above from being used to measure their activities. For samples eluted in the range of 0 – 0.5 M NaCl 10 µl of elution was added to 990 µl of Ellmans buffer and left for 3 min at which point the A_{412} was taken. For samples eluted in the range of 0.6 – 1 M NaCl the A_{412} was taken after 20 s and extrapolated to get the value after a 3 min incubation.

2.2.6 Sodium dodecyl sulphate polyacrylamide gel electrophoresis (SDS-PAGE).

Tris SDS-PAGE gels were made using the recipe shown in Table 4. The 12.5 % resolving gel was made first. The 10% ammonium persulfate (AMPS) and tetramethylethylenediamine (TEMED) were added last as they initiate the setting of the gel. Empty Novex gel cassettes were filled ¾ of the way up then 200 µl of water saturated butanol was added to the top of the unset gel to flatten the meniscus. After the resolving gel had set the butanol was washed off and the rest of the gel cassette was filled with stacking gel. The comb was then added to the stacking gel, this was then left to set.

Table 4. Composition of SDS-PAGE gels.

Reagent	12.5 % resolving gel	5 % Stacking gel
40 % Acrylamide	6.5 ml	1.25 ml
1.5 M Tris pH 8.8	5 ml	0 ml
0.5 M Tris pH 6.8	0 ml	1.25 ml
10 % SDS	200 µl	100 µl
H_2O	8.35 ml	7.3 ml
10 % AMPS	50 µl	50 µl
TEMED	14 µl	10 µl

A stock solution of 5 X loading buffer was made, this contained 0.25% Bromophenol blue, 0.5 M dithiothreitol (DTT), 50% Glycerol, 10% sodium dodecyl sulphate (SDS) and 0.25 M Tris, pH 6.8. This was diluted in the protein samples to a concentration of 1 X. After the loading buffer was added the samples were boiled for 2 minutes. In the case of pre and post induction samples, 0.5 ml of cell culture was taken and centrifuged at 13,000 g for 2 minutes. The supernatant was removed and 100 µl of 1 X loading buffer was added to the pre induction pellet. The volume of 1 X buffer added to the post induction pellet was adjusted based on its OD_{600} so both pre and post induction samples had the same protein concentrations. The samples were then boiled for 2 minutes. The samples were drawn up and down a Hamilton syringe to shear DNA, this was done until the viscosity of the samples had reduced. Gels were run at 75 mV until the dye front had passed into the resolving gel then the voltage was increased to 180 mV until the dye front reached the end of the gel cassette. The running buffer used contained 3 g/l Tris, 14.4 g/l Glycine and 1 g/l SDS. Precision plus molecular weight marker (BioRad) was used and the molecular weight standard on all gels.

2.2.7 Attempted refolding of AChE-d-TRX.

Shuffle *E. coli* that had been transformed with a plasmid containing the gene for AChE-d-TRX was grown in a 100 ml culture of 2YT media in a 500 ml conical flask, the cells were lysed as described above. A ground glass homogeniser was used to re-suspend the lysate pellet in 2.5 ml wash buffer which contained 50 mM Tris, 10 mM EDTA and 0.5 % Triton x-100 (pH 8). The sample was centrifuged at 15,000 g for 5 minutes. This was repeated once with wash buffer then again with Milli-Q water. The protein concentration was estimated by running a sample on an SDS-PAGE gel along with samples containing known amounts of bovine serum albumin (BSA).

The protein resuspension was then dissolved in solubilisation buffer (50 mM Tris, 5 M guanidinium chloride (GdmCl), 11 mM DTT, pH 8.75). Enough solubilisation buffer was used to give a protein concentration of 2 mg/ml. This was incubated at room temperature for 10 minutes to ensure complete disulphide bond reduction.

Half of the solubilised protein was added to a refolding buffer containing 50 mM Tris, 0.05 M GdmCl, 0.78 mM GSH and 0.44 mM oxidised glutathione (GSSH) at pH 8.75. The other half of the solubilised protein was added to a buffer with the same components as above but 0.5 M GdmCl instead of 0.05 M. The volume of the refolding buffers was 100 X the volume of the solubilised protein being added. Solubilised protein was added dropwise while stirring to avoid protein precipitation forming. The refolding samples were incubated at room temperature for 2 hours then over night at 4 ^{o}C whilst stirring.

Protein precipitate was removed by centrifugation at 15,000 g for 10 minutes, the supernatant was dialysed in 5 L of lysis buffer overnight at 4 ^{o}C and then concentrated with a centrifugal concentrator.

2.2.8 Sub cloning and Polymerase chain reaction (PCR).

The AChE-d gene was removed from the pET-32b vector using *NcoI* and *XhoI* restriction enzymes. The *NcoI* restriction site was between the TRX tag gene and the AChE-d gene so this released a DNA fragment containing only the AChE-d gene. This gene was then ligated into pET-23a using the same restriction sites. The AChE-d gene contained a stop codon which prevented the C terminal His tag of pET-23a being incorporated into the protein (Figure 15 A and B).

A modified pET-23b plasmid that had 6 histidine codons added after the T7 promotor (pLWRP51) (95) was used to produce N terminally His tagged AChE-d. PCR was used to copy the AChE-d gene out of the pET-23a construct, because pLWRP51 contained an *NdeI* restriction site instead of an *NcoI* site, the forward primer used in the PCR reaction contained the sequence for the *NdeI* site (CATATG) instead of the *NcoI* sequence (CCATGG). The *NdeI* and *XhoI* restriction sites were used to cut the AChE-d gene and the plasmid. The AChE-d gene contained a stop codon at the C terminus to prevent the C terminal His tag of pLWRP51 being incorporated into the protein (Figure 15 D). The sequence of the primers used is shown in Table 5.

Site directed mutagenesis to remove the stop codon from AChE-d was performed to allow the incorporation of the C terminal His tag in pET-23b (Figure 15 C). The primers used are shown in Table 5. The reverse primer was complimentary to the 3' end of

the AChE-d gene but the stop codon "TAA" was omitted from the primer. *NdeI* and *XhoI* were used to cut the ends of the PCR product which was then ligated into pET-23b that had been cut with the same restriction enzymes.

Phusion high fidelity DNA polymerase was used for all PCR reactions. All constructs were sequenced between the T7 promoter and T7 terminator sequence to ensure no mutations had occurred in the AChE-d gene.

The PCR conditions used were 30 cycles of 1 min at 94^{o}C for denaturation 2 min at 55^{o}C for primer annealing and 3 min at 72^{o}C for extension.

Table 5. Primers used to produce the AChE-d genes with a C terminal His tag (AChE-d C His) and N terminal His tag (AChE-d N His). pET-23a containing the AChE-d gene was used as the template in both PCR reactions.

AChE-d construct	Forward primer	Reverse primer
AChE-d C His	AAAAAACATATGGGAAGGCCGCGAAGATG	AAAAAACTCGAGCTCGTCGAGGGTGTCGGTGG
AChE-d N His	AAAAAACATATGGGAAGGCCGCGAAGATG	AAAAAATTACTCGAGCTCGTCGAGGGTGTCGG

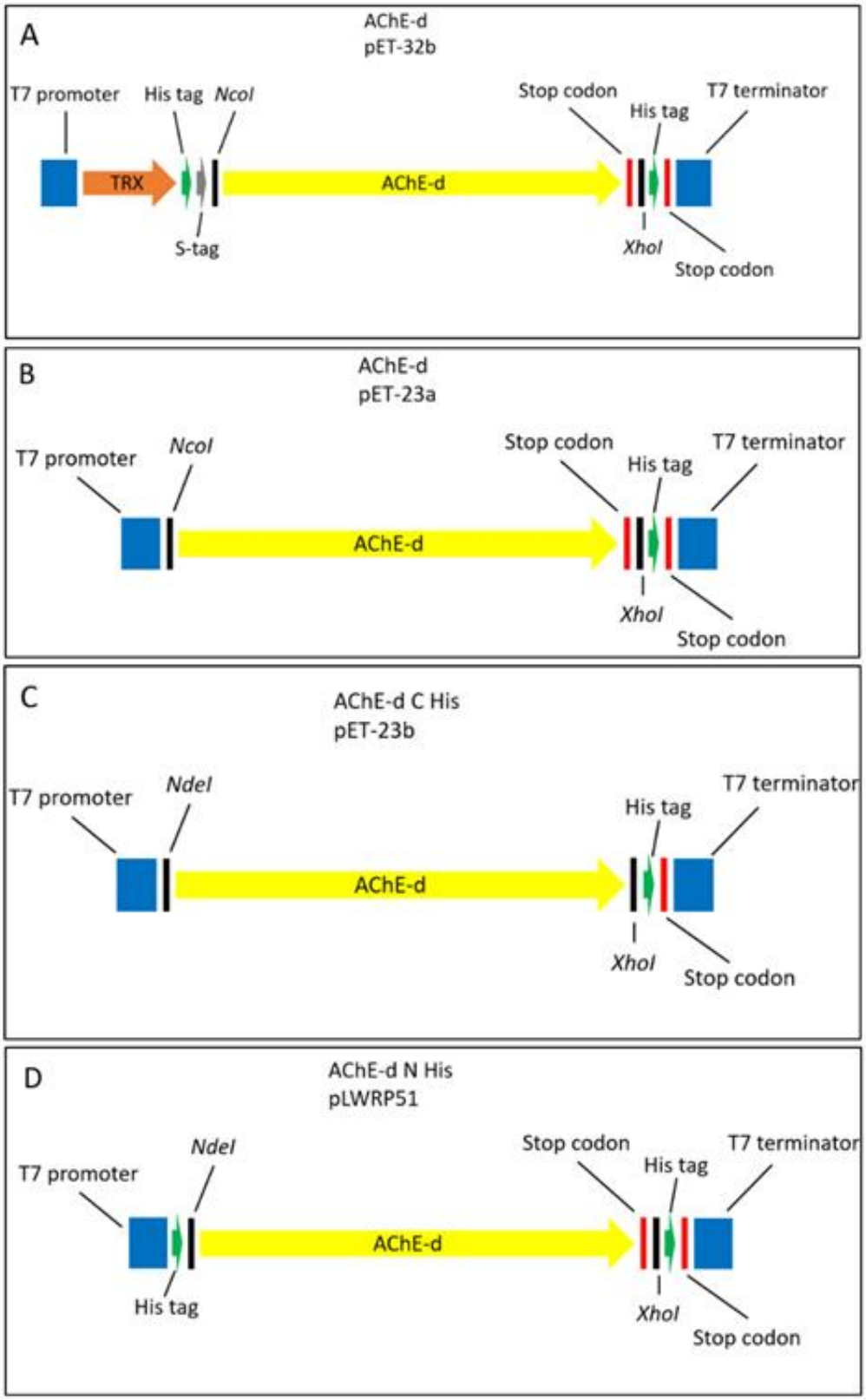

Figure 15. A cartoon representation of different AChE-d gene constructs. (A) AChE-d in pET-32b, this construct produced AChE-d TRX. (B) AChE-d in pET-23a, this construct produced AChE-d without a His tag. (C) AChE-d in pET-23b, this construct produced AChE-d with a C terminal His tag. (D) AChE-d in pLWRP51, this construct produced AChE-d with an N terminal His tag.

2.3 Results

2.3.1 Optimisation of the expression and purification of AChE-d-TRX.

Temperature and point of induction were both optimised to give the highest yield of soluble AChE-d-TRX expression by shuffle *E. coli*. Recombinant expression of the protein was induced by addition of IPTG to the liquid cultures to a final concentration of 0.45 mM. The expression yields were compared using the Ellmans assay to measure the AChE-d activity in the lysate supernatant of each culture. First the optimal temperature of induction was investigated. The results are shown in Table 6. All cultures were induced at around an OD_{600} of 0.6. Cultures induced at 18 and 25^{o}C were induced overnight, cultures at 30 and 37^{o}C were induced for 4 hours.

Table 6. Effect of induction temperature on AChE-d-TRX yield.

Temperature ^{o}C	Activity (A_{412} /min/10 µl lysate supernatant)
18	0.318
25	0.566
30	0.218
37	0.266

The optimal OD_{600} to induce expression of the protein was tested next. The cultures were induced at 25^{o}C overnight as the data in Table 6 indicated this would give maximum recombinant protein yield, the results are shown in Table 7.

Table 7. Effect of OD_{600} at induction on AChE-d-TRX yield.

OD_{600} at induction	Activity (A_{412}/min/10 µl lysate supernatant)
0.6	0.634
0.8	0.640
1.0	0.566
1.2	0.509

The data showed that the optimal OD_{600} to induce at was between 0.6 and 0.8. From this point on all cultures were induced between an OD_{600} of 0.6 and 0.8 at 25^{o}C overnight.

The protein contents of Shuffle *E. coli* expressing AChE-d-TRX can be seen in Figure 16. The mass of the AChE-d-TRX construct is 75.834 kDa. A band at the expected mass appears in the post induction lane but not the pre induction lane. The same band can be seen in the lysate pellet but not the lysate supernatant. This indicates that the vast majority of the expressed AChE-d-TRX is insoluble.

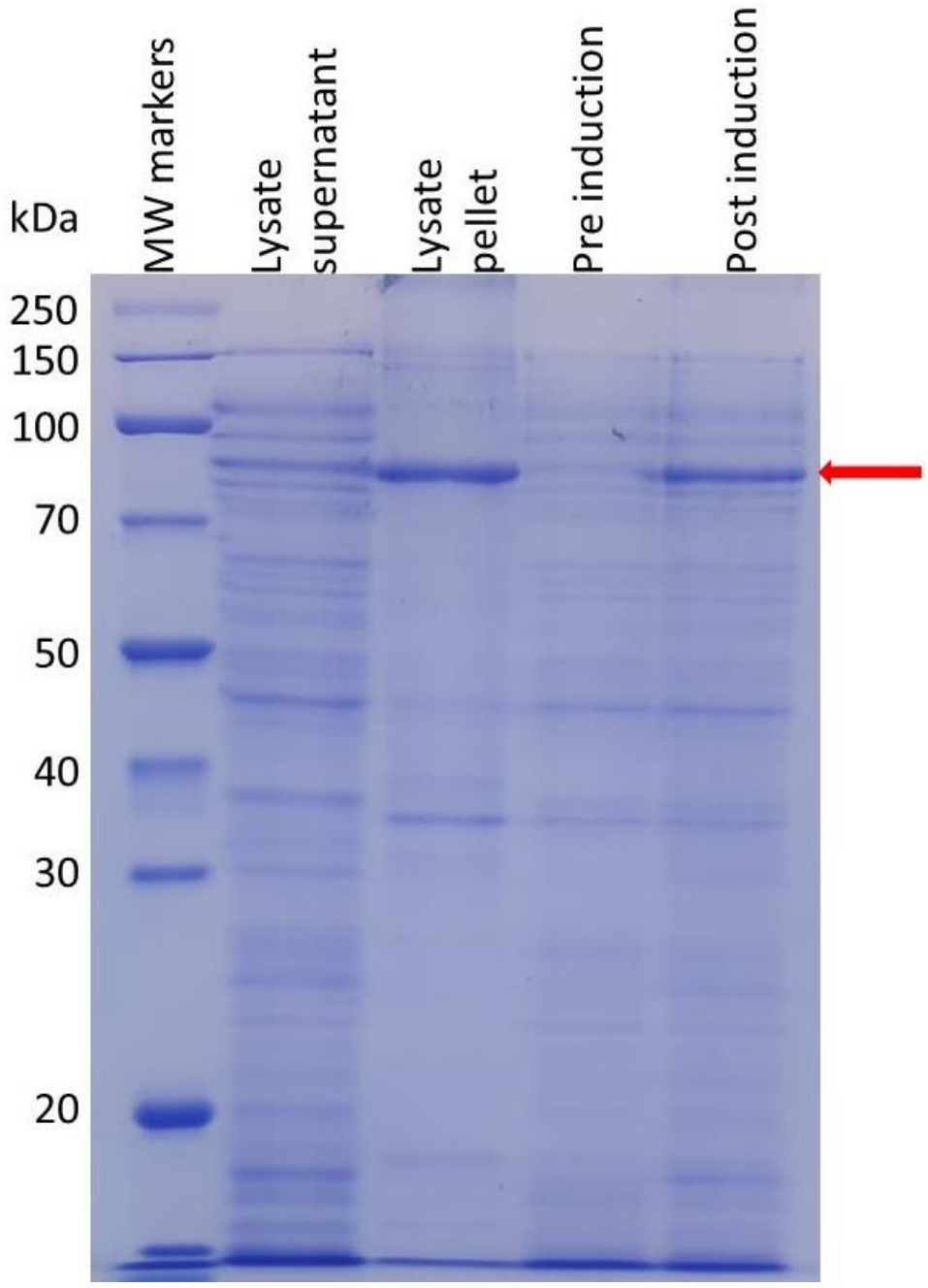

Figure 16. SDS-PAGE analysis of samples taken from a 50 ml growth of Shuffle *E. coli* expressing AChE-d-TRX. Samples prepared as described in 2.2.6. The red arrow shows the location of AChE-d-TRX.

2.3.2 AChE-d-TRXTRX refolding.

In order to investigate refolding of the lysate pellet, two refolding buffers were prepared, one with 0.05 M GdmCl and the other with 0.5 M GdmCl. The optimal concentration of GdmCl to use would be one that is high enough to keep proteins unfolded until they adopt their proper folded state, but not high enough to denature

properly folded protein. This concentration was not known, which necessitated the use of two concentrations which would allow their effectiveness to be compared.

The lysate pellet was washed and re-suspended in 2.5 ml Milli-Q water with a ground glass homogeniser. Different volumes were run on an SDS-PAGE gel with known concentrations of BSA. This was done to estimate the protein concentration in the lysate pellet suspension. This gel is shown in Figure 17.

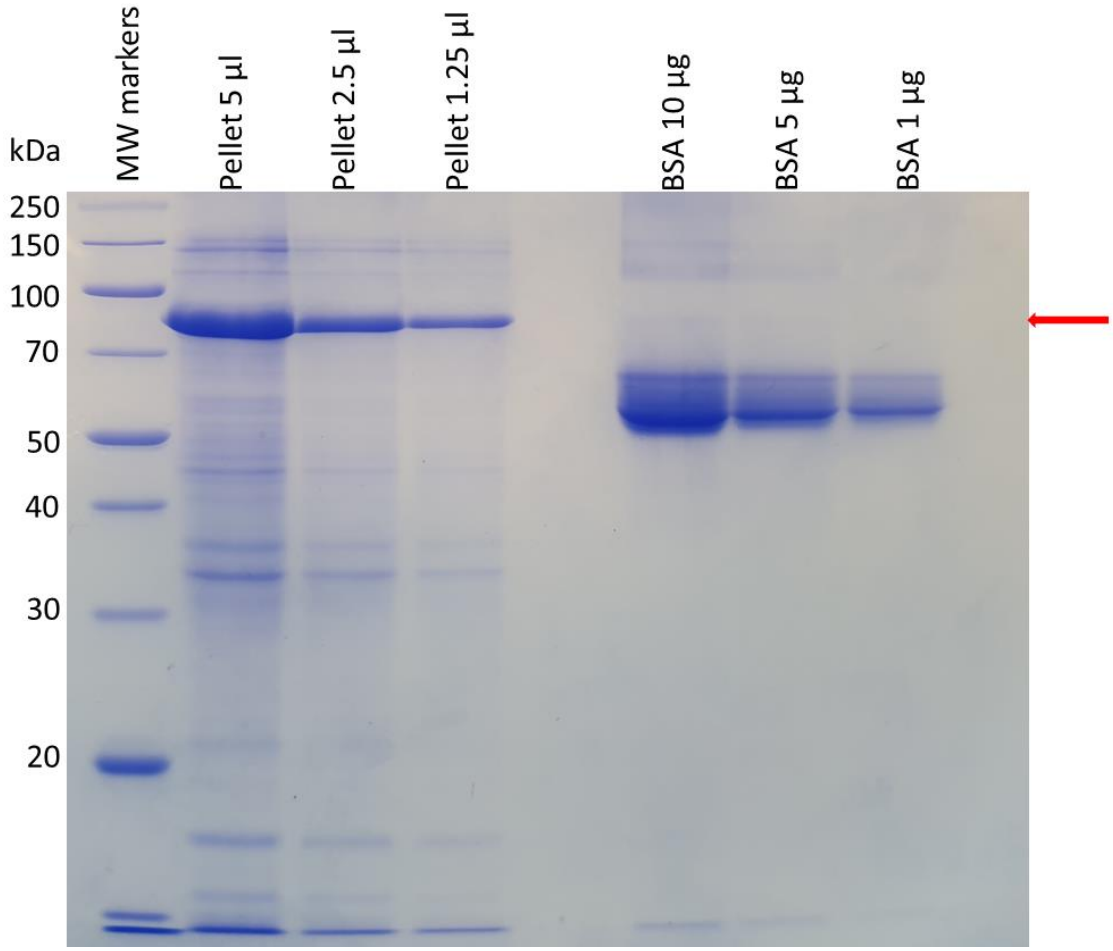

Figure 17. SDS-PAGE gel of varying volumes of AChE-d-TRX lysate pellet suspension and several known amounts of BSA. A red arrow marks the position of AChE-d-TRX.

Based on Figure 17 it was estimated that the total protein concentration in the lysate pellet suspension was around 3 mg/ml, meaning the 2.5 ml sample contained approximately 7.55 mg of protein. The protein was dissolved in 3.75 ml of solubilisation buffer which gave a protein concentration of 2 mg/ml.

As Figure 18 shows pellets formed in both refolding conditions, in both cases no AChE-d activity could be detected in the refolding supernatant but this wasn't

unexpected due to the fact that any correctly folded AChE-d-TRX would be very dilute at this point in the refolding process. The supernatants of both refolding buffers were concentrated to roughly 0.5 ml using 15 ml 50 kDa cut off centrifugal concentrators. No AChE-d-TRX could be seen in the concentration supernatant lane for either refolding condition and no activity could be detected. This showed that all of the AChE-d-TRX was in the pellet that formed in the refolding buffers.

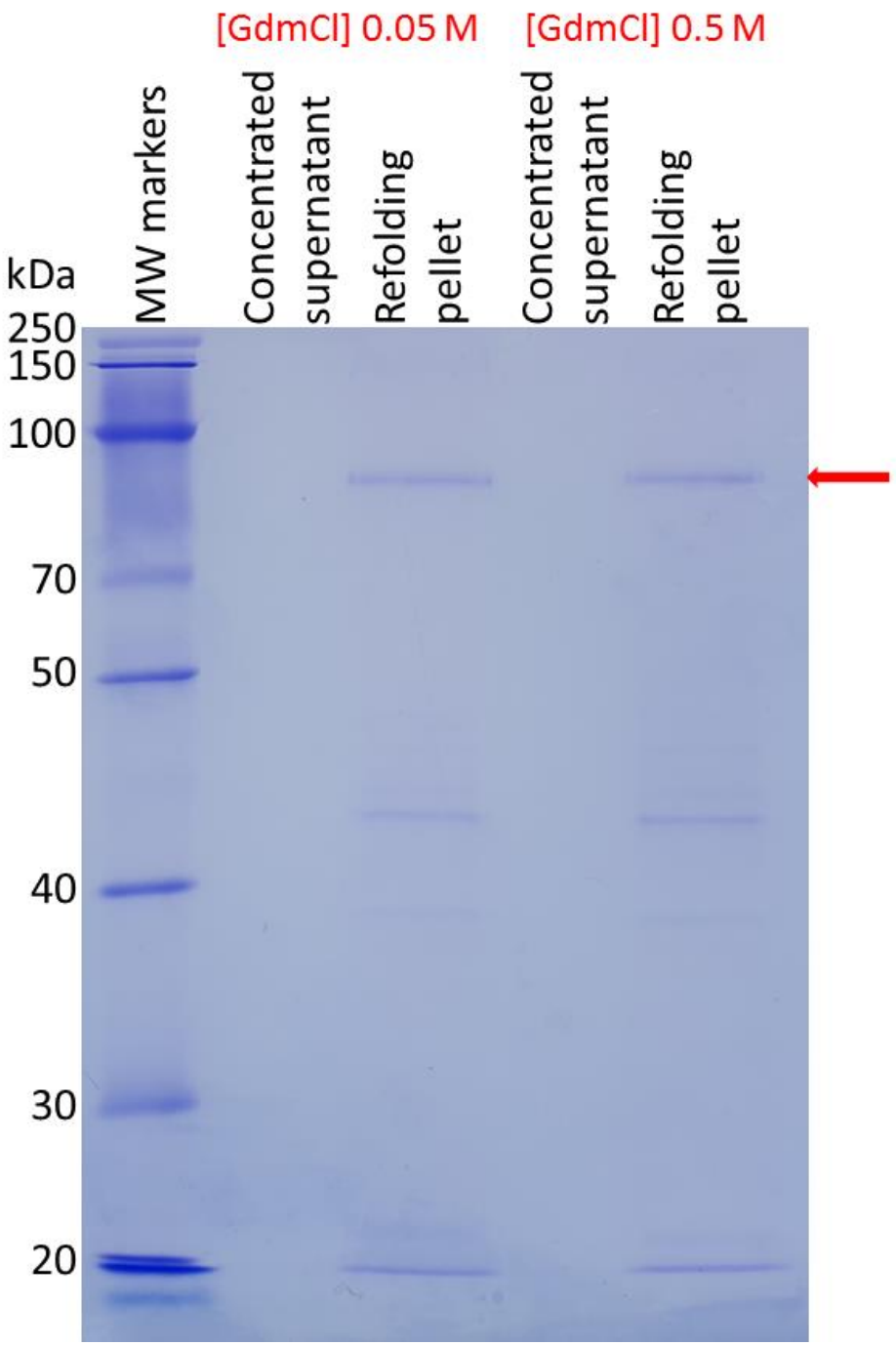

Figure 18. SDS-PAGE analysis of the products of refolding in two different buffers with different concentrations of GdmCl. Refolding pellet refers to the pellet that formed during the incubation in refolding buffer. Concentrated supernatants are samples taken from the spin concentrator. A red arrow marks the position of AChE-d-TRX.

2.3.3 Ni affinity chromatography of AChE-d-TRX.

The AChE-d-TRX construct contained a His tag located between the AChE-d and TRX subunits (Figure 1 A) so Ni affinity chromatography was attempted to purify the soluble AChE-d-TRX from the lysate supernatant.

Figure 19 A shows the elution profile of AChE-d-TRX from the Ni column, a large proportion of the total AChE-d-TRX came off the column in the wash. Figure 19 B shows that even after washing the column with lysis buffer containing 40 mM imidazole many contaminating proteins remain in the elution, and because around 33 % of the AChE-d-TRX was already washed off the column at this concentration of imidazole, increasing the concentration further would have likely resulted in the amount of AChE-d-TRX recovered being too low to provide us with an adequate supply of enzyme for kinetic and NMR experiments.

As the affinity of AChE-d-TRX for the Ni matrix was too low for this method of purification to be practical, and the majority of AChE-d-TRX produced by *E. coli* was insoluble, it was decided that refolding would be attempted again. However, the TRX tag was removed for this second attempt. It was thought that the AChE-d and TRX domains could be interacting with each other during the refolding process which could be preventing the correct folding of both domains. The structure of this new construct is shown in Figure 1 B. It was assumed that more insoluble AChE-d would be produced after the removal of the TRX tag as the purpose of this tag is to aid in the solubilisation of recombinant proteins. This presumed increase in AChE-d yield was seen as an added benefit of the TRX tag removal.

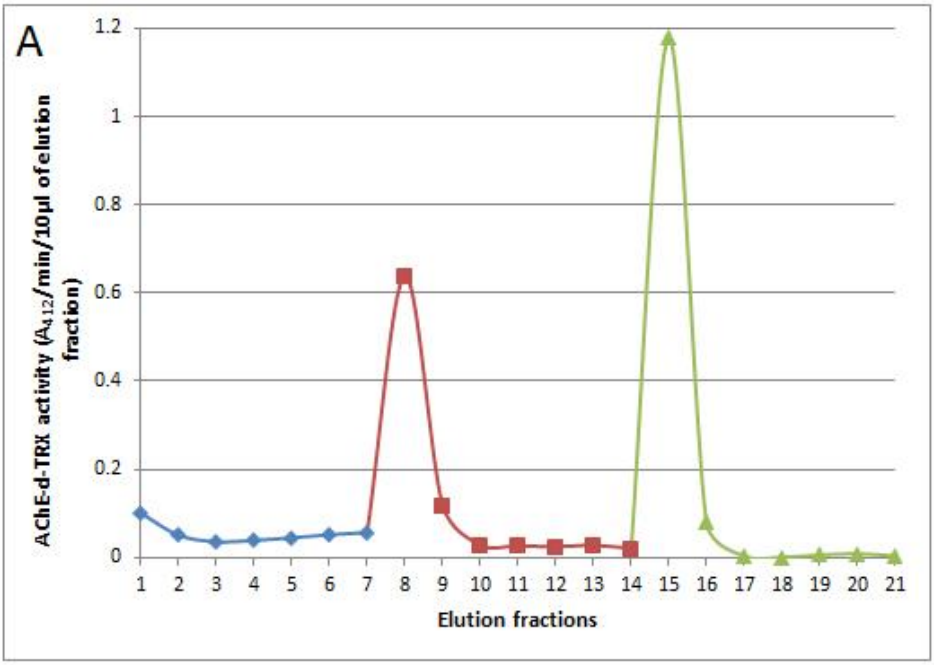

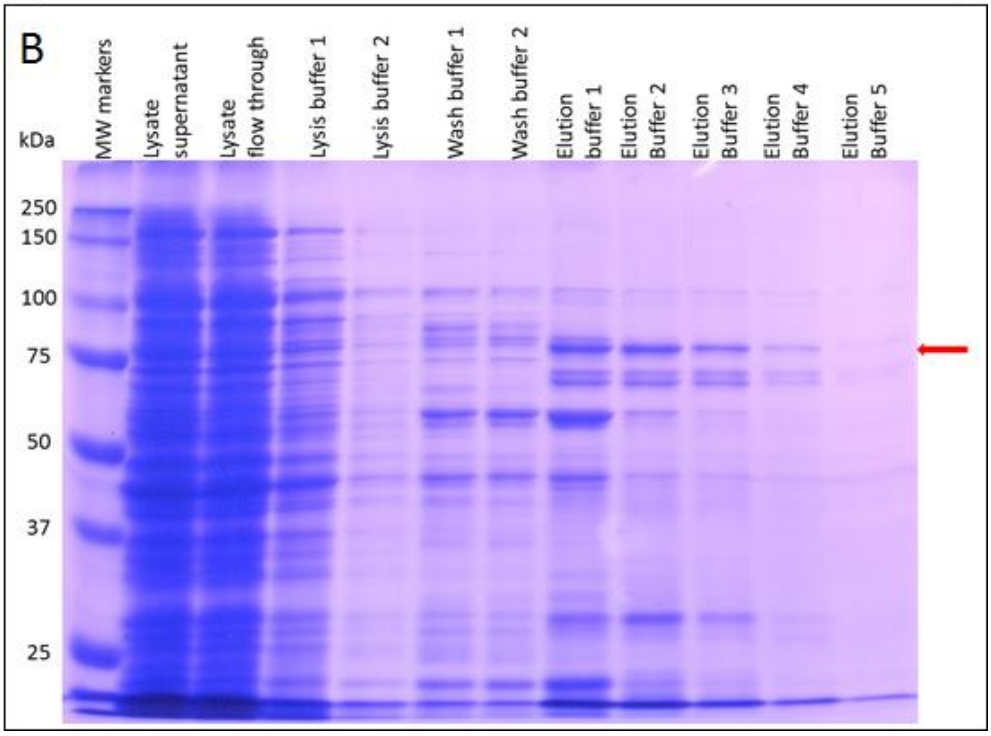

Figure 19. (A) The elution profile of AChE-d-TRX from a Ni affinity column based on AChE-d-TRX activity. Fractions 1 -7 were washed with lysis buffer (blue), 8-14 were washed with lysis buffer containing 40 mM imidazole (red) and fractions 15-20 were eluted with lysis buffer containing 20 mM EDTA (green). An SDS-PAGE of a selection of these samples is shown in Figure 19 B. (B) SDS-PAGE analysis of purification fractions from the Ni affinity chromatography of AChE-d-TRX. The AChE-d-TRX activity of these samples is shown in Figure 19 A. Lanes labelled lysis buffer 1 and 2 correspond to fractions 1 and 2 respectively in Figure 19 A, wash buffer 1 and 2 correspond to fractions 8 and 9 in Figure 19 A and Elution buffer 1 – 5 correspond to fractions 15 – 19 in Figure 19 A. A red arrow marks the position of AChE-d-TRX.

2.3.4 Optimisation of the expression and purification of AChE-d.

The mass of AChE-d without the TRX tag is 62.517 kDa, in Figure 20 no clear band can be seen in the lysate pellet lane at this mass. 10 µl of AChE-d lysate supernatant gave an activity of 3.240 A_{412}/min, whereas the same amount of lysate supernatant from an AChE-d-TRX growth of the same size gave an activity of 0.634 A_{412}/min (Table 8). This indicated that the soluble expression had increased fivefold but the overall expression had dropped significantly. This is shown by the large band of AChE-d-TRX seen in Figure 16 compared to the lack of any visible AChE-d band seen in Figure 20.

This AChE-d construct didn't have a His tag so it was decided that a cholinesterase specific affinity purification matrix called procainamide Sepharose, the chemical structure of which is shown in Figure 21, should be investigated for its ability to purify AChE-d. Procainamide Sepharose consists of the reversible AChE inhibitor procainamide bound to Sepharose through an amide linkage (96). The suggested binding and elution buffers were a 20 mM phosphate, 100 mM NaCl buffer for binding and washing, then to elute with 20 mM phosphate, 1 M NaCl buffer. It was decided that a range of NaCl concentrations should be tested to optimise the wash step.

Figure 22 shows that a large number of proteins were eluted from the procainamide Sepharose at all the NaCl concentrations tested between 0 and 1 M. Figure 23 shows the activity of each of these samples and Figure 24 shows the proteins that remained bound to procainamide Sepharose after elution with 1 M NaCl. This data showed that NaCl didn't selectively elute AChE-d from procainamide Sepharose and even after 1 M NaCl elution many proteins remained bound including over 50 % of the AChE-d. Procainamide Sepharose was deemed unsuitable for the purification of AChE-d, it was decided that a His tag should be added to AChE-d to aid purification.

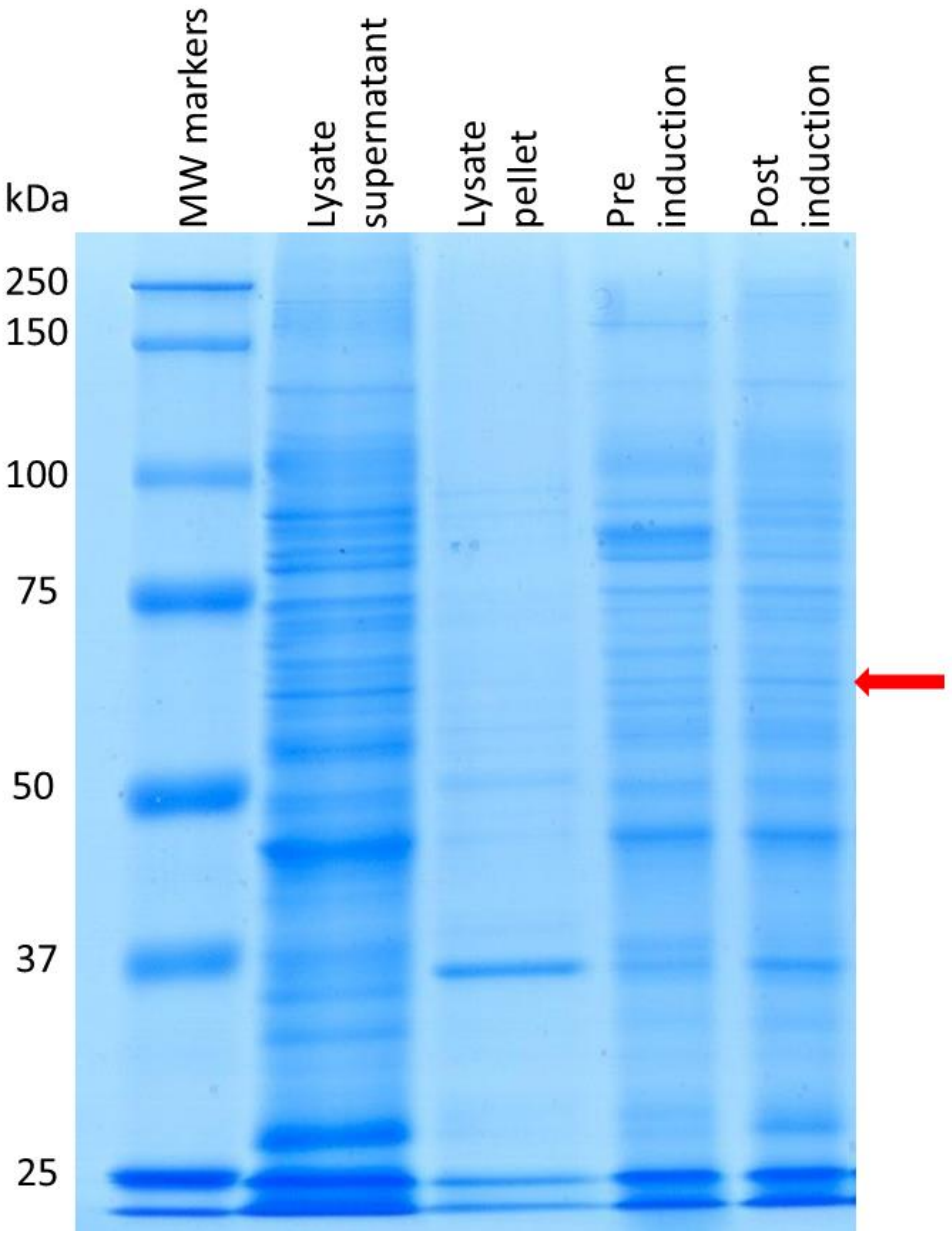

Figure 20. SDS-PAGE gel of samples of a Shuffle *E. coli* growth expressing AChE-d. The soluble and insoluble proteins from the growth are shown as well as samples from the media before and after induction with IPTG. The conditions of this gel are the same as used in Figure 2. A red arrow indicates the expected position of the AChE-d band.

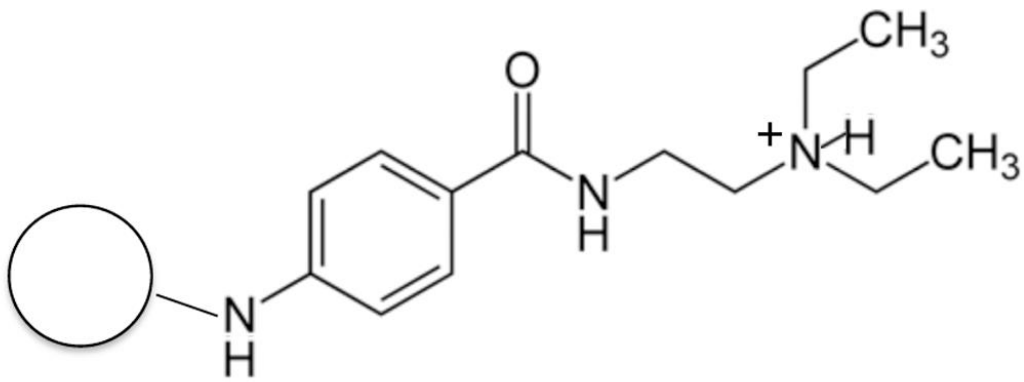

Figure 21. Chemical structure of procainamide bound to a bead of Sepharose.

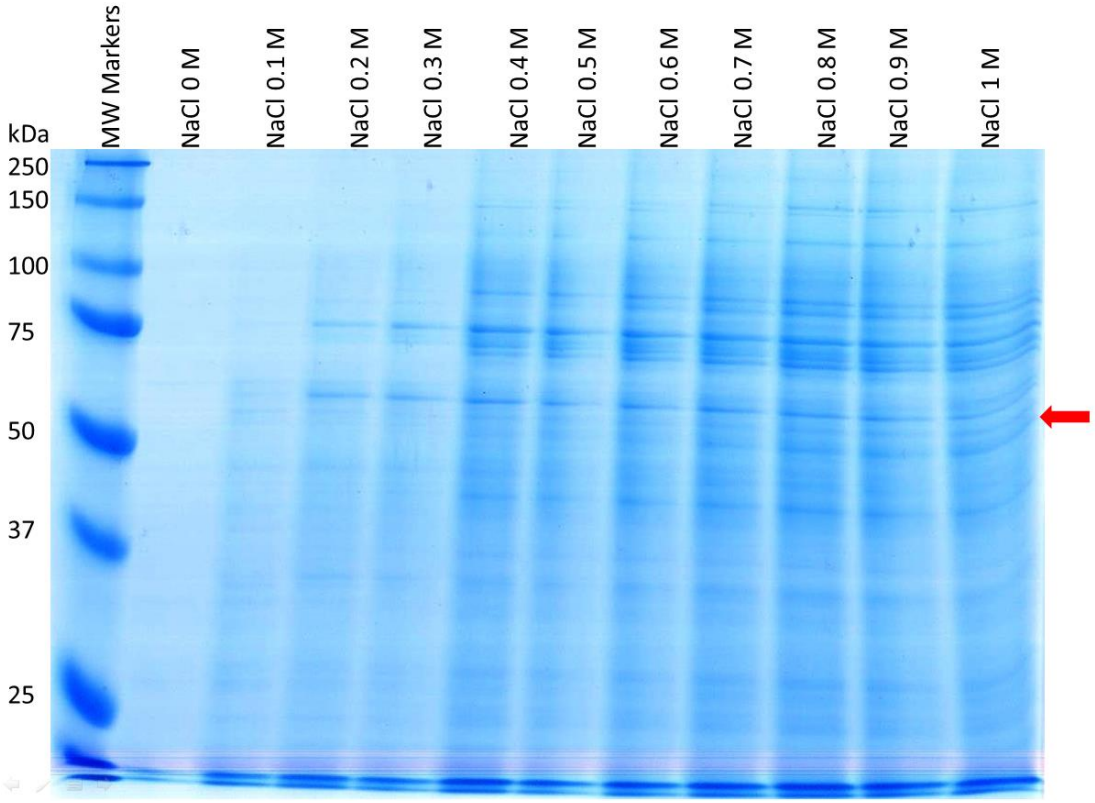

Figure 22. SDS-PAGE gel of AChE-d eluted from procainamide Sepharose in batch with varying NaCl concentrations. A red arrow marks the approximate position of AChE-d.

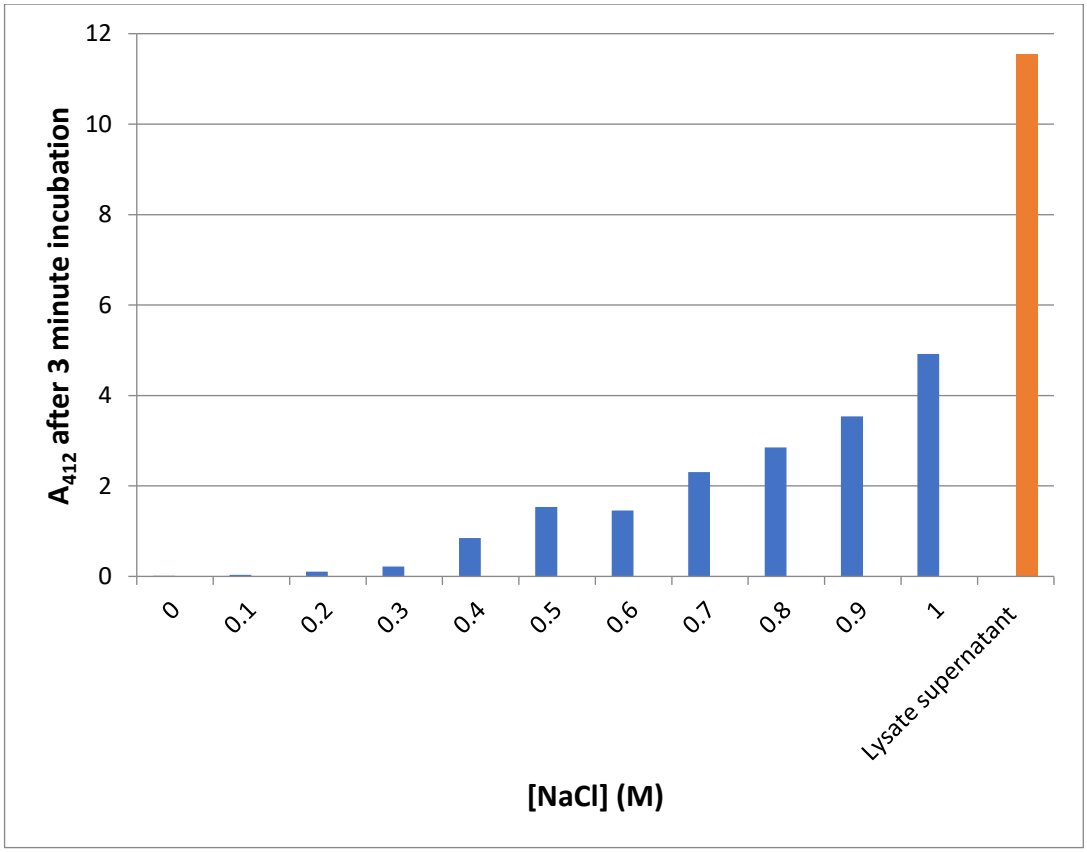

Figure 23. Bar chart showing the AChE-d activity of samples eluted from procainamide Sepharose with varying NaCl concentrations. Samples of lysate supernatant were incubated with procainamide Sepharose in batch then washed with 20 mM sodium phosphate buffer. For elution 20 mM sodium phosphate buffer containing the concentration of NaCl indicated on the x axis was added. AChE-d activity was measured with the Ellman's assay to assess the relative AChE-d concentrations. The AChE-d activity of lysate supernatant is shown in orange for comparison. n =1.

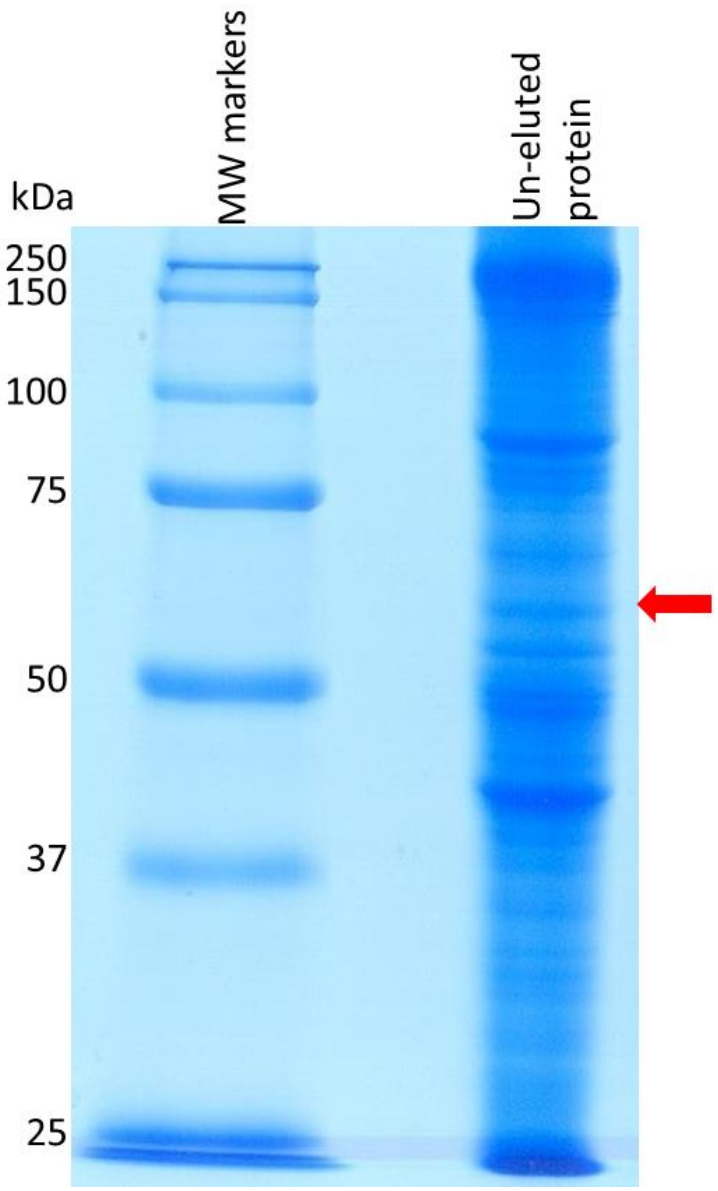

Figure 24. SDS-PAGE gel showing the proteins that remain bound to procainamide Sepharose after elution with 20 mM sodium phosphate buffer containing 1 M NaCl at pH 7.3. After the elution 40 µl of beads were mixed with 10 µl of 5 X sample buffer and boiled for 2 minutes, 10 µl of this was loaded onto the SDS-PAGE gel.

2.3.5 Purification optimisation of His tagged AChE-d.

Two different constructs of His tagged AChE-d were made; one had an N-terminal tag and the other a C-terminal tag. No active AChE-d could be produced from the construct with the N-terminal His tag but the C-terminally His tagged AChE-d showed unchanged expression when compared with the untagged AChE-d. When SDS-PAGE was used to analyse the lysate of *E. coli* expressing the C-terminally His tagged AChE-

d (Figure 25) no large band could be seen at the mass of AChE-d (62.517 kDa) in any of the lanes.

The AChE-d activity of the lysate supernatant was 3.887 A_{412}/min/10 µl, whilst without the His tag the activity was 3.240 A_{412}/min/10 µl (Table 8). This further confirmed that the addition of the tag did not greatly alter the expression yield.

The concentration of imidazole to wash the Ni affinity column with was optimised, Figure 26 A shows the elution fractions of this experiment.

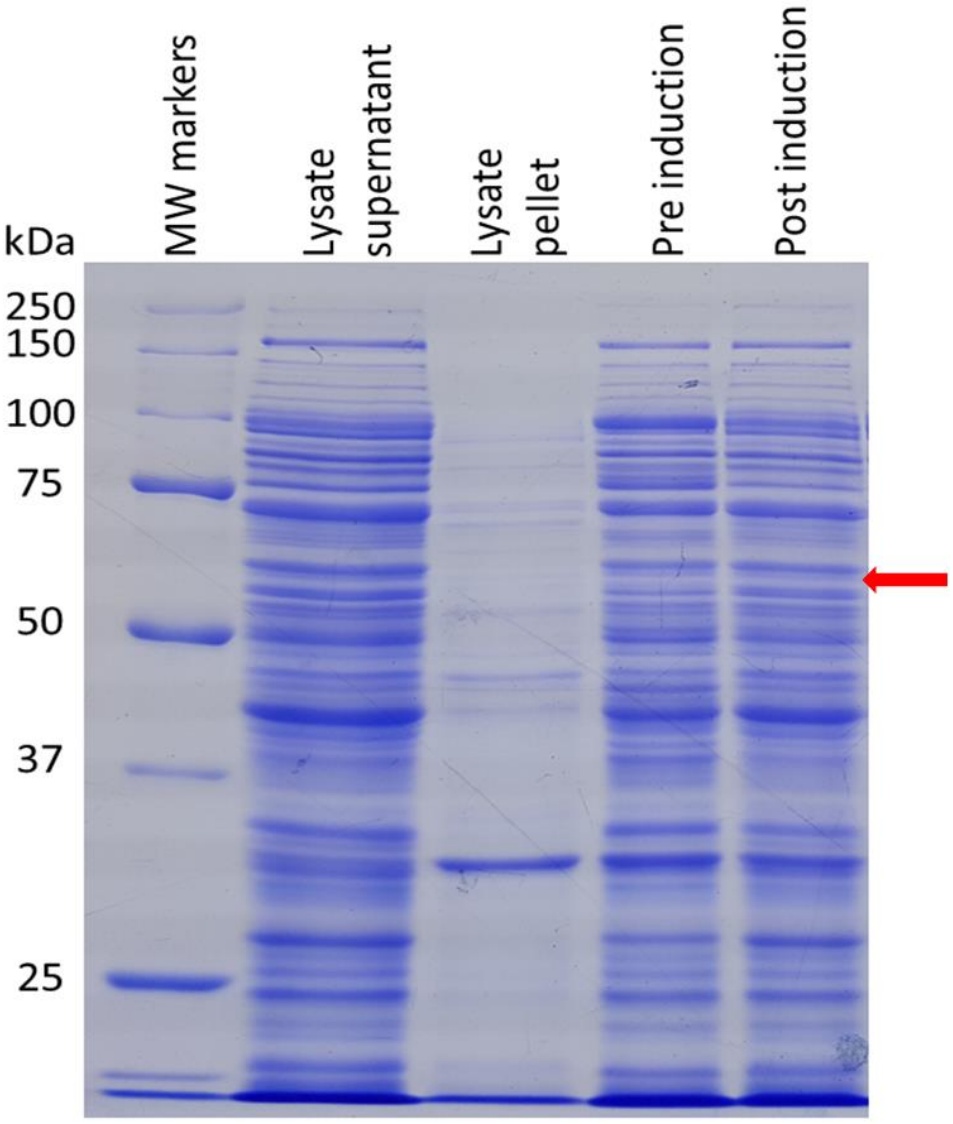

Figure 25. SDS-PAGE analysis of samples of a Shuffle *E. coli* growth expressing AChE-d C-His. The lysate supernatant and pellet from the growth are shown as well as samples from the media before and after induction with IPTG. A red arrow indicates the expected position of the AChE-d band.

The vast majority of the bound proteins were eluted at 40 mM imidazole but some contaminating proteins remained bound until EDTA was used to strip the Ni from the column. Figure 26 B shows the AChE-d activity of the samples shown in Figure 26 A. It was decided that 50 mM imidazole should be used in the wash step as the vast majority of contaminating proteins were removed at this concentration but only around 4 % of the total AChE-d activity was lost.

As Figure 26 A shows contaminating proteins were present after the wash with 50 mM imidazole so it was decided that gel filtration should be used to try and separate AChE-d from the low molecular weight contaminants that remain after Ni affinity chromatography.

Figure 27 shows the chromatogram from the size exclusion chromatography, fractions 28-35 were run on an SDS-PAGE gel shown in Figure 28 A to assess the purity of the elutions. Based on this gel, fractions 28-33 were concentrated, the purity of this sample can be seen in Figure 28 B. The A_{280} indicated that around 2 mg of AChE-d can be recovered from every litre of Shuffle *E. coli* in 2YT media. The identity of the band in figure 26 A marked by a red arrow was confirmed as AChE-d by in gel digestion and subsequent peptide mass fingerprinting.

Table 8. AChE-d activity in 10 µl of lysate supernatant of each of the AChE-d constructs.

AChE-d construct	**Activity (A_{412}/min/10 µl lysate supernatant)**
AChE-d-TRX	0.634
AChE-d	3.240
AChE-d C-His	3.887
AChE-d N-His	NA

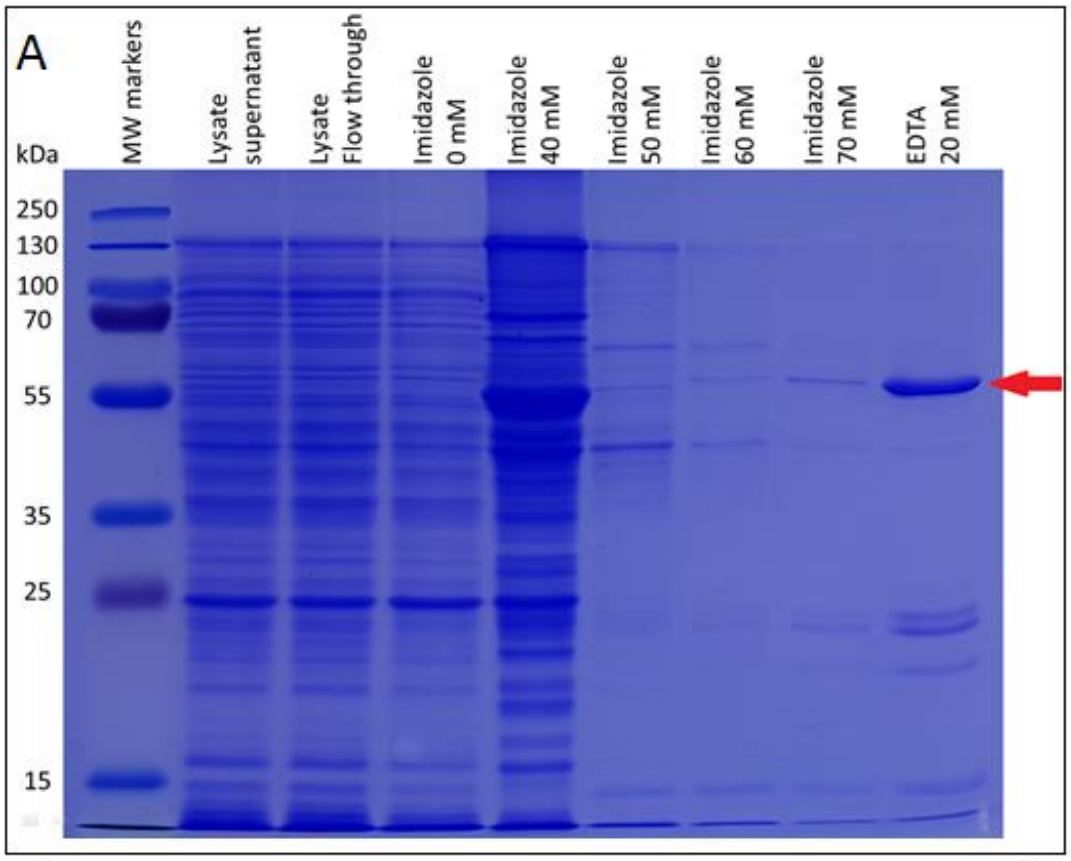

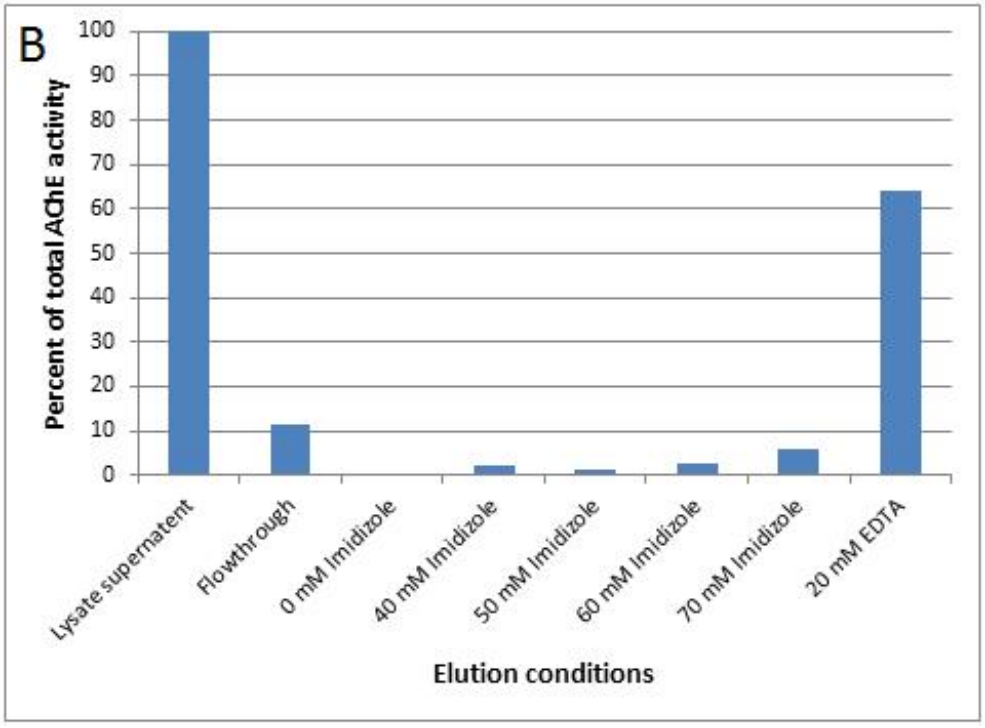

Figure 26 A. (A) SDS-PAGE analyses of the proteins in the lysate supernatant and the proteins that were eluted from the Ni column by different buffers. EDTA or imidazole was added to 20 mM sodium phosphate buffer that contained 100 mM NaCl and pH was adjusted to 7.4. (B) AChE-d activity in 10µl of the samples shown in (A). This experiment was done with successive elutions with different buffers (10 cv each) on the same 2 ml Ni column loaded with 20 ml lysate supernatant.

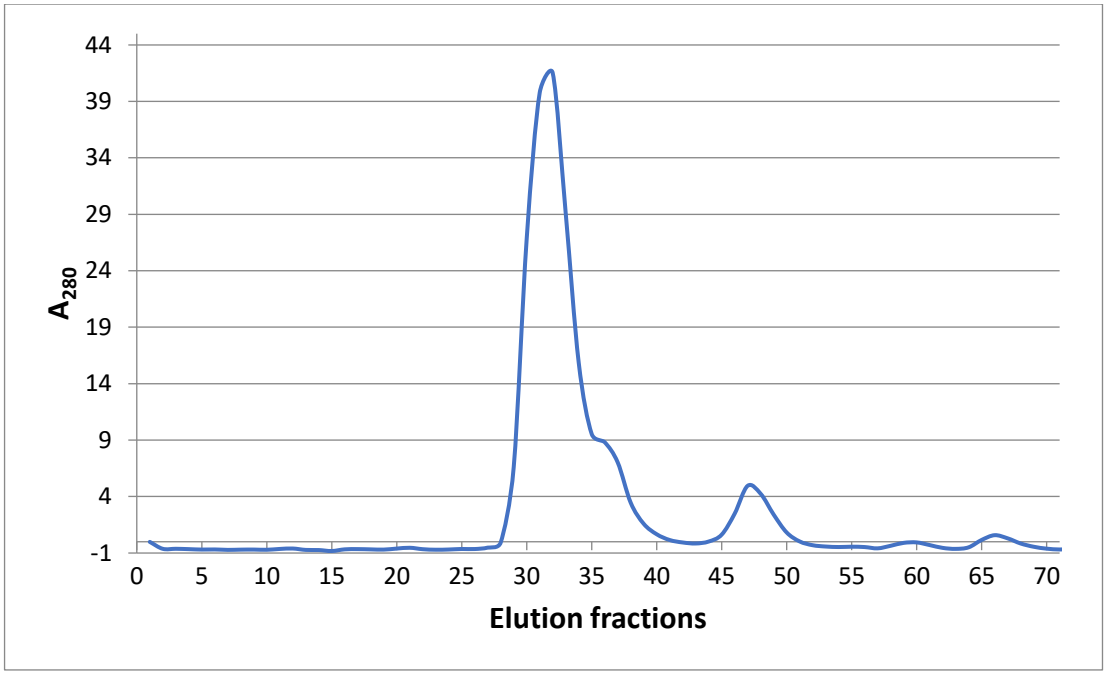

Figure 27. A_{280} of each fraction eluted from the size exclusion column.

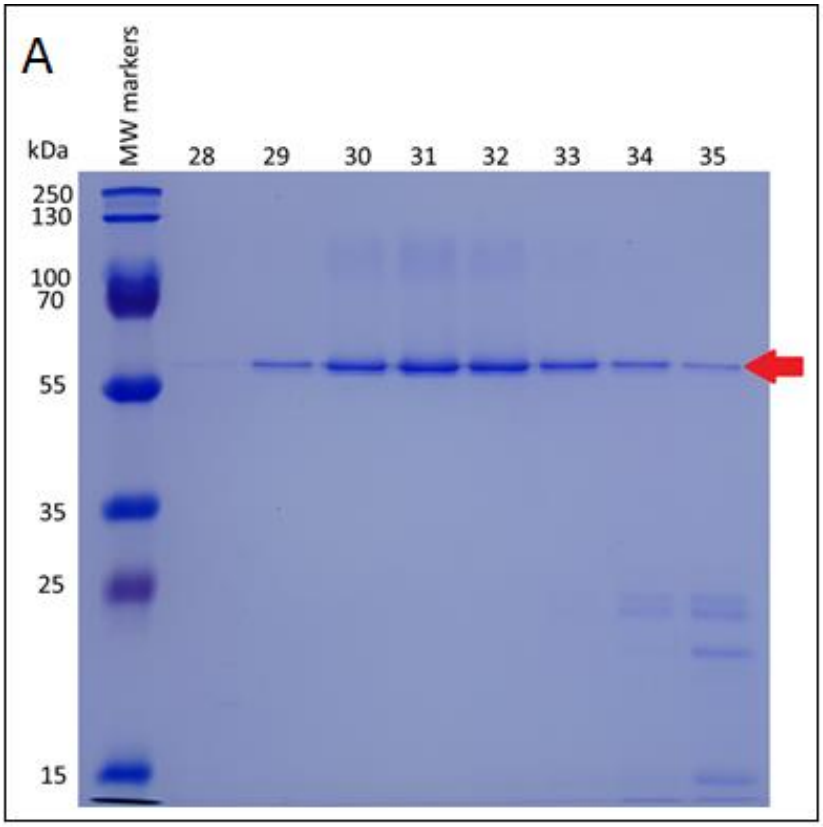

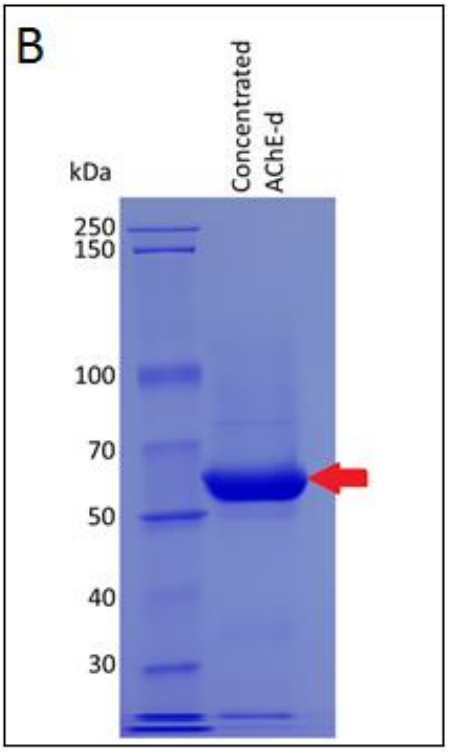

Figure 28. (A) SDS-PAGE analysis of fractions taken across the major peak seen on size exclusion chromatography of an AChE-d sample after Ni affinity chromatography. (B) SDS-PAGE analysis of fractions 28-33 from (A) after concentration. 10 µg of AChE-d loaded onto gel. Red arrows mark the position of AChE-d.

2.4 Discussion

2.4.1 Refolding.

The two refolding buffers used were exactly the same apart from the concentration of GdmCl, the two concentrations used were 0.05 M and 0.5 M. The hope was that one would produce more soluble and active AChE-d-TRX than the other, conditions could then be slightly altered, and the amount of active AChE-d-TRX measured with the Ellman's assay to assess the impact of the change in conditions on yield. This process would then be continued until no further gains in AChE-d-TRX refolding were seen. The pH, ratio of GSH to GSSH, protein concentration and GdmCl concentration can all affect the outcome of refolding. Because no activity was seen in either refolding condition, all these factors would need to be screened with no guarantee that any of them would produce soluble AChE-d-TRX. It was for this reason that Ni affinity purification of the soluble AChE-d-TRX from the lysate supernatant was attempted.

2.4.2 TRX tag removal.

In order to improve the probability of producing soluble and active AChE-d from the refolding experiment the TRX tag was removed. It was assumed that removing the TRX tag would cause *E. coli* to produce more insoluble and easier to refold AChE-d. The hypothesis was that because TRX tags have been shown to increase the yield of soluble recombinant protein (97)(98), removal of the tag would produce a higher yield of insoluble AChE-d and less soluble AChE-d. This was advantageous as only insoluble material can be used in refolding experiments. It has been shown that a fusion protein of Dihydrofolate reductase and H-Ras produced insoluble material after expression. Attempts to refold the inclusion bodies were unsuccessful. However, attempts to refold a mixture of the two un-fused proteins produced soluble H-Ras and Dihydrofolate reductase (99). It was thought that a similar result could be achieved by removing the TRX tag from AChE-d-TRX as the TRX tag could be interfering with the refolding. Interactions between the AChE-d and TRX subunits in the unfolded state of the fusion protein could prevent the correct fold of each of the

subunits from forming, so by removing the TRX tag a source of interference in the refolding proses would be removed.

As Table 8 shows the yield of active AChE-d in the lysate supernatant increased fivefold after the removal of the TRX tag but interestingly, the overall AChE-d expression dropped to a yield that couldn't be detected in the lysate supernatant, lysate pellet or post induction sample by SDS-PAGE analysis (Figure 20) whereas the AChE-d-TRX construct had produced a large band in the lysate pellet and post induction samples (Figure 16). The new AChE-d construct without the TRX tag was expressed in BL21 *E. coli*, the activity in the lysate supernatant was 0.383 A_{412}/min/10 µl of lysate supernatant. When expressed in Shuffle the activity was 3.865 A_{412}/min/10 µl of lysate supernatant. No band at the correct MW could be seen in the lysate supernatant or pellet after SDS-PAGE analysis of the BL21 expression of AChE-d (data not shown). In the paper reporting the creation of AChE-d (80), wild type AChE-TRX was expressed in Shuffle *E. coli* but no activity was recovered in the lysate supernatant. This indicated that the combination of Shuffle and the mutations present in AChE-d are required to get usable quantities (> 0.5 mg/l of *E. coli* culture) of cholinesterase.

The increase in soluble protein seen after the TRX tag removal was surprising but even more surprising was the disappearance of any insoluble AChE-d which could indicates a drop in recombinant protein production or that removal of the TRX tag allowed the Shuffle *E. coli* to produce a partially folded form of AChE-d which was soluble but more susceptible to proteolysis than the insoluble AChE-d-TRX. Because no band was seen in the lysate pellet of the BL21 expression of AChE-d the *E. coli* strain didn't noticeably affect the amount of insoluble AChE-d produced. Further experiments are needed to explain the apparent drop in recombinant protein expression after the removal of the TRX tag. Unfortunately, the effect of reducing agents on AChE-d activity could not be tested because reducing agents would interfere with the Ellmans assay by reacting with DTNB. However, it was assumed that the soluble and active AChE-d expressed by Shuffle had all of its disulphide bonds correctly oxidised as the cytoplasm of Shuffle *E. coli* was designed to be more oxidising than that of BL21.

Other cases of protein tags having a detrimental effect on soluble expression of certain proteins have been published (100)(101). There is published data that shows TRX tags can increase overall expression but reduce soluble expression for proteins over 25 kDa (102). The mechanism behind this remains unclear. The AChE-d construct with an N-terminal His tag failed to produce any soluble protein and no large band was seen in the lysate pellet. The C-terminal variant showed unchanged expression yields. The AChE-d-TRX construct had the TRX tag at the N-terminus. Considering even a comparatively small N-terminal hexa His tag prevented the expression of active AChE-d, any further addition of residues to the N-terminus of AChE-d could reduce the expression of active protein. So it's possible that a C-terminal TRX tag would have produced more soluble active protein.

2.4.3 AChE-d purification.

The removal of the TRX tag from the AChE-d gene also removed the His tag, this was not seen as a problem at the time as an affinity matrix specific for cholinesterases was commercially available and it had been used successfully to purify foetal bovine AChE from serum (103) and human BChE from serum (104). We can't know for certain whether the batch of procainamide Sepharose that was used in our experiments was defective, or if *E. coli* proteins happen to have a higher affinity for procainamide than serum proteins. However the latter seems unlikely as such a large proportion of the total *E. coli* proteins bound to the procainamide Sepharose with a similar affinity to AChE-d as illustrated in Figures 8, 9 and 10. It was decided that a second batch of procainamide would not be bought due to its high cost of around £1000/l. It was for this reason that the His tags were added to AChE-d. After optimisation of the Ni affinity and size exclusion chromatography protocols, pure and active AChE-d could be recovered at around 2 mg/l of 2YT culture which meant we could produce enough for kinetic and homonuclear NMR experiments.

This purified material was confirmed to be AChE-d as it had the correct molecular weight, catalytic activity and was enriched after Ni affinity purification. The cell lysate of Shuffle *E. coli* that had not been transformed with the AChE-d gene gave no signal in the Ellmans assay confirming that the signal seen in cell lysate of AChE-d transformed cells was due to the presence of AChE-d.

Chapter 3. Isotopic labelling of a designed isoform of acetylcholinesterase

3.1 Introduction

3.1.1 NMR background.

H, N and C are the most widely studied elements in biological NMR. This is because of their abundance in proteins, however, only certain isotopes of these elements can be used for high resolution NMR due to their spin ½ nuclei (105). When a spin½ isotope is placed in a magnetic field it will either align with the field or against it. It is more energetically favourable for the nucleus to align with the magnetic field so in a population of spin½ nuclei there will be a small excess of nuclei aligned with the magnetic field. The magnitude of this excess increases with the strength of the magnetic field. If electromagnetic radiation is applied at the correct frequency it can cause the nucleus to rotate out of line to the magnetic field. When the application of the electromagnetic radiation stops the nucleus will rotate around the magnetic field as it returns to alignment with it. This rotation can induce an alternating electric charge in a coil which is shown in NMR spectroscopy as the chemical shift.

Table 9 shows the spin and natural abundance of a selection of isotopes relevant to NMR. ^{1}H is a spin ½ nuclei and has a natural abundance of approximately 99.99% making it the most intrinsically sensitive nucleus to observe in protein NMR. However, its usefulness is limited by its abundance in proteins and its limited chemical shift range. AChE-d produces a spectrum with around 4000 ^{1}H signals. ^{1}H signals typically occur in a spectral width of around 13 ppm, because of this there will be significant peak overlap. This problem is exacerbated for large proteins which have slower tumbling rates which gives rise to broader signals (106). This causes detailed interpretation of 1D ^{1}H spectra to become very difficult. ^{15}N and ^{13}C are spin ½ nuclei, but have natural abundances of 0.36% and 1.11% respectively, and their gyromagnetic ratios of 10.14 and 6.73 10^{7} rad/T/s are smaller than that of ^{1}H (26.75

rad/T/s) (Table 9). If signals from these isotopes are to be observed in an NMR spectrum within a reasonable timescale, isotopic labelling needs to be done. This is achieved by growing *E. coli* in a minimal media with ^{13}C and or ^{15}N compounds being the sole source of these elements (107). This results in uniformly labelled protein being expressed. If two NMR sensitive nuclei are present in a protein, 2D heteronuclear spectra can be collected which greatly reduce the complexity of the spectrum. For instance, if a ^{1}H, ^{15}N Heteronuclear Single Quantum Coherence (HSQC) spectrum is collected, one peak will be observed for every ^{1}H bound to a ^{15}N (108) meaning a ^{1}H, ^{15}N HSQC spectrum of AChE-d would contain around 700 signals. The interpretation of a 2D spectrum is also helped by the reduced peak overlap caused by the peaks being separated across a plane instead of a single axis. Heteronuclear Multiple Quantum Coherence Selective Optimized Flip Angle Short Transient (HMQC-SOFAST) experiments function in a very similar way to HSQC experiments but they have improved signal to noise at the expense of resolution. Figure 29A and 28B shows the pulse sequences of the two different experiments.

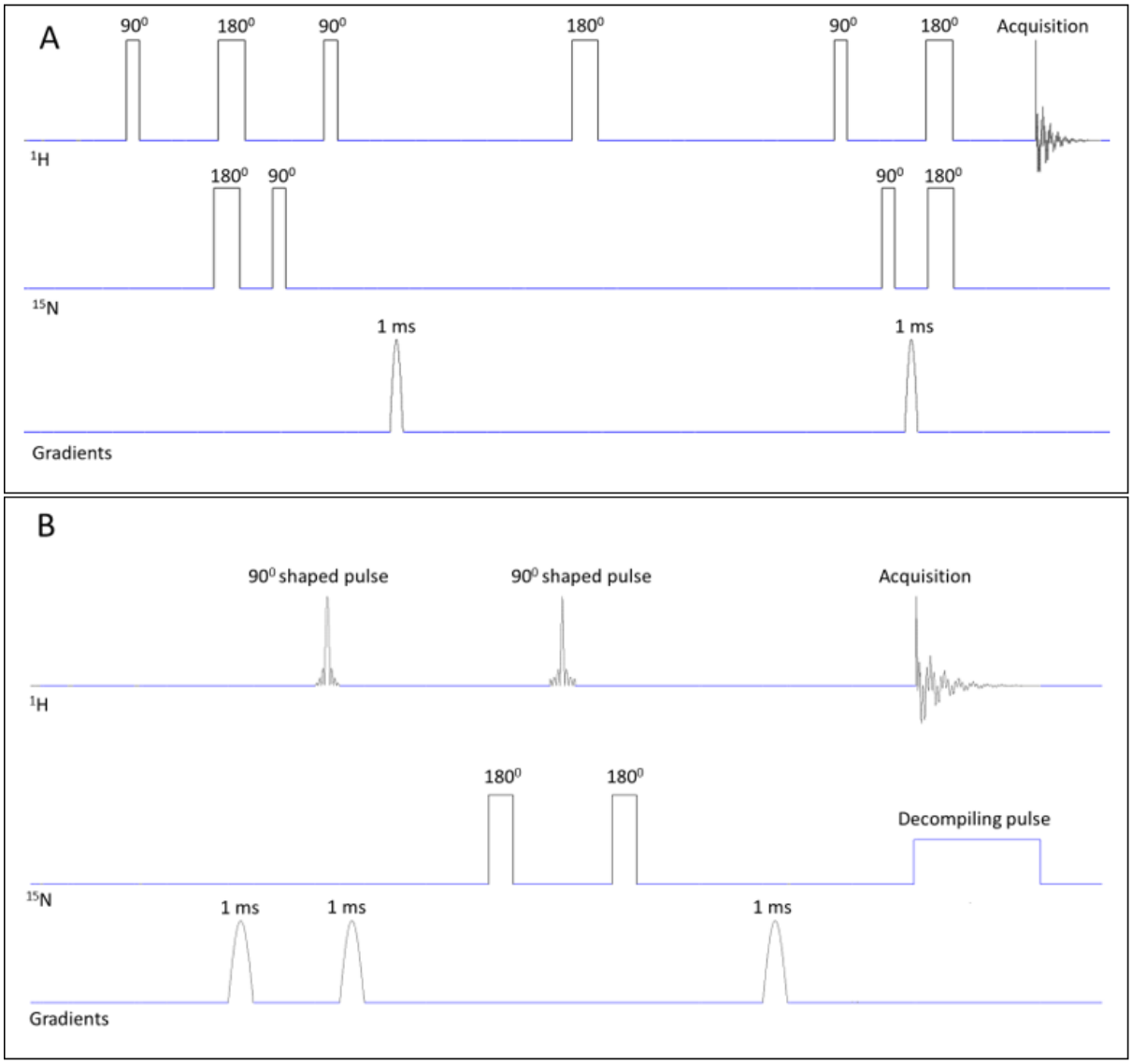

Figure 29A. Pulse sequence of a HSQC experiment (109). 28B. Pulse sequence of a HMQC-SOFAST experiment (110).

HMQC-SOFASTs Improve speed and the signal to noise ratio by using a shaped pulse to selectively excite only the amide protons in the protein, the aliphatic and aromatic protons remain unperturbed by the shaped pulse. The magnetization is efficiently transferred via dipolar coupling to the unperturbed protons, resulting in the amide protons having shorter T1 relaxation times. The reduced T1 relaxation time allows a faster repetition rate of the experiment allowing more scans to be taken in a unit time compared to a standard HSQC. The drawback of HMQC-SOFASTs is that the homonuclei (^{15}N in this case) are affected by J-coupling to the protons, this is not seen in HSQCs. The J-couplings result in the broadening of the detected peaks

resulting in reduced resolution (111). There is also no TROSY effect in HMQC-SOFAST experiment which also contributes to the broader peaks seen in these experiments (112). As the yield of protein was low (0.6 mg/l minimal media culture) HMQC-SOFAST experiments were used in this work.

Table 9. Isotope spin, natural abundance and gyromagnetic ratio of the elements that are commonly found in proteins or are used to label proteins.

Isotope	Spin	Natural abundance (%)	Gyromagnetic ratio (10^7 rad/T/s)
^{1}H	1/2	99.99	26.75
^{2}H	1	0.02	4.12
^{12}C	0	98.90	N/A
^{13}C	1/2	1.10	6.73
^{14}N	1	99.6	-7.23
^{15}N	1/2	0.365	10.14
^{19}F	1/2	100	25.18
^{31}P	1/2	100	10.84

3.1.2 Uniform ^{15}N vs ^{13}C labelling.

For this work ^{15}N labelling was chosen over ^{13}C partly due to ^{15}N minimal media costing around £13/l (compared to £170 for ^{13}C), and because ^{1}H, ^{15}N HMQC-SOFAST give one peak for every residue, excluding prolines, the n terminal residue and each of the sidechain amides adds a pair of peaks. ^{1}H, ^{13}C HMQC-SOFAST produce a larger number of peaks due to all residues containing multiple C-H bonds. As AChE-d has a mass of 62.517 kDa, reducing the complexity of its NMR spectra was a high priority.

3.1.3 ^{19}F labelling.

^{19}F labelling was also attempted, for this to work *E. coli* were grown in minimal media containing a fluorinated precursor of an amino acid. It is more energy efficient for the *E. coli* to use the ^{19}F labelled precursor to make an amino acid than to make the

amino acid from raw materials so the ^{19}F precursor gets incorporated into the expressed protein (113). For this work fluorinated precursors of tryptophan and phenylalanine were investigated. ^{19}F labelling offers the advantage of reduced spectral complexity as ^{19}F is not naturally occurring in proteins so only the residues labelled will produce signals. AChE-d contains 14 tryptophan and 28 phenylalanine residues so labelling either of these would produce a greatly simplified NMR spectrum compared to uniform ^{15}N labelling which would produce around 700 peaks. ^{19}F labelled precursors can negatively affect the expression yield of recombinant proteins, this is most likely caused by the larger electronegativity of ^{19}F atom compared to the ^{1}H it replaces in the precursor. This can interfere with the correct folding of the protein. The effect of precursors containing the ^{19}F in different positions on the tryptophan or phenylalanine aromatic ring needs to be tested to find the ones that give the highest yield of recombinant protein (114).

3.1.4 Specific ^{15}N labelling.

Specific residues can be ^{15}N labelled in a similar way to ^{19}F labelling. *E. coli* were grown in minimal media containing $^{14}NH_4Cl$ and ^{15}N labelled amino acids. The *E. coli* take up the ^{15}N labelled amino acids and use them to make the recombinantly expressed protein. All other amino acids are made using the $^{14}NH_4Cl$ so don't produce NMR signals. The opposite, known as un-labelling, can also be done where *E. coli* are grown in minimal media containing $^{15}NH_4Cl$ and specific residues are unlabelled by adding amino acids with natural abundance isotopes. This method selectively removes certain residues signals from the ^{1}H, ^{15}N HMQC-SOFAST (115). One of the downsides of all selective labelling techniques is that *E. coli* can use certain amino acids as precursors for other amino acids in a process known as scrambling. This can result in the isotopic label being transferred to amino acids that weren't intended for labelling which increases the background seen in the spectrum. Scrambling can also result in ^{14}N being incorporated in amino acids that were intended to be ^{15}N labelled which reduces the signal intensity of the peaks (115). Figure 30 gives an overview of the intensity that each amino acid will scramble to other residues, it shows that Asp, Gln and Glu can't be selectively labelled with ^{15}N because the amino groups of these amino acids are transferred to all other amino acids (115). Other residues like Met

and His are very amenable to selective ^{15}N labelling as they show no scrambling and some residues like Ile, Leu and Val can only be selectively labelled together as attempts to selectively label one will cause strong scrambling to the others.

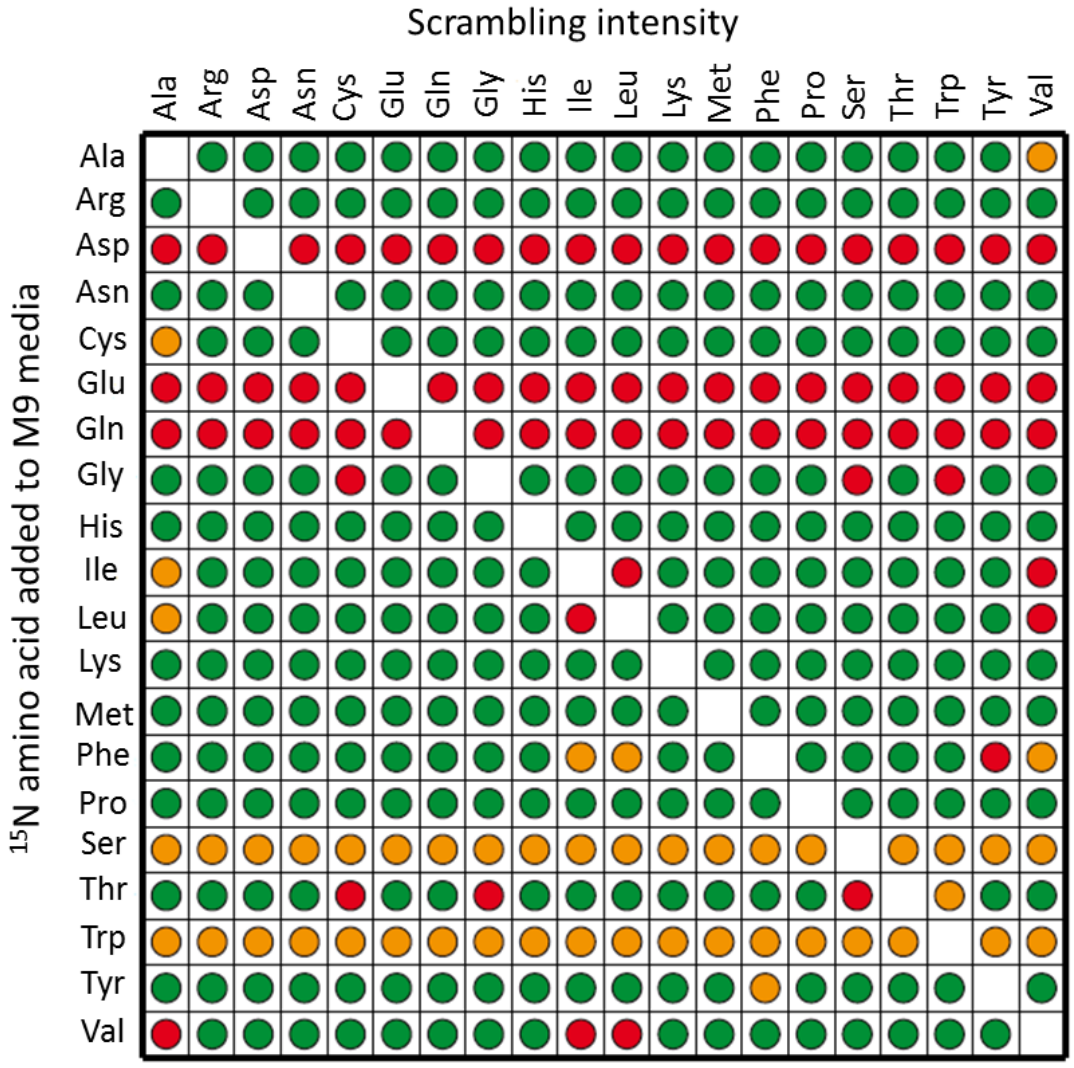

Figure 30. The degree of ^{15}N scrambling in *E. coli* for each amino acid. A green dot represents no noticeable scrambling, an orange dot represents mild but not prohibitive scrambling and a red dot indicates that selective labelling will result in the indicated residue being labelled as well as the added amino acid. This is an adapted version of Figure 32 from (115)**.**

3.1.5 Deuteration.

The HSQC and HMQC-SOFAST spectra of a protein can be improved by growing the *E. coli* and expressing the protein in D_2O instead of H_2O minimal media. This results in the expressed protein having around 70% of its protons replace with deuterons (116). The protein is purified in H_2O buffers as usual which causes the exchangeable

amide deuterons to be replaced by protons while all non-exchangeable deuterons remain bonded to the protein.

In a non-deuterated protein, the protons can transfer magnetization to each other in a process called spin diffusion (Figure 31 A), this broadens signals because each of the magnetisation transfer pathways alter the environment of the protons involved, resulting in them having a slightly different chemical shift. Normal oscillations in proteins mean that the different relaxation pathways can affect any given proton to varying degrees in different protein molecules in the sample. This causes the signal from the given proton to be spread out over a wider range of chemical shifts resulting in broader peaks. If the concentration of protons in the protein are reduced by deuteration (Figure 31 B) then there are less magnetization transfer pathways to interact with any given proton so the chemical shift range that each proton signal is spread out over is smaller, resulting in sharper peaks. This improves ^{1}H, ^{15}N HMQC-SOFAST spectra by increasing the signal to noise ratio and resolution. This technique is particularly valuable when looking at proteins over 30 kDa as the linewidths increase and the signal to noise ratio decreases with increasing protein size. In addition to this, ^{2}H has a lower gyromagnetic ration than ^{1}H (Table 9) meaning it couples more weakly to other nuclei so will have less of an effect on their chemical shifts which also aids the narrowing of linewidths (117).

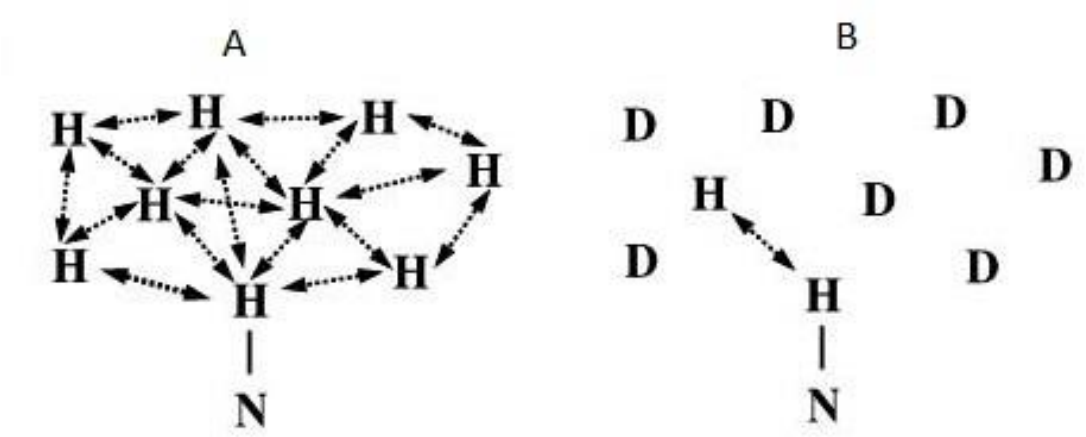

Figure 31. (A) shows a protonated protein with all of the magnetization transfer pathways between protons. (B) Shows a deuterated protein with greatly reduced pathways for magnetization transfer between protons. An altered version of Figure 2 from (118)**.**

3.1.6 Aims of the chapter.

Each of the labelling methods have different benefits and limitations. Each of them was tried and the results were compared to first of all, see if the labelling method could be used to produce NMR spectra and secondly, see which one would provide the best NMR spectra to identify peak shifts after ligand binding and to infer on structural changes in AChE-d after inhibition with an OP.

3.2 Materials and methods

3.2.1 Protein expression.

An altered M9 media was used for expressing labelled AChE-d, the components are shown in Table 10. The compounds were dissolved in Milli-Q water.

Table 10. Composition of altered M9 minimal media used to express isotopically labelled proteins. If the expressed protein was intended to be ^{15}N labelled $^{14}NH_4Cl$ was substituted for $^{15}NH_4Cl$.

Compound	Final concentration (g/l)
NH_4Cl	1
Na_2HPO_4	6.8
KH_2PO_4	3
NaCl	0.5
Na_2SO_4	0.05
EDTA	0.1
$CuCl_2 \bullet 2\ H_2O$	$2x10^{-5}$
$ZnCl_2$	$1x10^{-4}$
$MnCl_2 \bullet 4\ H_2O$	$3.2x10^{-3}$
$CoCl_2 \bullet 6\ H_2O$	$2x10^{-5}$
$FeCl_3$	$1x10^{-3}$
H_3BO_3	$2x10^{-5}$
$MgSO_4 \bullet 7\ H_2O$	0.25
$CaCl_2 \bullet 2\ H_2O$	0.04
d-Biotin	$1x10^{-6}$
Thiamine	$1x10^{-6}$
d-Glucose	4
Ampicillin	0.1

Test growths were carried out in 250 ml conical flasks containing 50 ml of cell culture. Large growths that were intended to produce protein for NMR experiments were carried out in 2.5 L baffled conical flasks containing 1 L of culture.

For specific labelling with either ^{15}N amino acids, or ^{19}F amino acid precursors, main cultures containing $^{14}NH_4Cl$ were inoculated at an OD_{600} of 0.2 from minimal media starter cultures and incubated at 37°C with shaking at 180 rpm until OD_{600} 0.4 was reached. The temperature was then lowered to 25°C until an OD_{600} of 0.6 was reached. For selective ^{15}N labelling, 100 mg of ^{15}N labelled leucine and isoleucine was dissolved in 10 ml of Milli-Q water and filter sterilised then added to the cultures at a concentration of 100 mg/l. The culture was left for 15 minutes at 25°C and then induced by the addition of IPTG to a final concentration of 0.45 mM. For ^{19}F labelling, the ^{19}F precursors were added when the culture reached an OD_{600} of 0.6. The precursors used were 4-fluoroindole, 5-fluoroindole, 6-fluoroindole, 7-fluoroindole and 4-fluorophenylacetic acid, all of which were purchased from Sigma-Aldrich. These resulted in 4-fluorotryptophan, 5-fluorotryptophan, 6-fluorotryptophan, 7-fluorotryptophan and 4-fluorophenyalanine being incorporated into the protein respectively. Each of the precursors were dissolved in DMSO to a concentration of 12 mg/ml and kept at 4°C. The chosen precursor was added from the DMSO stock to a final concentration of 60 µg/ml in the *E. coli* culture and left for 15 minutes at 25°C before being induced. Cultures were incubated overnight at 25°C with shaking at 180 rpm.

For un-labelling, minimal media was made with all the ingredients in Table 10 using $^{15}NH_4Cl$ and 0.5 g/l of all amino acids apart from leucine, isoleucine, valine, tryptophan and cysteine. The media was then filter sterilised by passing it through at 0.2 µm filter. The media was pre incubated at 25°C and inoculated to an OD_{600} of 0.5 from minimal media starter cultures. The inoculated cultures were then incubated at 25°C, with shaking at 180 rpm for 30 minutes until the OD_{600} reached 0.6. Expression was then induced by the addition of IPTG to 0.45 mM. The cultures were then returned to the incubator and left to express the recombinant protein overnight.

For the deuterated sample, all of the compounds in Table 10 were dissolved in 1 L of D_2O and filter sterilised. Shuffle *E. coli* was grown in 3 L of 2YT media at 37 °C to an OD_{600} of 0.5 and the cultures centrifuged at 4000 g for 20 minutes at 4°C. The supernatant was discarded and the cell pellet was re-suspended in 3 L minimal media

to get them back to their original volume, these cultures were then centrifuged at 4000 g for 20 minutes at 4°C. The supernatant was discarded, and the pellets were washed one more time in the same volume of sterile minimal media. The pellets were then re-suspended in 1 L D_2O minimal media in a 2.5 L baffled conical flask. The flask was placed in a shaking incubator at 25°C with shaking at 180 rpm for 45 minutes. Protein production was then induced by the addition of IPTG to a concentration of 0.45 mM. The flask was then returned to the incubator at 25°C with shaking at 180 rpm and left overnight. This method is an altered version of the protocol described in (119).

For all labelling methods, the cell lysis and protein purification procedures were the same as previously described in 2.2.3 and 2.2.4.

3.2.2 NMR experiments.

All samples were run at 35 °C on a Bruker Avance III 600 MHz (14.1 Tesla) 4-channel 5-amplifier NMR spectrometer with a QCI-F cryoprobe. All samples were in 20 mM phosphate buffer (pH 7.3) containing 100 mM NaCl. 5 % (v/v) D_2O was also added to all samples. Samples were collected in a 5 mm Shigemi tube with a volume of 320 µl. The noise base level used for all HMQC-SOFAST spectra was 28957.7 unless otherwise stated. All spectra were referenced on the water peak as tetramethylsilane bound not be added to the sample as it bound to AChE-d.

The ^{1}H 1D experiments used excitation sculpting for water suppression, 32768 points, 4 dummy and 16 real scans were collected. The spectral width was 16.0242 ppm.

^{1}H, ^{15}N HMQC-SOFAST experiments had 1024 points in the F2 (^{1}H) dimension and 100 points in the F1 (^{15}N) dimension. 4 dummy and 1888 real scans were collected. The spectral width was 14.0279 and 36 ppm for F2 and F1 respectively. A gaussian window function with a position of 0.2 was applied to all spectra and -25 line broadening was used.

The frequency range that a ^{19}F signal can occur at is larger than the bandwidth than can be collected in a single ^{19}F 1D experiment, so 4 different ^{19}F 1D spectra were

collected on the same sample, each of which looked at a different frequency range. The 4 spectra were displayed together using Topspins spectra overlay feature. Each of the 4 spectra had a spectral width of 40.2570 ppm and were collected for 4 dummy scans and 2560 real scans, 8192 points were collected. The O1P was altered in each experiment so that spectra 1-4 detected a ppm range of -40 - -80, -80 - -120, -120 - -160 and -160 - -200 ppm respectively.

All NMR data was viewed and processed using Brukers Topspin software package.

3.3 Results

3.3.1 ^{1}H NMR.

Figure 32 shows a ^{1}H 1D spectrum of AChE-d. There is significant peak overlap caused by a combination of the large number and broad linewidths of the peaks. This makes ^{1}H 1D spectra of large proteins like AChE-d of little use in analysing structural changes or dynamics in the protein as changes in individual peaks can't be observed.

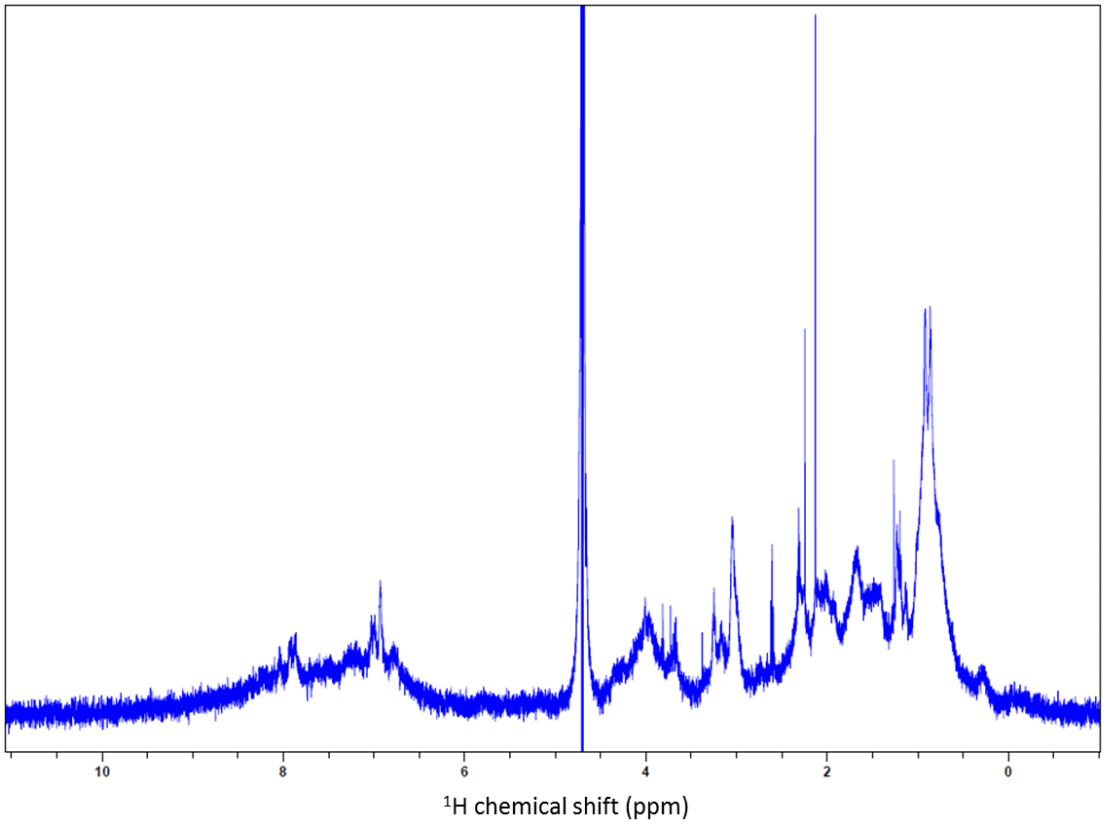

Figure 32. ^{1}H 1D of AChE-d collected for 16 scans and 32K points in the free induction decay (FID) at 35 ^{o}C. The sample was 28 µM in a 5 mm Shigemi tube.

3.3.2 ^{19}F labelling of AChE-d.

The reduction in expression of active AChE-d caused by recombinant labelling with various fluorinated amino acids ranged from 39% caused by 4-fluorophenylalanine to 98% caused by 4-fluorotryptophan (Table 11). A drop in the AChE-d activity in the lysate supernatant could have indicated either, less AChE-d had been produced or, labelled AChE-d had been produced but the resulting protein had a changed specific activity or a mixture of the two. None of these scenarios were desirable so 4-

fluorophenylalanine was chosen for further study as it caused the smallest reduction in AChE-d activity in the lysate supernatant. AChE-d was expressed in 2 L minimal media containing 4-fluorophenyalanine (60 μg/ml). The concentration of the resulting ^{19}F-Phe-AChE-d sample was 21.8 μM. The ^{19}F NMR spectrum of this sample can be seen in Figure 33, no peaks can be seen in the spectrum even though it was acquired overnight.

5-fluorotryptophan labelling caused the second lowest drop in AChE-d activity (91%). Assuming the AChE-d labelled with this precursor had the same specific activity as the 4-fluorophenylalanine, a 2 L growth would produce a 3 μM sample which would not be usable for NMR experiments. Alternatively, if the yield of AChE-d was higher it would have had a greatly reduced specific activity indicating that it wasn't comparable to AChE-d without ^{19}F labelling, therefore any data gained using 4-fluorotryptophan would not be relevant to wild type enzyme. For this reason, it was decided that ^{19}F labelling wouldn't be suitable for analysing OP inhibition of AChE-d.

Table 11. AChE-d activities in the lysate supernatant of Shuffle *E. coli* culture grown with different fluorinated amino acid residue precursors. A growth with no fluorinated precursor is included for comparison. Protein expression was induced at an OD_{600} of 0.6 in all cultures. All cultures contained 0.5 % DMSO as it was required to ensure the solubilisation of the ^{19}F labelled precursors.

Fluorinated amino acid residue	% of AChE-d activity compared to unlabelled growth	OD_{600} at harvest
unlabelled	100	1.89
4-Fluorotryptophan	2.2	1.62
5-Fluorotryptophan	8.6	1.66
6-Fluorotryptophan	5.9	1.82
7-Fluorotryptophan	2.1	1.61
4-Fluorophenylalanine	60.9	1.81

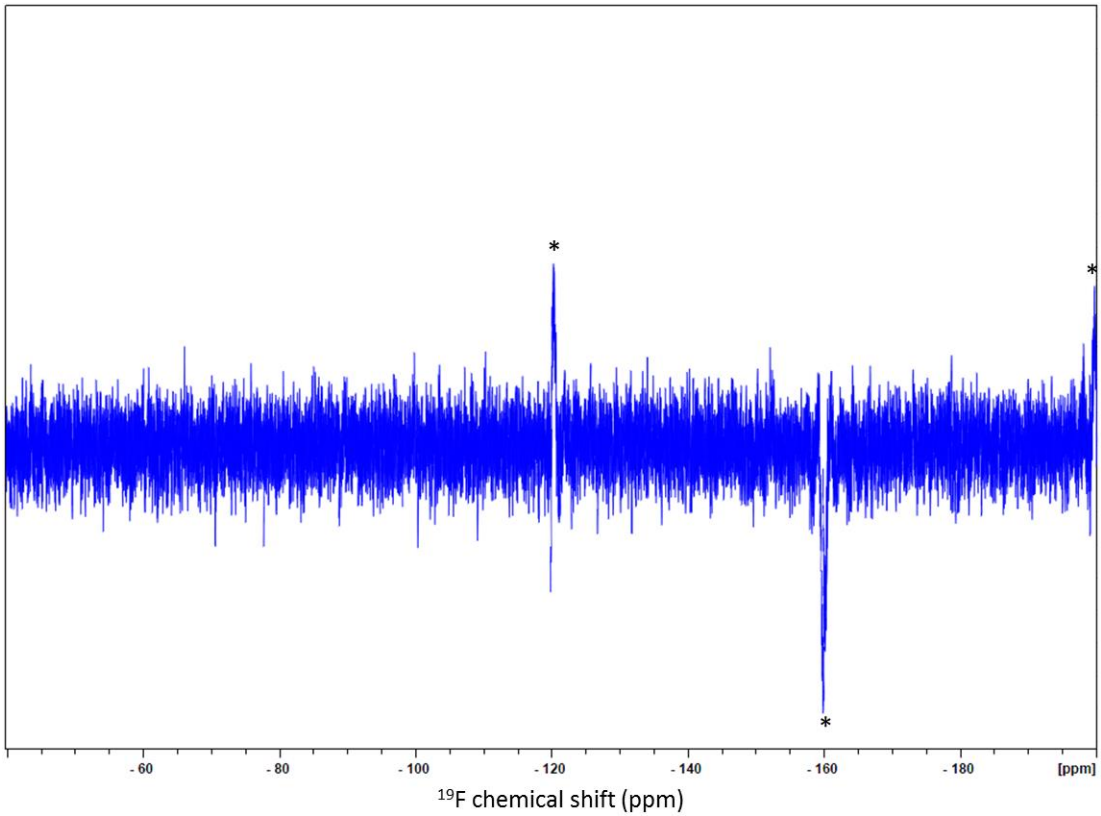

Figure 33. ^{19}F 1D of 4-fluorophenylalanine labelled AChE-d. Four separate spectra were collected on the same 21.8 µM sample. Each spectrum was collected for 2560 scans with 8 K points in the FID at 35 ^{o}C, each of the four spectra covered a different 40 ppm region these were combined to create this figure. The peaks seen at -120, -160 and -200 ppm (marked with *) are artefacts of the signal filtering and don't represent real NMR signals.

3.3.3 Uniform ^{15}N labelling and deuteration.

Figures 32 A and B show the same ^{1}H, ^{15}N HMQC-SOFAST spectrum of uniformly ^{15}N labelled AChE-d with the noise base level set to two different values. As expected the spectrum had very poor resolution due to the large number of peaks and, the broad nature of those peaks caused by the large size (62.517 kDa) of AChE-d. The vast majority of peaks are so overlapped that attempts to track their movement after inhibition with an OP would be impossible. However Figure 34 A shows that the spectrum contained a number of peaks around the edge which could be used to track ligand binding. Figure 34 B shows several high intensity peaks in the more crowded central region. The high intensity of these peaks compared to the others in the spectrum indicates they are the peaks of residues in a particularly mobile region of AChE-d, for instance un-structured loops or the C-terminus of the protein. If they

were caused by residues on the C-terminal tail they would not likely be affected by ligand binding so changes in their chemical shift after inhibition with an OP would not be expected.

Uniform ^{15}N labelling was also attempted in conjunction with ^{2}H labelling, the *E. coli* failed to express suitable amounts of active AChE-d when grown in D_2O. Table 12 shows a comparison of the AChE-d activity in the lysate supernatant of *E. coli* grown in D_2O minimal media and the standard H_2O minimal media. Even though the *E. coli* grew to a similar OD_{600} in D_2O and H_2O minimal media, protein expression in D_2O resulted in approximately 10 times less active AChE-d being produced. 1 L of minimal media produced around 0.6 mg of AChE-d which was enough for roughly 1 NMR samples. This meant that to make 1 sample of deuterated AChE-d 10 L of D_2O minimal media would be needed. The cost of D_2O was around £350/l from Cambridge Isotope Laboratories meaning £3500 would need to be spent. The D_2O could be used for 3-4 growths by distilling it after each growth to remove small molecule impurities, but the H_2O content rises after each distillation meaning the deuterium content of the recombinant protein is reduced for every successive expression. For these reasons it was decided that producing enough deuterated AChE-d to be used in the project would be too expensive to be practical.

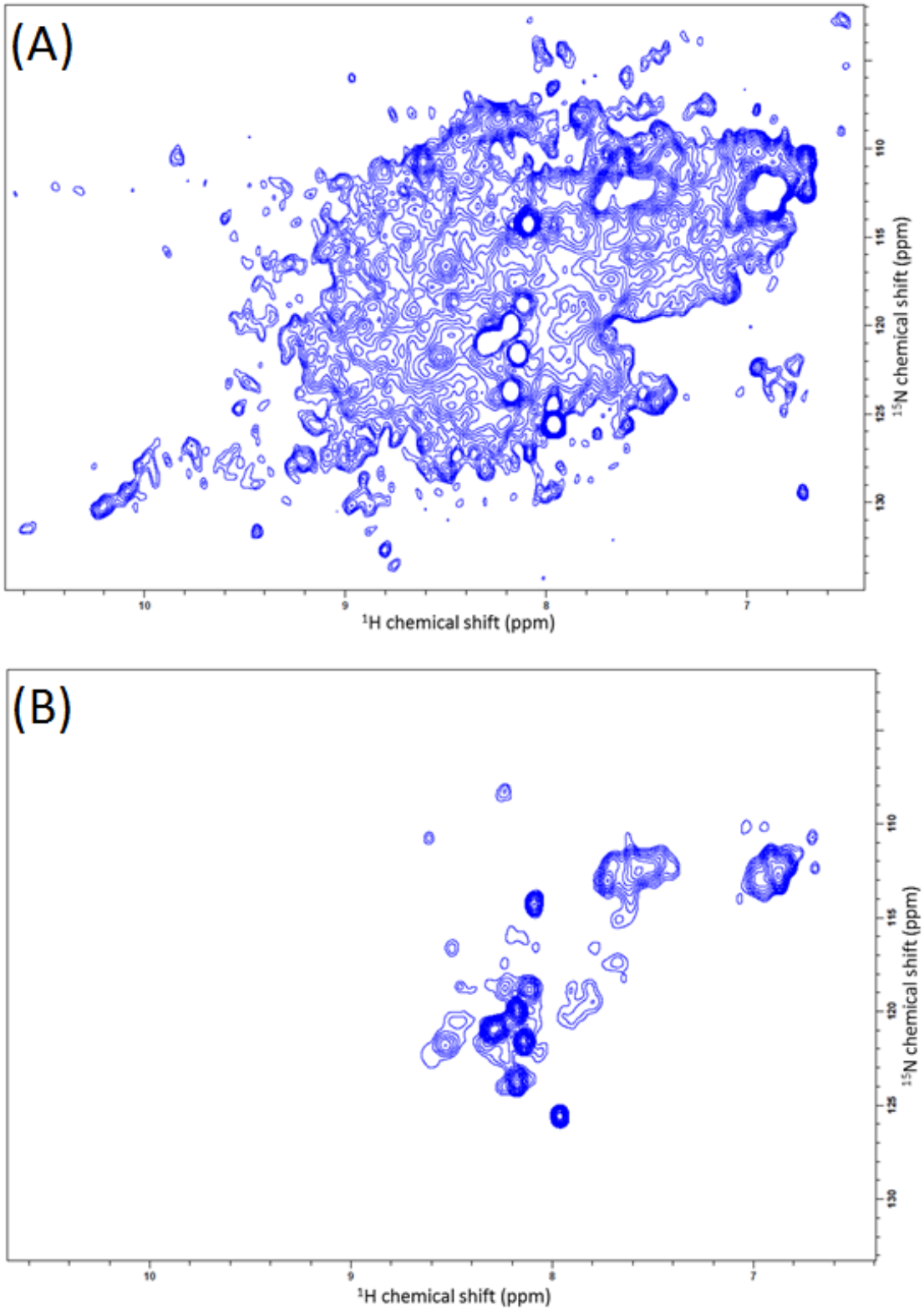

Figure 34. ^{1}H, ^{15}N HMQC-SOFAST of uniformly ^{15}N labelled AChE-d. Collected for 1888 scans with 1024 points in the ^{1}H dimension and 100 points in the ^{15}N dimension at 35 ^{o}C. The sample concentration was 24 µM. (A) the noise base level was set to 28957.7. (B) The same spectrum as Figure 34 A but the noise base level was set to 194803.4 to simplify the spectrum

Table 12. Comparison of the AChE-d activity in the lysate supernatant of *E. coli* grown in H_2O and D_2O minimal media using the protocol in 3.2.1. Both cultures were induced at an OD_{600} of 1.5.

Growth media	Activity (A_{412}/min/10 µl lysate supernatant)	OD_{600} at harvest
D_2O minimal media	0.261	3.2
H_2O minimal media	2.427	3.7

3.3.4 Selective ^{15}N labelling.

Several different methods were used to selectively ^{15}N label AChE-d, first ^{15}N labelled isoleucine and leucine were added to minimal media cultures. The AChE-d from this growth was purified and analysed by NMR to produce the spectrum shown in Figure 35. The AChE-d concentration in this sample was 24 µM which would be enough to get a HMQC-SOFAST spectrum of a uniformly ^{15}N labelled sample, however, Figure 35 shows that only four signals were detected. AChE-d contains 12 isoleucines and 52 leucines, these amino acids also scramble strongly to valine (115) of which there are 47 so 111 signals were expected. It was thought that aminotransferase could be partially responsible for the weak signals because it catalyses the transfer of amino acid amino groups to α-ketoglutarate which is a precursor for several other amino acids (115). By doing this aminotransferase essentially dilutes the ^{15}N of the labelled leucine and isoleucine into other amino acids. It has been previously shown that the addition of α-aminooxyacetic acid (an inhibitor of the aminotransferases) to the culture can increase the signals seen by reducing the ^{15}N dilution caused by aminotransferase (120). This was attempted but α-aminooxyacetic acid seemed to prevent the growth of the *E. coli* which meant a low yield of active AChE-d was obtained as shown in Table 13.

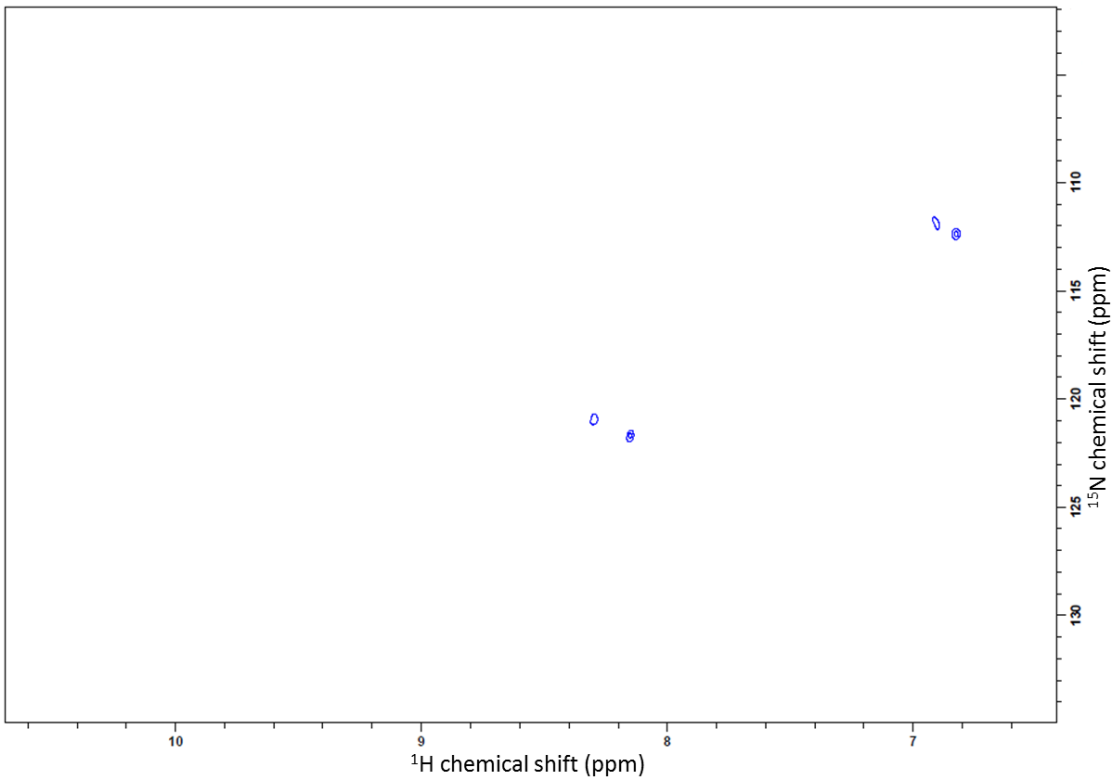

Figure 35. ^{1}H ^{15}N HMQC-SOFAST of AChE-d specifically labelled by the addition of ^{15}N leucine and isoleucine to the growth media. The sample concentration was 24 µM, the spectrum was collected for 1888 scans with 1024 points in the ^{1}H dimension and 100 points in the ^{15}N dimension at 35 ^{o}C. The noise base level was set to 28957.7 (same as Figure 34 A and 8).

Un-labelling was studied next, for this experiment Shuffle *E. coli* were grown in minimal media containing $^{15}NH_4Cl$. All amino acids were added to the media apart from leucine, isoleucine, valine, cysteine and tryptophan in their unlabelled form. Table 13 shows that roughly double the active AChE-d was produced with this method than with a standard minimal media growth. The spectrum of the purified AChE-d from this growth is shown in Figure 36.

Table 13. Comparison of the AChE-d activity in the lysate supernatants of differently labelled *E. coli* cultures. All cultures were grown in standard minimal media with the additions specified in the methods section. All cultures were induced at an OD_{600} of 0.6.

Labelling method	Activity (A_{412}/min/10 µl lysate supernatant)	OD_{600} at harvest
None	2.079	1.89
Un-labelling	4.357	5.4
Addition of ^{15}N Ile and Leu	2.264	3.8
Addition of ^{15}N Ile, Leu and α-aminooxyacetic acid	0.007	0.66

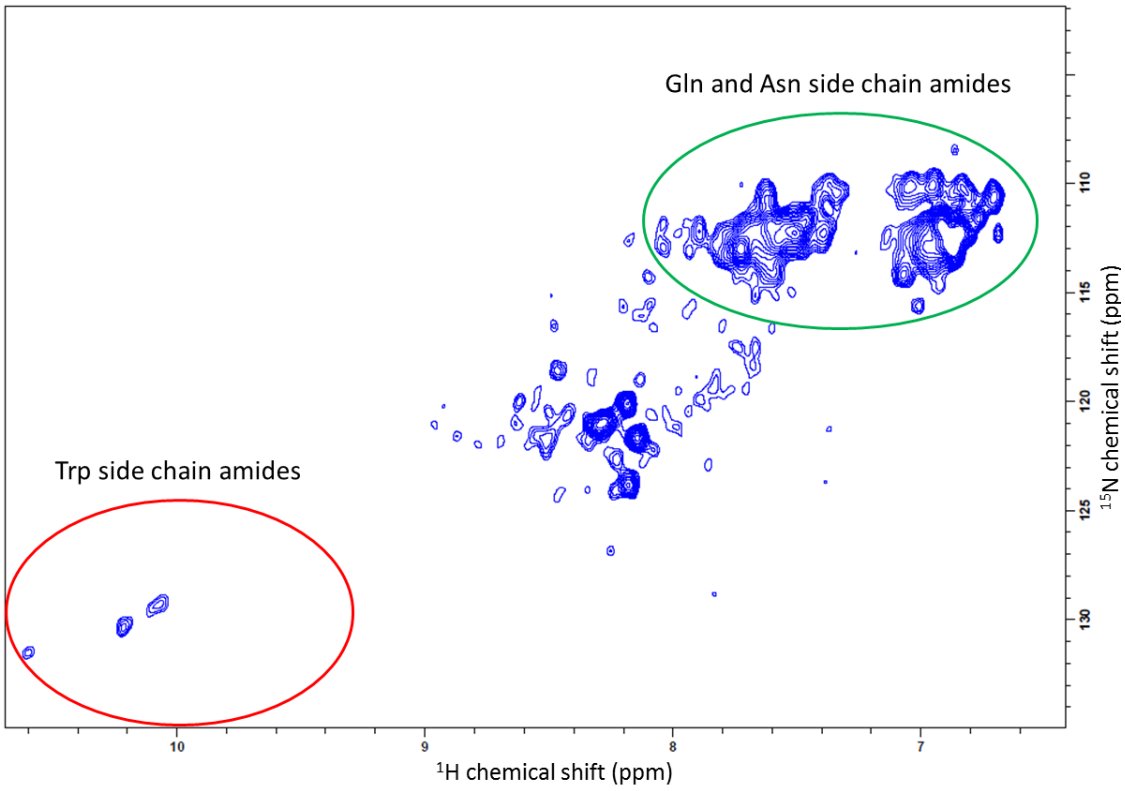

Figure 36. ^{1}H ^{15}N HSQC-SOFAST of AChE-d with ^{15}N labelling of leucine, isoleucine, valine, cysteine and tryptophan residues. This sample was produced with the un-labelling method described 3.2.1 and had a concentration of 24 µM. The spectrum was collected for 1888 scans with 1024 points in the ^{1}H dimension and 100 points in the ^{15}N dimension at 35 ^{o}C. The noise base level was set to 28957.7 (same as Figure 34 A and 33). The Trp side chain amides are circled in red, the Asn and Gln side chains are circled in green.

3.4 Discussion

3.4.1 AChE-d expression in minimal media.

Expressing recombinant proteins in minimal media has been reported to cause a drop in yield (121), so the reduced expression yield seen in this work (2 mg/l in 2YT media to 0.6 mg/l in minimal media) was expected. ^{15}N labelled yeast extract (product name, Celtone Base Powder (^{15}N, 98%+)) can be purchased from Cambridge Isotope Laboratories which allows for the uniform ^{15}N labelling of recombinant proteins without a drop in protein yield, but these products cost around £70/l of culture making it more cost effective to grow larger volumes of minimal media instead as there is only a 30% drop in yield and standard minimal media costs around £13/l.

3.4.2 Effects of AChE-d expression in D_2O minimal media.

Deuteration of AChE-d would have greatly improved the signal to noise and resolution of spectra obtained (118). Unfortunately, growing *E. coli* in D_2O has been shown to reduce overall expression of proteins and increase the doubling time of the *E. coli*, this is mainly caused by the deuterons being more slowly exchanged than protons which leads to a slowing of all reactions involving the transfer of protons. To overcome this the *E. coli* need to upregulate the expression of proteins associated with these reactions which increases the stress on the cells and decreases the resources that are available for other processes (122). It was thought that because Shuffle *E. coli* are under oxidative stress caused by the mutations needed to produce the strain (94), that the added stress of deuteration might be to toxic for them. However monoclonal antibodies have been successfully deuterated in Shuffle *E. coli* (123), and the Shuffle *E. coli* grew to similar OD_{600} in H_2O and D_2O minimal media (3.7 and 3.2 respectively) in this work. This indicates that the difficulty in producing deuterated AChE-d is protein specific. Deuteration of non-exchangeable protons has been shown to reduce the stability of proteins (124)(114) and it has been shown that deuteration can affect the structure of proteins (125). It's possible that these effects

of deuteration could be the cause of the reduction of soluble and active AChE-d expression in D_2O but further work is needed to confirm this.

3.4.3 Effect of ^{19}F labelling on AChE-d expression.

As Table 13 shows the fluorotryptophans had a much larger effect on the AChE-d activity in the lysate supernatant than fluorophenylalanine, and as all cultures grew to a similar OD_{600} it's unlikely that the difference is due to the fluorotryptophan precursors being toxic to the *E. coli*. The position of the ^{19}F on the indole ring of tryptophan has previously been shown to affect the yield of labelled protein, this is because fluorine is more electronegative than the proton it replaces which can disrupt the correct folding of the protein (126). Therefore several different ^{19}F precursors were tested.

The level of precursor uptake will also influence the AChE-d activity in the lysate supernatant, for instance the 4-fluorophenylalanine could have a very large detrimental effect on the folding of AChE-d which would lead to a low yield, but if the *E. coli's* uptake of the precursor is very poor then this effect won't be seen. AChE-d contains 14 tryptophans and 28 phenylalanines so fluorine labelling of phenylalanine is more likely to interfere with the correct folding of the protein as more changes have been introduced. Table 11 shows that *E. coli* cultures grown with the precursor to 4-fluorophenylalanine had the highest AChE-d activity in its lysate supernatant so it seems likely that there was a low incorporation of the 4-fluorophenylalanine precursor into the protein. No examples of specific ^{19}F labelling of phenylalanine using 4-fluorophenylacetic acid as a precursor could be found, but as phenylacetic acid is a known precursor to phenylalanine (127) it was decided that the possibility of using it as a specific label should be investigated.

Figure 33 shows the ^{19}F 1D NMR spectrum of the 4-fluorophenylalanine labelled AChE-d. No peaks can be seen. This could be because there was poor uptake of the 4-fluorophenylanine precursor or the substantial line broadening of ^{19}F signals caused by the combination of the chemical shift anisotropy (CSA) of ^{19}F (128) and large size of AChE-d (62.517 kDa). Mass spectrometry has been used to measure the incorporation of isotopic labels into recombinantly expressed proteins. However,

getting intact masses of larger proteins comes with significant difficulties (129) which prohibited the acquisition of mass spectrometry data on AChE-d without a significant investment of time into optimisation. If AChE-d had been selectively labelled with 4-fluorophenylalanine (which seems unlikely) then Figure 33 showed that the peaks produced by the ^{19}F labels were too broad to be detected. If the relatively high activity of 4-fluorophenylalanine labelled AChE-d (Table 11) indicated that the incorporation of the label had been poor, then successful fluorination of the Phe residues would likely result in a substantial drop in AChE-d activity as seen with the fluorinated Trp residues, especially considering that AChE-d contains double the number of Phe residues compared to Trp. For this reason further investigation of the 4-fluorophenylacetic acid incorporation efficiency didn't seem like an efficient use of time.

The correlation time can affect the amount of peak broadening caused by a nuclei's CSA, increasing correlation time leads to less efficient averaging of the CSA which leads to broader peaks (130). ^{19}F has a relatively high CSA, meaning that it will produce different chemical shifts depending on the direction it's measured relative to the magnetic field, in solution the tumbling of the molecule containing the ^{19}F atom will cause these differences to average out but will result in a broader peak than would be caused by isotropic nuclei (131). The combination of this with the peak broadening caused by the fast T2 relaxation rate of AChE-d due to its large size was expected to cause very broad peaks. Although the acquisition of high resolution ^{19}F spectra with good signal to noise ratios was not expected, it was thought that ^{19}F labelling experiments should be tried as they were relatively simple and there was the possibility that a ^{19}F labelled residue would be in a particularly flexible region of the protein and would result in a better than expected signal. The probability of gaining usable ^{19}F AChE-d spectra was low, so after the failure of initial attempts to produce usable quantities of a ^{19}F labelled AChE-d it was decided that further attempts to ^{19}F label AChE-d would not be made.

3.4.4 Selective ^{15}N labelling of AChE-d.

Selective ^{15}N labelling of leucine and isoleucine by the addition of ^{15}N labelled amino acids is known to be problematic due to high levels of scrambling (132), the ^{15}N is

strongly transferred to Val and Ala (Figure 30) leading to isotope dilution. Auxotrophic strains of *E. coli* have been developed that prevent scrambling by deleting genes associated with the production of certain amino acids (133). These auxotrophs are only commercially available in C43(DE3) *E. coli*, however, Shuffle *E. coli* is needed to express AChE-d so this method of selective labelling wasn't pursued any further.

Spectral simplification was the main goal of this work so whilst not ideal, some scrambling could be tolerated as it would still result in a spectrum with less peaks than uniformly ^{15}N labelled AChE-d. It was for this reason that the selective ^{15}N labelling of leucine and isoleucine was attempted. It was expected that leucine and isoleucine peaks would have a reduced signal intensity compared to uniformly ^{15}N labelled AChE-d and several other residue types would also produce relatively weak signals. Unfortunately, the scrambling was so severe that the ^{15}N concentration of each affected residue was too low to be detected. It was shown in (120) that the addition of the aminotransferase inhibitor α-aminooxyacetic acid could prevent the scrambling of the ^{15}N isotope on leucine so its addition to the growth media was tested but resulted in the growth of *E. coli* being halted and a negligible amount of AChE-d activity being detected in the lysate supernatant (Table 13). In reference (120), the *E. coli* strain BL21 (DE3) were used with good results, however, Shuffle *E. coli* are already under considerable oxidative stress and hence may cope less well with the additional stress of aminotransferase inhibition, resulting in the cessation of cell growth and no recombinant protein production.

The intention of the un-labelling experiment was to simplify the HMQC-SOFAST of AChE-d by removing the peaks from all residues except leucine, isoleucine, valine, tryptophan and cysteine. These residues were chosen for a variety of reasons. Leucine, isoleucine and valine make up 20% of residues in AChE-d so having just these ^{15}N labelled would produce a HMQC-SOFAST spectrum with 111 peaks, it was thought that this would sufficiently simplify the spectrum whilst still providing enough peaks to track movement on inhibition of the enzyme with an OP. Tryptophan was included because of its abundance in the active site gorge of AChE-d where it plays an important role in binding ligands which are then hydrolysed by

the catalytic triad at the base of the gorge (24). The tryptophan sidechain amides occupy a sparsely populated region of the spectrum from a ^{1}H, ^{15}N HMQC-SOFAST experiment and are seen in the bottom left hand corner of Figures 34 circled in red. This is an added bonus as it provides extra peaks to analyse whilst not increasing the complexity of the main body of the spectrum. Cysteine could not be included in the growth media as it inhibits the production of leucine, isoleucine, valine and threonine which stops the *E. coli* from growing (134). AChE-d only contains 6 cysteines so their inclusion into the HMQC-SOFAST spectra wasn't a major concern.

The un-labelling doesn't seem to have worked as expected, in Figure 36 the sidechain amide peaks of Asp and Gln can be seen as the two clusters of peaks in the top right corner of the spectrum circled in green. These amino acids were added in the same concentrations as all the others. It has been shown that the sidechains of Asp and Gln can be selectively ^{15}N labelled by expressing proteins in minimal media containing all amino acids (including Asp and Gln) with $^{15}NH_4Cl$ (135). For this reason, it's unlikely that their removal from the spectrum would be simple.

3.4.5 Conclusions.

Figures 32, and 34 have the noise base level set to the same value, meaning that only peaks above an intensity level of 28957.7 are shown in all spectra. When comparing the spectra it's apparent that Figure 36 (^{15}N sample all residues un-labelled apart from Ile, leu, Val, Cys and Trp) has a greatly simplified spectrum compared to Figure 34 A (uniformly ^{15}N labelled). However, many of the peaks on the periphery of Figure 34 A are lost in Figure 36. Any change in these peaks position after inhibition of AChE-d by an OP would be relatively easy to observe as the reduced spectral density around the perimeter of the spectrum reduces peak overlap. The loss of these peaks in Figure 36 is a disadvantage of the un-labelling method. However, several peaks in the central region of Figure 36 become better resolved due to un-labelling. Figure 34 B is taken from the same spectrum as Figure 34 A but the noise base level is set higher to remove more of the spectrum. Compared to Figure 36 there are less peaks because the less intense peaks were below the higher noise base level but several peaks remain which show limited overlap so could still be used to track peak shifts. Although un-labelling did make several new peaks available to study it seemed to

remove even more viable peaks on the periphery of the spectrum. For this reason, uniform ^{15}N labelling was chosen as the labelling method to use for studying OP inhibition of AChE-d.

Chapter 4. Kinetic analysis of organophosphate inhibition and oxime reactivation.

4.1 Introduction.

4.1.1 Organophosphate (OP) inhibition of AChE-d.

A schematic overview of the inhibition of AChE-d by an OP is shown in Figure 37, the first step is the reversible binding of the OP to AChE-d (Figure 37 A). Once bound the oxygen of the active site serine can form a covalent bond with the phosphorus atom of the OP which causes the bond between the phosphorus and the leaving group to break. This leaves the phosphate adduct covalently bound to the active site serine (Figure 37 B) which prevents AChE-d from catalysing the hydrolysis of ATCh (58). Oximes, which have an R=NOH functional group (R being any other chemical group) can be used to remove the phosphate adduct from OP inhibited AChE-d. The O of the oxime group forms a covalent bond with the phosphorus atom of the adduct by a nucleophilic attack reaction, this causes the bond between the phosphorus atom and the O of the active site serine to break releasing reactivated AChE-d and a phosphorylated oxime (141) (Figure 37 C).

The phosphate adduct can also undergo spontaneous hydrolysis, this is where a covalent bond is formed between the phosphate and the O of a water molecule, causing the release of a H^+ from the water and the phosphate adduct from AChE (142) (Figure 37 D). The R_2 group is susceptible to hydrolysis as well, this produces a negatively charged phosphate adduct that can't be reactivated with oximes and doesn't undergo spontaneous hydrolysis as the negative charge on the adduct protects it from nucleophilic attack (143) (Figure 37 E). The susceptibility of each OP to the post inhibition reaction pathways is different, for example the chemical warfare agent soman has an extremely fast ageing half-life of around 4 minutes (144), most other OPs have ageing half lives in the range of hours (145)(146). Tabun which is another chemical warfare agent OP is roughly 10 times more resistant to reactivation by the two most commonly used oximes (Figure 38) than sarin and VX

(65) which are also organophosphorus chemical warfare agents. The half-lives of spontaneous hydrolysis of OP inhibited AChE ranges from 1 – 40 hours (146)(147) which means spontaneous hydrolysis has little relevance to the toxicity of an OP as after acute poisoning with an OP death would occur before any significant spontaneous hydrolysis.

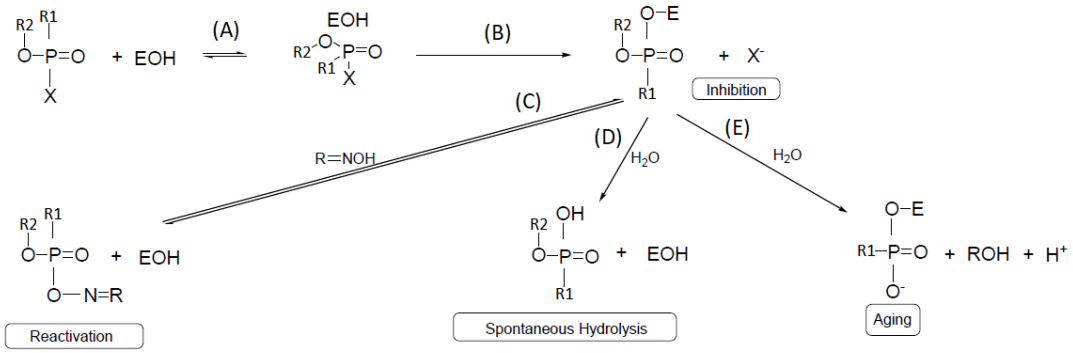

Figure 37. Schematic diagram of the inhibition of AChE by an OP and the subsequent reactions of the OP inhibited AChE. E represents the enzyme R_1 and R_2 represent any other chemical group and X represents the leaving group of the OP. This Figure is an altered version of one taken from (58)**.**

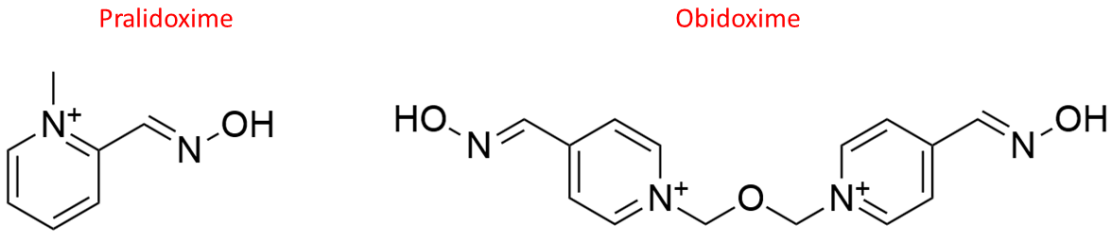

Figure 38. Structures of the two oximes used in this work.

4.1.2 Experimental aims.

The main aims of this chapter were to measure kinetic data for the inhibition of AChE-d by several OPs (Figure 39) and the subsequent oxime mediated reactivation of the OP-AChE-d conjugates using the oximes in Figure 38. This data was intended to be compared with NMR data on the interaction of OPs with AChE-d to see if OPs with different kinetic parameters perturbed different residues in AChE-d. This could suggest that the adducts were causing structural changes in AChE-d which could help explain the differences in the OPs rates of reactivation or determine if association of the adduct with certain residues had a protective effect against reactivation. Saturation transfer difference (STD) NMR was used to try and identify chemical

groups on OPs that were in particularly close proximity to AChE-d, this information could be used to infer which chemical groups were important for binding. The inhibition rates were collected to see if they correlated with the LD_{50}s of the OPs, which would mean they had predictive value in assessing the OP toxicity.

The inhibition and reactivation kinetics could only be determined for pesticide OPs as the collaborating laboratory at Defence Science and Technology Laboratory were unable to support the analysis to obtain kinetic data on the chemical warfare agents covered by this study. The inhibition and reactivation rates for chemical warfare agent and pesticide OPs with human AChE had been published (65). Therefore an additional aim of this work was to compare the reactivation rates of the pesticide inhibited human AChE in reference (65) with experimentally determined values using AChE-d. If the ranking of relative reactivation rates for the pesticide OPs was the same for human AChE and AChE-d then it would be likely that the organophosphorus chemical warfare agents would follow the same trend in both isoforms.

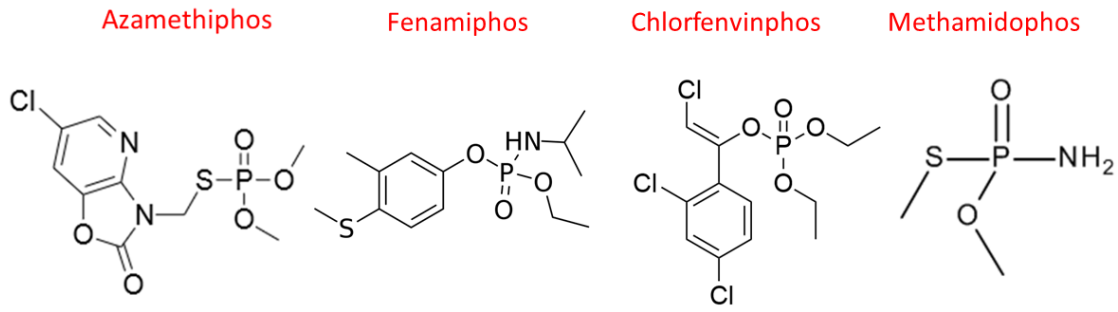

Figure 39. The OP pesticides used in this work.

4.2 Methods.

4.2.1 Determination of AChE-d stability.

The effect of BSA concentration on the degradation rate of AChE-d was tested. For this experiment five different 100 µl samples of 100 nM AChE-d were made with varying BSA concentrations. The BSA concentrations were, 0, 0.1, 0.2, 0.3 and 0.4 mg/ml. These were left at room temperature for one hour, every 10 minutes 10 µl of each sample was taken and used to determine the rate of AChE-d mediated breakdown of ATCh according to 2.2.5.

4.2.2 Determination of OP inhibition rates and affinities for AChE-d.

Stock solutions of 50 mM OP were made up in methanol just before use and kept on ice, these were then used to make stock solutions 10 X the concentration that was needed in the assay (Table 14). A stock solution of 1 µM AChE-d and 1mg/ml BSA was made in phosphate buffer (20 mM sodium phosphate, 100 mM NaCl, pH 7.4) and kept on ice. Samples for measuring the rate of inhibition were made by adding 10 µl of the AChE-d/BSA stock solution to 80 µl of phosphate buffer, 10 µl of the appropriate 10 X OP stock solutions was then added. Periodically 10 µl of the sample was taken for rate determination according to 2.2.5. This was done after 1, 2 and 3 minutes for methamidophos and 2, 4 and 6 minutes for fenamiphos. A rate determination assay can be done every 1 min. (21 s for the experiment to run and the rest of the time is used pipetting and changing cuvettes), azamethiphos and chlorfenvinphos inhibited AChE-d rapidly meaning in their inhibition assays samples needed to be taken after 10, 20 and 30 and 20, 40 and 60 seconds of incubation respectively, because the activity can only be taken once every minute one sample could not be used for all measurements, so separate samples were made for each time point. This was done for each of the OP concentrations in triplicate.

Table 14. The concentration of each OP used in assays to determine the inhibition potencies and K_ds for each OP.

[Azamethiphos] (mM)	[Methamidophos] (mM)	[Fenamiphos] (mM)	[Chlorfenvinphos] (mM)
0.05	2	0.1	0.1
0.1	4	0.25	0.2
0.15	6	0.5	0.3
0.2	8	0.75	0.4
0.3	10	1	0.5
0.4	12	1.5	0.75
	14	3	

The rate of inhibition was measured and the natural logarithm derived, these were then plotted against incubation time and fitted to a straight-line using Excel, and this was repeated for each OP concentration. The slope of the straight line gave the pseudo first order rate constant (k') (148) for the reaction of the OP with AChE-d. In reference (149) the oxime induced reactivation of OP inhibited human AChE was shown to follow Michalis-Menten kinetics which lead them to derive the altered Michalis-Menten equation given in Equation 2. The reaction scheme for OP inhibition is identical to the oxime induced reactivation (Figure 40 A and B) meaning the Michalis-Menten equation can be used to approximate the kinetics for OP inhibition. The Michalis-Menten equation was fit to plots of k' against OP concentration using the non-linear regression tool in the KaleidaGraph software package. This allowed values for k_r and K_d to be determined.

$$k_{obs} = \frac{k_r * [oxime]}{K_d + [oxime]}$$

Equation 2. Micaelis-Menten equation with parameters named according to reference (65)**. K_{obs} is the observed rate of reaction, k_r is the maximal rate of reaction and K_d is the dissociation constant. The derivation of this equation can be found in references (150) and (65).**

Figure 40. Reaction scheme for OP inhibition of AChE-d (A) and oxime mediated reactivation of OP inhibited AChE-d (B). E represents AChE-d, OPx the organophosphate with the leaving group (x) attached, EOPx the reversible complex between the OP and enzyme, EOP the phosphorylated enzyme and x the leaving group of the OP. OX represents the oxime, EOPOX the reversible complex between the phosphorylated enzyme and the oxime. OPOX represents the phosphorylated oxime. K_d is the concentration of either OP or oxime that give 50% maximum rate of reaction and k_r is the rate of reaction when the concentration of OP or oxime approach ∞.

4.2.3 Determination of OP stability.

Samples of each of the four OPs in Figure 39 were made at a concentration of 0.5 mM in phosphate buffer (20 mM sodium phosphate, 100 mM NaCl, pH 7.4) containing 5% deuterated methanol, the final sample volume was 600 µl and all samples were in 5 mm NMR tubes. The IconNMR mode of the TOPSPIN software package was used to automate the periodic collection of ^{1}H 1D spectra for each of these samples. It took 40 minutes to collect a spectrum on all the samples (10 min per sample), after this the process was repeated so a spectrum of each sample was collected every 40 minutes, this process was continued for 20 hours.

The ^{1}H 1D NMR experiments used excitation sculpting for water suppression, 32768 points, 4 dummy and 4 real scans were collected. The spectral width was 16.0242 ppm and the temperature was 25^{o}C.

The decrease in signal intensity of the OPs relative to the methanol signal was used to assess the breakdown of the OPs.

4.2.4 Reactivation of OP inhibited AChE-d.

To produce OP inhibited AChE-d, a 400 µl sample containing 5 µM AChE-d, 1 mM OP and 5% methanol was made in phosphate buffer (20 mM sodium phosphate, 100 mM NaCl, pH 7.4) and then, incubated at room temperature for 30 minutes after which its AChE-d activity was measured using methods described in 2.2.5 to make

sure over 95% of the AChE-d activity had been lost. Unreacted OP was removed from the sample by passing in through a 2 ml PD-10 desalt column (GE healthcare) which had been washed and pre equilibrated with phosphate buffer according to manufacturer's instructions. After the OP inhibited AChE-d sample had passed through the column its protein concentration was assessed by A_{280} measurement, it was then diluted in phosphate buffer to 1 µM and BSA was added to a concentration of 1 mg/ml, this stock solution was kept on ice. Appropriately concentrated stock solutions of oximes were made in phosphate buffer and kept on ice. Around 4 to 5 test samples were made containing 100 nM OP-AChE-d conjugate, 0.1 mg/ml BSA and varying concentration of oxime and periodically checked for AChE-d activity, this was done do determine the range of oxime concentrations necessary to achieve a saturation curve and the incubation time that would allow a detectable amount of AChE-d to be reactivated but not so much that all samples showed complete reactivation of AChE-d.

The oxime concentrations used to get saturation curves for oxime reactivation experiments were 0 - 1400 µM in 100 µM increments for all experiments apart from the obidoxime reactivation of chlorfenvinphos inhibited AChE-d. In that experiment the obidoxime concentrations were 0 - 3.9 mM in 0.3 mM increments. The rate of ATCh breakdown by AChE-d was measured at each oxime concentration after the pre-determined incubation time. These rates were then converted into the observed rate constant (k_{obs}) using Equation 3. The k_{obs} values were plotted against oxime concentration and the non-linear regression tool in the KaleidaGraph software package was used to fit Equation 2 to the data so kr and K_d could be determined.

$$k_{obs} = \frac{\left(Ln\frac{V0 - Vt}{V0 - Vi}\right)}{-t}$$

Equation 3. Used to convert the rate of reaction into the pseudo first order observed rate content (k_{obs}). V0 is the rate of uninhibited AChE-d, Vt is the rate of an OP-AChE-d conjugate at time t in the incubation with an oxime and Vi is the rate of OP-AChE-d conjugate before incubation with an oxime. The derivation of this equation can be found in references (65) and (150).

4.2.5 Measurement of oxime IC50s.

Stock solutions of each oxime were made in phosphate buffer (20 mM sodium phosphate, 100 mM NaCl, pH 7.4), the oxime concentrations of these stock solutions (in mM) were, 1000, 750, 500, 300, 200, 100, 50, 10, 5 and 1. A stock solution containing 100 nM AChE-d and 0.1 mg/ml BSA was made, this was kept on ice until needed along with the oxime stock solutions. Cuvettes containing 980 µl Ellmans buffer, 10 µl of the appropriate oxime stock and 10 µl of the AChE-d BSA stock were made. The AChE-d activity of these samples was obtained using the methods in 2.2.5. Three rate measurements were obtained for each oxime concentration. The oximes reacted with ATCh so the rate of oxime mediated breakdown of ATCh at each oxime concentration was measured by adding 10 µl of the appropriate oxime stock solution and 10 µl phosphate buffer to 980 µl of Ellmans buffer then measuring the rate of reaction using the same method as the samples containing AChE-d. The rate of oxime mediated breakdown of ATCh was subtracted from the rate of reaction obtained from the sample containing AChE-d and the corresponding concentration of oxime. The data was fitted to logarithmic equations using Excel which allowed the oxime concentration that gave 50% inhibition to be calculated.

4.3 Results

4.3.1 Stabilisation of AChE-d.

Dilute samples of AChE have been shown to be unstable at room temperature, this instability could be overcome by increasing the concentration of AChE in the sample (151). It was investigated weather BSA could also be used to prevent the breakdown of AChE-d, the results of this are given in Figure 41. The AChE-d sample containing no BSA lost roughly half of its activity over the hour long period it was observed and all samples containing BSA showed no significant drop in activity. All kinetic experiments from this point on included 0.1 mg/ml of BSA to prevent degradation of AChE-d, the lowest tested BSA concentration was chosen to minimise the chance of it affecting the kinetic assays by binding to the substrates, inhibitors or oximes.

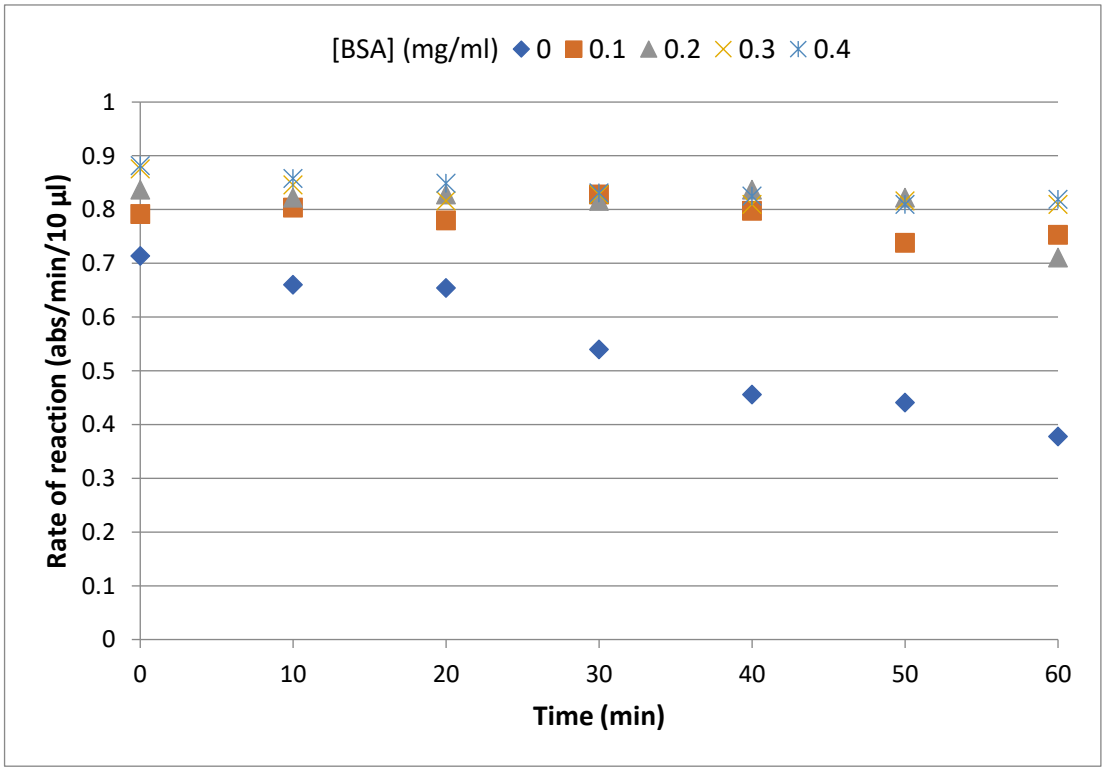

Figure 41. Activity of 100 nM samples of AChE-d containing varying concentrations of BSA over 1 hour at room temperature. n=1.

4.3.2 Organophosphate inhibition of AChE-d.

The maximum inhibition rate (k_r) and K_d of the four OP insecticides shown in Figure 39 were measured using the methods described in 4.2.2. The graphs of the pseudo

first order rate constant (k') for the inhibition of AChE-d by each of the OPs are shown in Figure 42, these were used to calculate the k_r and K_d for each inhibitor. The errors on the measurements of azamethiphos (Figure 42 A) were relatively large compared to the other OPs, this was because azamethiphos inhibited AChE-d at a very fast rate meaning only small amounts of the detectable product of the Ellmans assay could be generated resulting in the inherent noise of the assay being a more significant portion of the measured value.

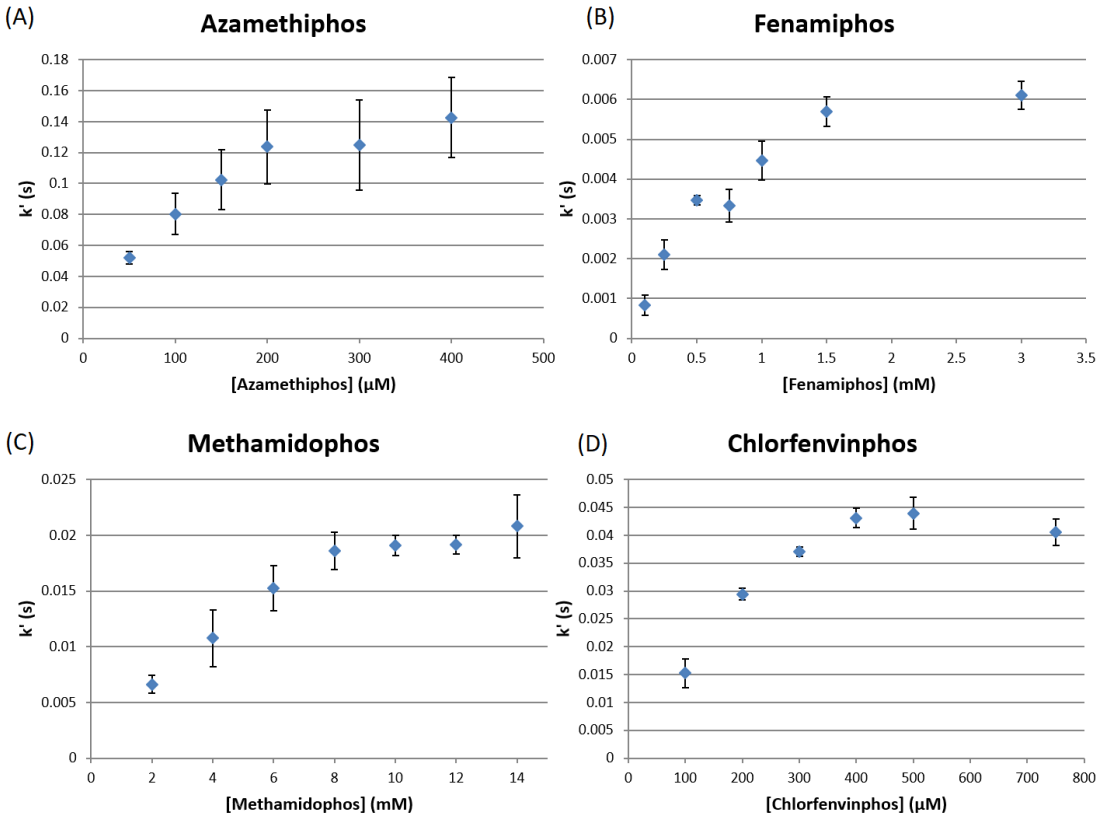

Figure 42. The pseudo first order rate constants of inhibition (k') plotted against OP concentration for azemethiaphos (A), fenamiphos (B), methamidophos (C) and Chlorfenvinphos (D). Each data point was the mean of three measurements and the error bars represent the standard deviation.

k_r and K_d values couldn't be determined for chlorfenvinphos because it started to precipitate at 400 µM meaning the plateau seen in Figure 42 D is due to the reaction buffer being saturated with chlorfenvinphos. However, from Figure 42 it can be determined that at an OP concentration of 100 µM chlorfenvinphos had the second highest k' and at 300 µM it had a k' of around 0.036 s which is higher than the

saturation point of methamidaphos and fenamiphos indicating it had a k_r larger than both of these OPs.

Table 15. The k_r and K_d values for each of the OP used to inhibit AChE-d. Chlorfenvinphos precipitated out of solution at 400 µM which was not high enough for it to saturate AChE-d so k_r and K_d could not be calculated. The errors were calculated by the KaleidaGraph software package. The LD_{50} values were measured on rats with the OP being administered orally and were taken from the references indicated next to the LD_{50} value.

OP	k_r (s)	K_d (µM)	LD_{50} (mg/kg)
Azamethiphos	0.186 ± 0.012	123.27 ± 21.69	1180 (152)
Fenamiphos	0.008 ± 0.001	726.02 ± 141.43	8.1 (153)
Methamidophos	0.031 ± 0.003	6792.5 ± 1369.8	30 (154)
Chlorfenvinphos	N/A	N/A	23 (155)

4.3.3 Measurement of OP stability.

It was thought that the degradation rate of the OPs could be affecting their inhibition rates, to test this, 0.5 mM samples of each of the OPs were made in phosphate buffer (20 mM sodium phosphate, 100 mM NaCl, pH 7.4) containing 5% deuterated methanol. ^{1}H 1D NMR spectra were collected of each of these samples every 40 minutes for 20 hours and the reduction in peak intensity was used to assess the breakdown of the OPs. Methamidophos was the only OP that showed noticeable degradation (25% over 20 hours) over the measured time (Figure 43).

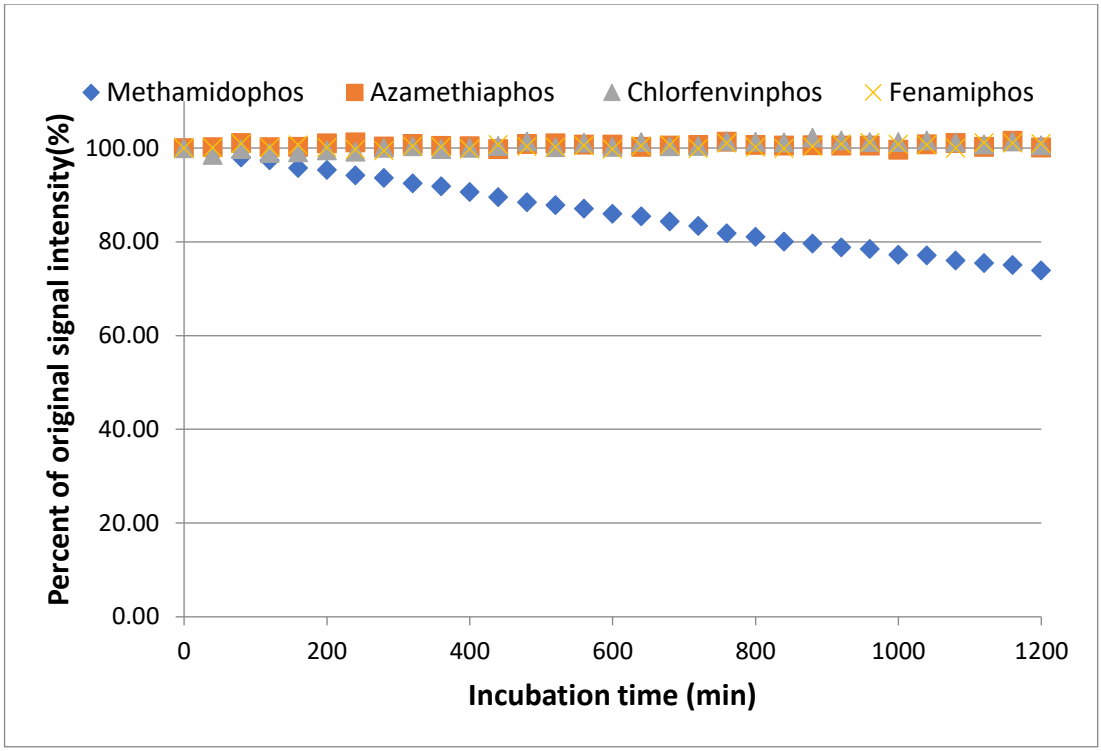

Figure 43. The reduction in signal intensity of each OP over a 20 hour period.

4.3.4 Oxime mediated reactivation of OP inhibited AChE-d.

The two oximes shown in Figure 38 were tested for their ability to reactivate AChE-d which had been inhibited by the OPs shown in Figure 39. Samples of OP inhibited AChE-d (100 nM) were incubated with varying concentrations of the chosen oxime for a predetermined period of time. Following incubation with oxime, 10 µl of the sample was added to 990 µl Ellmans buffer and the AChE-d activity measured. The AChE-d activity was then plotted against oxime concentration to produce the graphs shown in Figure 44.

The non-linear regression function of the KaleidaGraph software package was used to fit Equation 2 to the graphs in Figure 44. This allowed values for k_r and K_d to be determined. k_r gave the rate of reactivation at a saturating concentration of oxime and K_d gave the concentration of oxime that produced 50% of the maximum reactivation rate so represented the affinity of the oxime for the OP inhibited AChE-d. The values of k_r and K_d for each of the OP oxime pairs are given in Table 16 and shown graphically in Figure 45. Obidoxime showed a faster rate of reactivation than pralidoxime for all tested OPs (Figure 45 A). Methamidaphos had the fastest k_r for

both oximes (0.771 min for pralidoxime and 0.995 min for obidoxime), the k_r values for the other OPs ranged between 0.001 – 0.034 min for pralidoxime and 0.005 – 0.052 min for obidoxime. The K_d values showed that obidoxime was a weaker binder for all OP-AChE-d conjugates apart from methamidaphos (Figure 45 B) and that obidoxime had a surprisingly low affinity for chlorfenvinfos inhibited AChE-d, the K_d was roughly four times higher than that of the other OP-AChE-d conjugates.

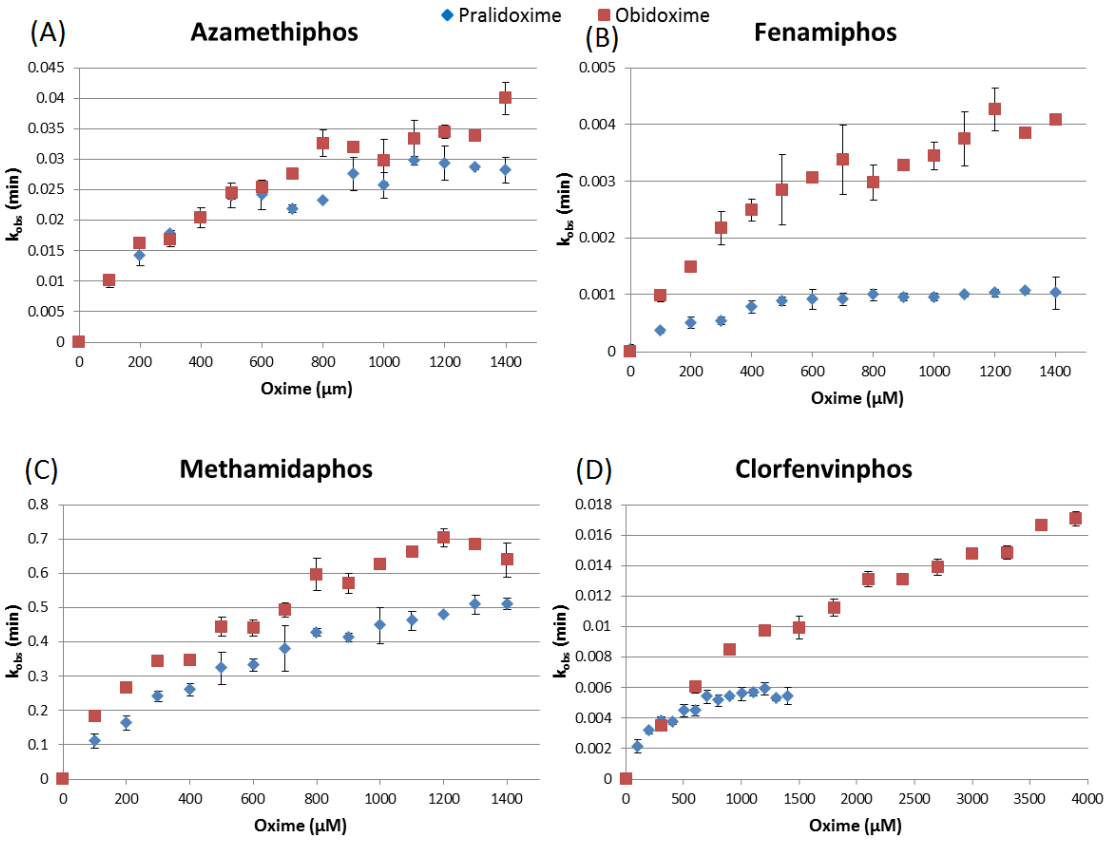

Figure 44. Reactivation rates (k_{obs}) of pralidoxime (blue) and obidoxime (red) for AChE-d inhibited by each of the four OP pesticides. Graphs (A), (B), (c) and (D) are for AChE-d inhibited by azamethiphos, fenamiphos, methamidaphos and chlorfenvinphos respectively. All data is the mean of two repeats and error bars represent the standard deviation.

Table 16. The reactivation rates (k_r) and dissociation constants (K_d) for two oximes and AChE-d inhibited with different OP insecticides. Data is a mean of two repeats, the standard deviation is given as the errors.

	Pralidoxime		Obidoxime	
OP used to inhibit AChE-d	**k_r (min)**	**K_d (μM)**	**k_r (min)**	**K_d (μM)**
Azamethiphos	0.034 ± 0.001	271.37 ± 41.28	0.049 ± 0.003	512.80 ± 86.46
Fenamiphos	0.001 ± 0.000	298.61 ± 42.29	0.005 ± 0.000	471.07 ± 72.05
Methamidaphos	0.771 ± 0.030	714.00 ± 60.58	0.996 ± 0.072	619.29 ± 104.35
Chlorfenvinphos	0.007 ± 0.000	232.68 ± 31.43	0.025 ± 0.001	1938.90 ± 222.00

The size of the phosphate aduct that inhibits AChE-d was thought to have an effect on the reactivatability of the OP-AChE-d conjugate, for this reason the size of the phosphate aduct was estimated for each of the four OPs. The atomic radi were taken from reference (156) and Equation 4 was used to calculate the atomic volume (Table 17). The size of the phosphate aducts were estimated by adding together the volumes of all the nuclei they contained (Table 18). The estimated molecular volumes are likely to be considerable overestimates because all atoms are asumed to have no overlaping sections, in reality the chemical bonds between atoms will cause significant overlap between atoms. However, for the purpose of comparing the size of the phosphate aducts to their reactivation rates the total volume of the aduct isn't particularly important as the errors will be consistent for all aducts meaning the molecular volume estimates will be comparable to each other.

Interestingly the larger phosphate aducts had slower reactivation rates. As Figure 46 A shows the relationship was aproximatly linear for azamethiphos, chlorfenvinphos and fenamiphos but the reactivation rate of methamidophos was too fast to fit the trend of the other three OPs. The K_ds of the oximes for the OP-AChE-d conjugates showed no obvious correlation with the size of the phosphate adduct (Figure 46 B).

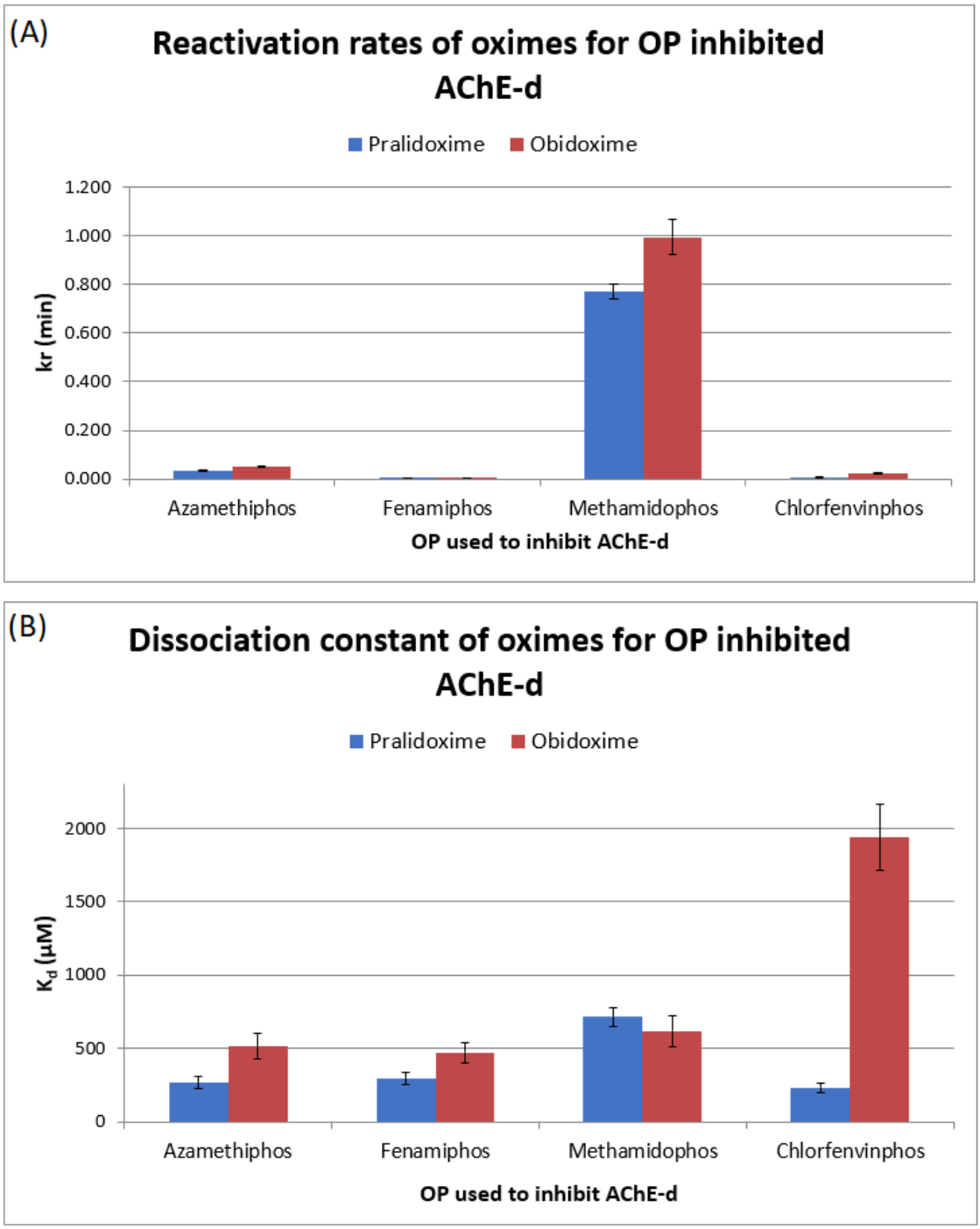

Figure 45. Graphical representation of the k_r (A) and K_d (B) values for the reactivation of OP inhibited AChE-d by pralidoxime and obidoxime.

$$V = \frac{4}{3}\pi r^3$$

Equation 4. Calculates the volume of a sphere. V is volume, π is pi and r is the radius.

Table 17. The atomic radi of several different elements found in OPs. The values of atomic radii were taken from reference (156)**, the volumes were calculated using Equation 4.**

Element	Radius (pm)	Volume (nm^3)
H	25	65
C	70	1400
N	65	1200
O	60	900
P	100	4200

Table 18. Estimate of the size of the phosphate adduct left bound to AChE-d after inhibition with each OP.

OP name	Chemical formula of adduct	Estimated volume (nm^3)
Fenamiphos	$O_2PH_{13}NC_5$	15045
Chlorfenvinphos	$O_3PH_{10}C_4$	13150
Azamethiphos	$O_3PH_6C_2$	12890
Methamidaphos	O_2PH_5NC	8925

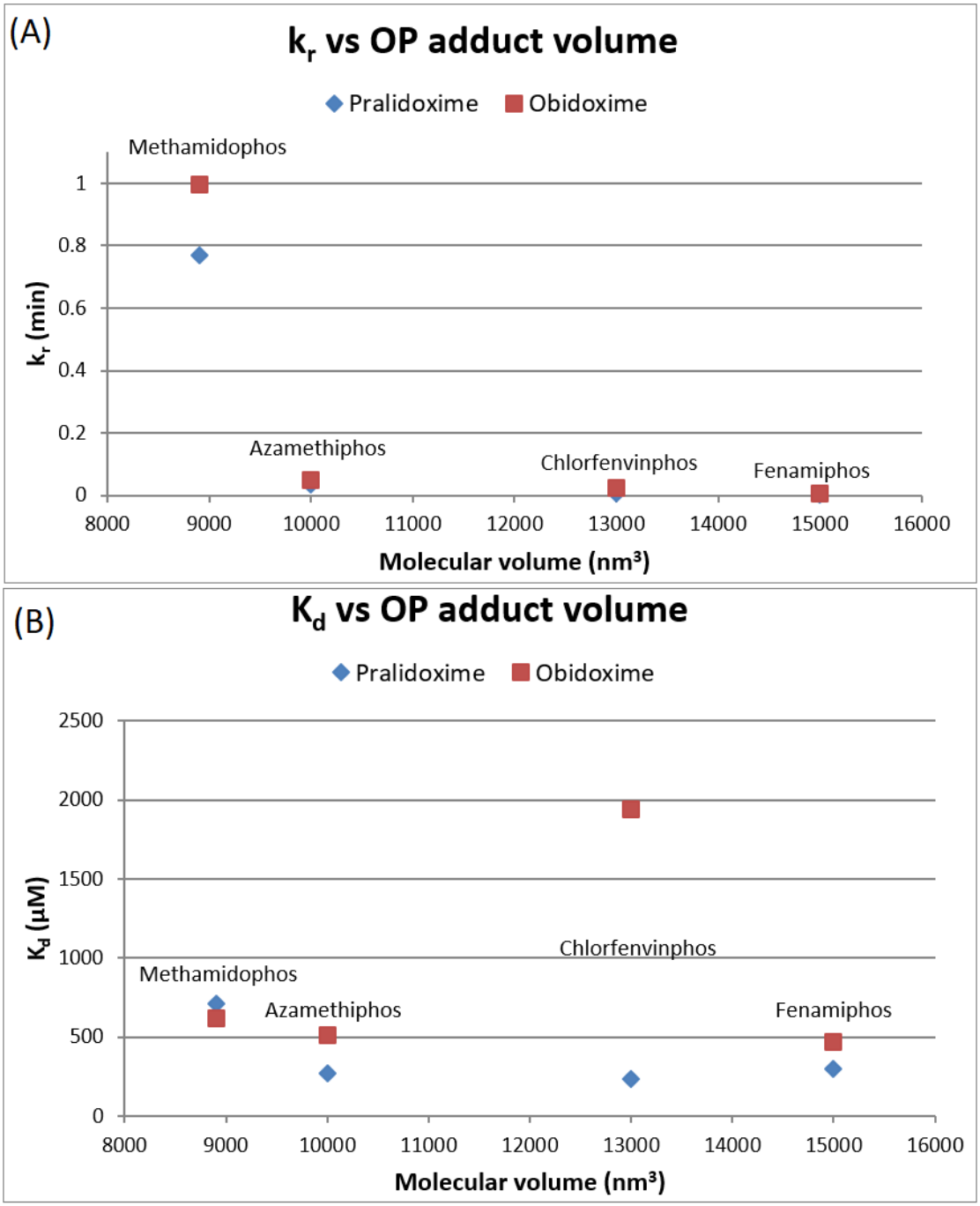

Figure 46. (A) The oxime mediated reactivation rates of AChE-d inhibited by four different OPs plotted against an estimate of the molecular volume of the phosphate groups left by the OPs after inhibition. (B) The K_ds of the oximes for each of the OP-AChE-d conjugates plotted against the estimated volume of phosphate adducts.

4.3.5 Oxime inhibition of AChE-d.

The AChE-d activity was measured in the presence of different concentrations of each of the oximes in Figure 38, this was done to obtain IC_{50} values for the oximes as AChE-d inhibitors. As shown in Figure 47 and Table 19 the IC_{50}s of the oximes were

very similar (pralidoxime 630.39 ± 131.94 and obidoxime 691.00 ± 49.51) and the errors of the measurements overlapped meaning there wasn't a significant difference in their inhibitory potencies.

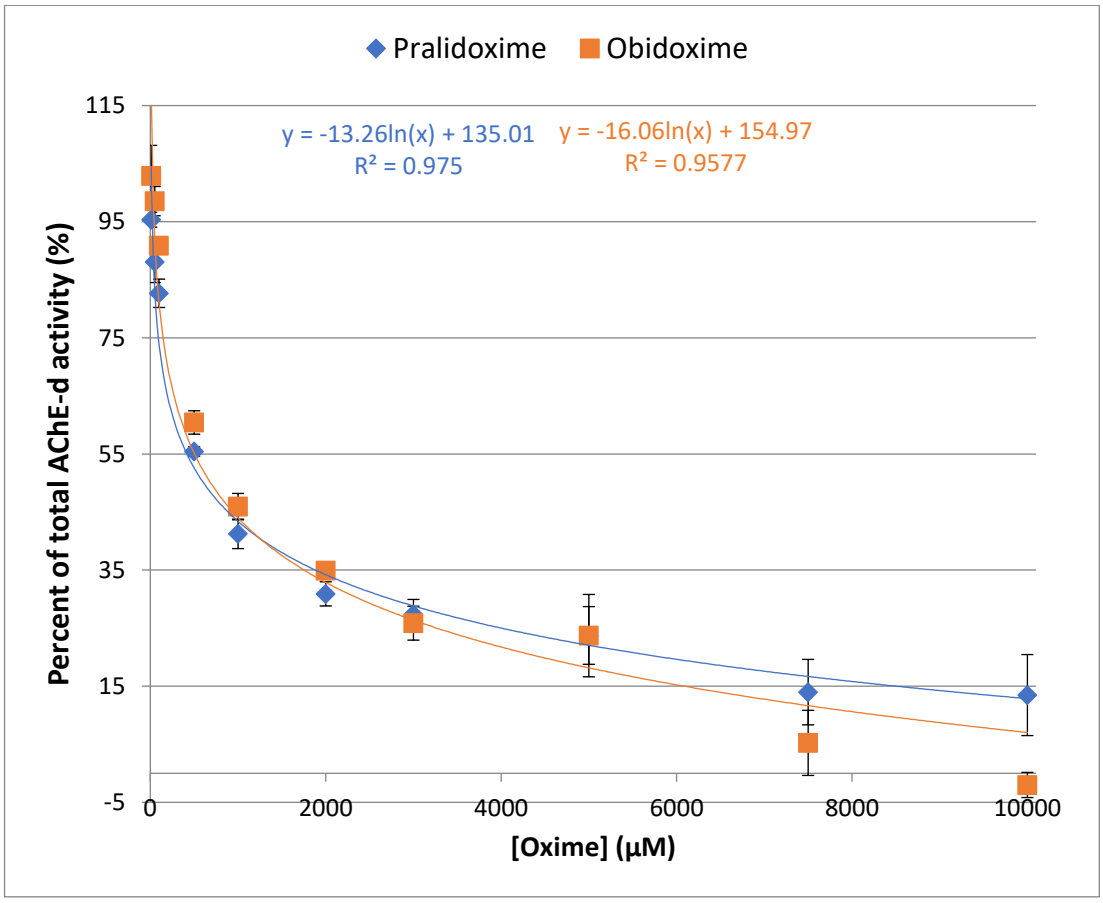

Figure 47. The percentage of total AChE-d activity in the presence of different concentrations of obidoxime and pralidoxime. The error bars represent the standard deviation of three measurements. The logarithmic equations fitted to each data set are shown in the corresponding colours.

Table 19. The IC_{50} values of obidoxime and pralidoxime for AChE-d. Values are the mean of three experiments and the errors are the standard deviation.

Oxime	IC_{50} (µM)
Pralidoxime	630.39 ± 131.94
Obidoxime	691.00 ± 49.51

4.4 Discussion.

4.4.1 Organophosphate inhibition rate and affinity as an indicator of toxicity.

Table 15 contains the k_r, K_d and LD_{50} values for each of the OPs in Figure 39. Azamethiphos was the least toxic (LD_{50} of 1180 mg/kg) but had the highest k_r (0.186 ± 0.012 s) meaning it was the most inhibitory OP. Fenamiphos which was the most toxic (LD_{50} 8.1 mg/kg) but had a k_r 23 times smaller than azamethiphos, this indicated that k_r was a poor indicator of the toxicity of an OP as a high k_r didn't indicate that an OP would be toxic. The K_d also proved to be a poor indicator of toxicity, azamethiphos had the lowest value (123.27 ± 21.69 µM) indicating it had the highest affinity for AChE-d, fenamiphos and methamidophos had K_ds 6 and 55 times higher respectively but their LD_{50}s were 146 and 39 times lower. The discrepancy between the efficacy of the OPs as AChE-d inhibiters and their toxicity could be caused by the fact that the LD_{50}s were obtained using rats, and as discussed in section 1.3.3, AChE-d and rat AChE have 83% sequence similarity. The differing 17% could cause the two AChE isoforms to have different susceptibilities to OP inhibition meaning that if the *in-vitro* kinetic experiments were repeated with rat AChE the inhibitory kinetics would show a closer correlation with the LD_{50} values. In section 1.2.1 it was demonstrated that the most toxic insecticide of a selection of OPs and carbamates varied between two different species of insects. *In vitro* experiments have also shown diisopropyl fluorophosphates (DFP) to inhibit human AChE 4 times faster than it does rat AChE. The same study also showed that nitrophenyl cyclohexyl methylphosphonate inhibited rat AChE 2 times faster than human (157). The species differences could explain the discrepancy between inhibition kinetics and LD_{50} but these experiments would need to be repeated with rat AChE to investigate this further.

A second possible explanation for the poor correlation between OP inhibition and toxicity is biological detoxification of the OP. An OP with a high inhibition rate will have a low toxicity if it is rapidly broken down *in vitro*. House flies were reported to have developed resistance to azamethiphos by upregulating OP degrading enzymes such as glutathione S transferase (GST) and cytochrome P450 (158) so *in vivo*

breakdown of OPs clearly has a significant effect on the toxicity of OPs and it is not unreasonable to hypothesize that different OPs could have different susceptibilities to the enzymes involved in their detoxification. It would be interesting to get *in vitro* data on the breakdown rates of different OPs by the main detoxifying enzymes (GST, cytochrome P450, paraoxonase and phosphotriesterase) and see if these values help to predict the toxicity of OPs.

In an attempt to make the data collected in this project comparable with previously published data on the inhibition and reactivation rates of chemical warfare agent OPs all data was analysed using the methods published in references (150) and (65).

4.4.2 OP degradation rate.

The only OP which degraded by a noticeable amount over the 20 hour time period measured was methamidophos. It took 2 hours for the sample to degrade by roughly 3% and as stocks of this OP weren't kept for longer than 2 hours the degradation of methamidaphos would have had a negligible effect on the results of the inhibition assay.

It was thought that the stability of the OPs could also have an effect on their LD_{50}s. Depending on the OP and the dose ingested, the symptoms of poisoning can manifest after several minutes to several hours (159) and as Figure 43 showed all OPs except methamidophos were stable for 20 hours. Even though methamidophos was the least stable it had only degraded by 30% after the 20 hour incubation at room temperature and physiological pH which would leave a large window of time for it to inhibit AChE in an organism before non-biological breakdown caused a significant reduction in its physiological concentration.

4.4.3 OP susceptibility to oxime reactivation.

It was interesting that for all tested OPs obidoxime had a faster reactivation rate than pralidoxime but showed a reduced affinity (apart from with methamidophos inhibited AChE-d). This indicated that obidoxime must have been more reactive towards the phosphate adduct of OP inhibited AChE-d than pralidoxime. A previous study showed obidoxime to be a faster reactivator of wild type human AChE inhibited

by the same OP adducts as the ones used in this study (65), however, obidoxime was shown to bind tighter than pralidoxime to all OP- human AChE conjugates apart from methamidophos. Interestingly the opposite result was obtained using AChE-d. The reactivation experiments in reference (65) were carried out at 37^{o}C, this would have contributed to the differences seen in the values obtained for k_r and K_d but the change in values should have been consistent for each OP-AChE-d conjugate, this was not the case. Reference (65) used human red blood cell ghosts as the source of AChE which had a 10% difference in sequence identity compared to AChE-d. These differences caused a change in the catalytic rate of AChE-d (80) so it is possible that they would also change the affinity of the enzyme for the two oximes. The use of red blood cell ghosts also meant that membranes were present in all stages of the protocol, and to overcome the degradation of AChE at low protein concentrations the red blood cell ghosts were re-suspended in human plasma that had been treated with soman to remove BChE activity and then dialysed to remove excess soman. The lipids and plasma proteins present in the OP inhibited human AChE sample could have interacted with the oximes which is another possible contribution to the differences seen in the reactivation rates. These differences meant that NMR data collected on organophosphorus chemical warfare agents interactions with AChE-d could not be compared to the kinetic data in reference (65) because the differences in the two AChE isoforms would likely cause AChE-d to have an altered ranking of k_r and K_d values for the OP chemical warfare agents than human AChE. This would mean that any changes a chemical warfare agent OP caused in the NMR spectrum of AChE-d could not be related to reactivation rate as this data was not available.

The data for the reactivation of chlorfenvinphos inhibited AChE-d by obidoxime (Figure 44 D) is interesting as it gave a K_d of around 1.9 mM, the other OPs had K_ds in the range of 250 – 750 µM. A new sample of chlorfenvinphos inhibited AChE-d was made and its reactivation by obidoxime was retested using the same methods as before, the K_d obtained in this repeat was around 1.5 mM. Although the repeat produced a smaller K_d it was still larger than would be expected based on the K_ds of other OPs. With the exception of chlorfenvinphos, all the K_ds for pralidoxime and obidoxime were within 300 µM when tested against the same OP. Chlorfenvinphos

showed a difference of over a mM in the K_ds for the two oximes. At the concentrations used in this assay the obidoxime induced hydrolysis of ATCh was insignificant so after accounting for it the K_d values were unchanged. Spontaneous hydrolyses of the phosphate adduct was unlikely to be the cause as the K_d of pralidoxime for chlorfenvinphos inhibited AChE-d would also have been high, in reality it was 233 µM.

Figure 46 A showed that the size of the phosphate adduct that was left covalently bound to the active site of AChE-d after inhibition by an OP was a relatively good indicator of how susceptible it would be to reactivation. Unsurprisingly the size of the adduct didn't appear to be the only factor effecting reactivation as the relationship between size and reactivation rate was not linear for all OPs but the trend did show that smaller adducts were reactivated faster. This trend was not seen when plotting K_d against phosphate adduct size which meant based on this data the size of the adduct had no predictive value on the affinity of oximes for OP inhibited AChE-d.

Only four OPs and two oximes were used in this work which was a small data set, this meant that more OPs and oximes needed to be tested to confirm these results. It would also be interesting to test OP oxime pairs with a wider range of reactivation rates, K_ds and molecular volumes than those presented in this data set. This would allow the relationship between reactivation kinetics and adduct size to be more accurately determined and help to identify if any relationships does exist between K_d/k_r and adduct size.

4.4.4 Inhibition potency of the oximes.

Based on pralidoxime having a lower K_d than obidoxime for all OP-AChE-d conjugates apart from methamidophos, it was assumed that pralidoxime would have a lower IC_{50} for AChE-d than obidoxime. However, as Figure 47 and Table 19 show, the difference between the IC_{50} values for the oximes ware not statistically significant.

For an oxime to reactivate OP inhibited AChE-d it would likely need a certain affinity for AChE-d but, as this work showed, two oximes with the same affinity for AChE-d had different reactivation kinetics for each OP. So the affinity of an oxime for AChE-

d is unlikely to be a good indicator of usefulness of an oxime as a countermeasure to OP poisoning.

Chapter 5. NMR investigation of the inhibition of a designed isoform of acetylcholinesterase by organophosphates.

5.1 Introduction.

5.1.1 Background to Saturation Transfer Difference (STD) NMR.

STD NMR was developed by Moriz Mayer and Bernd Meyer in 1999 (160), the technique was developed to allow the detection of small molecules binding to larger proteins using the small molecule signal as the reporter. The experiments utilised shaped pulses to specifically excite small (around 1 ppm) regions of the spectra (161). These shaped pulses saturate the resonances that they hit, meaning that the energy difference between the high and low energy spin states is equalised (162) and because NMR relies on this small difference in the energy levels of spin states to detect a signal (163), saturation results in the signal becoming undetectable.

The premise of the experiment was that two 1D spectra would be collected of a protein ligand sample, one spectrum would have the shaped pulse set far away from any protein or ligand resonances (around -30 ppm), this would result in a standard 1D spectrum and was referred to as the off resonance spectrum. The second spectrum or “on resonance spectrum” was collected with the shaped pulse in a region of the spectrum that would excite protein resonances but not the ligand resonances. A chemical shift between 0 and -2 ppm was usually chosen for the on resonance experiment (164). The fact that this ppm range was only sparsely populated by protein resonances was not a problem because the saturation that the shaped pule imparts on the protein resonances it excites quickly diffuses to all protein resonances, so as long as even a small part of the protein was excites with the pulse the whole protein became saturated, this happens more efficiently for larger proteins (165). If the ligand were to bind to the protein that had been saturated, some of the proteins saturation would be transferred to the bound ligand.

This would result in the ligand peaks having a lower intensity in the on resonance spectrum. The off resonance spectrum is then subtracted from the on resonance spectrum to produce the difference spectrum, so in theory, only the resonances of the bound ligand will be present in the difference spectrum (166) although artefacts and false positives can occur. Figure 48 gives a cartoon representation of this.

STD experiments are sensitive to binders with K_ds in the range of 10^{-3} – 10^{-8} M (160). During the saturation time of the experiment ligands need to bind to the protein, receive a transfer of saturation and then diffuse off the protein so another ligand can bind. Only the free ligand is detected as the bound ligand will produce very broad signals as it adopts the long correlation time of the protein it is bound to. If the ligand binds too tightly then the rate at which it diffuses off the protein will be very slow so new ligands can't bind to the protein and receive a saturation transfer. This results in the population of partially saturated ligand being low so no drop in signal in the on resonance spectrum is seen. If the binding is too weak the amount of ligand that binds and receive a saturation transfer is low so again, no drop in signal is seen in the on resonance spectrum (167). Despite STDs limitations in the direct detection of tight binding ligands, a method does exist that uses the displacement of a ligand with an STD observable affinity by a much tighter binder to be detected. This works by measuring the drop in the signal of the weaker ligand in the difference spectrum when the tighter binder is added. By using this method the affinities of different ligands can be ranked (168).

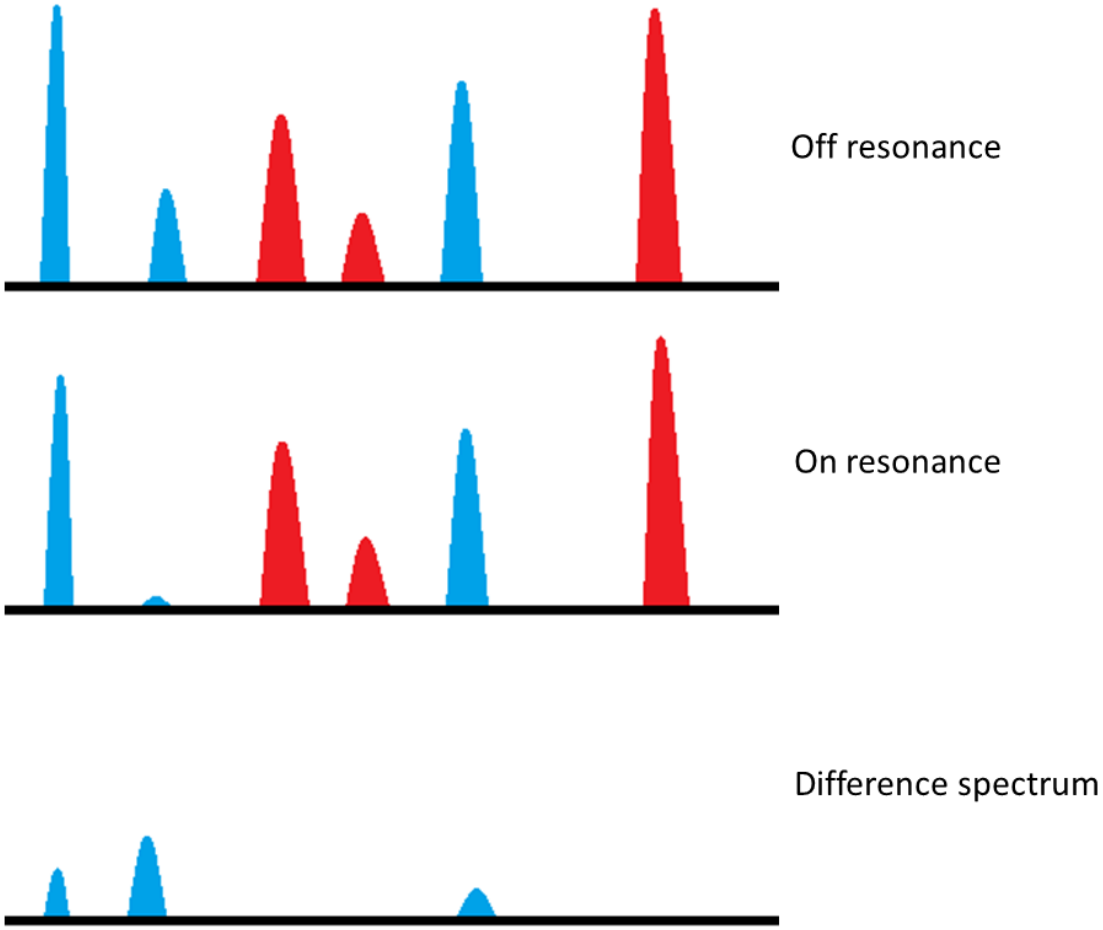

Figure 48. Cartoon representation of an STD experiment. A binding ligand is represented in blue and a non-binding ligand in red. The peaks with the largest intensity in the difference spectrum were in closest proximity to the protein. The difference spectrum is phased 180^{o} to the off and on resonance spectrum.

Another useful property of STD experiments is that nuclei that are in close proximity to the protein show a larger STD effect than the more distant nuclei. This can be used in conjunction with protein observe experiments to determine the orientation of the ligand in the active site (169).

5.1.2 2D NMR experiments in ligand binding studies.

The use of chemical shift perturbation in 2D NMR experiments (^{1}H, ^{15}N HMQC-SOFAST for example) has been extensively reported (170)(171)(172). The premise is that a 2D spectrum of isotopically labelled protein is collected, ligand can then be titrated into the sample. If the ligand binds, the residues in close proximity to it will be in an altered chemical environment resulting in their peaks being located at a

different chemical shift. This technique can be used for a range of different applications such as determining the K_d of a ligand for a protein (173). If the 2D NMR spectra of the protein is assigned and a structure of the protein has been determined then the binding site of the ligand can be determined by mapping the peak shifts onto the structure, this process can also be used to detect conformational change if the residues whose peaks move are in different parts of the protein (174). The benefit of protein observe methods is that a proteins response to the binding of the ligand can be studied at atomic resolution. The downsides include information on how the ligand is effected by binding is not obtained, the need for isotopically labelled protein, long acquisition times of 2D experiments, proteins over 30 kDa becomes difficult due to the crowded spectra of broad peaks and if detailed information on the structural changes in the protein is required, a large investment of time is needed to assign the peaks to the each residue (175).

Tight and week binding ligands can have different effects on the peaks observed in the NMR spectra. Week binding ligands will result in fast chemical shift exchange. This means that as the concentration of ligand is increased the effected peaks of the protein will migrate from the unbound position to the bound position in a dose dependent manner. When saturation is achieved the peak will remain in the same position. When a tight binding ligand is used the system is in slow exchange and two peaks will be present for each of the effected protein residues, one for unbound and one for bound. As the concentration of the ligand is increased the unbound peak will reduce in intensity and the intensity of the bound peak will increase. Figure 49 displays this point graphically. OPs are covalent inhibiters so will be in slow exchange, however AChE-d was incubated with OPs for a long enough time that the vast majority of the sample was inhibited so only one peak is present for each of the effected AChE-d residues.

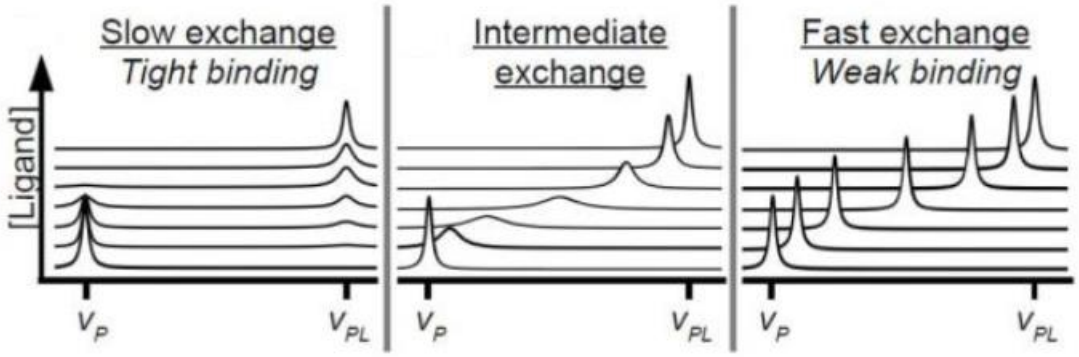

Figure 49. graphic representation of the different chemical exchange regimes. This Figure is an altered version of one found in (176).

5.1.3 Use of NMR to study AChE.

Papers have been published that used NMR to study AChE (177)(178)(179), all of which have been ligand observe experiments that either tried to identify reversible binders to be used as Alzheimers drugs (178) or as an alternative to the Ellman's assay to study the kinetics of AChE (177)(179). No studies could be found that used AChE with a mutated active site serine to study the affinities of OPs. This was surprising as papers have been published on the effect of mutations on the activity of AChE (137) and STD experiments have the potential to not only inform on affinity of an OP but also its chemical motifs that interact closely with AChE. As discussed in chapter 2, no studies using 2D NMR experiments on isotopically labelled AChE have been published. This has meant that the only studies on the effect of OP inhibition of AChE structure have been X-ray crystallography based. These studies have identified differences in the structure of paraoxon (74) and sarin (180) inhibited AChE. In (73) quantitative structure activity relationship regression analysis was used to derive an equation to predict the reactivation rate of OPs based on their molecular volume, the electronegativity of their chemical groups and their predicted orientation in the active site of AChE. The equation produced by this work was generally able to predict reactivation rate with enough accuracy to rank the rates relative to each other. However, the equation was not successful at predicting the reactivation rates of all the tested OPs which indicated that the equation was not taking all the necessary parameters into account. It was thought that the changes in the X-ray structures of AChE after inhibition with an OP could be contributing to the

reactivation rate so it was decided that NMR should be used to try and detect perturbation of residues caused by different OPs and see if there was a correlation with certain peak shifts and the reactivation rate of different AChE-OP complexes. The benefit this would have over the X-ray crystallography method was that the solution state of the enzyme would be observed, the data would be quicker to acquire and molecular dynamics information could potentially be obtained from the NMR spectra.

5.2 Methods.

5.2.1 Producing OP inhibited AChE-d samples.

OP inhibited samples were made using the methods in section 4.2.4 except the AChE-d concentration was 20 µM instead of 5 µM. The elution was used to make a 350 µl sample in phosphate buffer containing 5% D_2O with a 14 µM concentration of OP inhibited AChE-d. A 5 mm Shigemi tube was used in the data collection.

5.2.2 Collection and processing of HMQC-SOFAST data.

HMQC-SOFAST (111) data using azamethiphos, fenamiphos, methamidophos and chlorfenvinphos was collected on the NMR machine at Kent described in section 3.2.2. The data concerning tabun, soman, cyclosarin and VX was collected on an NMR spectrometer at Defence Science and Technology Laboratory (DSTL), Porton Down, which had the same specifications as the one at Kent.

^{1}H, ^{15}N HMQC-SOFAST experiments were collected and processed as described in section 3.2.2. The AChE-d concentration was 14 µM for all spectra.

The TOPSPIN software package was used to pick 43 peaks in the HMQC-SOFAST spectrum. To decide which peaks to pick two different spectra of un-inhibited AChE-d were used. These spectra had been collected under identical conditions on two separate samples of AChE-d. For a peak to be selected it had to be easily resolved from nearby peaks either because of its high intensity or because of its position in a sparsely populated region of the spectrum. The peak also had to be seen in both spectra of un-inhibited AChE-d, this was done to prevent noise from being mistaken as peaks. The two un-inhibited spectra also allowed the peak shift due to normal sample variation to be determined. If the peak shifts caused by OP inhibition were less than the peak shifts caused by sample variation they were discarded from the data set.

In the spectra of OP inhibited AChE-d the peaks in closest proximity to the position of the picked peak in the un-inhibited spectra were picked. The difference in peak positions between the two spectra was calculated as the hypotenuse after the ^{15}N

chemical shifts were adjusted by a factor of 0.26 to account for the different chemical shift ranges of ^{1}H and ^{15}N.

5.2.3 Production of AChE-d Ser 204 -> Ala mutant.

The active site serine of AChE-d was mutated to an alanine, this was done to produce an AChE-d mutant (AChE-d S204A) that would bind to OPs but not form a covalent bond with them. The quick change mutagenesis method was used to achieve this. The primers in Table 20 were designed to introduce this mutation. The mutagenic reaction was carried out using the protocol and reagents supplied by Agilent in their QuikChange II Site-Directed Mutagenesis Kit (181). The resulting plasmid was sent for sequencing to confirm that only the desired mutation had been introduced. The plasmid containing the AChE-d S204A gene was transformed into Shuffle *E. coli* cells. Protein expression and purification was carried out using the same protocol as AChE-d (Sections 2.2.2 – 2.2.4). The PCR conditions used were 30 cycles of 1 min at 94^{o}C for denaturation 2 min at 55^{o}C for primer annealing and 3 min at 72^{o}C for extension.

Table 20 . The primers used in the quick-change mutagenesis of Ser 204 to Ala in AChE-d.

Primer direction	Primer sequence
Forward	ACTGTTTGGTGAAGCAGCCGGTGCAGCAAG
Reverse	CTTGCTGCACCGGCTGCTTCACCAAACAGT

5.2.4 STD NMR analysis of OP binding to AChE-d S204A.

As with the NMR experiments in section 5.2.2, samples containing organophosphorus chemical warfare agents were run on the NMR at Porton Down and samples containing pesticide OPs were run on the NMR at the University of Kent.

The samples were made in in phosphate buffer (20 mM sodium phosphate, 100 mM NaCl, pH 7.4) containing 0.5 mM OP, 5% deuterated methanol and 5.5 µM AChE-d S204A, the final volume was 550 µl. Samples were collected in 5 mm NMR tubes. An exponential window function 0.3 Hz was applied to all spectra.

The STD experiments used 8 dummy and 256 real scans with a time domain of 32768 points and the spectral width was 16 ppm. The saturation time was 2 seconds and

the shaped pulse used for saturation was an Eburp2.100 pulse set at -30 ppm for the off resonance portion of the experiment and -2 ppm for the on resonance portion. All data was collected at 25^{o}C. All spectra were phased to 180^{o} from the reference spectra so binding was indicated by positive peaks in the difference spectrum.

To obtain the excitation profile of the Eburp2.1000 shaped pulse, a 550 µl sample of D_2O in a 5 mm NMR tube was used. In a ^{1}H 1D experiment using the Eburp2.1000 pulse as the source of excitation, a spectrum was collected for 1 scan every 0.1 ppm between 0 and 10 ppm. This was achieved by changing o1p. The intensity of the residual water peak was measured in every spectrum and the data was plotted using Excel. The experiment was carried out at 25^{o}C on the Bruker Avance III 600 MHz (14.1 Tesla) 4-channel 5-amplifier NMR spectrometer with a QCI-F cryoprobe at the University of Kent.

5.2.5 Measurement of ^{31}P chemical shifts.

Samples containing organophosphorus chemical warfare agents were run on the NMR at Porton Down and samples containing pesticide OPs were run on the NMR at the University of Kent.

The samples were 0.5 mM OP in phosphate buffer containing 5% deuterated methanol. The sample volume was 550 µl and all samples were collected in 5 mm NMR tubes.

The ^{31}P experiments used 4 dummy and 512 real scans with a time domain of 131072 and a spectral width of 396 ppm. Proton decoupling was employed. ^{19}F decoupling wasn't available so the peak position of OPs containing a ^{19}F was measured at the midpoint of the two ^{19}F coupled peaks. An exponential window function of 5 Hz was applied to all spectra.

5.3 Results.

5.3.1 HMQC-SOFAST experiments.

In an attempt to investigate whether inhibition of AChE-d by OPs with different reactivation rates caused perturbation of different residues, ^{1}H, ^{15}N, HMQC-SOFASTs were collected on un-inhibited AChE-d and AChE-d inhibited by each of the pesticide OPs shown in Figure 39, and tabun, soman, cyclosarin and VX (Figure 9 A and B). Figure 50 shows the structure of the phosphate adducts that were left bound to Ser 204 of AChE-d after inhibition with each of these OPs. Because unreacted OP was removed, these adducts would be responsible for any perturbation of residues seen in the NMR spectra of inhibited AChE-d.

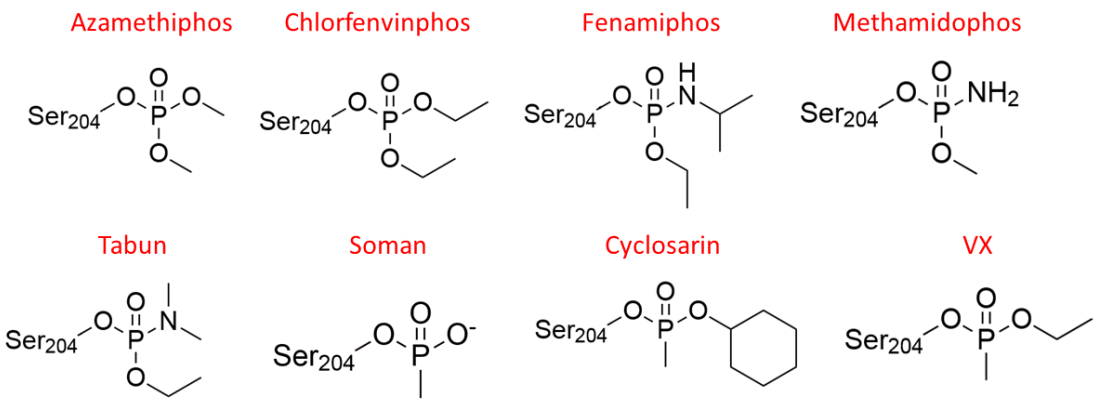

Figure 50. The phosphate adducts left bound to the active site serine of AChE-d after inhibition with different OPs. The aged form of soman is shown as this is rapidly produced after inhibition.

Figure 51 shows the peaks in the ^{1}H, ^{15}N HMQC-SOFAST that were chosen to assess the impact of OP inhibition on AChE-d. As AChE-d spectra were not assigned, if a peak moved after inhibition its new location could not be determined with any certainty. When comparing the spectra of uninhibited and inhibited AChE-d, the peak in the inhibited spectrum that was closest in proximity to the position of the peak in the uninhibited spectrum was picked. In an attempt to assess the variability of the measurements, a ^{1}H, ^{15}N HMQC-SOFAST was collected on two different samples of un-inhibited AChE-d that had undergone identical treatment. The differences in peak position between the two spectra were recorded and provided values for the magnitude in peak shift that could be expected due to sample variation alone. If the

magnitude of a peak shift caused by OP inhibition was lower than the peak shift between the two un-inhibited spectra it was discarded. Figure 52 shows the two un-inhibited spectra of AChE-d overlaid, the reproducibility was poor as not all peaks were in the same place. The cause of this was not known but noise was likely to be a significant factor. Only peaks that were in the same position in both spectra were picked to try and limit the effect the poor reproducibility would have had on the data. Figure 53 shows an example of the peak picking process and highlights the main problem associated with the method. In the chlorfenvinphos inhibited spectrum one peak was in the closest proximity to the positions of peak 41 and 42 in the uninhibited spectrum so it was picked as both of these peaks in the chlorfenvinphos inhibited spectrum. This was because the true position of either peaks could not be determined, it did not indicate that the two peaks had merged. Figure 54 shows the magnitude of the peak shift caused by each of the OP adducts in Figure 50 minus the shifts that were smaller than those between the two un-inhibited spectra. The magnitudes were useful in determining peak shifts that were larger than what could be expected by sample variation but, because the position of each peak could not be accurately determined after inhibition the magnitudes were not necessarily accurate representations of the peaks that had moved the most. For this reason the data was analysed on a binary basis with peaks being classed as having shifted or not based on whether the magnitude of their shift was larger than the control.

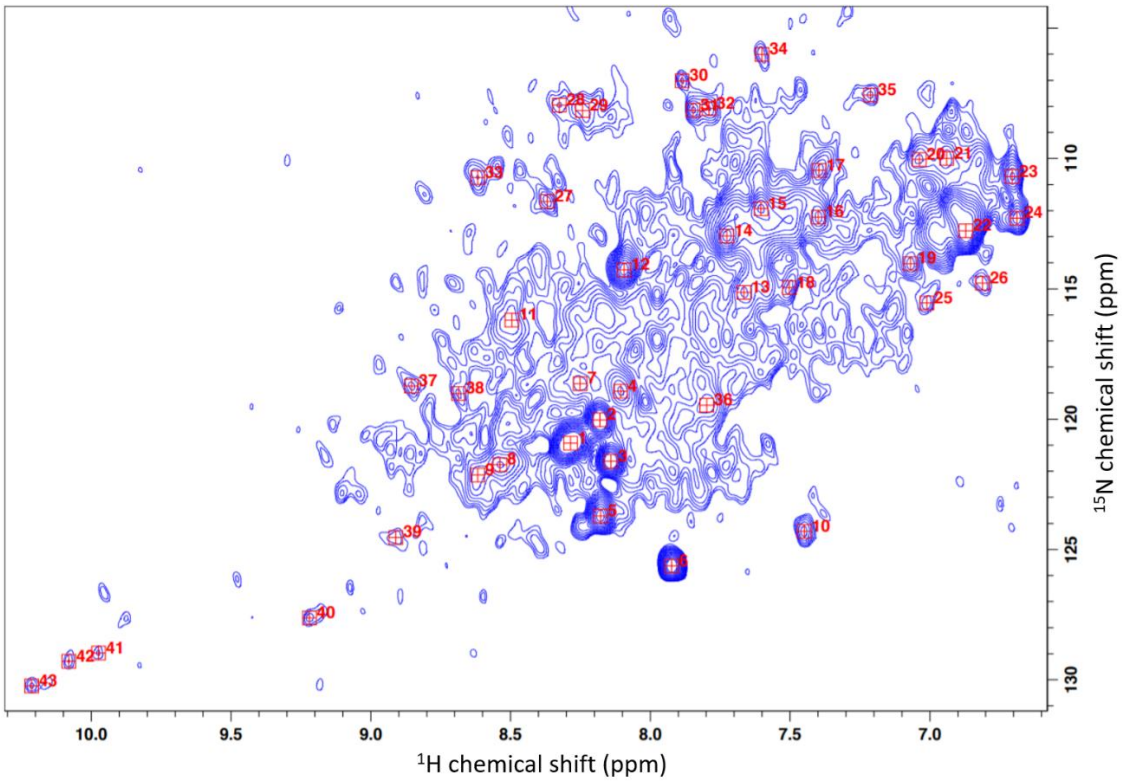

Figure 51. ^{1}H, ^{15}N HMQC-SOFAST of AChE-d with the position of the 43 peaks used to asses AChE-d inhibition indicated by red crosses. The concentration of AChE-d was 14 µM. The spectrum was collected for 1888 scans with 1024 points in the ^{1}H dimension and 100 points in the ^{15}N dimension at 35 ^{o}C. The noise base level was set to 26905.6.

If two OPs caused the same peak to shift this was classified as a peak shift in common. The number of peak shifts that each of the OPs had in common were counted (Table 21 and Figure 55), this was done to identify OPs that caused similar residue perturbations. The mean number of peak shifts in common was 22.3 ± a standard deviation of 4.3 so OPs that had more than 27 peak shifts in common had an above average similarity. These OP pairs and their number of shared peak shifts were, tabun – fenamiphos 28, azamethiphos – chlorfenvinphos 29, and chlorfenvinphos – fenamiphos 31. There were 12 peaks that all tested OPs caused a shift in, their peak numbers were 9, 11, 12, 15, 16, 17, 18, 25, 34, 36, 39, and 41.

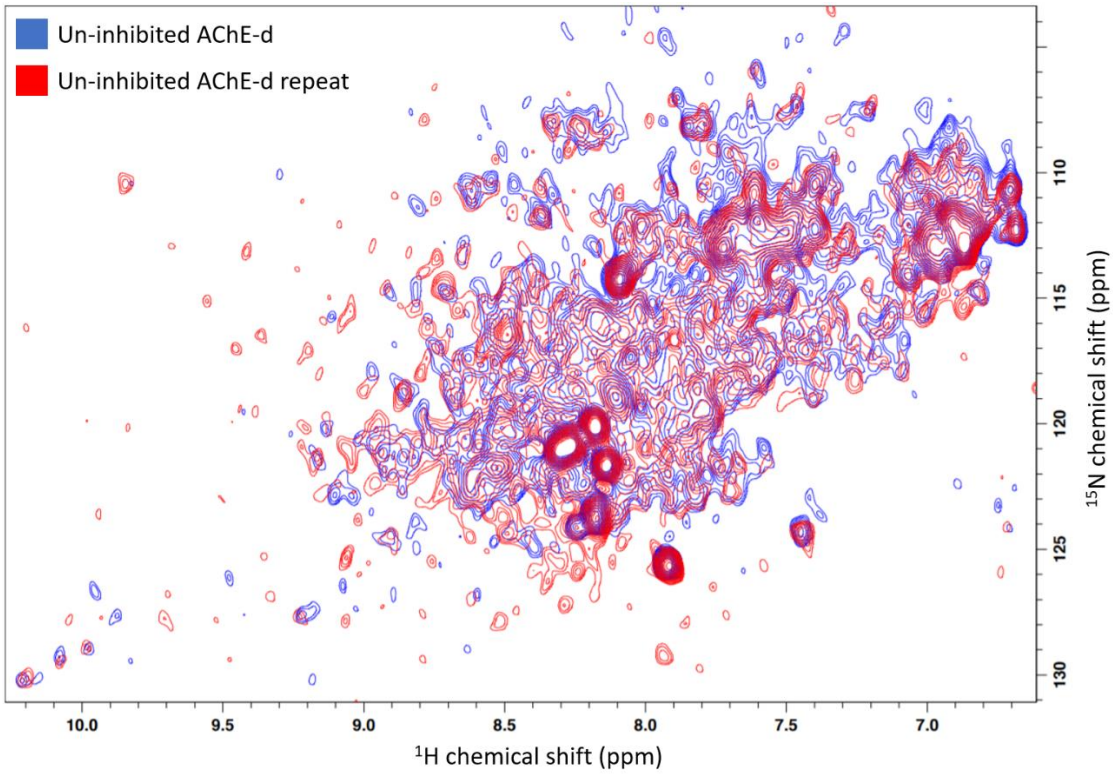

Figure 52. Overlay of the ^{1}H, ^{15}N HMQC-SOFAST spectra of 2 different but identically treated un-inhibited AChE-d samples. The concentration of AChE-d was 14 µM. The spectra were collected for 1888 scans with 1024 points in the ^{1}H dimension and 100 points in the ^{15}N dimension at 35 ^{o}C. The noise base level was set to 26905.6.

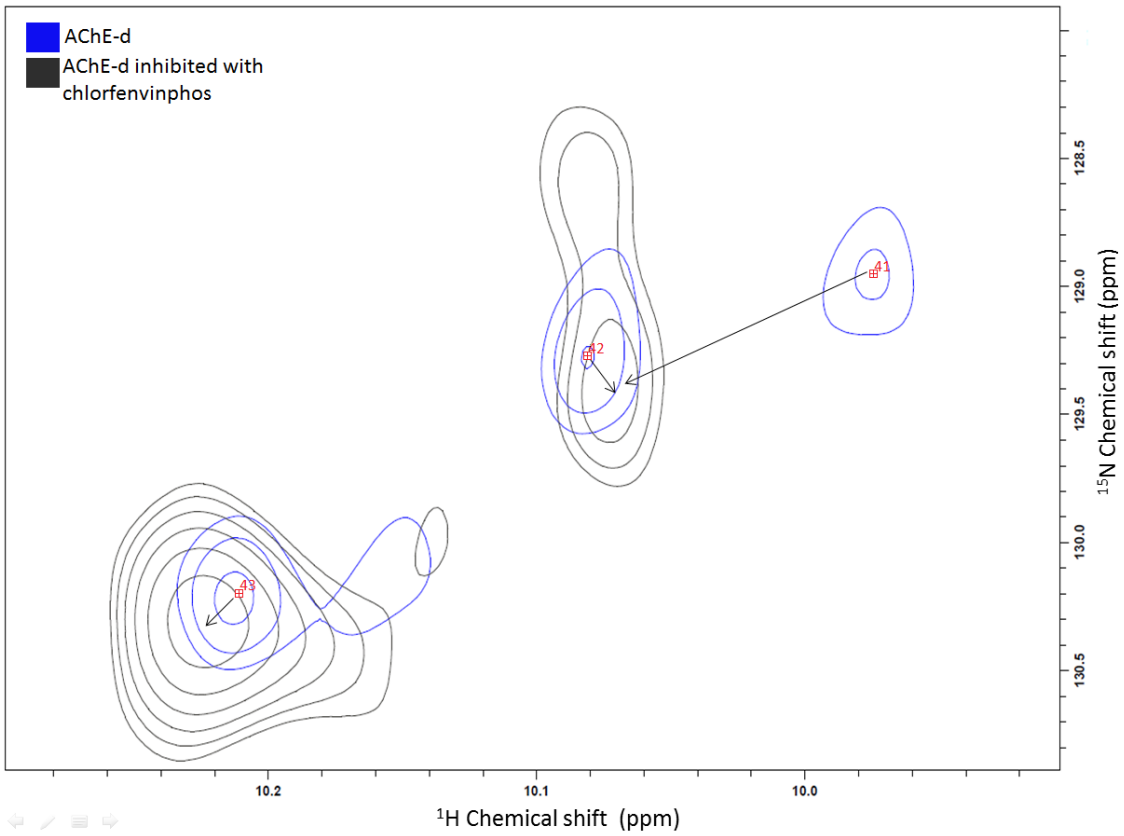

Figure 53. Overlaid ^{1}H, ^{15}N HMQC-SOFAST spectra of un-inhibited AChE-d (blue) and chlorfenvinphos inhibited AChE-d (gray). Arrows indicate assumed movement of the peaks between the two spectra.

The number of peak shifts each OP caused was also measured (Table 22). It was interesting to note that the OPs with the most peak shifts in common were also the ones with the most peak shifts. This could have indicated that the above average number of shared peak shifts was actually caused by the higher probability of having shared peaks due to these OPs having more peak shifts. However, even if this was the case the fact that these OPs caused a larger number of peak shifts was in itself a point of similarity.

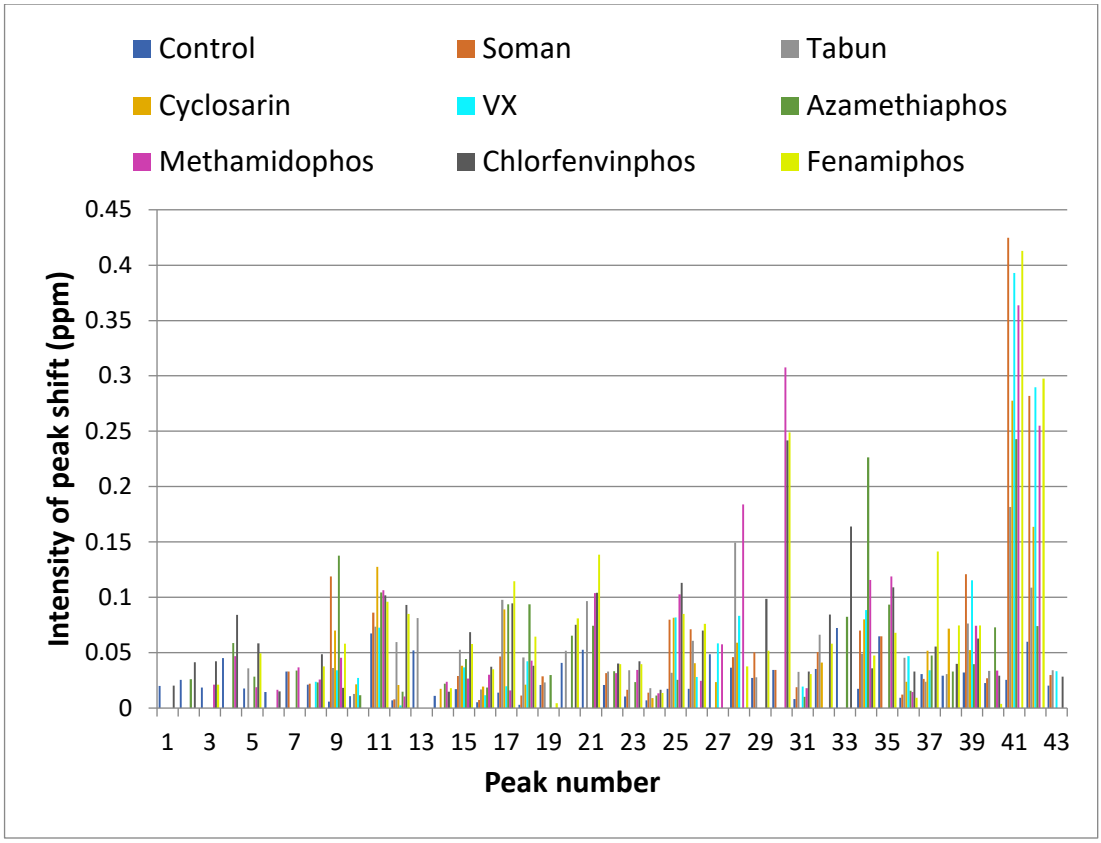

Figure 54. Magnitude of the peak shifts in ^{1}H, ^{15}N HSQC-SOFAST spectra caused by inhibition of AChE-d with OPs. The control data is the difference in peak position between two un-inhibited spectra of AChE-d. Any peak shift magnitudes that were smaller than the control data for a given peak were discarded.

If OPs with similar reactivation rates caused similar peak shifts then azamethiphos, fenamiphos and chlorphenvinphos should have had more peak shifts in common with each other than with methamidophos as the k_r of methamidophos for both oximes was close to 1 min and the other pesticides had k_r values ranging from 0.001 – 0.049 min meaning that methamidophos was much more susceptible to reactivation than the other 3 pesticides. Peaks 20, 37 and 38 were found to shift in the spectra of AChE-d inhibited by azamethiphos, fenamiphos and chlorfenvinphos but not methamidophos. Out of the pesticide OPs methamidophos was the only one that caused peak 27 to shift.

The reactivation data for the organophosphorus chemical warfare agents was collected on human erythrocyte AChE and as discussed in section 4.4.3 this could mean that the ranking of relative reactivation rates of these OPs might be different in AChE-d. However, the same trend in reactivation rates for VX, tabun and cyclosarin

was seen in a study using rat brain AChE (182) which suggests that their reactivation rates relative to each other are independent of AChE isoform. Assuming that AChE-d inhibited with VX and cyclosarin is relatively susceptible to reactivation and AChE-d inhibited with tabun is highly resistant, as seen with other AChE isoforms, then VX and cyclosarin should have had more peak shifts in common with each other than with tabun. The ^{1}H, ^{15}N HMQC-SOFAST data showed that no peaks shifted in response to inhibition with cyclosarin and VX but not tabun. Tabun caused peak 5, 13, 20, and 21 to shifts, the other two OP chemical warfare agents did not. Soman could not be reactivated due to its fast ageing rate (183).

Table 21. The number of peak shifts that each OP had in common with all other tested OPs.

	Soman	Tabun	Cyclosarin	VX	Azamethiphos	Methamidophos	Chlorfenvinphos	Fenamiphos
Soman		25	18	19	23	24	25	27
Tabun	25		19	19	25	22	26	28
Cyclosarin	18	19		18	18	18	18	20
VX	19	19	18		17	18	17	17
Azamethiphos	23	25	18	17		25	29	26
Methamidophos	24	22	18	18	25		27	26
Chlorfenvinphos	25	26	18	17	29	27		31
Fenamiphos	27	28	20	17	26	26	31	

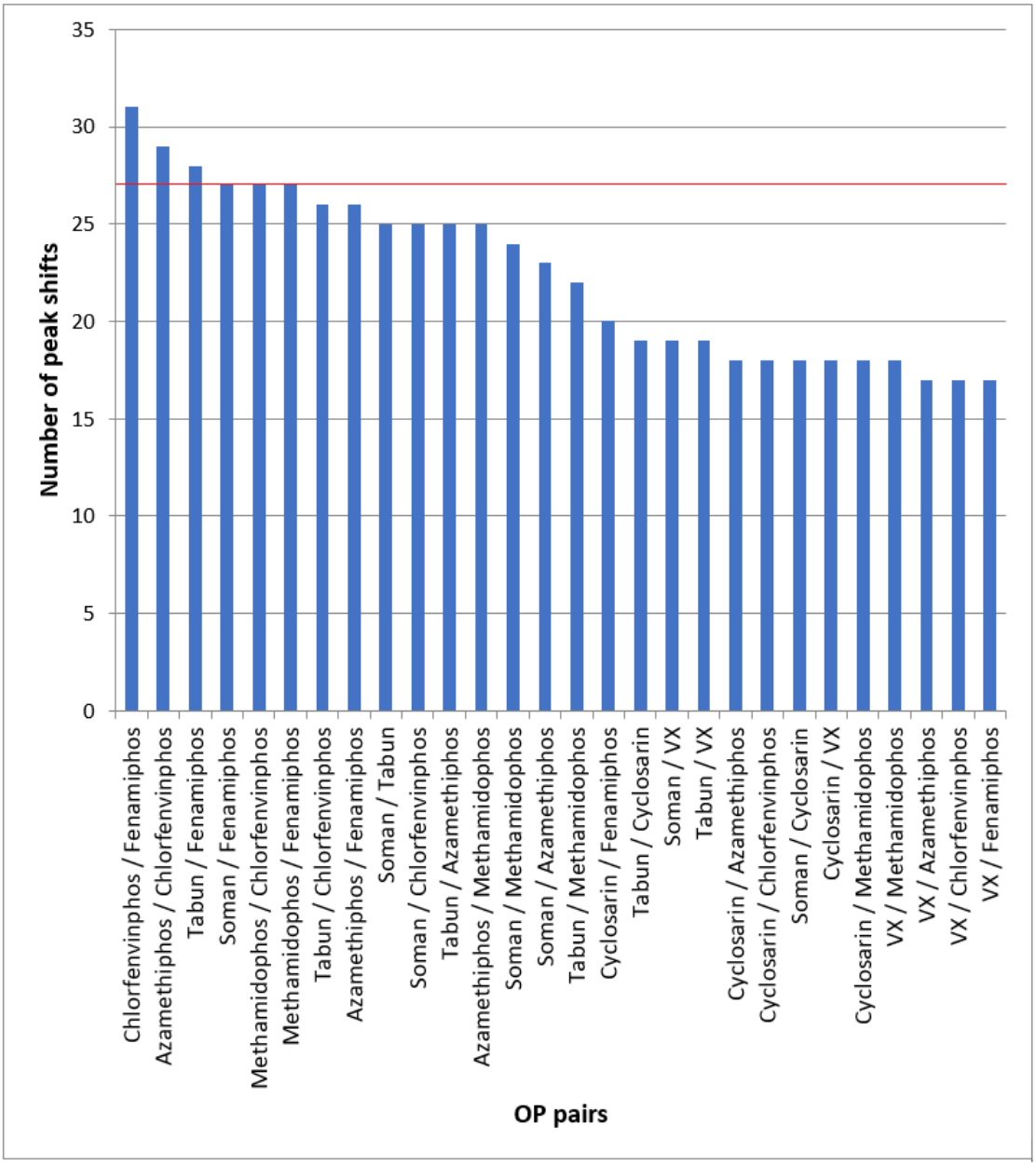

Figure 55. The number of peak shifts in common that each OP pair had, a red line at 27 was included to mark the mean plus one standard deviation of the data set

Table 22. The number of peak shifts in the ^{1}H, ^{15}N HSQC-SOFAST spectra of AChE-d inhibited by each of the OPs. In total 43 peaks were picked. The ^{1}H, ^{15}N HMQC-SOFAST spectra of OP inhibited AChE-d can be seen in appendix 1 – 9.

OP name	Number of peak shifts
Chlorfenvinphos	37
Azamethiphos	32
Tabun	31
Methamidophos	31
Soman	29
Fenamiphos	22
Cyclosarin	22
VX	22

5.3.2 STD analysis of OP binding to a mutated isoform of AChE-d.

Studying the reversible formation of the OP AChE-d complex had an inherent problem in that after an OP bound to AChE-d the phosphorylation of the active site serine occurred creating a new covalent complex. To overcome this, a mutant of AChE-d was made that had the active site serine mutated to an alanine. The hypothesis was that as none of the residues in the active site gorge were mutated the effect on the binding of an OP to AChE-d would be minimally affected, and because the alanine had no hydroxyl group no phosphorylation would occur. The mutant was confirmed to have no AChE-d activity by incubating a 1 µM sample of the protein in Ellman's buffer for 10 minutes, no increase in the absorbance at 412 nm could be detected. This mutant would allow us to only study the reversible part of the interaction of OPs with AChE-d. The mutated isoform of AChE-d was termed AChE-d S204A.

The excitation profile of the Eburp2.1000 pulse used in the STD experiment to selectively excite AChE-d S204A is shown in Figure 56. The tip of the peak which provided maximal saturation of any resonances it hits was relatively small (around 0.2 ppm), but the total peak including the base covered roughly 2 ppm and a small amount of excitation (larger than 1 % of maximum) was still detected out to around

1 and 9 ppm. When using this shaped pulse some saturation of the OP was to be expected because the point of maximal excitation needed to hit a protein resonance, these usually extend out to around -2 ppm. Any OP peak within 4 ppm of the point of maximal excitation (-2 ppm in this case) would be partially excited by the pulse.

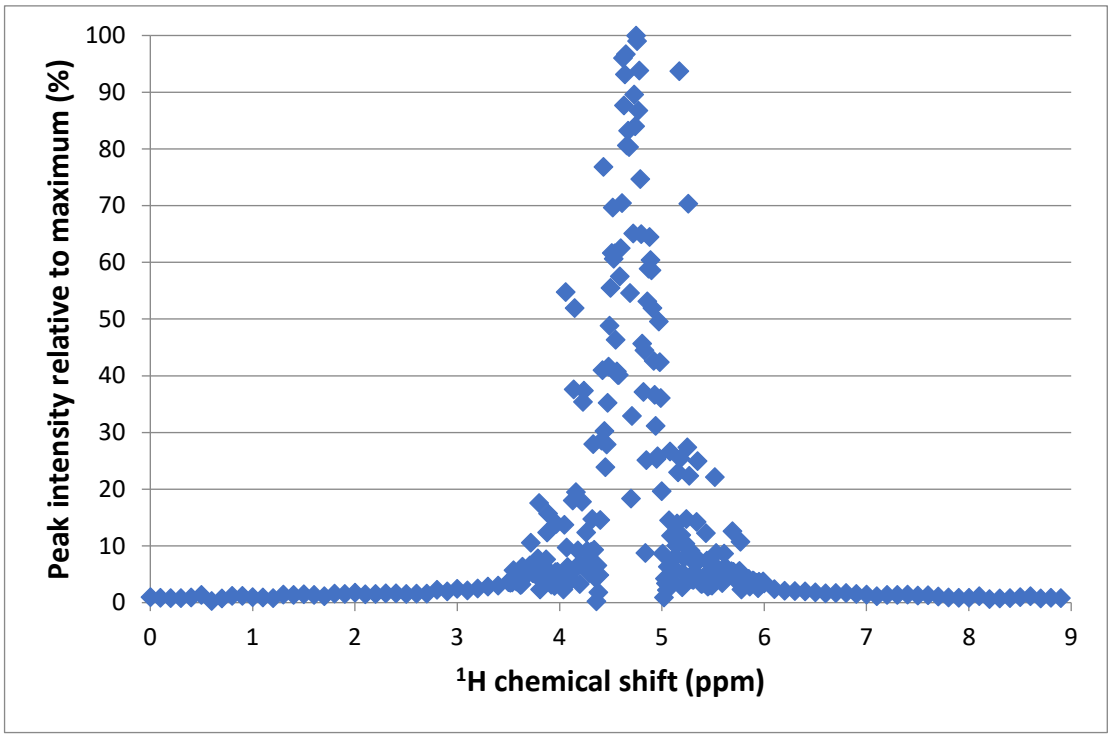

Figure 56. The excitation profile of the Eburp2.1000 shaped pulse centred on the water peak. This is the shaped pulse used to selectively excite proteins in STD experiments.

To identify false positive results, control experiments were done for all OPs, these involved running the STD experiments on samples containing only the OP. If the control experiments gave a positive result it confirmed that the Eburp2.1000 pulse was hitting the ligand. This was not a problem in all cases as if a larger STD effect was seen when the protein was added binding was confirmed (184). Figure 57 shows an example of this, a small peak in the STD spectra of only chlorfenvinphos can be seen at around 1.2 ppm (marked with red asterisk in Figure 57). In the STD spectrum of chlorfenvinphos and AChE-d S204A the peak becomes considerably larger. Because the chlorfenvinphos concentration and STD parameters were identical between the two spectra, the difference can only be explained by binding of chlorfenvinphos to AChE-d S204A.

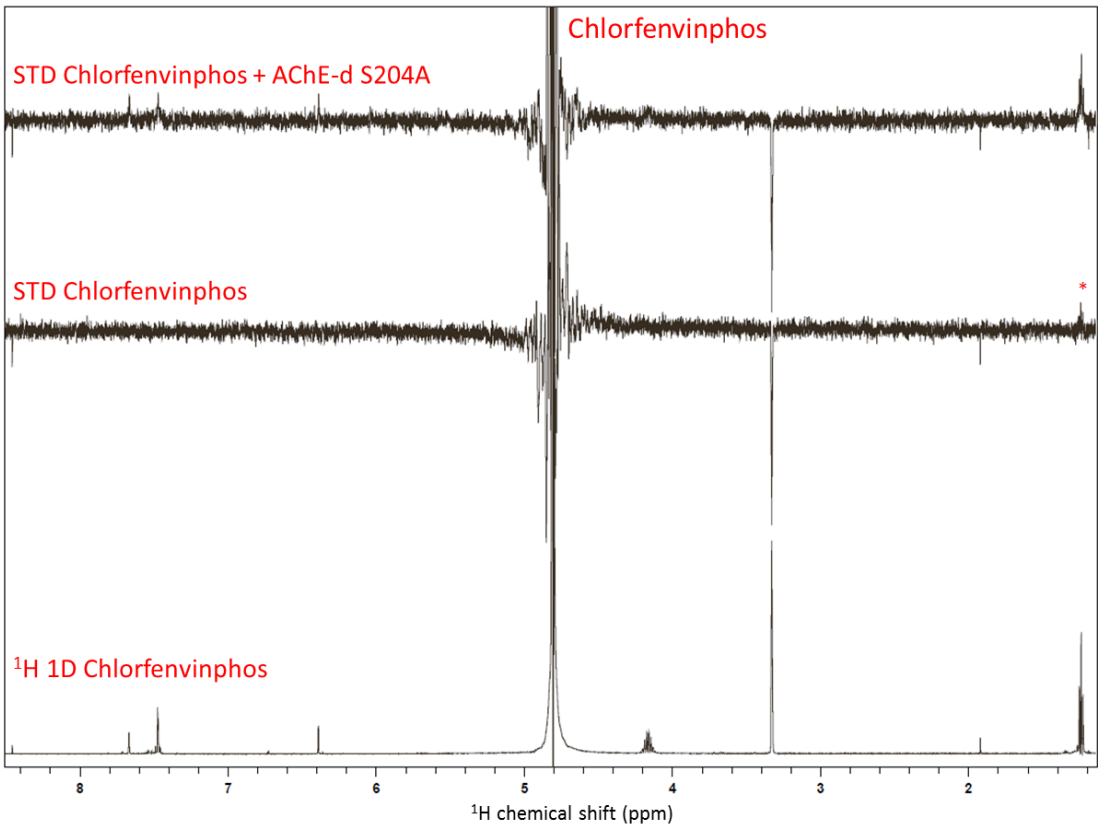

Figure 57. STD NMR experiment of chlorfenvinphos in the presence and absence of AChE-d S204A. Chlorfenvinphos concentrations were 0.5 mM and AChE-d S204A was 5.5 µM. The spectra were collected over 256 scans. The peak at 1.2 ppm in the control spectrum is marked with a red asterisk.

Another type of artefact often seen in STD spectra is intense peaks being present in the difference spectrum, this can occur if a peak has slight differences in its position in the on and off resonance experiments so subtraction of the off resonance experiment from the on resonance experiments doesn't totally remove the peak from the difference spectrum (164). This can be seen in Figure 57 as the methanol peak at around 3.2 ppm. These artefacts had a consistent intensity in the samples that did and did not contain protein so all changes in peak intensity seen in the OP peaks could be attributed to binding.

Binding of azamethiphos, chlorfenvinphos, VX and VM to AChE-d S204A could be detected by STD NMR (Table 24). No binding was detected for Fenamiphos, methamidophos and cyclosarin. The data for tabun was inconclusive as the molecule broke down rapidly meaning there was only a low concentration of tabun in the NMR tube so even if it was binding to AChE-d S204A with an appropriate K_d its concentration would be too low to detect.

It was interesting that binding was detected with VX and not cyclosarin because cyclosarin has been shown to inhibit human erythrocyte AChE at 4 times the rate of VX (65) so it was assumed to be a tighter binder. To test whether cyclosarin was binding AChE-d S204A too tightly to be detected by STD NMR a competition experiment was set up. For this 0.5 mM of VX and cyclosarin were mixed with AChE-d S204A and an STD experiment was performed with identical parameters as before. If cyclosarin had a higher affinity for AChE-d S204A than VX, the VX signal in the difference spectrum would be reduced (185) as cyclosarin would displace it in the active site of AChE-d S204A. As indicated by Figure 58 cyclosarin did not displace VX from the active site of AChE-d S204A as the VX signal at 1.4 ppm in the difference experiment with and without cyclosarin had the same intensity.

Table 24. Detection of binding of each OP to AChE-d S204A by STD NMR. The STD NMR spectra can be seen in Appendix 10-16, and Figure 57.

OP name	Binding detected
Azamethiphos	Yes
Chlorfenvinphos	Yes
Fenamiphos	No
Methamidophos	No
Soman	No
Tabun	Inconclusive
Cyclosarin	No
VX	Yes
VM	Yes

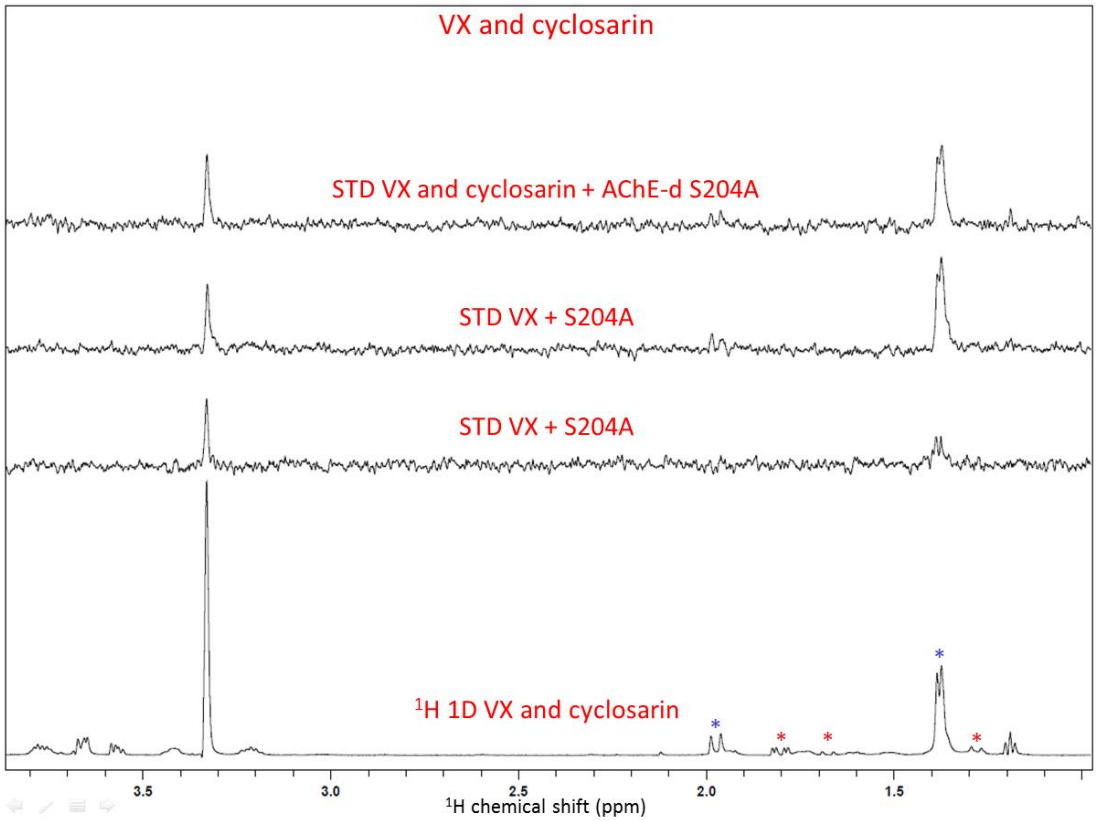

Figure 58. STD data for the competition binding experiment between cyclosarin and VX for AChE-d S204A. OP concentrations were 0.5 mM and AChE-d S204A was 5.5 µM. The spectra were collected over 256 scans. In the off resonance spectrum the VX peaks are marked with blue asterisk and the cyclosarin peaks are marked with red asterisk.

5.3.3 ^{31}P NMR spectra of OPs.

The electronegativity of the phosphate adducts was thought to affect their susceptibility to reactivation by oximes. The ^{31}P chemical shift is highly dependent on the electronegativity of the atoms in the phosphate adduct (186) so the chemical shift of the ^{31}P atom in the phosphate adduct was thought to be a good proxy to assess the electronegativity of the adduct. Attempts were made to inhibit AChE-d with OPs and then measure the ^{31}P chemical shift of the phosphate adducts bound to the protein. The hypothesis was that ^{31}P atoms that had more electronegative surroundings would show higher chemical shifts and in turn be more susceptible to reactivation by oximes. No phosphate signals could be detected in the NMR spectra of OP inhibited AChE-d even after running the experiments overnight (21000 scans), this was likely because of limited concentration of the samples (40 µM), and the large size of AChE-d (62.517 kDa) which would have broadening the phosphorus signals.

Measuring the ^{31}P chemical shift of the phosphate adduct covalently bound to the active site serine of AChE-d would have given the value that was most relevant to oxime reactivation but because this didn't appear to be practical the ^{31}P chemical shifts of the OPs were measured (Table 25).

Table 25. The ^{31}P chemical shifts of several OPs.

OP Name	^{31}P chemical shift (ppm)
VX	60.8
Methamidophos	42.56
Soman	36.26
Cyclosarin	34.03
Azamethiaphos	30.6
Tabun	11.4
Fenamiphos	6.79
Chlorfenvinphos	-6.51

The ^{31}P chemical shifts were plotted against reactivation rate (Figure 59 A and B). The data in Figure 59 A and B was not combined into a single graph because AChE-d was used to obtain the reactivation data of the pesticide OPs (Figure 59 A) at room temperature and the data in Figure 59 B was collected at 37^{o}C using human eurythrocite AChE (65), so as discused in chapter 4, the data were not directly comparable. However, it can be seen that in general OPs with higher ^{31}P chemical shift were reactivated at a faster rate by both oximes.

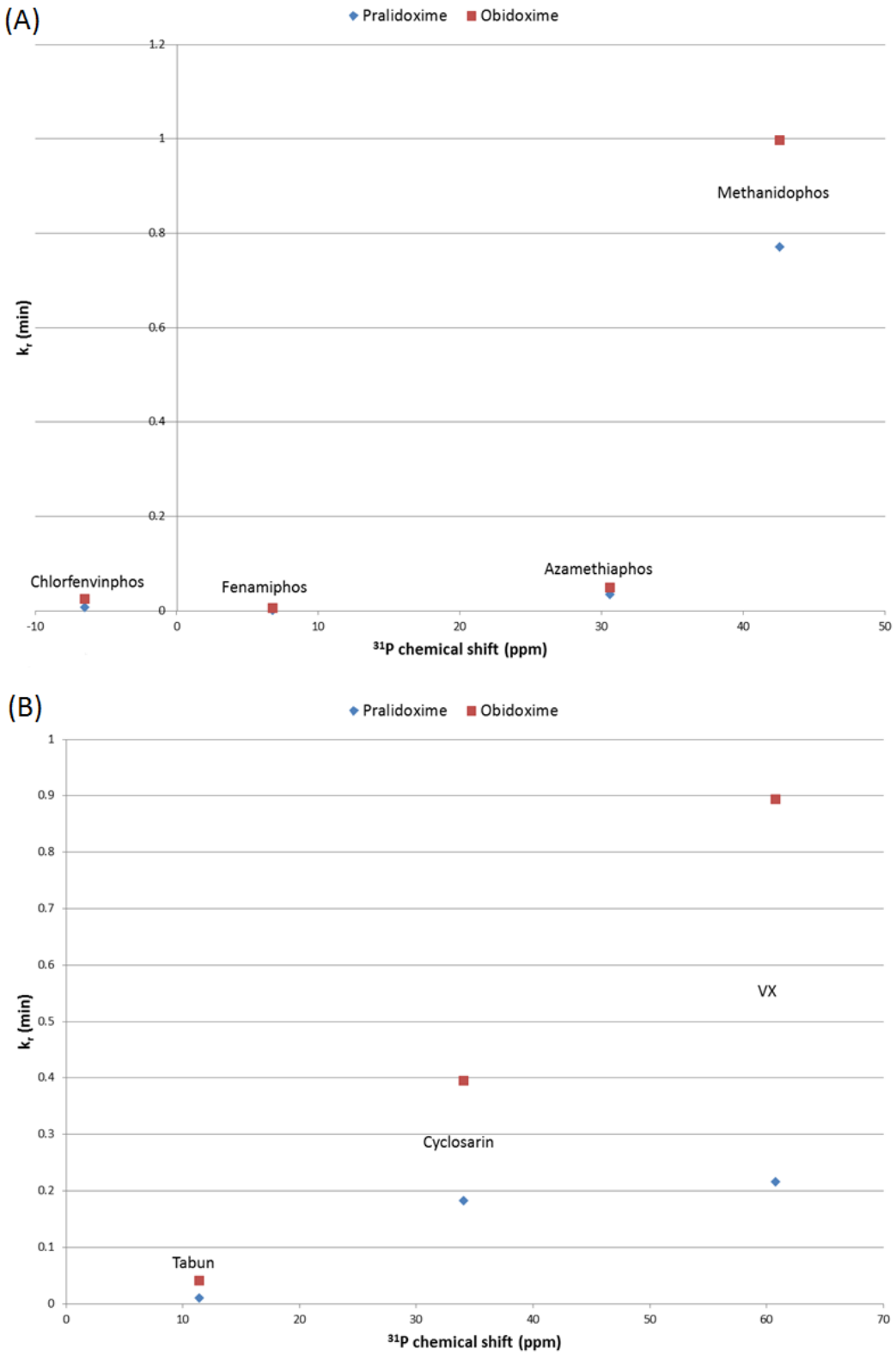

Figure 59. (A) The ^{31}P chemical shifts of azamethiaphos, Fenamiphos, methamidophos and chlorfenvinphos plotted against their reactivation rates by two different oximes. Reactivation rates were obtained using AChE-d (section 4.3.4). (B) The ^{31}P chemical shifts of tabun, cyclosarin and VX plotted against their reactivation rates by two different oximes, the reactivation rates were obtained using human erythrocyte AChE in reference (65).

5.4 Discussion.

5.4.1 ^{1}H, ^{15}N HMQC-SOFAST analysis of AChE-d inhibition.

The peaks that proved easiest to measure were those with a higher than average intensity. The fact that these peaks had higher than average intensities indicated that they were in a flexible and or disordered region of the protein, for instance the C-terminus. This flexibility would impart longer T1 and T2 relaxation times on the nuclei of these residues meaning they would relax at a slower rate so more signal could be detected (176). The active site gorge of AChE-d was not expected to have a higher than average flexibility compared to the rest of the enzyme (187) so the easiest to measure residues were unlikely to be the ones directly interacting with the phosphate adduct. Despite this several peak shifts were identified that were larger than the shifts seen between the two un-inhibited spectra. The peaks that shifted in all OP inhibited AChE-d spectra (peaks 9, 11, 12, 15, 16, 17, 18, 25, 34, 36, 39, and 41) were likely to be close to the active site serine which would explain why they were perturbed by all the OP adducts. Peaks 15, 16, 17 and 18 were in a region of the spectrum where it is common to find the peaks of Asn and Gln side chains (188). Gln 71 and Asn 87 both form part of the active site gorge (Figure 60) so were likely candidates for at least 2 of these peaks.

Peaks 41, 42 and 43 were in a region of the spectrum usually populated by the side chains of Trp residues (188) and as Figure 61 shows, 5 Trp residues were in close proximity to the Ser 204 residue. It was highly probable that some of these Trp residues were the 3 peaks in question.

These peaks could be useful to monitor when trying to detect if a ligand had bound to AChE-d, but in this work the aim was to see if OPs with similar reactivation rates caused similar peak shifts. These peaks were not particularly useful for this task as they shifted after inhibition by all OPs, regardless of the reactivation rate of the OP.

The number of peak shifts caused by each OP should have been related to the size of the phosphate adduct left by the OP as a larger adduct would interact with more residues. Table 26 shows the estimates of the chemical warfare agent OP adducts

volumes and the volume estimates of the insecticide OPs adducts that were calculated in section 4.3.4. Cyclosarin was expected to cause the most shifts in the ^{1}H, ^{15}N HSQC spectra as it had the largest volume but in reality it produced the lowest number of shifts (VX and fenamiphos) (Table 22). Chlorfenvinphos showed the largest number of shifts even though it had an estimated adduct volume of 13150 nm^3 which was very close to the median adduct volume of 12152 nm^3. When the estimated volume of the phosphate adducts were plotted against the number of peak shifts they caused (Figure 62) no correlation was seen. This indicated that the size of the phosphate adduct was not a good indicator of how many residues it would perturb. One reason for this could be that the active site gorge had enough room to accommodate even the larger adducts without any perturbation of the residues and it is the electronegativity of groups of the adduct that determine how residues interact with the adduct so in turn how many peaks shift.

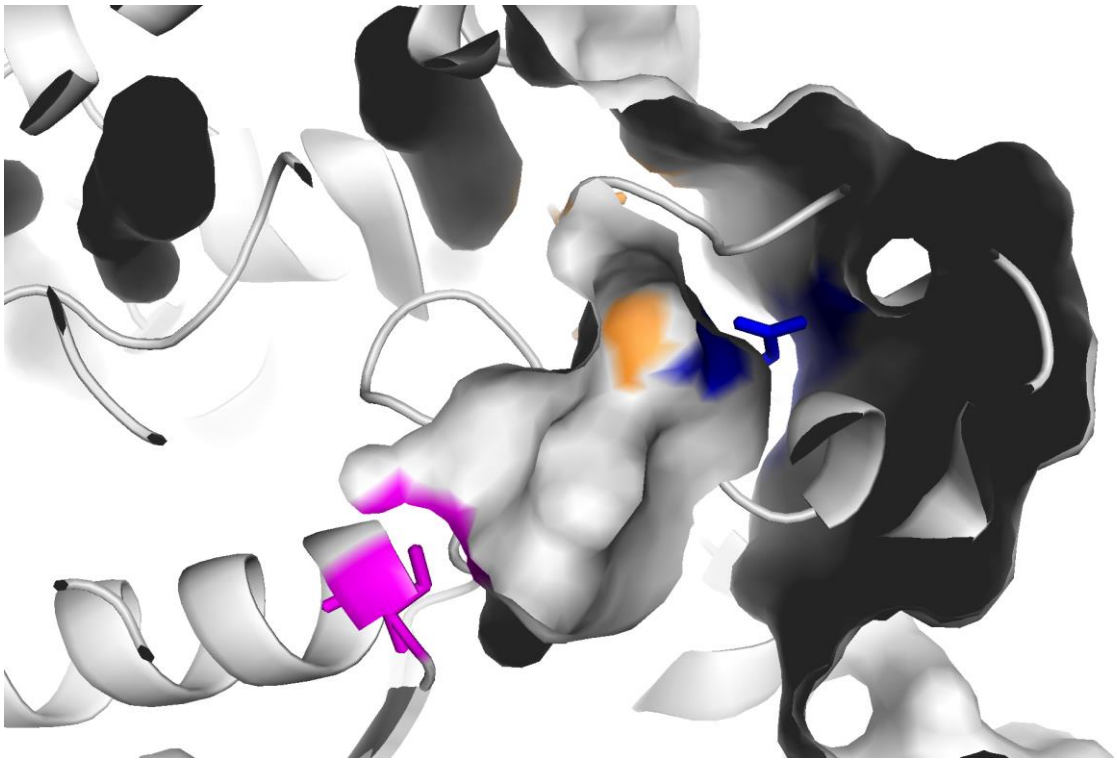

Figure 60. The base of the active site gorge of AChE-d with S204 in pink, Q71 in orange and N87 in blue. The PDB structure with id number 4pqe was used to generate this image.

Several peaks were identified that only appeared to shift in the spectra of AChE-d inhibited with OPs that had slow reactivation rates for pralidoxime and obidoxime. However, care needs to be taken when drawing conclusions from the data involving

organophosphorus chemical warfare agents as their reactivation rates were collected using the human erythrocyte isoform of AChE so these OPs could have different reactivation rates with AChE-d. Even the data collected on the insecticide OPs have problems that limit the conclusions that can be drawn from it. For instance, when the data is viewed in a binary way with peaks being classed as shifted or not shifted, a difference does seem to exist between the peaks shifted by OPs with different reactivation rates. It would be tempting to say that this is evidence that interaction of an adduct with certain residues can confer a certain degree of protection from reactivation. However, when the peak shifts are viewed on the NMR spectra the difference becomes less convincing. As can be seen in Figure 63, the shifts in the position of peaks 37 and 38 caused by inhibition with chlorfenvinphos and methamidophos were similar in magnitude but only the shifts caused by chlorfenvinphos were deemed significant as they were slightly larger. The small difference between peak shifts that were deemed significant (chlorfenvinphos) and insignificant (methamidophos) meant that factors like noise could potentially result in peaks either being included in the list of significant shifts or not. This problem was exacerbated by the low protein concentration (14 μM) used in the HMQC-SOFAST experiments.

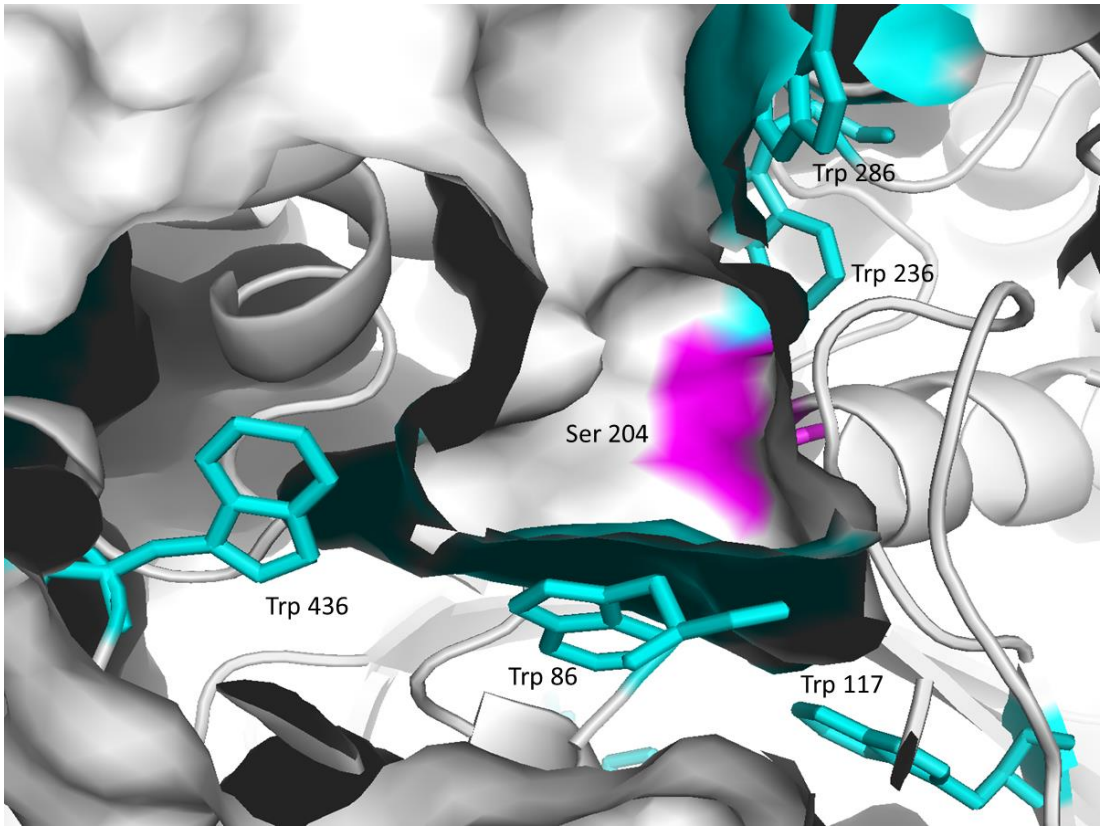

Figure 61. The active site gorge of AChE with Ser204 in pink and 5 Trp residues that were in close proximity to the Ser in cyan. The PDB structure with id number 4pqe was used to generate this image.

Table 26. Volume estimates for the phosphate adducts left bound to AChE-d after inhibition by each of the OPs. The volume estimates are ordered largest to smallest. The volume of somans aged form is given as the ageing process happens with a half-life of around 4 minutes (144) **so the aged form would have been present in the ^{1}H, ^{15}N HMQC-SOFAST experiment.**

OP name	Chemical formula of adduct	Estimated volume (nm^3)
Cyclosarin	$O_2PC_7H_{14}$	16710
Fenamiphos	$O_2PH_{13}NC_5$	15045
Tabun	$O_2PH_{11}NC_4$	13515
Chlorfenvinphos	$O_3PH_{10}C_4$	13150
Azamethiphos	$O_3PH_6C_2$	12890
VX	$O_2PC_3H_8$	10720
Methamidaphos	O_2PH_5NC	8925
Soman	O_2PCH_3	7595

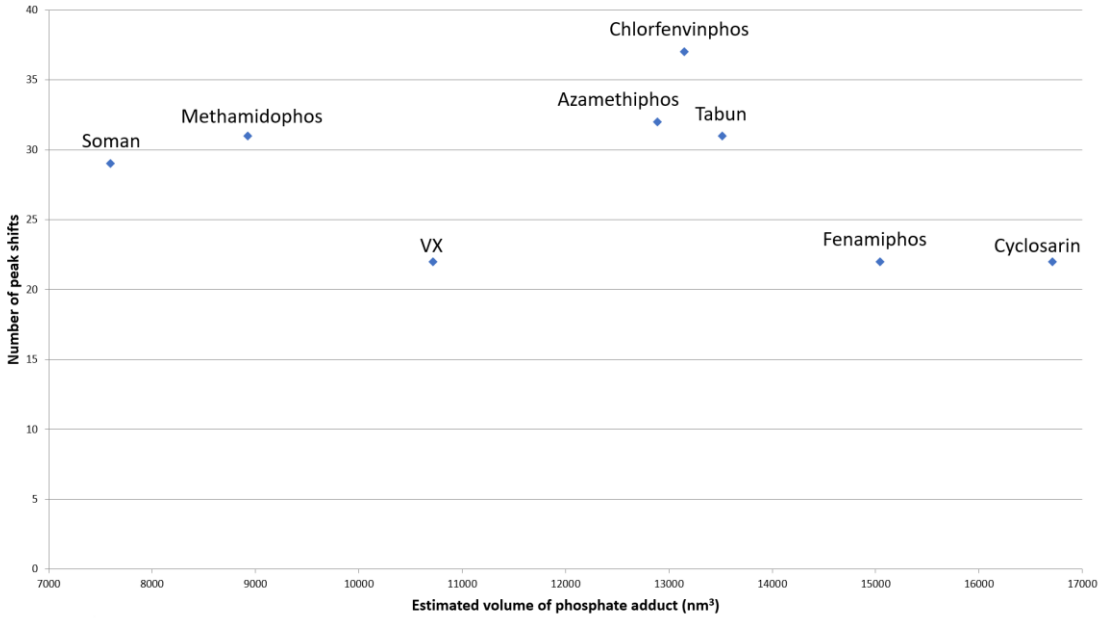

Figure 62. The estimated volume of the phosphate adducts of each on the OPs plotted against the number of peak shifts they caused in the ^{1}H, ^{15}N HMQC-SOFAST spectrum of AChE-d after inhibition.

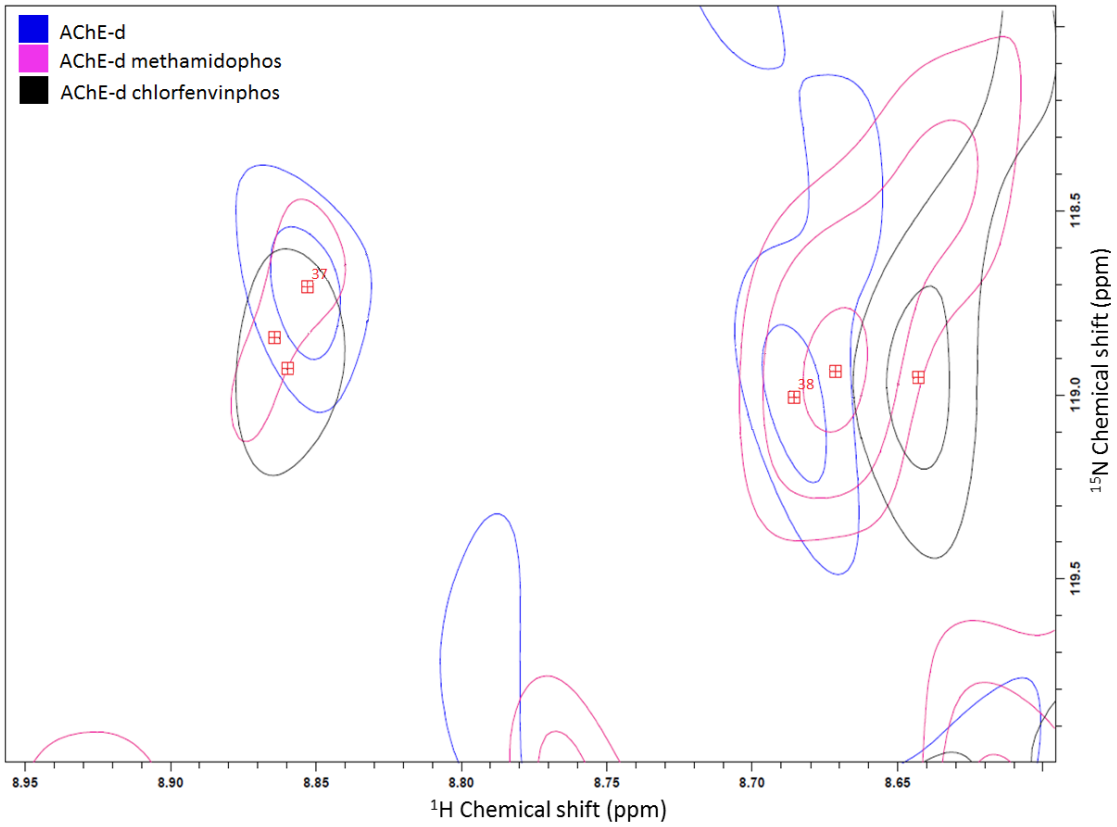

Figure 63. HMQC-SOFAST of un-inhibited AChE-d (blue), methamidophos inhibited AChE-d (pink) and chlorfenvinphos inhibited AChE-d (black). The protein concentration was 14 µM in all samples. The spectrum was collected for 1888 scans with 1024 points in the ^{1}H dimension and 100 points in the ^{15}N dimension at 35 ^{o}C.

5.4.2 Assessment of OP binding using STD NMR.

The fact that VX had a higher affinity for AChE-d S204A than cyclosarin was surprising as cyclosarin has been shown to inhibit AChE-d at a faster rate than VX in multiple isoforms of AChE (182)(65). This suggests that cyclosarin must be much more reactive to the active site serine of AChE than VX to make up for its lower affinity. Cyclosarin has F as a leaving group which has been shown to be a better leaving group than the 2-(diisopropylamino)ethane-1-thiol of VX. This is likely to account for the faster inhibition rate seen with cyclosarin.

STD NMR can reportedly detect binders with affinities ranging from around 10^{-3} – 10^{-8} M (189), this indicated that cyclosarin had a mM K_d for AChE-S204A which is remarkably weak for a compound that has an LD_{50} of 21.9 µg/kg (intravenous in pigs) (190). For VX to have a higher affinity for AChE-d S204A but a lower inhibition rate,

it must have to spend a considerable amount of time bound to the enzyme but not reacting with it, so the assumption can be made that the rate limiting step in the reaction of VX with AChE-d is the phosphorylation of the active site serine. Since cyclosarin was a relatively weak binder but had a faster inhibition rate, it can be assumed that the phosphorylation of the active site serine is the rate limiting step for this OP as well. It was not completely unsurprising that methamidophos and Fenamiphos binding could not be detected as they were both shown to be relatively poor inhibitors of AChE-d in section 4.3.2. It would be interesting to compare the binding affinities and inhibition rates of more OPs to see if the trend of phosphorylation being the rate limiting step is common to all OPs. Whilst the STD data gave some insight into the mechanism of OP inhibition it did not provide useful predictions on the toxicity of OPs as soman and cyclosarin showed no binding but were both highly toxic.

As AChE-d is not completely representative of wild type AChE, interpretation of the data requires care as there is the possibility that VX inhibits AChE-d at a faster rate than cyclosarin. AChE-d S204A had the added problem that a key residue in the enzyme was mutated, this would have affected the affinity of the OPs for the enzyme, but the degree of the affect is unknown.

5.4.3 ^{31}P NMR.

The chemical shift of the ^{31}P signal of an OP appeared to be a relatively good indicator of how susceptible the OP would be to reactivation by pralidoxime and obidoxime. The ^{31}P chemical shift was measured with the leaving group still attached to the OPs, this would have introduced a source of error as the leaving group would contribute to the chemical shift of the OP but was not present on the phosphate adduct that inhibits AChE-d. So the chemical shift measured were not completely representative of the phosphate adducts. A closer correlation could potentially be obtained by measuring the ^{31}P chemical shift of the phosphate adduct bound to AChE-d. High concentrations of the inhibited protein would be needed and a higher field NMR spectrometer would also improve the likelihood of detecting the adduct by increasing the signal to noise of the spectrum (191).

The ^{31}P spectra should have given an indication of the inhibition rates of the OPs because OPs with higher ^{31}P chemical shifts would have had a more de-shielded ^{31}P nucleus meaning it would be more susceptible to nucleophilic attack by the O of the active site serine. As Table 25 shows the ^{31}P chemical shifts were poor indicators of the inhibition rate of the OPs. Chlorfenvinphos had the lowest chemical shift (-6.51 ppm) but inhibited AChE-d faster than fenamiphos and methamidophos which had chemical shifts of 6.79 and 42.56 ppm respectively. This indicated that the leaving group and structure of the OP were likely to be the determining factors of the inhibition rate.

Chapter 6. General conclusions.

6.1 Summary of thesis.

The expression and purification of a designed isoform of human acetylcholinesterase (AChE-d) was optimised resulting in the recovery of around 2 mg of purified AChE-d for every litre of Shuffle *E. coli* grown in 2YT media. Different isotopic labelling schemes were investigated as follows. Uniform ^{15}N labelling, specific ^{15}N labelling of I, L and V residues, specific ^{15}N un-labelling of all residues apart from I, L, V, W and C, specific ^{19}F labelling of W and F residues and uniform ^{15}N and ^{2}H labelling. Uniform ^{15}N labelling produced around 0.6 mg of purified AChE-d for every litre of Shuffle *E. coli* grown in minimal media. Specific ^{15}N labelling of I, L and V residues only produced 10s of µg/l of AChE-d, most likely because an inhibiter of the enzyme that transfers amino groups between residues was added which appeared to be toxic to the cells. The un-labelling method produced around 3 mg/l of purified AChE-d, well resolved peaks on the periphery of the NMR spectrum were lost and several well resolved peaks in the central region of the spectrum were gained (Figure 36). All the ^{19}F labelled precursors for W and F residues caused a drop in AChE-d expression ranging from a 40 % to a 98 % reduction in the AChE-d activity in the lysate supernatant, when an NMR sample was made using AChE-d labelled with the precursor that caused the smallest drop in activity (4-fluorophenylacetic acid), no signal could be detected in the 1D ^{19}F NMR spectrum. Attempts to uniformly label AChE-d with ^{2}H as well as ^{15}N resulted in around 60 µg/l of AChE-d being produced. Uniform ^{15}N labelling of AChE-d was chosen as the best method of labelling AChE-d as it produced a relatively good yield of protein and the NMR spectra of this protein had more well resolved peaks than protein produced using the un labelling method.

The kinetics of the inhibition of AChE-d by four organophosphate (OP) pesticides (Figure 39) were studied and the results were compared with the data published in (65) which presented the inhibition and reactivation rates of human erythrocyte AChE by methamidophos, Fenamiphos, paraoxon-methyl and paraoxon-ethyl. In this thesis paraoxon-methyl and paraoxon-ethyl were replaced with azamethiphos and

chlorfenvinphos respectively as the paraoxons were deemed to be too toxic. Paraoxon-methyl leaves the same phosphate adduct bound to AChE-d after inhibition as azamethiphos, the same is true for paraoxon-ethyl and chlorfenvinphos. The OP pairs that have the same phosphate adduct will give the same result in reactivation experiments as the phosphate adduct is what gets covalently attached to the active site serine of AChE-d so is the only relevant part of the OP. However, these OP pairs will not have the same inhibition rates as the leaving groups are different which will alter the affinity and reactivity of the OP for the AChE-d active site. Methamidophos was shown to be a more potent inhibitor than fenamiphos for both AChE-d and human AChE. This could indicate the two AChE isoforms have the same relative susceptibilities to inhibition by OPs but more OPs would need to be tested to confirm this. Based on methamidophos and fenamiphos alone the data in (65) concerning organophosphorus chemical warfare agents could not be assumed to be representative of AChE-d. The same analysis was done with the reactivation rates of two oximes (Figure 38) for AChE-d inhibited with each of the OPs and the two isoforms were shown to follow different trends (Table 27).

Table 27. Relative ranking of the reactivation rates of AChE-d and human AChE inhibited by OPs. Paraoxon-methyl has the same phosphate adduct as azamethiphos meaning that AChE inhibited by these OPs are identical. The same is true for paraoxon-ethyl and chlorfenvinphos. The data for reactivation of OP inhibited human AChE was taken from (65)**.**

Reactivation rate	OP inhibited AChE-d	OP inhibited human AChE
Fast	Methamidophos	Paraoxon-methyl
	Azamethiphos	Methamidophos
	Chlorfenvinphos	Paraoxon-ethyl
Slow	Fenamiphos	Fenamiphos

Using identical conditions, ^{1}H, ^{15}N HMQC-SOFAST spectra were obtained of AChE-d inhibited with four pesticides and four organophosphorus chemical warfare agents and the peak shifts caused by the inhibition were measured. The OPs that had the slowest reactivation rates appeared to cause the most peak shifts and have more peak shifts in common with each other than with OPs with faster reactivation rates.

However, the magnitudes of the peak shifts were small and the concentration of protein was low (14 µM) which meant noise due to sample variation and hardware limitations could have had a substantial influence on results. Figure 64 shows the ^{1}H, ^{15}N HSQC spectra of lysozyme in the presence of different concentrations of histamine, black arrows show the significant peak shifts which were several times larger than those seen in this work (Figure 63 for example). When it comes to using protein observe NMR to study ligand binding, lysozyme has an advantage over AChE-d, lysozyme is around 14 kDa meaning its spectra is much less crowded and its peaks much sharper so movement of the peaks is easier to track.

The active site serine of AChE-d was mutated to an alanine, this produced a variant of AChE-d (AChE-d S204A) that could bind to OPs but not be phosphorylated by them. Saturation transfer difference NMR was used to study the binding between AChE-d S204A and OPs. Binding could not be detected for all OPs and, for cyclosarin it was shown that the lack of signal in the STD spectra was not due to the binding being too tight which indicated that cyclosarin had a very low affinity for AChE-d.

The ^{31}P NMR spectra of OP inhibited AChE-d were collected but no signal could be detected. This was likely due to the large size of AChE-d (62.517 kDa) making the peak of the phosphate adduct very broad, and together with the low concentration of the sample (40 µM), resulting in low signal intensity. ^{31}P NMR spectra have successfully been collected on a 42 kDa protein but a concentration of around 800 µM was used (192). Getting an 800 µM sample of OP inhibited AChE-d was not feasible so the ^{31}P spectra of the OPs were collected instead. The OPs with faster reactivation rates were found to have higher chemical shifts.

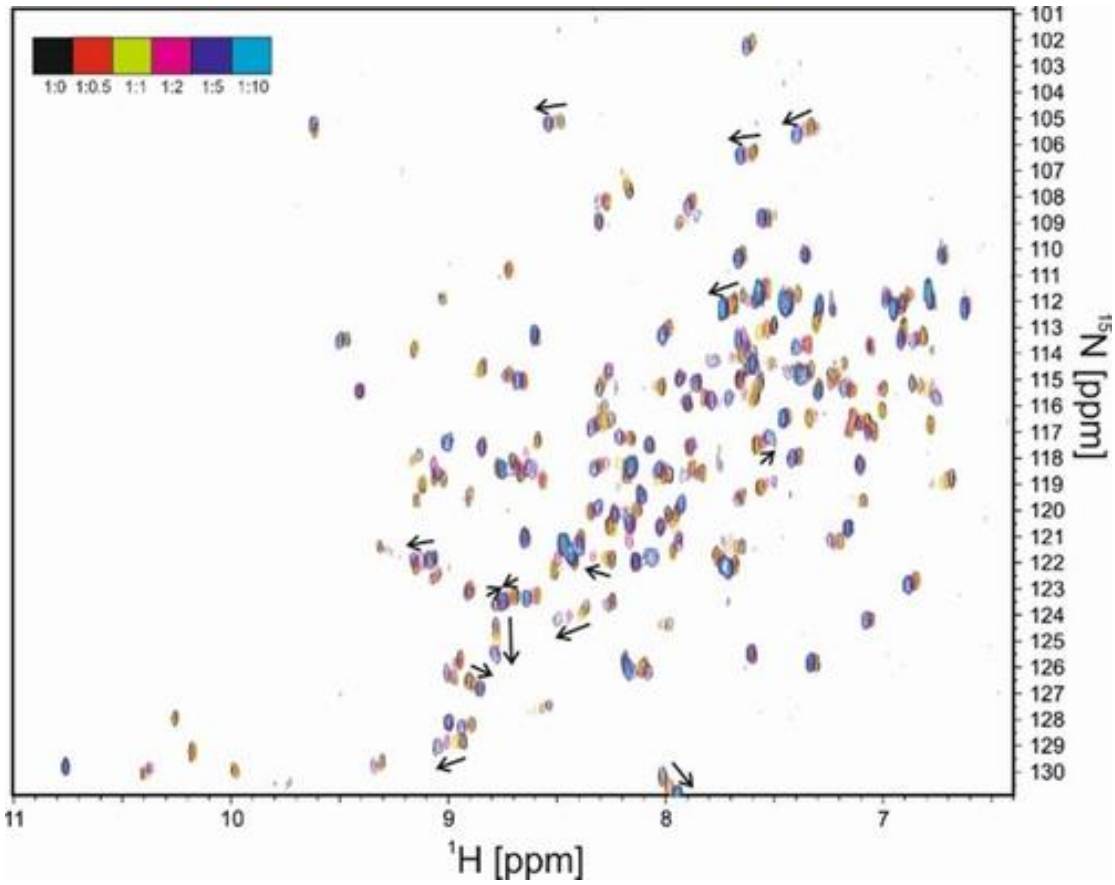

Figure 64. Natural abundance ^{15}N, ^{1}H HSQC spectra of a 5 mM lysozyme sample with different concentrations of histamine. The ratio of lysozyme to histamine is shown in the top left hand corner. This figure was taken from (193)**.**

6.2 Outcomes of the project.

As outlined in section 1.3.3 of the thesis, the aims of this project were to:

- Find a cost-effective source of high purity AChE with the highest possible similarity to wild type human AChE-S.

- Develop NMR methods to study the interactions of AChE with a range of OPs, and to develop protocols for use in assessing the threat of any newly discovered OPs.

- To gain data on the mechanism of inhibition and reactivation that could be used to understand whether inhibition of AChE by certain OPs causes structural changes in the protein that could lower the affinity of certain oximes for that particular OP AChE conjugate. This would help to explain the different reactivation rates that oximes have for different OP AChE conjugates.

  In Chapter 2 it was clearly demonstrated that pure AChE-d could be obtained after recombinant expression in *E. coli*, the benefit this had over the recombinant expression in insect (90) and mammalian cells (89) was that isotopic labelling could be carried out in a cost effective manner. The downside of using an *E. coli* expression system was that only AChE-d could be expressed. This isoform was shown to have an 11% reduction in the turnover rate of ATCh when compared to human AChE (80). In Sections 4.3.2 and 4.3.4 it was shown that the relative ranking of the reactivation rates of pesticide inhibited AChE-d by oximes differed from the ranking of reactivation rates in human AChE. So AChE-d was shown to not be completely representative of human AChE but as it was the only isoform that could be isotopically labelled its use was continued and all data had to be interpreted with this caveat in mind.

  Both protein and ligand observe NMR methods were developed. Attempts to simplify the NMR spectrum of AChE-d were unsuccessful which resulted in low resolution ^{1}H, ^{15}N HMQC-SOFAST spectra of uniformly ^{15}N labelled AChE-d being used to study OP inhibition. The results of this experiment indicated that OPs with

slow reactivation rates may produce different peak shifts in the NMR spectra than OPs with fast reactivation rates, but due to the low resolution and signal-to-noise of the spectra, definitive conclusions could not be draw from the data. Although this method could potentially identify residues important in protecting OPs from reactivation it is unlikely to have any predictive value in estimating OP toxicity as no correlation was seen between peak shifts caused by an OP and its toxicity. The ligand observe method using STD NMR and AChE-d S204A was able to detect the binding of some OPs to the mutated enzyme, but the fact that the binding of all OPs could not be detected meant that STD NMR was not useful in estimating the toxicity of an OP because highly toxic OPs like soman and cyclosarin did not show any binding. Due to the low signal to noise (around 3:1) of the STD experiments the relative intensities of the peaks in the difference spectrum could not be analysed to determine a chemical group's proximity to the enzyme, so chemical groups that had close interactions with the enzyme could not be identified.

The resolution and signal to noise of the ^{1}H, ^{15}N HMQC-SOFAST spectrum was low, so although a larger number and similar peak shifts were seen in AChE-d inhibited with slow reactivating OPs, the results need to be viewed with cation. With this in mind, the data could be seen as preliminary evidence that interaction of a phosphate adduct with certain residues can have a protective effect against oxime-mediated reactivation. The STD data indicated that the phosphorylation step in the inhibition of AChE-d was the rate limiting part of the reaction so the affinity of the OP for AChE-d is not as important as the rate of the phosphorylation step.

6.3 Future work.

Obtaining the inhibition and reactivation rates for the organophosphorus chemical warfare agents with AChE-d should be a main priority as the relative ranking of these values for several OPs was shown to be different for AChE-d and human AChE. This introduced problems in interpreting the AChE-d ^{1}H, ^{15}N HMQC-SOFAST spectra of OP chemical warfare agent inhibited AChE-d as the only available kinetic data for organophosphorus chemical warfare agents was produced with human AChE. This meant that the OPs could not definitively be classed as having a fast or slow reactivation rate, and as one of the aims of this work was to look for common peak shifts in OPs with common kinetic parameters, the kinetic parameters need to be clearly defined.

Attempts should also be made to express usable quantities of deuterated AChE-d as this would allow more detailed NMR studies of the enzyme to be undertaken. In this work the only method of deuteration tried was the "condense and grow" method (119) in which *E. coli* is grown in 3 L of rich media to an OD_{600} of round 0.6. These cultures are then centrifuged, and the cell pellets are washed with phosphate buffer then re-suspended in 1 L of D_2O minimal media, recombinant expression is then induced after a 45 minute equilibration period. *E. coli* need to alter their protein composition to survive in D_2O growth media (122) so the abrupt change from protonated to deuterated media used in this method could stress the *E. coli* cells, reducing the yield of recombinant protein. Other deuteration methods equilibrate *E. coli* to D_2O by growing the cells in minimal media with a gradually increasing percentage of D_2O. First the cells are grown in minimal media containing 50% D_2O, once the culture reaches stationary phase cells are spreads on an agar plate containing 50% D_2O. A colony from this plate is used to inoculate a 90% D_2O minimal media culture which is then used to produce colonies to inoculate a 100% D_2O culture (194). This method selects for cells that can tolerate D_2O and will result in cells having the necessary proteome to grow in D_2O at the start of the experiment resulting in less stress on the cells which could give a better yield of recombinant AChE-d.

If AChE-d was successfully deuterated then the assignment of the backbone residues could become possible. The largest enzyme that has been assigned is malate synthase which has a molecular weight of 81 kDa (195). However, malate synthase was likely chosen for assignment as it produced unusually good NMR spectra for a protein of its size, the samples also had a concentration of 900 µM. Achieving a concentration that high with AChE-d is unlikely to be feasible. If the ^{1}H, ^{15}N spectra of deuterated AChE-d was not assignable, then the selective ^{13}C labelling of Isoleucine, leucine and valine (ILV) could be investigated. This involves expressing the protein in the presence of ILV precursors that have the methyl group selectively ^{13}C labelled and all protons apart from those of the methyl replaced with deuterons. In a ^{1}H, ^{13}C NMR spectra one peak will be observed for each of the ILV residues (196) resulting in a greatly simplified spectra. Assigning the spectrum of deuterated AChE-d with either uniform ^{15}N or ILV ^{13}C labelling would involve a substantial amount of work and there is no guarantee it is possible. However, if successful, studying the dynamics of AChE-d would become easier which would lead to valuable information on how AChE-d is structurally affected by inhibition and reactivation. There is clearly an appetite for this type of research as papers are routinely published that use X-ray crystallography and computer simulations to study the structural dynamic of human AChE. Some examples are, estimating the flexibility of aromatic residues in the gorge (197), and estimating how fluctuations in the volume of the active site gorge after inhibition with different OPs could affect reactivation (198). Other studies have taken a purely computational simulation approach to try and understand the protein structural changes that are important for the inhibition by OPs (199) and their ageing (144). NMR could enhance these studies by providing information on dynamics and the residues that interact with OPs and oximes, this data could be used as refinements in molecular dynamics simulations and to validate X-ray crystallography data. This could aid the rational design of safer OP insecticides and Alzheimer's drugs and more effective oxime reactivators.

The mutation introduced into AChE-d S204A would have had an effect on the binding affinity of ligands such as OPs and oximes. To determine the magnitude of this effect

the K_d of several reversible inhibitors (Alzheimer's drugs for example) should be determined using AChE-d and AChE-d S204A.

The inhibition rates of OPs did not correlate with their toxicity, because of this it was thought that their degradation *in vevo* could influence toxicity. To better predict OP toxicity their breakdown by cytochrome p450, glutathione s transferase and paraoxonases should be investigated using *in vitro* assays as these enzymes are known to breakdown OPs in organisms (200). It is possible that the less toxic OPs are more readily broken down by these enzymes.

7. References.

1. Bon, S., F. Coussen, and J. Massoulié. 1997. Quaternary associations of acetylcholinesterase. II. The polyproline attachment domain of the collagen tail. J. Biol. Chem. 272: 3016–3021.

2. Massoulié, J., A. Anselmet, S. Bon, E. Krejci, C. Legay, N. Morel, and S. Simon. 1999. The polymorphism of acetylcholinesterase: Post-translational processing, quaternary associations and localization. In: Chemico-Biological Interactions. . pp. 29–42.

3. Barnard, E.A. 1974. Neuromuscular Transmission—Enzymatic Destruction of Acetylcholine. In: The Peripheral Nervous System. . pp. 201–224.

4. Liao, J., H. Heider, M. -C Sun, and U. Brodbeck. 1992. Different Glycosylation in Acetylcholinesterases from Mammalian Brain and Erythrocytes. J. Neurochem. 58: 1230–1238.

5. Saldanha, C. 2017. Human erythrocyte acetylcholinesterase in health and disease. Molecules. 22.

6. Tousoulis, D., A.-M. Kampoli, C. Tentolouris, N. Papageorgiou, and C. Stefanadis. 2012. The role of nitric oxide on endothelial function. Curr. Vasc. Pharmacol. 10: 4–18.

7. Kaufer, D., A. Friedman, S. Seidman, and H. Soreq. 1998. Acute stress facilitates long-lasting changes in cholinergic gene expression. Nature. 393: 373–377.

8. Darreh-Shori, T., E. Hellström-Lindahl, C. Flores-Flores, Z.Z. Guan, H. Soreq, and A. Nordberg. 2004. Long-lasting acetylcholinesterase splice variations in anticholinesterase-treated Alzheimer's disease patients. J. Neurochem. 88: 1102–1113.

9. Soreq, H., and S. Seidman. 2001. Acetylcholinesterase--new roles for an old actor. Nat. Rev. Neurosci. 2: 294–302.

10. Hall, L.M., and P. Spierer. 1986. The Ace locus of Drosophila melanogaster: structural gene for acetylcholinesterase with an unusual 5' leader. EMBO J. 5: 2949–2954.

11. Futerman, A.H., M.G. Low, K.E. Ackermann, W.R. Sherman, and I. Silman. 1985. Identification of covalently bound inositol in the hydrophobic membrane-anchoring domain of Torpedo acetylcholinesterase. Biochem. Biophys. Res. Commun. 129: 312–317.

12. Krejci, E., F. Coussen, N. Duval, J.M. Chatel, C. Legay, M. Puype, J. Vandekerckhove, J. Cartaud, S. Bon, and J. Massoulié. 1991. Primary structure of a collagenic tail peptide of Torpedo acetylcholinesterase: co-expression with catalytic subunit induces the production of collagen-tailed forms in transfected cells. EMBO J. 10: 1285–1293.

13. Cousin, X., C. Créminon, J. Grassi, K. Méflah, G. Cornu, B. Saliou, S. Bon, J. Massoulié, and C. Bon. 1996. Acetylcholinesterase from Bungarus venom: A monomeric species. FEBS Lett. 387: 196–200.

14. Patocka, J., K. Kuca, and D. Jun. 2004. Acetylcholinesterase and butyrylcholinesterase--important enzymes of human body. Acta medica (Hradec Kral. 47: 215–28.

15. Boeck, A.T., D.L. Fry, A. Sastre, and O. Lockridge. 2002. Naturally occurring mutation, Asp70His, in human butyrylcholinesterase. Ann. Clin. Biochem. 39: 154–156.

16. Schwarz, M., Y. Loewenstein-Lichtenstein, D. Glick, J. Liao, B. Norgaard-Pedersen, and H. Soreq. 1995. Successive organophosphate inhibition and oxime reactivation reveals distinct responses of recombinant human cholinesterase variants. Mol. Brain Res. 31: 101–110.

17. Herkert, N.M., N. Aurbek, P. Eyer, H. Thiermann, and F. Worek. 2010. Comparative study of oxime-induced reactivation of erythrocyte and muscle AChE from different animal species following inhibition by sarin or paraoxon. Toxicol. Lett. 194: 94–101.

18. Quinn, D.M. 1987. Acetylcholinesterase: Enzyme Structure, Reaction Dynamics, and Virtual Transition States. Chem. Rev. 87: 955–979.

19. Bar-Even, A., E. Noor, Y. Savir, W. Liebermeister, D. Davidi, D.S. Tawfik, and R. Milo. 2011. The moderately efficient enzyme: Evolutionary and physicochemical trends shaping enzyme parameters. Biochemistry. 50: 4402–4410.

20. ZHOU, G. -Q, and W. -Z ZHONG. 1982. Diffusion-Controlled Reactions of Enzymes: A

Comparison between Chou's Model and Alberty-Hammes-Eigen's Model. Eur. J. Biochem. 128: 383–387.

21. Johnson, J.L., B. Cusack, M.P. Davies, A. Fauq, and T.L. Rosenberry. 2003. Unmasking tandem site interaction in human acetylcholinesterase. Substrate activation with a cationic acetanilide substrate. Biochemistry. 42: 5438–5452.

22. Mallender, W.D., T. Szegletes, and T.L. Rosenberry. 2000. Acetylthiocholine binds to Asp74 at the peripheral site of human acetylcholinesterase as the first step in the catalytic pathway. Biochemistry. 39: 7753–7763.

23. Felder, C.E., S.A. Botti, S. Lifson, I. Silman, and J.L. Sussman. 1997. External and internal electrostatic potentials of cholinesterase models. J. Mol. Graph. Model. 15: 318–327.

24. Dvir, H., I. Silman, M. Harel, T.L. Rosenberry, and J.L. Sussman. 2010. Acetylcholinesterase: From 3D structure to function. Chem. Biol. Interact. 187: 10–22.

25. Botti, S.A., C.E. Felder, S. Lifson, J.L. Sussman, and I. Silman. 1999. A modular treatment of molecular traffic through the active site of cholinesterase. Biophys. J. 77: 2430–2450.

26. Steitz, T.A., and R.G. Shulman. 2003. Crystallographic and NMR Studies of the Serine Proteases. Annu. Rev. Biophys. Bioeng. 11: 419–444.

27. Zhou, Y., S. Wang, and Y. Zhang. 2010. Catalytic reaction mechanism of acetylcholinesterase determined by born-oppenheimer Ab initio QM/MM molecular dynamics simulations. J. Phys. Chem. B. 114: 8817–8825.

28. Umeyama, H., A. Imamura, C. Nagata, and M. Hanano. 1973. A molecular orbital study on the enzymic reaction mechanism of α-chymotrypsm. J. Theor. Biol. 41: 485–502.

29. Naray-Szabo, G., A. Warshel, F. Sussman, and J.K. Hwang. 1989. How do serine proteases really work? Biochemistry. 28: 3629–3637.

30. Pohanka, M. 2011. Cholinesterases, a target of pharmacology and toxicology. Biomed. Pap. 155: 219–230.

31. Shohami, E., D. Kaufer, Y. Chen, S. Seidman, O. Cohen, D. Ginzberg, N. Melamed-Book, R. Yirmiya, and H. Soreq. 2000. Antisense prevention of neuronal damages following head injury in mice. J. Mol. Med. 78: 228–236.

32. Campanari, M.L., F. Navarrete, S.D. Ginsberg, J. Manzanares, J. Sáez-Valero, and M.S. García-Ayllón. 2016. Increased Expression of Readthrough Acetylcholinesterase Variants in the Brains of Alzheimer's Disease Patients. J. Alzheimer's Dis. .

33. Bartus, R.T., R.L. Dean, B. Beer, and A.S. Lippa. 1982. The cholinergic hypothesis of geriatric memory dysfunction. Science. 217: 408–14.

34. Selkoe, D. 1994. Normal and Abnormal Biology of the Beta-Amyloid Precursor Protein. Annu. Rev. Neurosci. 17: 489–517.

35. Inestrosa, N.C., A. Alvarez, C.A. Pérez, R.D. Moreno, M. Vicente, C. Linker, O.I. Casanueva, C. Soto, and J. Garrido. 1996. Acetylcholinesterase accelerates assembly of amyloid-β-peptides into Alzheimer's fibrils: Possible role of the peripheral site of the enzyme. Neuron. 16: 881–891.

36. Kutty, K.M., and R.H. Payne. 1994. Serum pseudocholinesterase and very-low-density lipoprotein metabolism. J. Clin. Lab. Anal. 8: 247–250.

37. PERRY, E.K., R.H. PERRY, G. BLESSED, and B.E. TOMLINSON. 1978. Changes in Brain Cholinesterases in Senile Dementia of Alzheimer Type. Neuropathol. Appl. Neurobiol. 4: 273–277.

38. Geula, C., and M.M. Mesulam. 1995. Cholinesterases and the pathology of Alzheimer disease. Alzheimer Dis. Assoc. Disord. 9 Suppl 2: 23–8.

39. Ashani, Y., S. Shapira, D. Levy, A.D. Wolfe, B.P. Doctor, and lily raveh. 1991. Butyrylcholinesterase and acetylcholinesterase prophylaxis against soman poisoning in mice. Biochem. Pharmacol. 41: 37–41.

40. Fukuto, T.R. 1990. Mechanism of action of organophosphorus and carbamate insecticides. In: Environmental health perspectives. . pp. 245–54.

41. Gupta, R. 2006. Toxicology of Organophosphate & Carbamate Compounds. .

42. Turusov, V., V. Rakitsky, and L. Tomatis. 2002. Dichlorodiphenyltrichloroethane (DDT):

Ubiquity, persistence, and risks. Environ. Health Perspect. 110: 125–128.

43. Bondarenko, S., J. Gan, D.L. Haver, and J.N. Kabashima. 2004. Persistence of selected organophosphate and carbamate insecticides in waters from a coastal watershed. Environ. Toxicol. Chem. 23: 2649–54.

44. Desneux, N., A. Decourtye, and J.-M. Delpuech. 2006. The Sublethal Effects of Pesticides on Beneficial Arthropods. Annu. Rev. Entomol. 52: 81–106.

45. Eckert, J.E. 2015. The Effect of DDT on Honeybees. J. Econ. Entomol. 38: 369–374.

46. Antary, T.M. Al. 2010. Toxicity of Certain Insecticides to the Parasitoid Diaeretiella Rapae (Mcintosh)(Hymenoptera : Aphidiidae) and its Host , the Cabbage Aphid Brevicoryne Brassicae L . (Homoptera : Aphididae). Current. 4: 994–1000.

47. 2010. Toxicological Profile for DDT, DDE, and DDD. In: ATSDR's Toxicological Profiles. .

48. DuBois, K.P. 1971. The toxicity of organophosphorus compounds to mammals. Bull. World Health Organ. 44: 233–240.

49. UK, G. 2019. Pesticides registration. http://www.hse.gov.uk/pesticides/topics/pesticide-approvals/pesticides-registration.htm. Heal. Saf. Exec. .

50. Hertfordshire, U. of. 2019. parathion-methyl. https://sitem.herts.ac.uk/aeru/ppdb/en/Reports/507.htm. Pestic. Prop. DataBase. .

51. Karki, P., S.G. Hansdak, S. Bhandari, A. Shukla, and S. Koirala. 2001. A clinico-epidemiological study of organophosphorus poisoning at a rural-based teaching hospital in eastern Nepal. Trop. Doct. 31: 32–34.

52. Hossard, L., A. Philibert, M. Bertrand, C. Colnenne-David, P. Debaeke, N. Munier-Jolain, M.H. Jeuffroy, G. Richard, and D. Makowski. 2014. Effects of halving pesticide use on wheat production. Sci. Rep. 4.

53. Oerke, E.C. 2006. Crop losses to pests. J. Agric. Sci. 144: 31–43.

54. E., Y., E. A., and E. J. 2012. Insecticides for Vector-Borne Diseases: Current Use, Benefits, Hazard and Resistance. In: Insecticides - Advances in Integrated Pest

Management. .

55. Kapesa, A., E.J. Kweka, H. Atieli, Y.A. Afrane, E. Kamugisha, M.C. Lee, G. Zhou, A.K. Githeko, and G. Yan. 2018. The current malaria morbidity and mortality in different transmission settings in western Kenya. PLoS One. 13.

56. Delfino, R.T., T.S. Ribeiro, and J.D. Figueroa-Villar. 2009. Organophosphorus compounds as chemical warfare agents: A review. J. Braz. Chem. Soc. 20: 407–428.

57. EMBER, L. 2010. Chemical Weapons Convention. Chem. Eng. News. 76: 9.

58. Čolović, M.B., T.D. Lazarević-Pašti, A.M. Bondžić, V.M. Vasić, and D.Z. Krstić. 2013. Acetylcholinesterase inhibitors: Pharmacology and toxicology. Curr. Neuropharmacol. 11: 315–335.

59. Aker, W.G., X. Hu, P. Wang, and H.M. Hwang. 2008. Comparing the relative toxicity of malathion and malaoxon in blue catfish Ictalurus furcatus. Environ. Toxicol. 23: 548–554.

60. Buratti, F.M., M.T. Volpe, A. Meneguz, L. Vittozzi, and E. Testai. 2003. CYP-specific bioactivation of four organophosphorothioate pesticides by human liver microsomes. Toxicol. Appl. Pharmacol. 186: 143–154.

61. Feyereisen, R. 1999. Insect P450 Enzymes. Annu. Rev. Entomol. 44: 507–533.

62. Hollingworth, R.M. 1971. Comparative metabolism and selectivity of organophosphate and carbamate insecticides. Bull. World Health Organ. 44: 155–170.

63. Siegfried, B.D., and M.E. Scharf. 2011. Mechanisms of Organophosphate Resistance in Insects. In: Biochemical Sites of Insecticide Action and Resistance. . pp. 269–291.

64. Whyard, S., R.J. Russell, and V.K. Walker. 1994. Insecticide resistance and malathion carboxylesterase in the sheep blowfly, Lucilia cuprina. Biochem. Genet. 32: 9–24.

65. Worek, F., H. Thiermann, L. Szinicz, and P. Eyer. 2004. Kinetic analysis of interactions between human acetylcholinesterase, structurally different organophosphorus compounds and oximes. Biochem. Pharmacol. 68: 2237–2248.

66. Franca, T.C.C., D.A.S. Kitagawa, S.F. d. A. Cavalcante, J.A.V. da Silva, E. Nepovimova,

and K. Kuca. 2019. Novichoks: The dangerous fourth generation of chemical weapons. Int. J. Mol. Sci. 20.

67. Scott, A.L. 2014. Atropine. In: Encyclopedia of Toxicology: Third Edition. . pp. 339–341.

68. Eddleston, M., N.A. Buckley, P. Eyer, and A.H. Dawson. 2008. Management of acute organophosphorus pesticide poisoning. Lancet. 371: 597–607.

69. Worek, F., N. Aurbek, M. Koller, C. Becker, P. Eyer, and H. Thiermann. 2007. Kinetic analysis of reactivation and aging of human acetylcholinesterase inhibited by different phosphoramidates. Biochem. Pharmacol. 73: 1807–1817.

70. Eddleston, M. 2002. Oximes in acute organophosphorus pesticide poisoning: a systematic review of clinical trials. Qjm. 95: 275–283.

71. Worek, F., J. Von Der Wellen, K. Musilek, K. Kuca, and H. Thiermann. 2012. Reactivation kinetics of a homologous series of bispyridinium bis-oximes with nerve agent-inhibited human acetylcholinesterase. Arch. Toxicol. 86: 1379–1386.

72. Marrs, T.C., and J.A. Vale. 2006. Management of organophosphorus pesticide poisoning. In: Toxicology of Organophosphate & Carbamate Compounds. . pp. 715–733.

73. Maxwell, D.M., K.M. Brecht, and R.E. Sweeney. 2013. A common mechanism for resistance to oxime reactivation of acetylcholinesterase inhibited by organophosphorus compounds. In: Chemico-Biological Interactions. . pp. 72–76.

74. Franklin, M.C., M.J. Rudolph, C. Ginter, M.S. Cassidy, and J. Cheung. 2016. Structures of paraoxon-inhibited human acetylcholinesterase reveal perturbations of the acyl loop and the dimer interface. Proteins Struct. Funct. Bioinforma. 84: 1246–1256.

75. Deshpande, S.S., G.B. Viana, F.C. Kauffman, D.L. Rickett, and E.X. Albuquerque. 1986. Effectiveness of physostigmine as a pretreatment drug for protection of rats from organophosphate poisoning. Toxicol. Sci. 6: 566–567.

76. Albuquerque, E.X., E.F.R. Pereira, Y. Aracava, W.P. Fawcett, M. Oliveira, W.R. Randall, T.A. Hamilton, R.K. Kan, J.A. Romano, and M. Adler. 2006. Effective countermeasure

against poisoning by organophosphorus insecticides and nerve agents. Proc. Natl. Acad. Sci. 103: 13220–13225.

77. Maxwell, D.M., K.M. Brecht, I. Koplovitz, and R.E. Sweeney. 2006. Acetylcholinesterase inhibition: Does it explain the toxicity of organophosphorus compounds? Arch. Toxicol. 80: 756–760.

78. Despain, K.E., J.H. McDonough, J.D. McMonagle, M.J. McGinley, and J. Evans. 2007. The toxicity of soman in the African green monkey (Chlorocebus aethiops). Toxicol. Mech. Methods. 17: 255–264.

79. Pereira, E.F.R., Y. Aracava, L.J. DeTolla, E.J. Beecham, G.W. Basinger, E.J. Wakayama, and E.X. Albuquerque. 2014. Animal Models That Best Reproduce the Clinical Manifestations of Human Intoxication with Organophosphorus Compounds. J. Pharmacol. Exp. Ther. 350: 313–321.

80. Goldenzweig, A., M. Goldsmith, S.E. Hill, O. Gertman, P. Laurino, Y. Ashani, O. Dym, T. Unger, S. Albeck, J. Prilusky, R.L. Lieberman, A. Aharoni, I. Silman, J.L. Sussman, D.S. Tawfik, and S.J. Fleishman. 2016. Automated Structure- and Sequence-Based Design of Proteins for High Bacterial Expression and Stability. Mol. Cell. 63: 337–346.

81. Cadieux, C.L., C.A. Broomfield, M.G. Kirkpatrick, M.E. Kazanski, D.E. Lenz, and D.M. Cerasoli. 2010. Comparison of human and guinea pig acetylcholinesterase sequences and rates of oxime-assisted reactivation. Chem. Biol. Interact. 187: 229–233.

82. Santillo, M.F., and Y. Liu. 2015. A fluorescence assay for measuring acetylcholinesterase activity in rat blood and a human neuroblastoma cell line (SH-SY5Y). J. Pharmacol. Toxicol. Methods. 76: 15–22.

83. Brossi, A., B. Schönenberger, O.E. Clark, and R. Ray. 1986. Inhibition of acetylcholinesterase from electric eel by (-)- and (+)-physostigmine and related compounds. FEBS Lett. 201: 190–192.

84. Morton, C.L., and P.M. Potter. 2000. Comparison of Escherichia coli, Saccharomyces cerevisiae, Pichia pastoris, Spodoptera frugiperda, and COS7 cells for recombinant gene expression: Application to a rabbit liver carboxylesterase. Appl. Biochem. Biotechnol. - Part B Mol. Biotechnol. 16: 193–202.

85. Goto, N.K., and L.E. Kay. 2000. New developments in isotope labeling strategies for protein solution NMR spectroscopy. Curr. Opin. Struct. Biol. 10: 585–592.

86. Fischer, M., A. Ittah, I. Liefer, and M. Gorecki. 1993. Expression and reconstitution of biologically active human acetylcholinesterase fromEscherichia coli. Cell. Mol. Neurobiol. 13: 25–38.

87. Fischer, M., A. Ittah, M. Gorecki, and W. MM. 1995. Recombinant human acetylcholinesterase expressed in Escherichia coli: refolding, purification and characterization. Biotechnol. Appl. Biochem. 21: 295–311.

88. Ruark, C., R. Chapleau, D. Mahle, and J. Gearhart. 2015. Organophosphorus Inhibition and Characterization of Recombinant Guinea Pig Acetylcholinesterase. Protein Pept. Lett. 22: 862–868.

89. Wang, X.J., H.X. Wu, S.S. Ye, L.Y. Pan, and Y.C. Qian. 2014. Expression of recombinant human acetylcholinesterase and its application in screening its inhibitors. Yaoxue Xuebao. 49: 50–54.

90. Radić, Z., G. Gibney, S. Kawamoto, K. MacPhee-QuigleyJ, C. Bongiorno, and P. Taylor. 1992. Expression of Recombinant Acetylcholinesterase in a Baculovirus System: Kinetic Properties of Glutamate 199 Mutants. Biochemistry. 31: 9760–9767.

91. Rosenberg, Y.J., J. Walker, X. Jiang, S. Donahue, J. Robosky, M. Sack, J. Lees, and L. Urban. 2015. A highly stable minimally processed plant-derived recombinant acetylcholinesterase for nerve agent detection in adverse conditions. Sci. Rep. 5.

92. Strauss, A., F. Bitsch, G. Fendrich, P. Graff, R. Knecht, B. Meyhack, and W. Jahnke. 2005. Efficient uniform isotope labeling of Abl kinase expressed in Baculovirus-infected insect cells. J. Biomol. NMR. 31: 343–349.

93. Hansen, A.P., A.M. Petros, A.P. Mazar, T.M. Pederson, A. Rueter, and S.W. Fesik. 1992. A Practical Method for Uniform Isotopic Labeling of Recombinant Proteins in Mammalian Cells. Biochemistry. 31: 12713–12718.

94. Lobstein, J., C.A. Emrich, C. Jeans, M. Faulkner, P. Riggs, and M. Berkmen. 2012. SHuffle, a novel Escherichia coli protein expression strain capable of correctly folding

disulfide bonded proteins in its cytoplasm. Microb. Cell Fact. 11.

95. Alanen, H.I., R.A. Williamson, M.J. Howard, A.K. Lappi, H.P. Jäntti, S.M. Rautio, S. Kellokumpu, and L.W. Ruddock. 2003. Functional characterization of ERp18, a new endoplasmic reticulum-located thioredoxin superfamily member. J. Biol. Chem. 278: 28912–28920.

96. Ralston, J.S., a R. Main, B.F. Kilpatrick, and a L. Chasson. 1983. Use of procainamide gels in the purification of human and horse serum cholinesterases. Biochem. J. 211: 243–50.

97. Bell, M.R., M.J. Engleka, A. Malik, and J.E. Strickler. 2013. To fuse or not to fuse: What is your purpose? Protein Sci. 22: 1466–1477.

98. Young, C.L., Z.T. Britton, and A.S. Robinson. 2012. Recombinant protein expression and purification: A comprehensive review of affinity tags and microbial applications. Biotechnol. J. 7: 620–634.

99. Netzer, W.J., and F.U. Hartl. 1997. Recombination of protein domains facilitated by co-translational folding in eukaryotes. Nature. 388: 343–349.

100. Yuan, S., J. Xu, Y. Ge, Z. Yan, G. Du, and N. Wang. 2013. Prokaryotic Ubiquitin-Like ThiS Fusion Enhances the Heterologous Protein Overexpression and Aggregation in Escherichia coli. PLoS One. 8.

101. Sati, S.P., S.K. Singh, N. Kumar, and A. Sharma. 2002. Extra terminal residues have a profound effect on the folding and solubility of a Plasmodium falciparum sexual stage-specific protein over-expressed in Escherichia coli. Eur. J. Biochem. 269: 5259–5263.

102. Hammarström, M., E.A. Woestenenk, N. Hellgren, T. Härd, and H. Berglund. 2006. Effect of N-terminal solubility enhancing fusion proteins on yield of purified target protein. J. Struct. Funct. Genomics. 7: 1–14.

103. De La Hoz, D., B.P. Doctor, J. Scott Ralston, R.S. Rush, and A. David Wolfe. 1986. A simplified procedure for the purification of large quantities of fetal bovine serum acetylcholinesterase. Life Sci. 39: 195–199.

104. Saxena, A., C. Luo, and B.P. Doctor. 2008. Developing procedures for the large-scale purification of human serum butyrylcholinesterase. Protein Expr. Purif. 61: 191–196.

105. Marion, D. 2013. An Introduction to Biological NMR Spectroscopy. Mol. Cell. Proteomics. 12: 3006–3025.

106. Yu, H. 2002. Extending the size limit of protein nuclear magnetic resonance. Proc. Natl. Acad. Sci. 96: 332–334.

107. Hoopes, J.T., M.A. Elberson, R.J. Preston, P.T. Reddy, and Z. Kelman. 2015. Protein Labeling in Escherichia coli with 2H, 13C, and 15N. In: Methods in Enzymology. . pp. 27–44.

108. Bodenhausen, G., and D.J. Ruben. 1980. Natural abundance nitrogen-15 NMR by enhanced heteronuclear spectroscopy. Chem. Phys. Lett. 69: 185–189.

109. Fardus-Reid, F., J. Warren, and A. Le Gresley. 2016. Validating heteronuclear 2D quantitative NMR. Anal. Methods. .

110. Ghosh, S., A. Sengupta, and K. Chandra. 2017. SOFAST-HMQC—an efficient tool for metabolomics. Anal. Bioanal. Chem. .

111. Schanda, P., E. Kupĉe, and B. Brutscher. 2005. SOFAST-HMQC experiments for recording two-dimensional deteronuclear correlation spectra of proteins within a few seconds. J. Biomol. NMR. 33: 199–211.

112. Pervushin, K., R. Riek, G. Wider, and K. Wuthrich. 1997. Attenuated T2 relaxation by mutual cancellation of dipole-dipole coupling and chemical shift anisotropy indicates an avenue to NMR structures of very large biological macromolecules in solution. Proc. Natl. Acad. Sci. U. S. A. 94: 12366–12371.

113. Crowley, P.B., C. Kyne, and W.B. Monteith. 2012. Simple and inexpensive incorporation of 19F-Tryptophan for protein NMR spectroscopy. Chem. Commun. 48: 10681–10683.

114. Curtis-Marof, R., D. Doko, M.L. Rowe, K.L. Richards, R.A. Williamson, and M.J. Howard. 2014. 19 F NMR spectroscopy monitors ligand binding to recombinantly fluorine-labelled b ’ x from human protein disulphide isomerase (hPDI). Org. Biomol.

Chem. 12: 3808–3812.

115. Lacabanne, D., B.H. Meier, and A. Böckmann. 2018. Selective labeling and unlabeling strategies in protein solid-state NMR spectroscopy. J. Biomol. NMR. 71: 141–150.

116. Yamazaki, T., D.R. Muhandiranv, L.E. Kay, W. Lee, and C.H. Arrowsmith. 1994. A Suite of Triple Resonance NMR Experiments for the Backbone Assignment of 15N, 13C, 2H Labeled Proteins with High Sensitivity. J. Am. Chem. Soc. 116: 11655–11666.

117. LeMaster, D.M. 1990. Uniform and selective deuteration in two-dimensional NMR of proteins. Annu. Rev. Biophys. Biophys. Chem. 19: 243–266.

118. Sattler, M., and S.W. Fesik. 1996. Use of deuterium labeling in NMR: Overcoming a sizeable problem. Structure. 4: 1245–1249.

119. Marley, J., M. Lu, and C. Bracken. 2001. A method for efficient isotopic labeling of recombinant proteins. J. Biomol. NMR. 20: 71–75.

120. Lopukhov, L. V., A.A. Ponomareva, and L.O. Yagodina. 2007. Selective 15N labeling of barstar in a T7 polymerase system. Biophysics (Oxf). 52: 13–15.

121. Sivashanmugam, A., V. Murray, C. Cui, Y. Zhang, J. Wang, and Q. Li. 2009. Practical protocols for production of very high yields of recombinant proteins using Escherichia coli. Protein Sci. 18: 936–948.

122. Opitz, C., E. Ahrné, K.N. Goldie, A. Schmidt, and S. Grzesiek. 2019. Deuterium induces a distinctive Escherichia coli proteome that correlates with the reduction in growth rate. J. Biol. Chem. 294: 2279–2292.

123. Reddy, P.T., R.G. Brinson, J.T. Hoopes, C. McClung, N. Ke, L. Kashi, M. Berkmen, and Z. Kelman. 2018. Platform development for expression and purification of stable isotope labeled monoclonal antibodies in Escherichia coli. MAbs. 10: 992–1002.

124. Hattori, A., H.L. Crespi, and J.J. Katz. 1965. Effect of Side-Chain Deuteration on Protein Stability. Biochemistry. 4: 1213–1225.

125. Liu, X., B.L. Hanson, P. Langan, and R.E. Viola. 2007. The effect of deuteration on protein structure: A high-resolution comparison of hydrogenous and perdeuterated haloalkane dehalogenase. Acta Crystallogr. Sect. D Biol. Crystallogr. 63: 1000–1008.

126. Curtis-Marof, R., D. Doko, M.L. Rowe, K.L. Richards, R. a Williamson, and M.J. Howard. 2014. 19F NMR spectroscopy monitors ligand binding to recombinantly fluorine-labelled b'x from human protein disulphide isomerase (hPDI). Org. Biomol. Chem. 12: 3808–12.

127. Doroshenko, V.G., V.A. Livshits, L.G. Airich, I.S. Shmagina, E.A. Savrasova, M. V. Ovsienko, and S. V. Mashko. 2015. Metabolic engineering of Escherichia coli for the production of phenylalanine and related compounds. Appl. Biochem. Microbiol. 51: 733–750.

128. Li, C., G.F. Wang, Y. Wang, R. Creager-Allen, E.A. Lutz, H. Scronce, K.M. Slade, R.A.S. Ruf, R.A. Mehl, and G.J. Pielak. 2010. Protein 19F NMR in Escherichia coli. J. Am. Chem. Soc. 132: 321–327.

129. Forbes, A.J., M.T. Mazur, H.M. Patel, C.T. Walsh, and N.L. Kelleher. 2001. Toward efficient analysis of >70 kDa proteins with 100% sequence coverage. Proteomics. 1: 927–933.

130. Tang, S., and D.A. Case. 2011. Calculation of chemical shift anisotropy in proteins. J. Biomol. NMR. 51: 303–312.

131. Gerig, J.T. 1994. Fluorine NMR of proteins. Prog. Nucl. Magn. Reson. Spectrosc. 26: 293–370.

132. O'Grady, C., B.L. Rempel, A. Sokaribo, S. Nokhrin, and O.Y. Dmitriev. 2012. One-step amino acid selective isotope labeling of proteins in prototrophic Escherichia coli strains. Anal. Biochem. 426: 126–128.

133. Lin, M.T., L.J. Sperling, H.L. Frericks Schmidt, M. Tang, R.I. Samoilova, T. Kumasaka, T. Iwasaki, S.A. Dikanov, C.M. Rienstra, and R.B. Gennis. 2011. A rapid and robust method for selective isotope labeling of proteins. Methods. 55: 370–378.

134. KARI, C., Z. NAGY, P. KOVACS, and F. HERNADI. 2009. Mechanism of the Growth Inhibitory Effect of Cysteine on Escherichia coli. J. Gen. Microbiol. 68: 349–356.

135. Cao, C., J.L. Chen, Y. Yang, F. Huang, G. Otting, and X.C. Su. 2014. Selective 15N-labeling of the side-chain amide groups of asparagine and glutamine for applications

in paramagnetic NMR spectroscopy. J. Biomol. NMR. 59: 251–261.

136. Ellman, G.L., K.D. Courtney, V. Andres, and R.M. Featherstone. 1961. A new and rapid colorimetric determination of acetylcholinesterase activity. Biochem. Pharmacol. 7: 88–95.

137. Shafferman, A., C. Kronman, Y. Flashner, M. Leitner, H. Grosfeld, A. Ordentlich, Y. Gozes, S. Cohen, N. Ariel, D. Barak, M. Harel, I. Silman, J.L. Sussman, and B. Velan. 1992. Mutagenesis of human acetylcholinesterase. Identification of residues involved in catalytic activity and in polypeptide folding. J. Biol. Chem. 267: 17640–17648.

138. Vaughan, A., T. Rocheleau, and R. Ffrench-Constant. 1997. Site-directed mutagenesis of an acetylcholinesterase gene from the yellow fever mosquito Aedes aegypti confers insecticide insensitivity. Exp. Parasitol. 87: 237–244.

139. Bartling, A., F. Worek, L. Szinicz, and H. Thiermann. 2007. Enzyme-kinetic investigation of different sarin analogues reacting with human acetylcholinesterase and butyrylcholinesterase. Toxicology. 233: 166–172.

140. Worek, F., P. Eyer, and H. Thiermann. 2012. Determination of acetylcholinesterase activity by the Ellman assay: A versatile tool for in vitro research on medical countermeasures against organophosphate poisoning. Drug Test. Anal. 4: 282–291.

141. Wong, L., Z. Radić, R.J.M. Brüggemann, N. Hosea, H.A. Berman, and P. Taylor. 2000. Mechanism of oxime reactivation of acetylcholinesterase analyzed by chirality and mutagenesis. Biochemistry. 39: 5750–5757.

142. Hovanec, J.W., C.A. Broomfield, G.M. Steinberg, K.W. Lanks, and C.N. Lieske. 1977. Spontaneous reactivation of acetylcholinesterase following organophosphate inhibition. I. An analysis of anomalous reactivation kinetics. BBA - Enzymol. 483: 312–319.

143. Curtil, C., and P. Masson. 1993. [Aging of cholinesterase after inhibition by organophosphates]. Ann. Pharm. Fr. 51: 63–77.

144. Sirin, G.S., Y. Zhou, L. Lior-Hoffmann, S. Wang, and Y. Zhang. 2012. Aging mechanism of soman inhibited acetylcholinesterase. J. Phys. Chem. B. 116: 12199–12207.

145. SUN, M. -c, Z. -g CHANG, M. -z SHAU, R. -h HUANG, and T. -c CHOU. 1979. The Mechanism of Ageing of Phosphonylated Acetylcholinesterase. Eur. J. Biochem. 100: 527–530.

146. Mason, H.J., C. Sams, A.J. Stevenson, and R. Rawbone. 2000. Rates of spontaneous reactivation and aging of acetylcholinesterase in human erythrocytes after inhibition by organophosphorus pesticides. Hum. Exp. Toxicol. 19: 511–516.

147. Langenberg, J.P., L.P.A. De Jong, M.F. Otto, and H.P. Benschop. 1988. Spontaneous and oxime-induced reactivation of acetylcholinesterase inhibited by phosphoramidates. Arch. Toxicol. 62: 305–310.

148. Stroberg, W., and S. Schnell. 2017. On the validity and errors of the pseudo-first-order kinetics in ligand–receptor binding. Math. Biosci. 287: 3–11.

149. Worek, F., P. Eyer, and L. Szinicz. 1998. Inhibition, reactivation and aging kinetics of cyclohexylmethylphosphonofluoridate-inhibited human cholinesterases. Arch. Toxicol. 72: 580–587.

150. Su, C.T., P.H. Wang, R.F. Liu, J.H. Shih, C. Ma, C.H. Lin, C.Y. Liu, and M.T. Wu. 1986. Kinetic studies and structure-activity relationships of bispyridinium oximes as reactivators of acetylcholinesterase inhibited by organophosphorus compounds. Toxicol. Sci. .

151. Estrada-Mondaca, S., and D. Fournier. 1998. Stabilization of recombinant Drosophila acetylcholinesterase. Protein Expr. Purif. 12: 166–172.

152. Hertfordshire, U. of. azamethiphos (Ref: GCA 18809). PPDB Pestic. Prop. DataBase. .

153. Cornell Cooperative Extension. fenamiphos (Nemacur) Chemical Profile 2/85. Pestic. Manag. Educ. Progr. .

154. Cornell Cooperative Extension. methamidophos (Monitor) Chemical Profile 4/95. Pestic. Manag. Educ. Progr. .

155. Hutson, D.H., and C.J. Logan. 1986. Detoxification of the organophosphorus insecticide chlorfenvinphos by rat, rabbit and human liver enzymes. Xenobiotica. 16: 87–93.

156. Slater, J.C. 1964. Atomic radii in crystals. J. Chem. Phys. 41: 3199–3204.

157. Coban, A., R.L. Carr, H.W. Chambers, K.O. Willeford, and J.E. Chambers. 2016. Comparison of inhibition kinetics of several organophosphates, including some nerve agent surrogates, using human erythrocyte and rat and mouse brain acetylcholinesterase. Toxicol. Lett. 248: 39–45.

158. Kristensen, M., M. Knorr, A.G. Spencer, and J.B. Jespersen. 2009. Selection and Reversion of Azamethiphos-Resistance in a Field Population of the Housefly <I>Musca domestica</I> (Diptera: Muscidae), and the Underlying Biochemical Mechanisms. J. Econ. Entomol. 93: 1788–1795.

159. Peter, J.V., T. Sudarsan, and J. Moran. 2014. Clinical features of organophosphate poisoning: A review of different classification systems and approaches. Indian J. Crit. Care Med. 18: 735–745.

160. Mayer, M., and B. Meyer. 1999. Characterization of ligand binding by saturation transfer difference NMR spectroscopy. Angew. Chemie - Int. Ed. 38: 1784–1788.

161. Freeman, R. 1991. Selective Excitation in High-Resolution NMR. Chem. Rev. 91: 1397–1412.

162. Spencer, R.G.S., J.A. Ferretti, and G.H. Weiss. 1989. NMR saturation factors in the presence of chemical exchange. J. Magn. Reson. 84: 223–235.

163. James Keeler. 2006. Understanding NMR spectroscopy. Choice Rev. Online. 43: 43-5896-43–5896.

164. Viegas, A., J. Manso, F.L. Nobrega, and E.J. Cabrita. 2011. Saturation-transfer difference (STD) NMR: A simple and fast method for ligand screening and characterization of protein binding. J. Chem. Educ. 88: 990–994.

165. Kalk, A., and H.J.C. Berendsen. 1976. Proton magnetic relaxation and spin diffusion in proteins. J. Magn. Reson. 24: 343–366.

166. Haselhorst, T., A.C. Lamerz, and M. Von Itzstein. 2009. Saturation transfer difference NMR spectroscopy as a technique to investigate protein-carbohydrate interactions in solution. Methods Mol. Biol. 534: 375–386.

167. Wagstaff, J.L., S.L. Taylor, and M.J. Howard. 2013. Recent developments and applications of saturation transfer difference nuclear magnetic resonance (STD NMR) spectroscopy. Mol. Biosyst. 9: 571–577.

168. Wang, Y. Sen, D. Liu, and D.F. Wyss. 2004. Competition STD NMR for the detection of high-affinity ligands and NMR-based screening. Magn. Reson. Chem. 42: 485–489.

169. Mayer, M., and B. Meyer. 2001. Group epitope mapping by saturation transfer difference NMR to identify segments of a ligand in direct contact with a protein receptor. J. Am. Chem. Soc. 123: 6108–6117.

170. Furukawa, A., T. Konuma, S. Yanaka, and K. Sugase. 2016. Quantitative analysis of protein-ligand interactions by NMR. Prog. Nucl. Magn. Reson. Spectrosc. 96: 47–57.

171. Yu, Z., P. Li, and K.M. Merz. 2017. Using Ligand-Induced Protein Chemical Shift Perturbations To Determine Protein-Ligand Structures. Biochemistry. 56: 2349–2362.

172. Stark, J., and R. Powers. 2008. Rapid protein-ligand costructures using chemical shift perturbations. J. Am. Chem. Soc. 130: 535–545.

173. Peng, C., S.W. Unger, F. V. Filipp, M. Sattler, and S. Szalma. 2004. Automated evaluation of chemical shift perturbation spectra: New approaches to quantitative analysis of receptor-ligand interaction NMR spectra. J. Biomol. NMR. 29: 491–504.

174. Williamson, M.P. 2013. Using chemical shift perturbation to characterise ligand binding. Prog. Nucl. Magn. Reson. Spectrosc. 73: 1–16.

175. Takeuchi, K., and G. Wagner. 2006. NMR studies of protein interactions. Curr. Opin. Struct. Biol. 16: 109–117.

176. Kleckner, I.R., and M.P. Foster. 2011. An introduction to NMR-based approaches for measuring protein dynamics. Biochim. Biophys. Acta - Proteins Proteomics. 1814: 942–968.

177. Da Cunha Xavier Soares, S.F., A.A. Vieira, R.T. Delfino, and J.D. Figueroa-Villar. 2013. NMR determination of Electrophorus electricus acetylcholinesterase inhibition and reactivation by neutral oximes. Bioorganic Med. Chem. 21: 5923–5930.

178. Tanoli, N.U., S.A.K. Tanoli, A.G. Ferreira, M. Mehmood, S. Gul, J.L. Monteiro, L.C.C.

Vieira, T. Venâncio, A.G. Correa, and Z. Ul-Haq. 2018. Characterization of the interactions between coumarin-derivatives and acetylcholinesterase: Examination by NMR and docking simulations. J. Mol. Model. 24.

179. Tanoli, N.U., S.A.K. Tanoli, A.G. Ferreira, S. Gul, and Z. Ul-Haq. 2015. Evaluation of binding competition and group epitopes of acetylcholinesterase inhibitors by STD NMR, Tr-NOESY, DOSY and molecular docking: An old approach but new findings. Medchemcomm. .

180. Ekström, F., A. Hörnberg, E. Artursson, L.G. Hammarström, G. Schneider, and Y.P. Pang. 2009. Structure of HI-6-sarin-acetylcholinesterase determined by x-ray crystallography and molecular dynamics simulation: Reactivator mechanism and design. PLoS One. 4.

181. Agilent Technologies. 2011. QuikChange II Site-Directed Mutagenesis Kit: Instruction Manual. Europe. 200523: 19.

182. Kuca, K., J. Patocka, J. Cabal, and D. Jun. 2004. Reactivation of organophosphate-inhibited acetylcholinesterase by quaternary pyridinium aldoximes. Neurotox. Res. 6: 565–570.

183. Michel, H.O., B.E. Hackley, L. Berkowitz, G. List, E.B. Hackley, W. Gillilan, and M. Pankau. 1967. Ageing and dealkylation of soman (pinacolylmethylphosphonofluoridate)-inactivated eel cholinesterase. Arch. Biochem. Biophys. 121: 29–34.

184. Vom, A., S. Headey, G. Wang, B. Capuano, E. Yuriev, M.J. Scanlon, and J.S. Simpson. 2013. Detection and prevention of aggregation-based false positives in STD-NMR-based fragment screening. Aust. J. Chem. 66: 1518–1524.

185. Pérez-Victoria, I., S. Kemper, M.K. Patel, J.M. Edwards, J.C. Errey, L.F. Primavesi, M.J. Paul, T.D.W. Claridge, and B.G. Davis. 2009. Saturation transfer difference NMR reveals functionally essential kinetic differences for a sugar-binding repressor protein. Chem. Commun. : 5862–5864.

186. A. AL-Jalali, M., and Y. M. Mahzia. 2014. Effect of electronegative elements on the NMR chemical shift in somesimple R-X organic compounds. IOSR J. Appl. Phys. 6: 45–

56.

187. Ghattyvenkatakrishna, P.K., N. Chavali, and E.C. Uberbacher. 2013. Flexibility of active-site gorge aromatic residues and non-gorge aromatic residues in acetylcholinesterase. Chem. Pap. 67: 677–681.

188. Krishnarjuna, B., G. Jaipuria, A. Thakur, P. D'Silva, and H.S. Atreya. 2011. Amino acid selective unlabeling for sequence specific resonance assignments in proteins. J. Biomol. NMR. 49: 39–51.

189. Meyer, B., and T. Peters. 2003. NMR spectroscopy techniques for screening and identifying ligand binding to protein receptors. Angew. Chemie - Int. Ed. 42: 864–890.

190. Hulet, S.W., D.R. Sommerville, D.B. Miller, J.A. Scotto, W.T. Muse, and D.C. Burnett. 2014. Comparison of sarin and cyclosarin toxicity by subcutaneous, intravenous and inhalation exposure in Gottingen minipigs. Inhal. Toxicol. 26: 175–184.

191. James, T.L. 1998. Chapter 1 Fundamentals of NMR. Control. .

192. Seifert, M.H.J., C.B. Breitenlechner, D. Bossemeyer, R. Huber, T.A. Holak, and R.A. Engh. 2002. Phosphorylation and flexibility of cyclic-AMP-dependent protein kinase (PKA) using 31P NMR spectroscopy. Biochemistry. 41: 5968–5977.

193. Becker, W., K.C. Bhattiprolu, N. Gubensäk, and K. Zangger. 2018. Investigating Protein–Ligand Interactions by Solution Nuclear Magnetic Resonance Spectroscopy. ChemPhysChem. 19: 895–906.

194. Duff, A.P., K.L. Wilde, A. Rekas, V. Lake, and P.J. Holden. 2015. Robust High-Yield Methodologies for 2H and 2H/15N/13C Labeling of Proteins for Structural Investigations Using Neutron Scattering and NMR. In: Methods in Enzymology. . pp. 3–25.

195. Tugarinov, V., R. Muhandiram, A. Ayed, and L.E. Kay. 2002. Four-dimensional NMR spectroscopy of a 723-residue protein: Chemical shift assignments and secondary structure of malate synthase G. J. Am. Chem. Soc. 124: 10025–10035.

196. Tugarinov, V., and L.E. Kay. 2003. Ile, Leu, and Val Methyl Assignments of the 723-Residue Malate Synthase G Using a New Labeling Strategy and Novel NMR Methods.

J. Am. Chem. Soc. 125: 13868–13878.

197. Xu, Y., J.P. Colletier, M. Weik, H. Jiang, J. Moult, I. Silman, and J.L. Sussman. 2008. Flexibility of aromatic residues in the active-site gorge of acetylcholinesterase: X-ray versus molecular dynamics. Biophys. J. 95: 2500–2511.

198. Ochoa, R., C.A. Rodriguez, and A.F. Zuluaga. 2016. Perspectives for the structure-based design of acetylcholinesterase reactivators. J. Mol. Graph. Model. 68: 176–183.

199. Wang, J., J. Gu, and J. Leszczynski. 2008. Theoretical modeling study for the phosphonylation mechanisms of the catalytic triad of acetylcholinesterase by sarin. J. Phys. Chem. B. 112: 3485–3494.

200. Alejo-González, K., E. Hanson-Viana, and R. Vazquez-Duhalt. 2018. Enzymatic detoxification of organophosphorus pesticides and related toxicants. J. Pestic. Sci. 43: 1–9.

8. Appendices.

8.1 ^{1}H, ^{15}N HMQC-SOFAST of OP inhibited AChE-d.

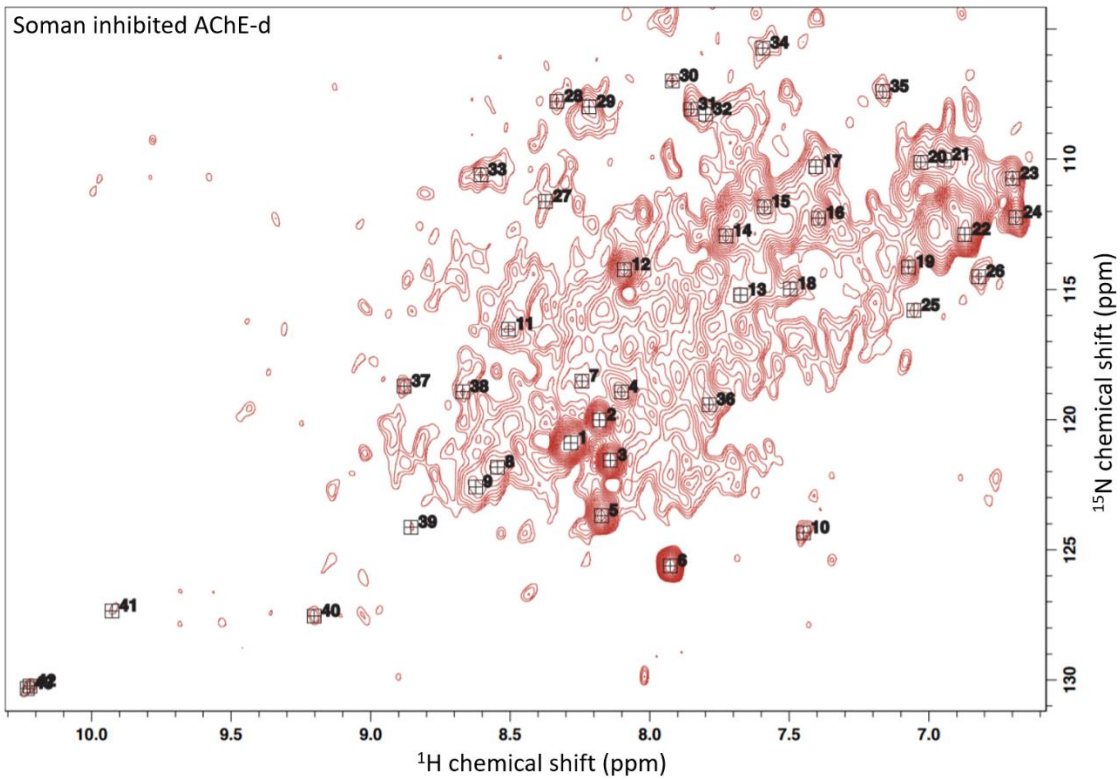

Appendix 1. ^{1}H, ^{15}N HMQC-SOFAST of soman inhibited AChE-d with the position of the 43 peaks used to asses AChE-d inhibition indicated by black crosses, the concentration of AChE-d was 14 µM. The spectrum was collected for 1888 scans with 1024 points in the ^{1}H dimension and 100 points in the ^{15}N dimension at 35 ^{o}C. The noise base level was set to 26905.6.

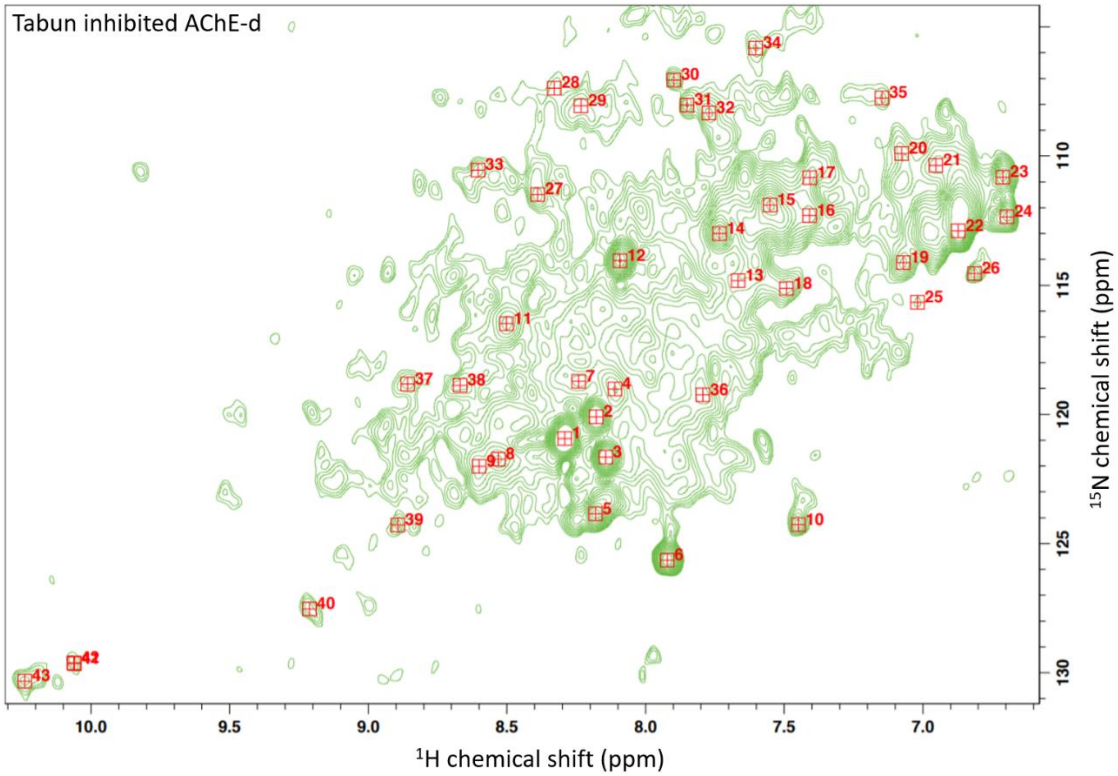

Appendix 2. ^{1}H, ^{15}N HMQC-SOFAST of tabun inhibited AChE-d with the position of the 43 peaks used to asses AChE-d inhibition indicated by red crosses, the concentration of AChE-d was 14 µM. The spectrum was collected for 1888 scans with 1024 points in the ^{1}H dimension and 100 points in the ^{15}N dimension at 35 ^{o}C. The noise base level was set to 26905.6.

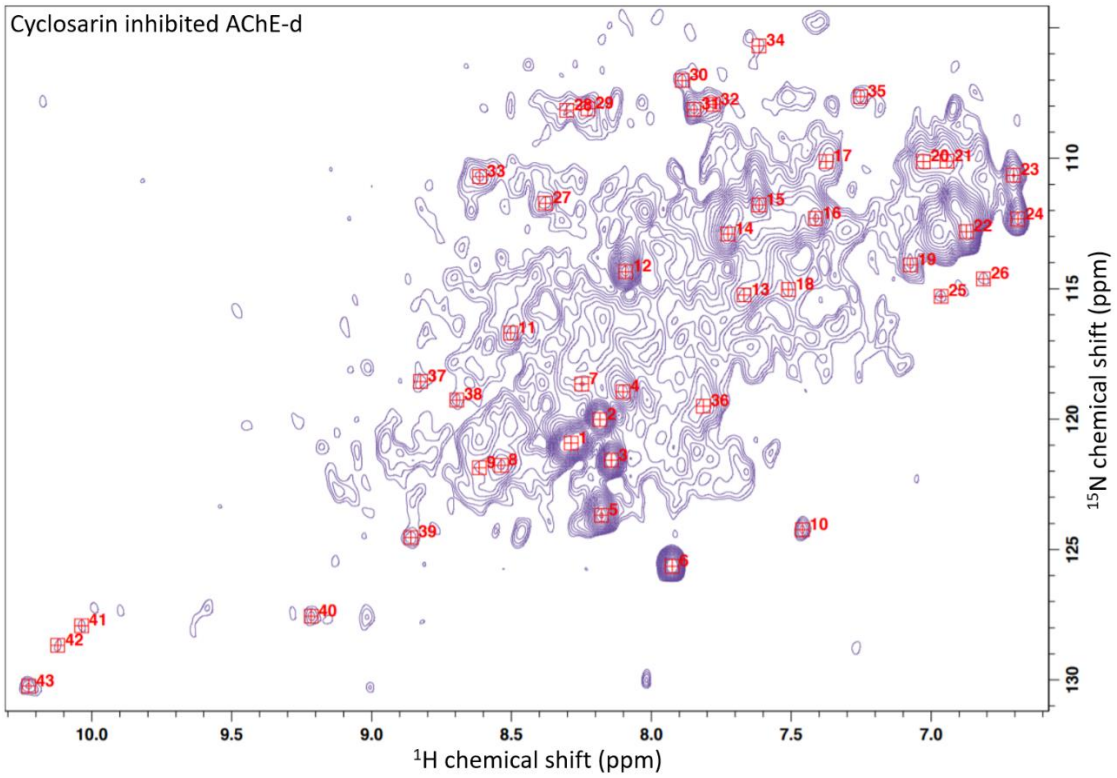

Appendix 3. ^{1}H, ^{15}N HMQC-SOFAST of cyclosarin inhibited AChE-d with the position of the 43 peaks used to asses AChE-d inhibition indicated by red crosses, the concentration of AChE-d was 14 µM. The spectrum was collected for 1888 scans with 1024 points in the ^{1}H dimension and 100 points in the ^{15}N dimension at 35 ^{o}C. The noise base level was set to 26905.6.

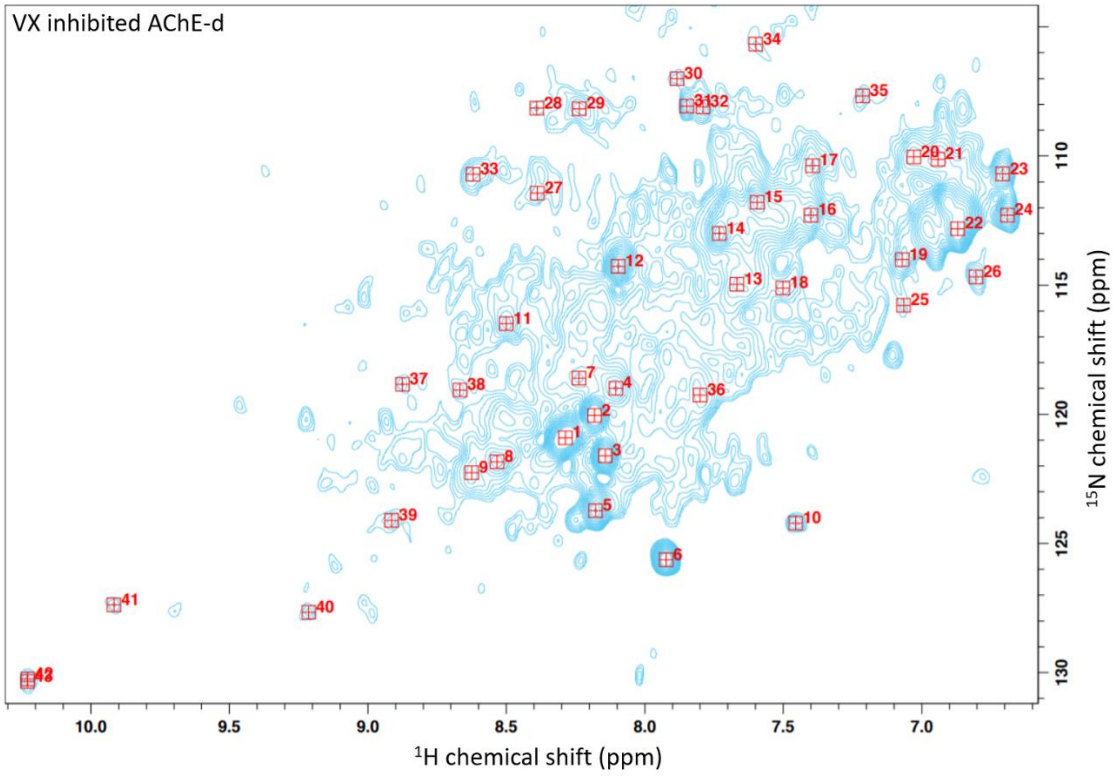

Appendix 4. ^{1}H, ^{15}N HMQC-SOFAST of VX inhibited AChE-d with the position of the 43 peaks used to asses AChE-d inhibition indicated by red crosses, the concentration of AChE-d was 14 µM. The spectrum was collected for 1888 scans with 1024 points in the ^{1}H dimension and 100 points in the ^{15}N dimension at 35 ^{o}C. The noise base level was set to 26905.6.

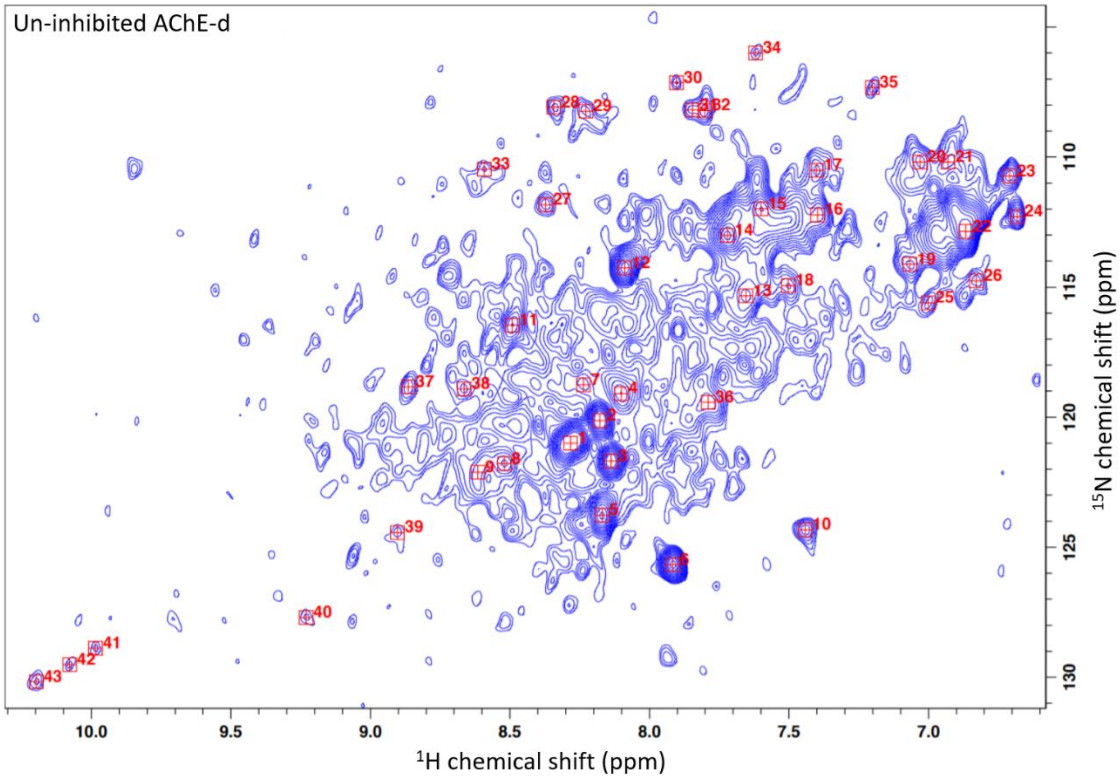

Appendix 5. ^{1}H, ^{15}N HMQC-SOFAST of un-inhibited AChE-d with the position of the 43 peaks used to asses AChE-d inhibition indicated by red crosses, the concentration of AChE-d was 14 µM. The spectrum was collected for 1888 scans with 1024 points in the ^{1}H dimension and 100 points in the ^{15}N dimension at 35 ^{o}C. The noise base level was set to 26905.6.

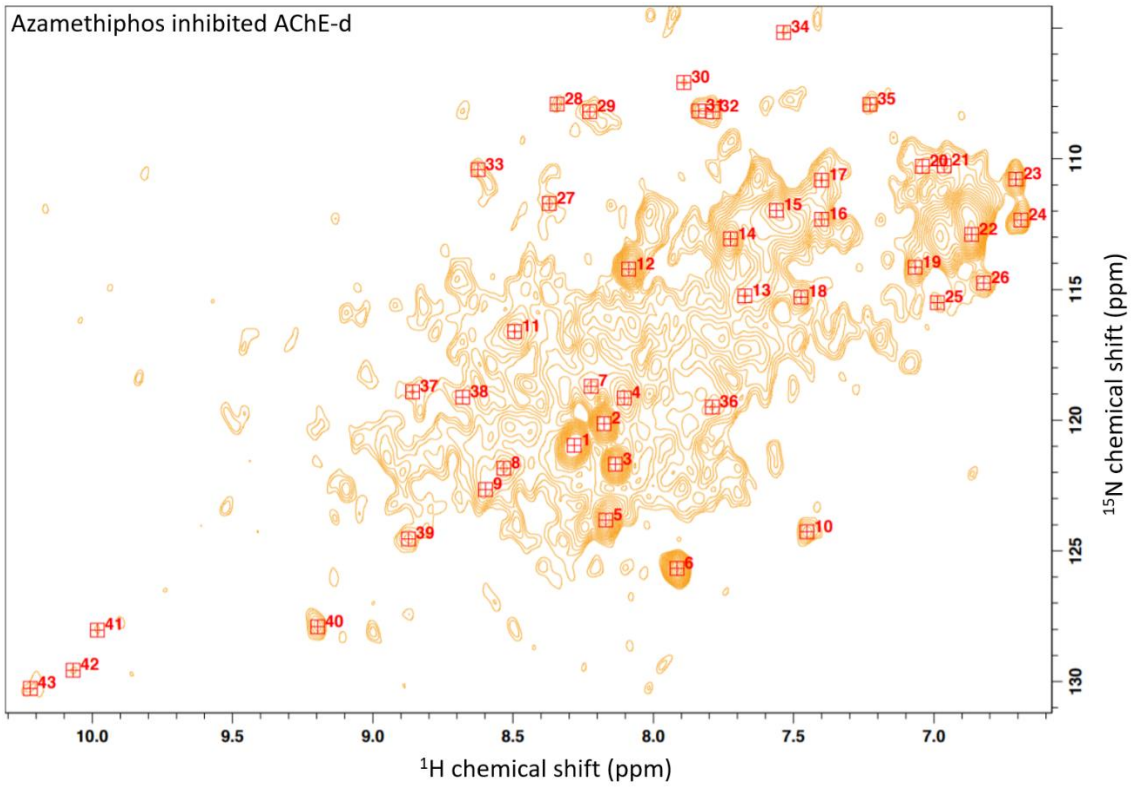

Appendix 6. ^{1}H, ^{15}N HMQC-SOFAST of azamethiphos inhibited AChE-d with the position of the 43 peaks used to asses AChE-d inhibition indicated by red crosses, the concentration of AChE-d was 14 µM. The spectrum was collected for 1888 scans with 1024 points in the ^{1}H dimension and 100 points in the ^{15}N dimension at 35 ^{o}C. The noise base level was set to 26905.6.

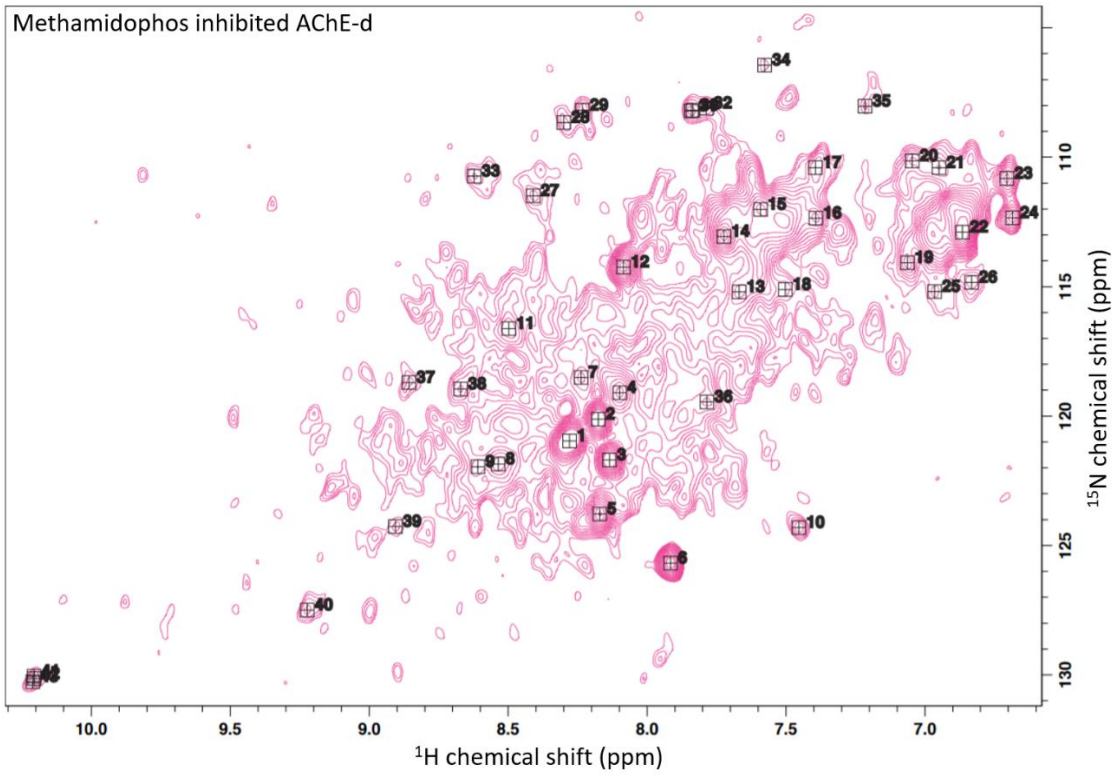

Appendix 7. ^{1}H, ^{15}N HMQC-SOFAST of methamidophos inhibited AChE-d with the position of the 43 peaks used to asses AChE-d inhibition indicated by black crosses, the concentration of AChE-d was 14 µM. The spectrum was collected for 1888 scans with 1024 points in the ^{1}H dimension and 100 points in the ^{15}N dimension at 35 ^{o}C. The noise base level was set to 26905.6.

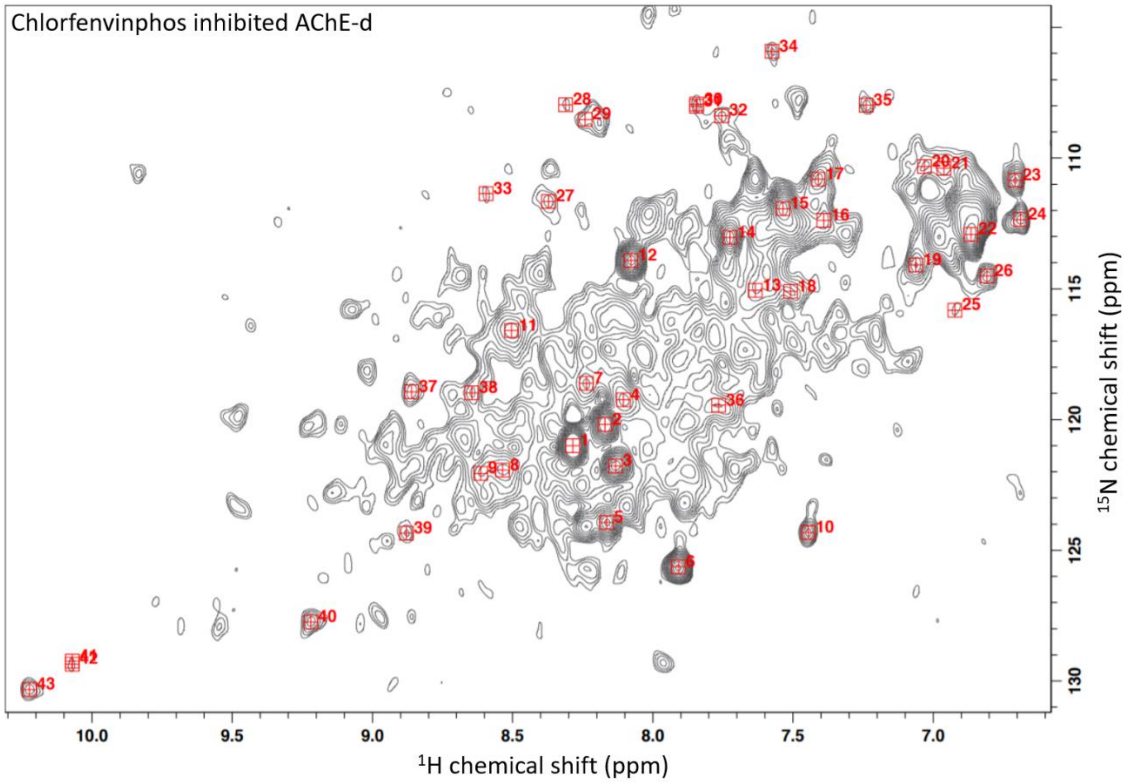

Appendix 8. ^{1}H, ^{15}N HMQC-SOFAST of chlorfenvinphos inhibited AChE-d with the position of the 43 peaks used to asses AChE-d inhibition indicated by red crosses, the concentration of AChE-d was 14 µM. The spectrum was collected for 1888 scans with 1024 points in the ^{1}H dimension and 100 points in the ^{15}N dimension at 35 ^{o}C. The noise base level was set to 26905.6.

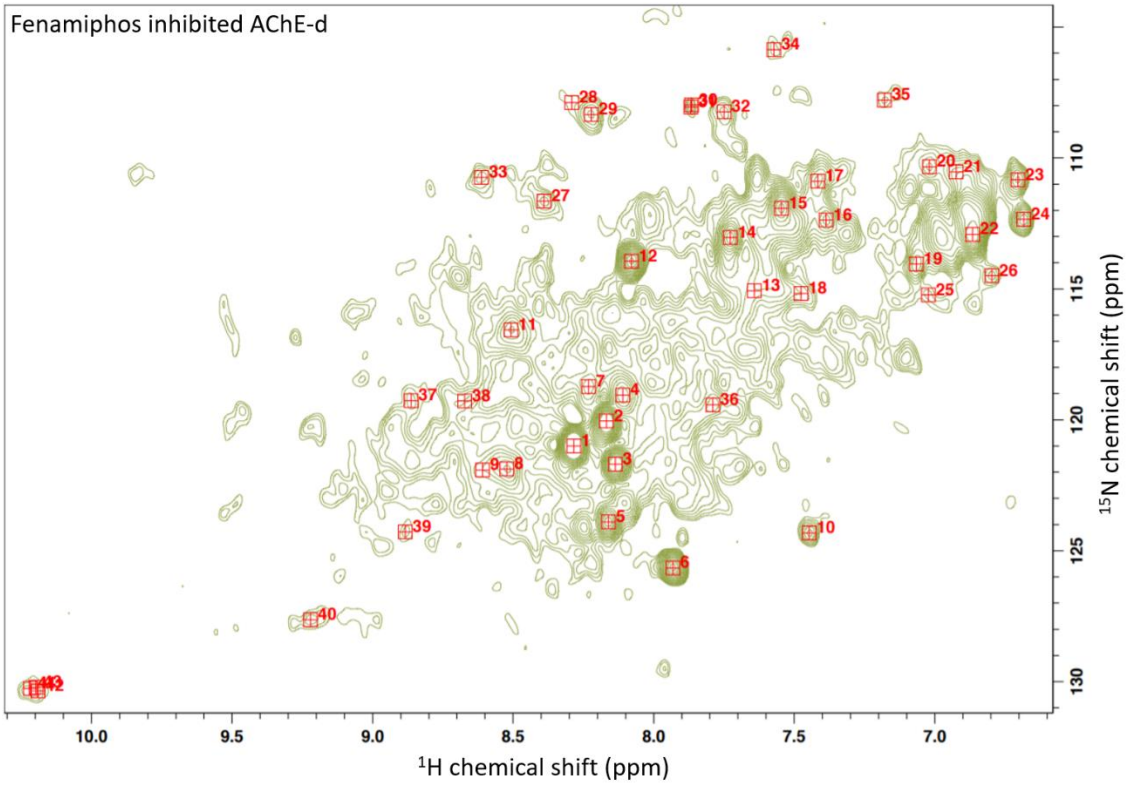

Appendix 9. ^{1}H, ^{15}N HMQC-SOFAST of fenamiphos inhibited AChE-d with the position of the 43 peaks used to asses AChE-d inhibition indicated by red crosses, the concentration of AChE-d was 14 µM. The spectrum was collected for 1888 scans with 1024 points in the ^{1}H dimension and 100 points in the ^{15}N dimension at 35 ^{o}C. The noise base level was set to 26905.6.

8.2 STD data of OPs binding to AChE-d S204A.

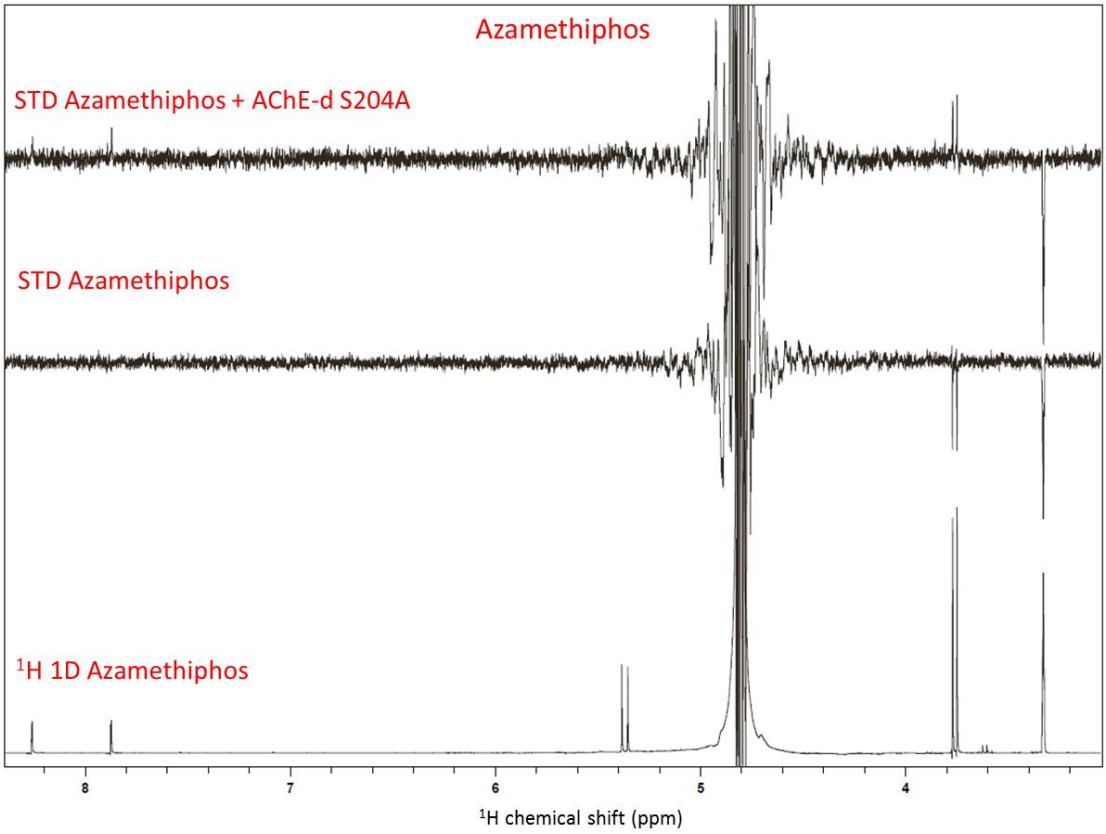

Appendix 10.STD NMR experiment of azamethiphos in the presence and absence of AChE-d S204A. Azamethiphos concentrations were 0.5 mM and AChE-d S204A was 5.5 µM. The spectra were collected over 256 scans.

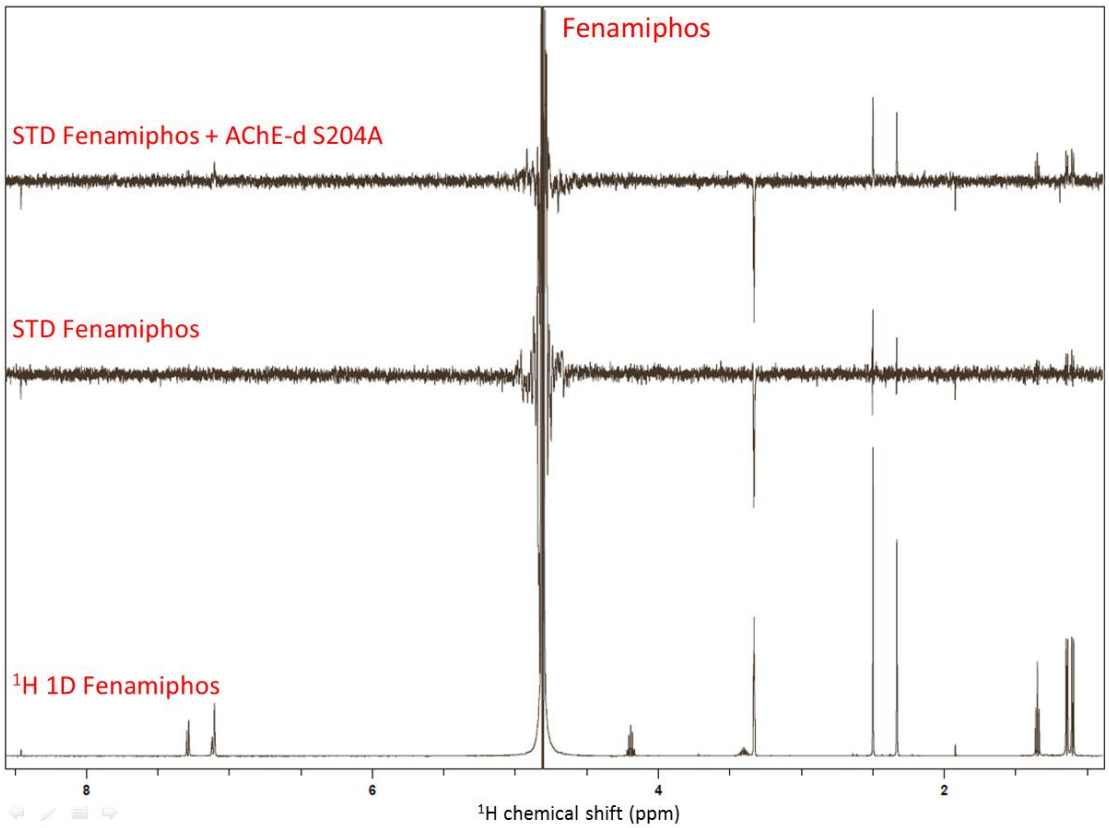

Appendix 11. STD NMR experiment of fenamiphos in the presence and absence of AChE-d S204A. Fenamiphos concentrations were 0.5 mM and AChE-d S204A was 5.5 µM. The spectra were collected over 256 scans.

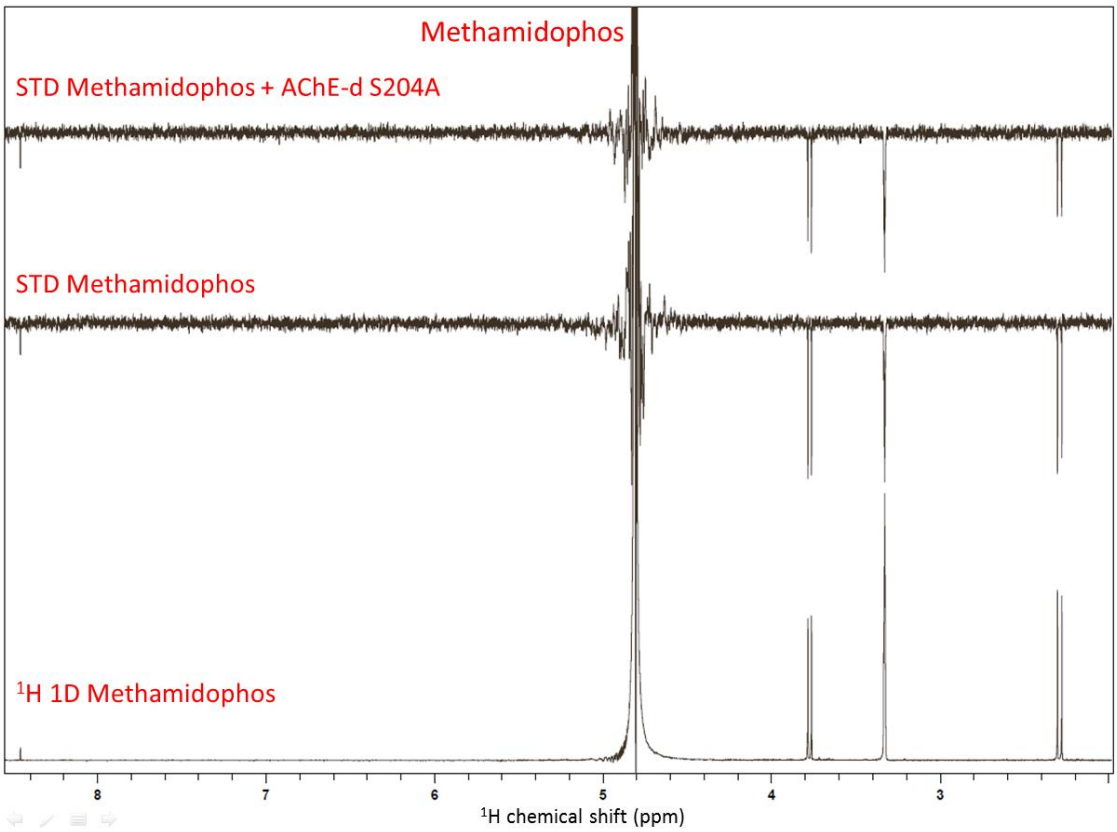

Appendix 12. STD NMR experiment of methamidophos in the presence and absence of AChE-d S204A. Methamidophos concentrations were 0.5 mM and AChE-d S204A was 5.5 µM. The spectra were collected over 256 scans.

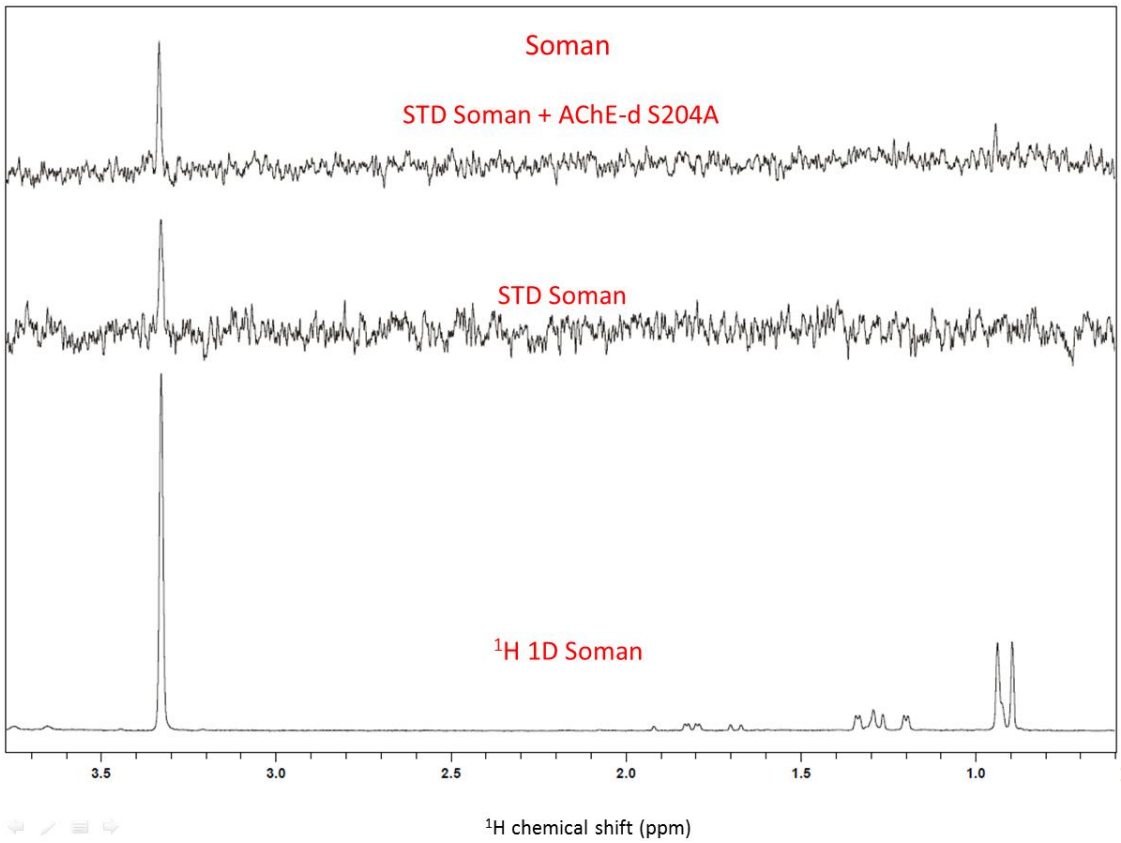

Appendix 13. STD NMR experiment of soman in the presence and absence of AChE-d S204A. Soman concentrations were 0.5 mM and AChE-d S204A was 5.5 µM. The spectra were collected over 256 scans.

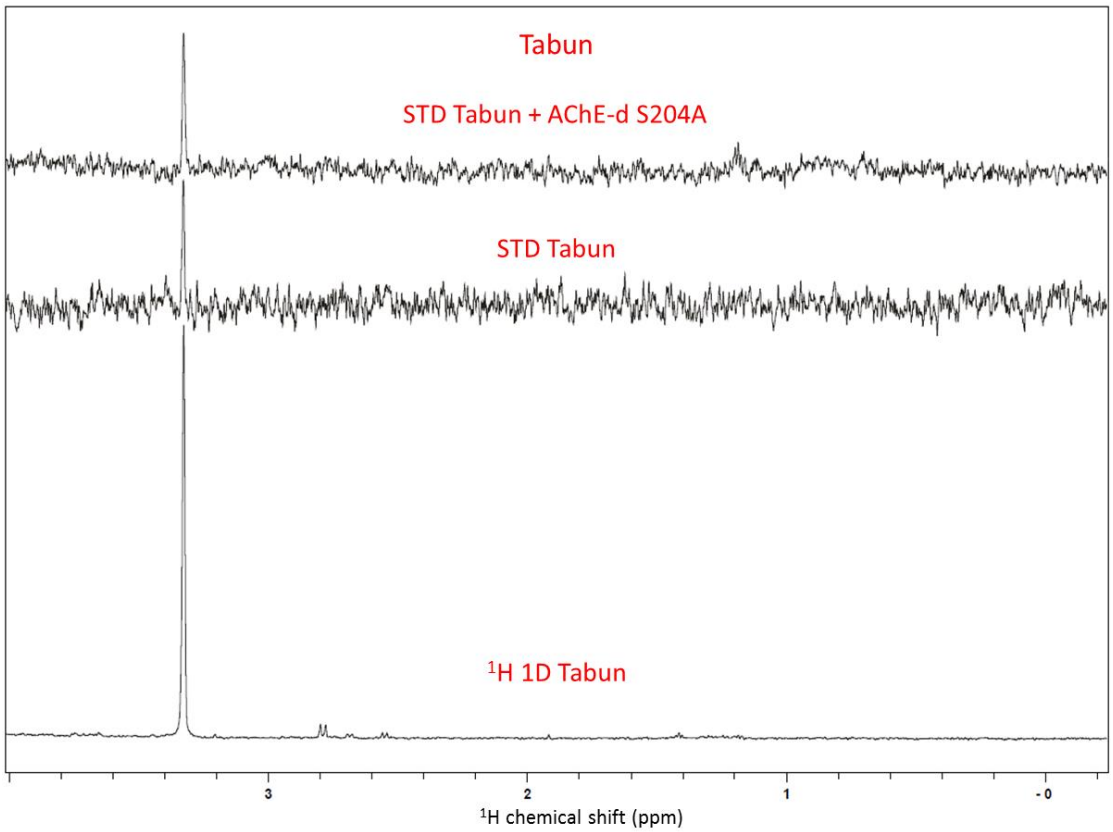

Appendix 14. STD NMR experiment of tabun in the presence and absence of AChE-d S204A. Tabun concentrations were 0.5 mM and AChE-d S204A was 5.5 µM. The spectra were collected over 256 scans.

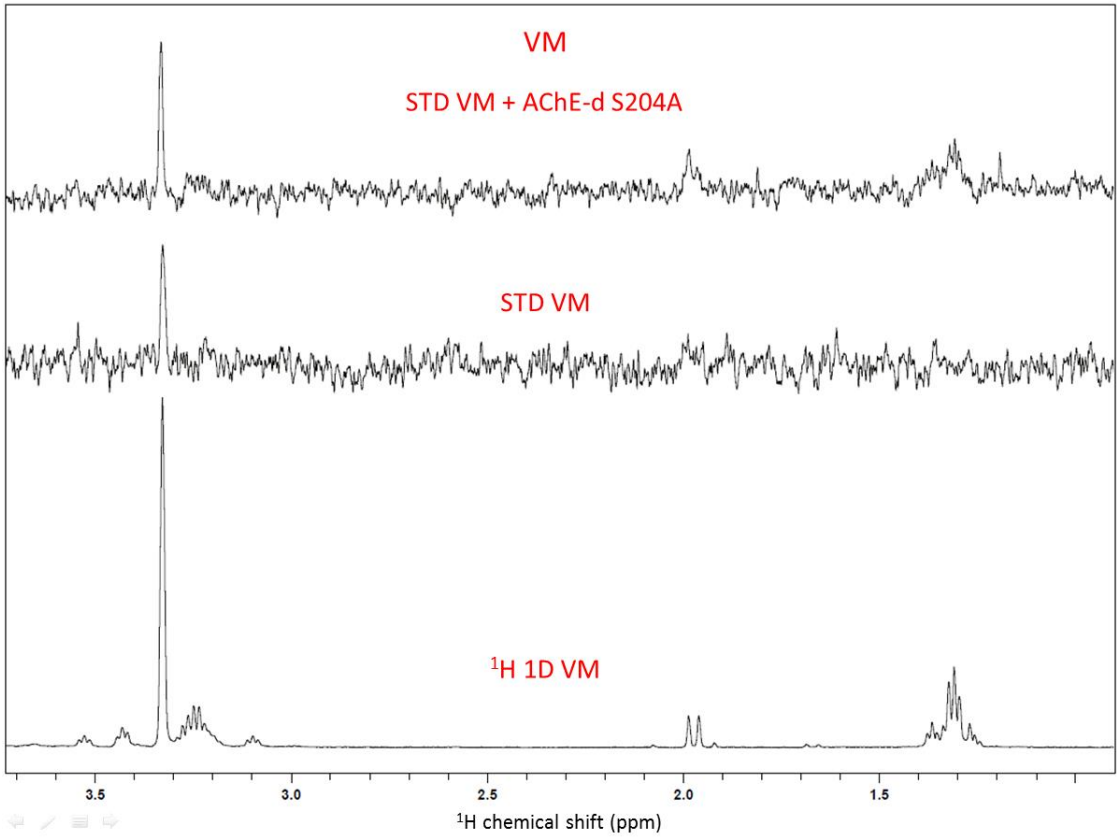

Appendix 15. STD NMR experiment of VM in the presence and absence of AChE-d S204A. VM concentrations were 0.5 mM and AChE-d S204A was 5.5 µM. The spectra were collected over 256 scans.

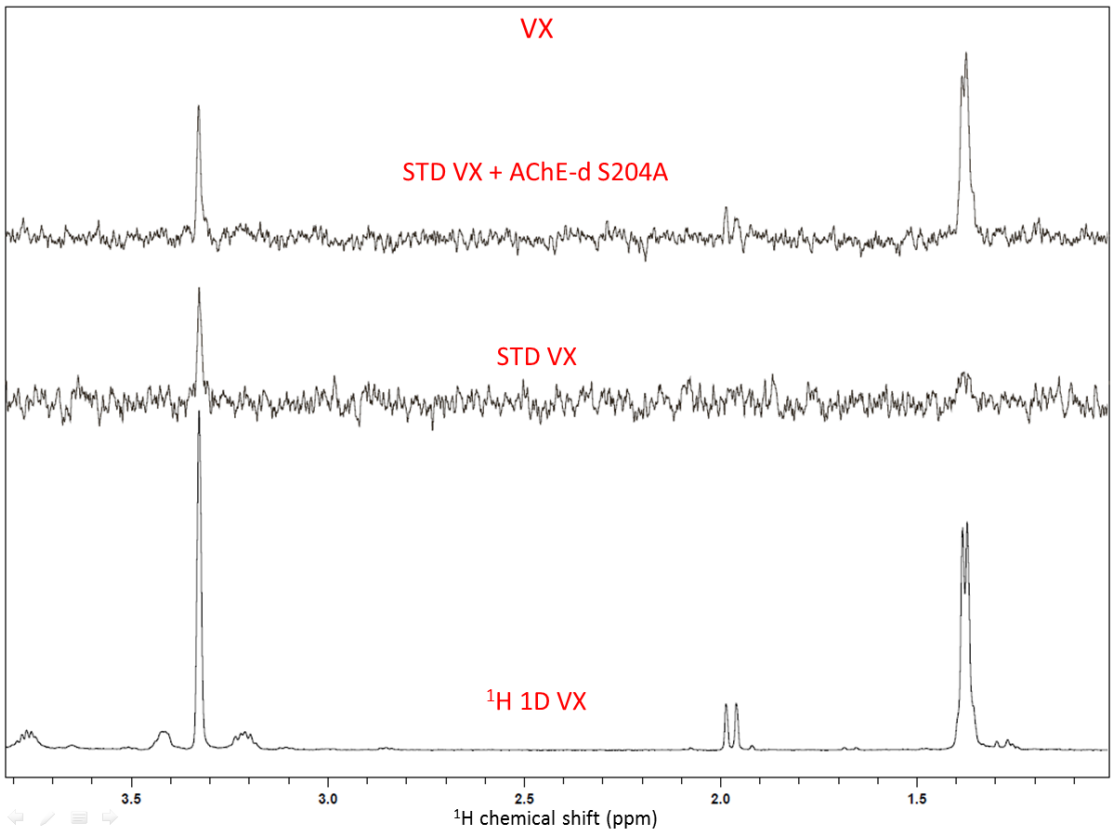

Appendix 16. STD NMR experiment of VX in the presence and absence of AChE-d S204A. VX concentrations were 0.5 mM and AChE-d S204A was 5.5 µM. The spectra were collected over 256 scans.

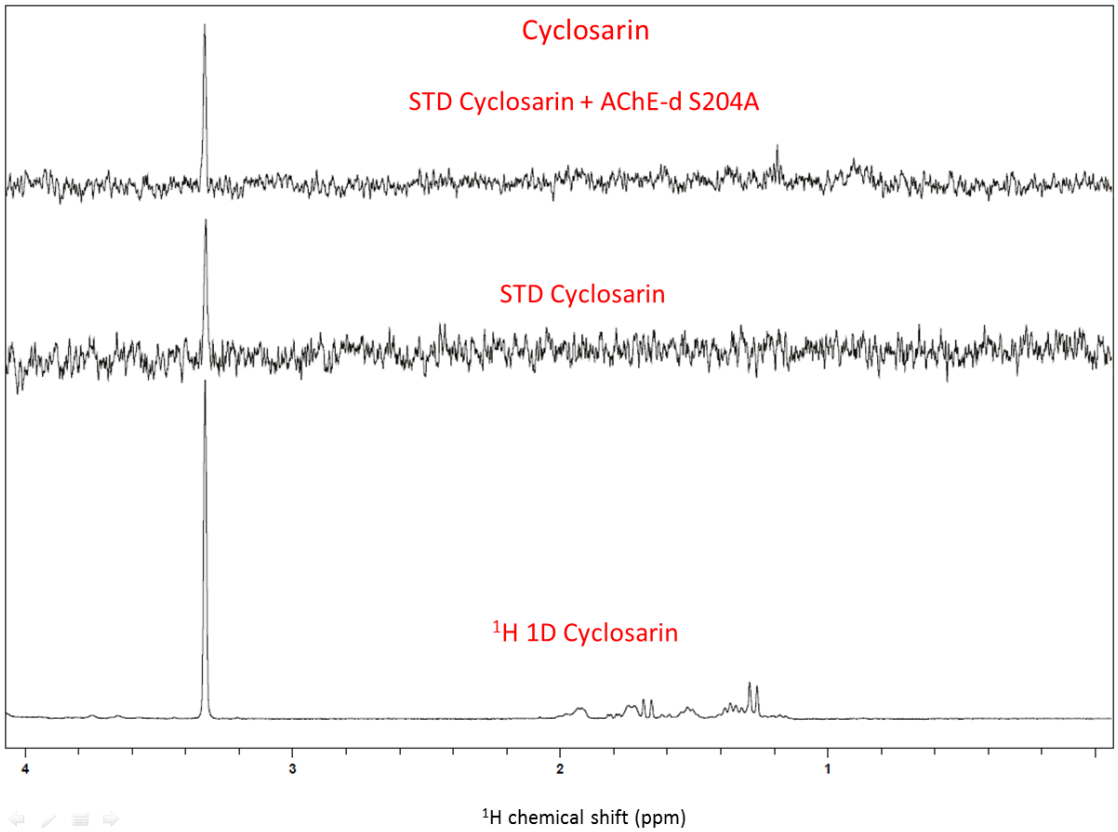

Appendix 17. STD NMR experiment of cyclosarin in the presence and absence of AChE-d S204A. Cyclosarin concentrations were 0.5 mM and AChE-d S204A was 5.5 µM. The spectra were collected over 256 scans.